UNIVERSITÄT BAYREUTH

SYNTHESE UND WIRKOPTIMIERUNG ANTITUMORALER PLATINKOMPLEXE MIT N-HETEROZYKLISCHEN CARBENEN

DISSERTATION

zur Erlangung des akademischen Grades eines

Doktors der Naturwissenschaften (Dr. rer. nat.)

im Fach Chemie

an der Fakultät für Biologie, Chemie und Geowissenschaften

Universität Bayreuth

vorgelegt von

Tobias Rehm

aus Radolfzell am Bodensee

Ravensburg, 2020

Die vorliegende Arbeit wurde in der Zeit von Januar 2015 bis März 2018 in Bayreuth am Lehrstuhl Organische Chemie I unter Betreuung von Herrn Professor Dr. Rainer Schobert angefertigt.

Vollständiger Abdruck der von der Fakultät für Biologie, Chemie und Geowissenschaften der Universität Bayreuth genehmigten Dissertation zur Erlangung des akademischen Grades eines Doktors der Naturwissenschaften (Dr. rer. nat.).

Dissertation eingereicht am: 07.11.2019

Zulassung durch die Promotionskommission: 04.12.2019

Wissenschaftliches Kolloquium: 09.03.2020

Amtierender Dekan: Prof. Dr. Matthias Breuning

Prüfungsausschuss:

Prof. Dr. Rainer Schobert	(Gutachter)
Prof. Dr. Birgit Weber	(Gutachterin)
Prof. Dr. Birte Höcker	(Vorsitz)
Prof. Dr. Peter Strohriegl	

„Alle Dinge sind Gift, und nichts ist ohne Gift:

allein die Dosis machts, daß ein Ding kein Gift sei."

Paracelsus, 1538

INHALTSVERZEICHNIS

ABKÜRZUNGSVERZEICHNIS

Ac	Acyl-
Ac_2O	Essigsäureanhydrid
AcOH	Essigsäure
Ar	Aryl-
Bzl	Benzyl-
CA-4	Combretastatin A-4
COX	Cyclooxygenasen
DCC	Dicyclohexylcarbodiimid
DMSO	Dimethylsulfoxid
eq	Äquivalente
exs.	excess
Et	Ethyl-
EtOH	Ethanol
et al.	*et alii* (und andere)
FOLFOX	Chemotherapie-Schema mit Folinsäure, 5-Fluorouracil und Oxaliplatin
HDAC	Histon-Deacetylasen
IC_{50}	mittlere inhibitorische Konzentration
KO^tBu	Kalium-*tert*-butanolat
L	Ligand
M	Metall
Me	Methyl-
MTT	3-(4,5-Dimethylthiazol-2-yl)-2,5-diphenyltetrazolium-bromid
mw	Mikrowelle
n-Bu	*n*-Butyl-
NHC	*N*-Heterozyklisches Carben
NMR	Kernspinresonanz (*nuclear magnetic resonance*)
Nu	Nukleophil
n-Oct	*n*-Octyl-
OMe	Methoxy-
Ph	Phenyl-
ROS	Reaktive Sauerstoffspezies
rt	Raumtemperatur
Tos	Tosyl-
TosMIC	Tosylmethylisocyanid
Üs.	Überschuss
versch.	verschiedene

ZUSAMMENFASSUNG

Seit dem Ende der 1970er Jahre besitzen Platinkomplexe wie Cisplatin eine führende Rolle in der Behandlung von Tumorerkrankungen, sind aber trotz fortschrittlicher Therapieschemata bis heute mit schweren Nebenwirkungen behaftet. Bei der Forschung nach immer neuen und besser verträglichen Zytostatika rückten zuletzt weitere Übergangsmetalle in den Fokus der Wissenschaft. Ein Grund dafür sind die mittlerweile gut erforschten und vor allem sehr variabel einsetzbaren *N*-heterozyklischen Carbene (NHCs). Mit diesen als Liganden ergaben sich gänzlich neue Metallotherapeutika, mit besser justierbaren pharmakologischen Eigenschaften als jemals zuvor. In der vorliegenden kumulativen Dissertationsschrift ist in vier wissenschaftlichen Publikationen die Synthese und Wirkoptimierung antitumoraler Platinkomplexe mit solchen NHC-Liganden dargestellt. Dabei sollten unter Verwendung von NHCs neuartige, cisplatin-ähnliche Strukturtypen entwickelt werden, die eine Alternative zu den etablierten Platinzytostatika bieten könnten.

Einen synthetischen Zugang dazu lieferten – ausgehend von Imidazolium- bzw. Benzimidazoliumsalzen synthetisierte – *cis*-[$Pt^{II}Cl_2$(DMSO)(NHC)]-Komplexe wie **65** und **71**. Deren labile, *cis*-ständige DMSO-Liganden wurden unter Erhalt der Stereochemie gegen andere Liganden ausgetauscht. Zunächst konnten Phosphine in *cis*-Position zu verschiedenen Imidazol- und Benzimidazol-NHC-Liganden eingeführt werden, wodurch die neutralen Komplexe **66** und **72** sowie mit einem Überschuss an PPh_3 die geladenen Komplexe **67** und **73** erhalten wurden. Im Vergleich mit den beiden *trans*-Komplexen **68** und **69**, die keine Interaktion mit DNA zeigten, wurden die neuen Verbindungen mit Hilfe einiger Kooperationspartner auf ihre Struktur-Wirkungs-Beziehung hin untersucht. Dabei wurde beobachtet, dass die Phosphin-Komplexe, insbesondere die geladenen, eine ungewöhnliche Aggregation von DNA herbeiführen, während die Verbindungen mit DMSO-Liganden eine DNA-Bindung vergleichbar mit Cisplatin eingehen. Die Komplexe **71**-**73** mit sehr unterschiedlich substituierten Benzimidazol-NHC-Liganden, wiesen zudem im Bezug auf Größe und Lipophilie eine klare strukturelle Abhängigkeit ihrer zytotoxischen

Eigenschaften auf, vorwiegend aufgrund der durch die Substituenten stark beeinflusste Zellaufnahme der Verbindungen.

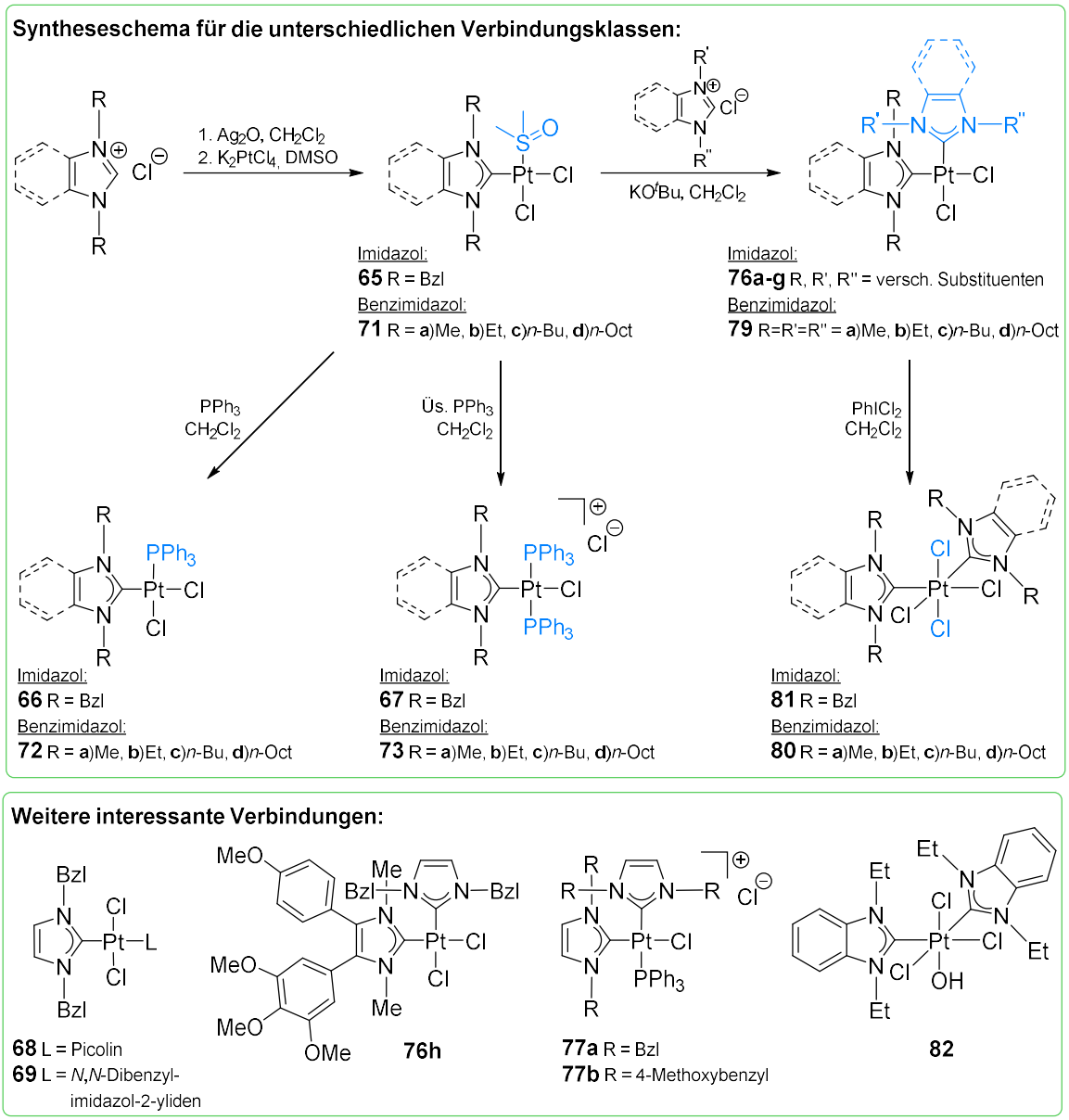

Abbildung 1: Oben: Zusammenfassendes Schema zur Synthese der unterschiedlichen Verbindungsklassen dieser Arbeit. Unten: Weitere wichtige synthetisierte Verbindungen, unter anderem die postulierte Struktur von Pt^{IV}-Hydroxo-Komplex **82**.

Ein solch starker Einfluss der Substituenten auf die Wirksamkeit der Komplexe weckte das Interesse, die DMSO- bzw. Phosphin-Liganden durch einen besser justierbaren, zweiten NHC zu ersetzen, mit dem die physikochemischen Eigenschaften noch präziser angepasst werden könnten. Zum Ausganspunkt dieser Arbeit waren allerdings nur symmetrische *cis*-$[Pt^{II}Cl_2(NHC)_2]$-Komplexe bekannt, woraufhin für die Synthese von neuartigen unsymmetrischen *cis*-$[Pt^{II}Cl_2(NHC)^1(NHC)^2]$-Komplexen eine eigene Methode entwickelt

werden musste. Durch Generierung eines freien NHC^1 aus einem (Benz-)Imidazoliumsalz mit KO^tBu in trockenem CH_2Cl_2 und anschließender Umsetzung mit einem *cis*-$[Pt^{II}Cl_2(DMSO)(NHC^2)]$-Komplex gelang es, eine Vielzahl unterschiedlichster Kombinationen von NHC-Liganden in *cis*-Positionierung am Platin zu koordinieren. Die Zytotoxizität der zehn erhaltenen Komplexe **76** und **77** war, wie erwartet, stark abhängig von den eingesetzten NHC-Liganden und deren Substituenten. Besonders interessant war dabei die auffallend hohe Selektivität von **76h** – mit einem Combretastatin A-4 (CA-4) abgeleiteten NHC-Liganden – gegenüber einigen ausgewählten Krebszelllinien.

Die Robustheit der neu entwickelten Methode zeigte sich im Weiteren bei der Umsetzung mit stabileren, alkylierten Benzimidazol-Liganden, wobei die sterisch stark unterschiedlich abgeschirmten Komplexe **79** problemlos erhalten wurden. Neben einer Gegenüberstellung mit den analogen Imidazol-Komplexen sollten diese Pt^{II}-Verbindungen auch als Ausgangssubstanzen für Oxidationsversuche dienen. Pt^{IV}-Prodrugs wie die hierbei angestrebten, gelten als prinzipiell weniger toxische und selektivere Hoffnungsträger unter den Platinzytostatika, wurden aber in Verbindung mit NHC-Liganden bislang äußerst selten untersucht. Durch Umsetzung mit Iodbenzoldichlorid ($PhICl_2$) konnten die Pt^{IV}-Komplexe **80** sowie **81** mit sehr guten Ausbeuten erhalten werden. Versuche, *cis,cis,trans*-$[Pt^{IV}Cl_2(NHC)_2(OH)_2]$ bzw. $[Pt^{IV}Cl_3(NHC)_2(OH)]$-Komplexe zu synthetisieren, die zusätzliche Funktionalisierungen an den axialen Hydroxo-Liganden ermöglichen würden, scheiterten an einer intrinsischen Instabilität solcher Komplexe mit den hier eingesetzten Liganden. Allerdings konnte die kurzzeitige Existenz eines Komplexes mit der postulierten Struktur **82** mittels NMR-Spektren nachgewiesen werden. Bei der Untersuchung der zytotoxischen Wirkung war für die Pt^{II}-Verbindungen **79** erneut ein starker Einfluss durch die Substituenten der NHC-Liganden und bei den Pt^{IV}-Komplexen **80** und **81** zudem eine Selektivität gegenüber Krebszellen im Vergleich zu nicht-malignen Fibroblasten zu erkennen. Überdies zeigten einige *cis*- wie auch *trans*-Pt^{IV}-Komplexe sogar niedrigere mikromolare IC_{50}-Werte als deren analoge Pt^{II}-Verbindungen.

SUMMARY

Platinum complexes such as cisplatin have been at the forefront of tumor treatment since the late 1970s, but despite advanced therapies, they still present severe side effects. In the research for new and more tolerable cytostatic drugs, most recently further transition metals have become of interest in the scientific community. One reason for this growing interest are the by now well-researched and, above all, highly variable *N*-heterocyclic carbenes (NHCs) as ligands which allow to synthesize entirely new metallotherapeutics with better adjustable pharmacological properties than ever before. In the present cumulative dissertation, four scientific publications illustrate the synthesis and optimisation of antitumoral platinum complexes with such NHC ligands. Applying NHCs, novel cisplatin-like structure types should be developed, which could offer an alternative to the established platinum cytostatics.

A synthetic approach is given by *cis*-[$Pt^{II}Cl_2$(DMSO)(NHC)] complexes such as **65** and **71** – synthesized from imidazolium or benzimidazolium salts – whose labile *cis*-standing DMSO ligands are exchangeable for other ligands while retaining the stereochemistry of the complex. Thus, phosphines are introduced in *cis*-position to various imidazole and benzimidazole NHC ligands, yielding the neutral complexes **66** and **72** as well as the charged complexes **67** and **73** by applying an excess of PPh_3. In comparison to the two *trans*-complexes **68** and **69** – which show no interaction with DNA – the new compounds were investigated for their structure-activity relationship in cooperation with scientific partners. It was observed that the phosphine complexes, the charged ones in particular, cause an unusual aggregation of DNA, while the compounds with DMSO ligands undergo a DNA binding comparable to that of cisplatin. Complexes **71**-**73** with very different substituted benzimidazole NHC ligands additionally show a clear structural dependence of their cytotoxic properties as they increase in size and lipophilicity. This is probably mainly due to the cellular uptake, which is strongly influenced by the substituents.

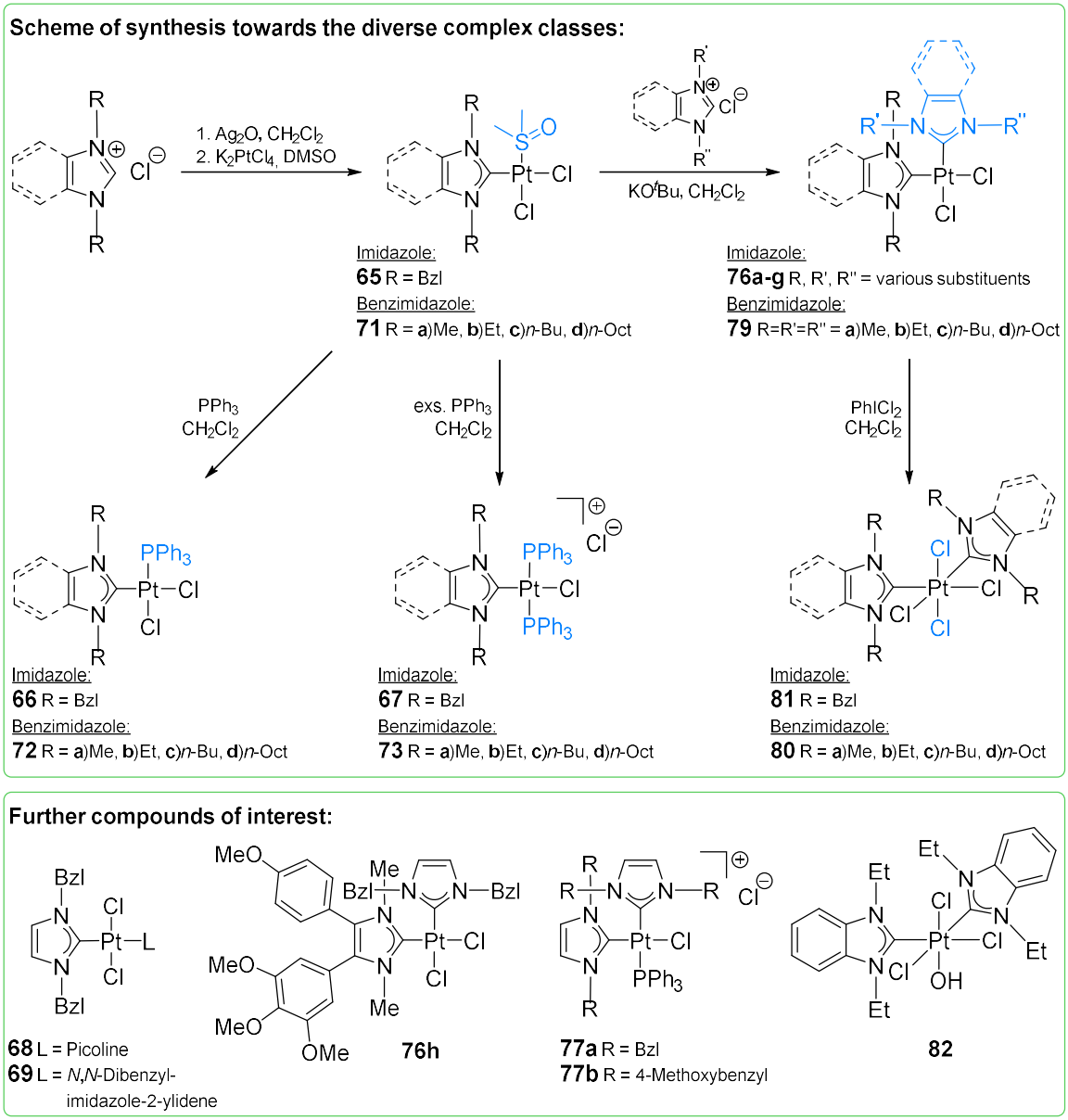

Figure 1: Top: Summarizing scheme of synthesis towards the complex classes obtained in this work. Bottom: Further compounds of interest including the postulated structure of Pt^{IV} hydroxo complex **82**.

Such a strong influence of the substituents on the efficacy of the complexes has awakened the desire to replace the DMSO or phosphine ligands by a more adjustable second NHC in order to adapt their physicochemical properties more precisely. However, only symmetrical *cis*-[$Pt^{II}Cl_2(NHC)_2$] complexes were known at this point. For this reason, a unique method for the synthesis of novel unsymmetric *cis*-[$Pt^{II}Cl_2(NHC)^1(NHC)^2$] complexes needed to be developed. By generating a free NHC^1 from a (benz)imidazolium salt and KO^{t}Bu in dry CH_2Cl_2 followed by the subsequent reaction with a *cis*-[$Pt^{II}Cl_2(DMSO)(NHC^2)$] complex, a variety of different combinations of NHC ligands in *cis*-coordination at the platinum are obtained. The cytotoxicity of the ten resulting

complexes **76** and **77** is strongly dependent on the coordinated NHC ligands and their substituents, as expected. The strikingly high selectivity on just a few cancer cell lines of **76h** – carrying a combretastatin A-4 derived NHC ligand – is particularly interesting.

Processing more stable alkylated benzimidazole ligands demonstrates the robustness of the newly developed method by delivering the sterically varied complexes **79** without any difficulties. In addition to a comparison with the analogue imidazole complexes, these Pt^{II} compounds should also serve as starting materials for oxidation experiments. The intended Pt^{IV} prodrugs are considered to be less toxic and more selective bearers of hope for platinum cytostatics but have so far rarely been investigated in association with NHC ligands. By reaction with iodobenzene dichloride ($PhICl_2$) the Pt^{IV} complexes **80** and **81** are obtained in high yields. Attempts to synthesize *cis*,*cis*,*trans*-$[Pt^{IV}Cl_2(NHC)_2(OH)_2]$ or $[Pt^{IV}Cl_3(NHC)_2(OH)]$ complexes, which would allow additional functionalization at the axial hydroxo ligands, failed due to an intrinsic instability of such complexes with the ligands used. However, the short-lived existence of a complex with the postulated structure **82** could be detected by NMR spectra. Examination of the cytotoxic effects reveal again a strong influence of the substituents of the NHC ligands for the Pt^{II} compounds and, in the case of the Pt^{IV} complexes also a selectivity towards cancer cells compared to non-malignant fibroblasts. In addition to that, some *cis*- as well as *trans*-Pt^{IV} complexes show even lower micromolar IC_{50} values than their analogous Pt^{II} compounds.

1 EINLEITUNG

1.1 METALLE IN DER MEDIZIN

Die große Mehrheit der heutzutage medizinisch eingesetzten Wirkstoffe sind organische Verbindungen und die pharmazeutische Forschung konzentriert sich zunehmend auf Biopharmazeutika wie Peptide und Antikörper. Dennoch sind Metalle bei vielen medizinischen Anwendungen nicht wegzudenken und besitzen lebenswichtige biologische Funktionen wie das Eisen im Hämoglobin oder Zink in der Alkohol-Dehydrogenase. Zudem verfügen sie über Eigenschaften, die mit organischen Verbindungen nicht nachstellbar sind und eröffnen dadurch gänzlich andere Ansätze zur Entwicklung neuer Medizinprodukte.[1]

Metalle und Metallverbindungen fanden schon in der Antike medizinische Anwendung. Im alten Ägypten wurden, neben einer Vielfalt pflanzlicher Heilmittel, Kupfersulfat zur Sterilisation und Zink für eine beschleunigte Wundheilung eingesetzt, während in Arabien und China Goldzubereitungen zu verschiedenen Zwecken verwendet wurden.[1] Diese teils auf folgerichtigen Beobachtungen, teils auf Mythen begründete Medizin wurde bis in die Renaissance vollzogen. Dabei wurden unter anderem hochgiftiges Quecksilber und Quecksilberchlorid (Kalomel) als Diuretikum, Laxans und zur Bekämpfung der Syphilis-Epidemie eingesetzt.[2] Der wohl bekannteste Mediziner des 15. und 16. Jahrhunderts, Theophrastus Bombast von Hohenheim, bekannt als PARACELSUS, erkannte später jedoch die Toxizität des Quecksilbers und wies auf dessen vorsichtige Dosierung hin. In diesem Zusammenhang entstand sein berühmtes Zitat:

„Alle Dinge sind Gift, und nichts ist ohne Gift; allein die Dosis machts, daß ein Ding kein Gift sei.“ (Paracelsus, 1538)[3]

Nach dem unbedachten Einsatz toxischer Metallverbindungen in der Vergangenheit war die moderne Medizin Metallotherapeutika gegenüber lange Zeit skeptisch eingestellt bis Anfang des 20. Jahrhunderts mit PAUL EHRLICHS Salvarsan (**1**) eine Verbindung des Halbmetalls Arsen den Markt eroberte.[4] Als eines der ersten antimikrobiell wirkenden Medikamente wurde es trotz starker Nebenwirkungen erfolgreich gegen die damals lebensgefährliche und weit verbreitete Syphilis eingesetzt bevor es durch die besser

verträglichen Penicillin-Antibiotika verdrängt wurde.[5] Während der 1930er Jahre begann man, nach Forschungen von FORESTIER, mit der Gabe von Goldsalzen gegen rheumatoide Arthritis.[6] Die Entwicklung dieser Therapien führte über verschiedene injizierbare Gold-Thiolatokomplexe zum heute noch eingesetzten, oral verfügbaren Auranofin (**2**).[1,7]

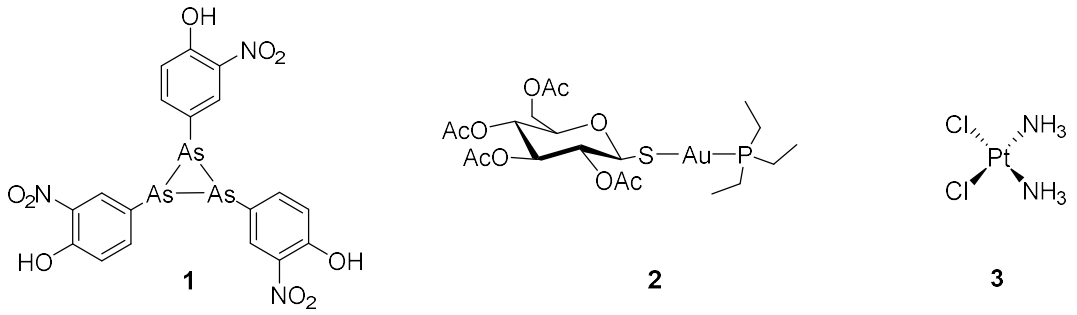

Abbildung 2: Strukturen der historisch bedeutenden, metallhaltigen Wirkstoffe Salvarsan (**1**), Auranofin (**2**) und Cisplatin (**3**).

Zwar betrifft die rheumatoide Arthritis fast 1% der Bevölkerung,[8] die wichtigste Gruppe der Metallodrugs bilden heute aber die platinbasierten Zytostatika. Deren Entdeckung geht auf BARNETT ROSENBERG zurück, der 1964 an der Michigan State University den Einfluss eines elektrischen Feldes auf die Zellteilung von *E. coli* Bakterien untersuchte. Dabei beobachtete er anstelle der Zellteilung ein filamentartiges Wachstum der Bakterien auf das 300- bis 400-fache ihrer ursprünglichen Länge.[9,10] Dies war jedoch nicht auf das elektrische Feld, sondern auf die Platinverbindungen *cis*-$[Pt^{IV}(NH_3)_2Cl_4]$ und *cis*-$[Pt^{II}(NH_3)_2Cl_2]$ (**3**) zurückzuführen, die sich aus der Platinelektrode im Nährmedium gebildet hatten. Diese zellteilungsinhibierende Wirkung konnte anschließend auch in Tierversuchen als antitumorale Aktivität nachgewiesen werden,[11] woraufhin 1974 in einer Studie der erste Krebspatient mit *cis*-$[Pt^{II}(NH_3)_2Cl_2]$ (**3**) behandelt wurde. Dieser schlicht Cisplatin getaufte Komplex wurde dann 1978 von der FDA zur Behandlung von Eierstock- und Hodenkrebs zugelassen und führte zu einem Durchbruch in der Krebstherapie. Wegen teils schwerer Nebenwirkungen wurde weiterhin intensiv am Therapieschema sowie an Nachfolgepräparaten geforscht, sodass Cisplatin (**3**) und seine Derivate, alleine oder in Kombination mit anderen Medikamenten, mittlerweile in vielen Chemotherapien gegen verschiedenste Krebsformen zur Standardtherapie gehören.[10,12]

Neben der Behandlung von Arthritis mit Goldverbindungen und der Krebstherapie mit Platinkomplexen werden Metalle in der Medizin heutzutage auch in vielen anderen

Feldern eingesetzt: Z. B. zur Behandlung von Diabetes (Vanadium), Blutarmut (Eisen), depressiven Erkrankungen (Lithium), Herpes (Zink), Hyperkalzämie (Gallium), Geschwüre (Bismut), Strahlentherapie (Radium) sowie in der Diagnostik (Technetium) und als MRT-Kontrastmittel (Gadolinium).[13]

1.2 PLATINKOMPLEXE IN DER CHEMOTHERAPIE

1.2.1 ENTWICKLUNG VON PLATINKOMPLEXEN MIT ANTITUMORALER WIRKUNG

Die Erfolgsgeschichte der Platinkomplexe in der Chemotherapie begann 1978 mit der Markteinführung von Platinol® (Cisplatin (**3**), Bristol-Myers Squibb) zur Behandlung von Hoden- und Eierstockkrebs. Insbesondere die enorm gesteigerten Heilungsraten bei Hodenkrebs von über 90% führten dazu, dass Cisplatin (**3**) zu einem der am häufigsten angewandten Antitumormittel weltweit wurde. Durch weiterentwickelte Supportivtherapien wird Cisplatin heute zusätzlich in der Therapie von Blasen-, Gebärmutterhals-, Kopf-Hals-, Speiseröhren- und Lungenkrebs eingesetzt, wodurch es in fast 50% aller krebsbezogenen Chemotherapien zu finden ist.[14,15]

Trotz der Behandlungserfolge, die dem ersten Platinzytostatikum zu verdanken sind, haben Patienten noch immer mit schweren Nebenwirkungen zu kämpfen. Neben der dosislimitierenden Nephrotoxizität (Nierenschädigung), die durch Prähydratisierung sowie forcierter Diurese gelindert wird, kann Cisplatin Nervenschädigung, Höhrschädigung und starke Übelkeit mit Erbrechen hervorrufen. Zudem wird die Behandlung häufig durch bereits vorhandene oder während der Therapie erworbene Resistenzen wieder zurückgeworfen.[16-18] Aus diesen Gründen wurde bereits vor dessen Zulassung nach strukturähnlichen Derivaten gesucht, die sowohl die Nebenwirkungen von Cisplatin verringern, sein Wirkspektrum erweitern als auch Resistenzmechanismen überwinden.

Im Laufe der intensiven Forschungen legten CLEARE und HOESCHELE die Leitstruktur für die Suche nach neuen Platinzytostatika als neutralen, quadratisch-planaren Komplex der generellen Formel *cis*-$[Pt^{II}(NH_2R)_2X_2]$ fest. Dabei sollten X_2 zwei *cis*-ständige, semilabile, anionische Abgangsgruppen und $(NH_2R)_2$ zwei inerte neutrale Aminliganden sein.[19,20] Genau diesem Schema entsprechen alle sechs weiteren bis heute behördlich zugelassen

Platin-Wirkstoffe: Carboplatin (**4**, weltweit), Oxaliplatin (**5**, weltweit), Nedaplatin (**6**, Japan), Lobaplatin (**7**, China), Heptaplatin (**8**, Korea) und kürzlich Miriplatin (**9**, Japan).[15,16,20-23]

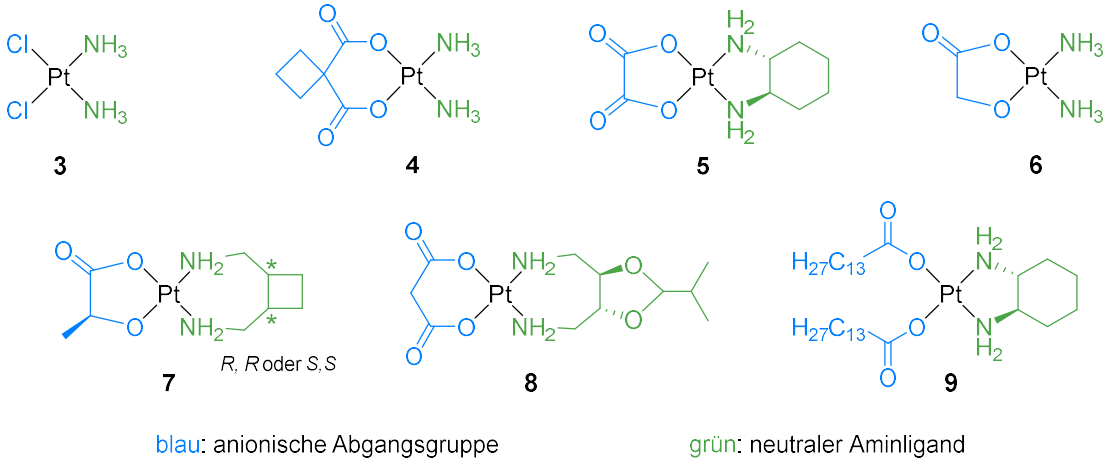

Abbildung 3: Weltweit und lokal zugelassene Platinzytostatika Cisplatin (**3**), Carboplatin (**4**), Oxaliplatin (**5**), Nedaplatin (**6**), Lobaplatin (**7**), Heptaplatin (**8**) und Miriplatin (**9**).

Unter dem Handelsnamen Paraplatin® kam 1986 Carboplatin (**4**) als erste Weiterentwicklung auf den Markt.[24] Die entscheidende Modifizierung an Carboplatin im Vergleich zu Cisplatin (**3**) ist der Austausch der labilen Chlorid-Abgangsgruppen gegen Cyclobutanodicarboxylat, einen stärker bindenden Chelatliganden. Carboplatin wird ebenfalls hauptsächlich zur Behandlung von Ovarial-, Bronchial- und Zervixkarzinomen sowie Kopf-Hals-Tumoren eingesetzt. Eine Myelosuppression stellt die dosislimitierende Nebenwirkung dar.[20,21,24]

Um das Wirkspektrum zu erweitern und Resistenzen zu brechen, wurden in der weiteren Entwicklung die Aminliganden derivatisiert und 1996 Oxaliplatin (**5**) zur klinischen Anwendung zugelassen.[25] Es ist auch in Cisplatin-resistenten Tumorentitäten wie dem kolorektalen Karzinom aktiv, wo es in der Kombinationstherapie FOLFOX zusammen mit 5-Fluoracil und Folinsäure erfolgreich eingesetzt wird.[20,21]

Nedaplatin (**6**) ist bereits seit 1995 in Japan zur Behandlung von Bronchialkarzinomen sowie von Tumoren im Kopf-Nacken-Bereich und der Speiseröhre zugelassen; dabei ähnelt es in Wirkung und Nebenwirkungen dem Carboplatin (**4**). Lobaplatin (**7**) und Heptaplatin (**8**) zeigen mit Cisplatin (**3**) und Carboplatin (**4**) vergleichbare Wirksamkeiten, weshalb sie nur lokal in China bzw. Korea als Chemotherapeutikum gegen Leukämie und Brustkrebs bzw. Magenkarzinome zugelassen sind.[21,22] Miriplatin (**9**) wird seit 2009 in

Japan eingesetzt. Dieser sehr lipophile Platinkomplex wird in iodierten Fettsäuren suspendiert und direkt in die Leberarterie verabreicht, um so eine Anreicherung im Lebergewebe und selektive Behandlung des Leberzellkarzinoms zu erreichen.[23,26]

Diese mittlerweile sieben zugelassenen Komplexe entstammen aus tausenden untersuchten Platinverbindungen, von denen über 30 präklinische und klinische Studien erreichten, einige davon mehrfach in verschiedenen Kombinationstherapien. Zurzeit befinden sich unter anderem Picoplatin (**10**), Lipoplatin™ (**11**), ProLindac™ (**12**) und Satraplatin (**13**) in klinischen Untersuchungen.[22,27] Während die drei erstgenannten wiederum Pt^{II}-Spezies beinhalten, handelt es sich bei Satraplatin (**13**) um einen Pt^{IV}-Komplex. In dieser Oxidationsstufe verspricht man sich stabile, nicht-toxische Prodrugs, die gegen Ligandensubstitution abgeschirmt sind und erst durch Reduktion in der hypoxischen Krebszelle den eigentlichen Pt^{II}-Wirkstoff freisetzen. Zudem eröffnen die zwei zusätzlichen axialen Liganden die Möglichkeit, die pharmakologischen Eigenschafften weiter zu optimieren.[28] Im Falle des Satraplatin (**13**) konnte so das erste oral verfügbare Platinpräparat synthetisiert werden, wodurch es besonderes Interesse erregt hat.[29]

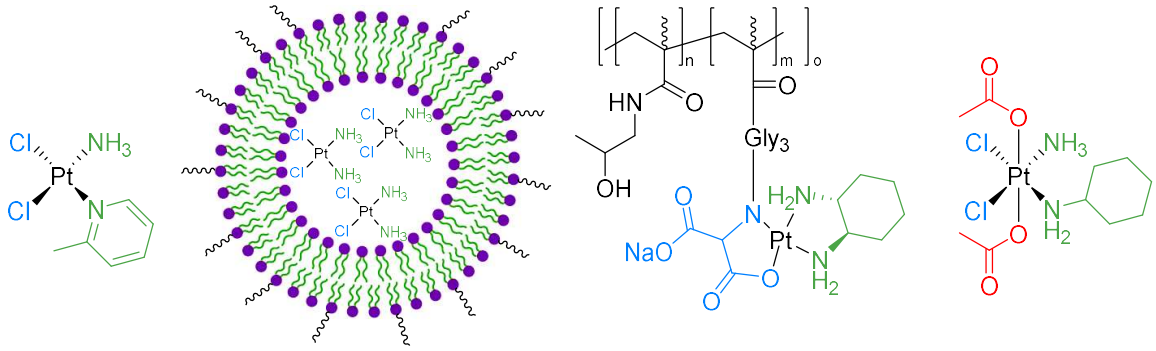

Abbildung 4: Strukturen bzw. Teilstrukturen von Picoplatin (**10**), Lipoplatin™ (**11**), ProLindac™ (**12**) und des Pt^{IV}-Prodrug Satraplatin (**13**).

1.2.2 PHARMAKOKINETIK UND WIRKMECHANISMUS ERFOLGREICHER PLATINVERBINDUNGEN

Platinkomplexe werden in ihrer Gesamtheit mittlerweile bei nahezu allen Krebsentitäten erfolgreich eingesetzt.[14,30] Diese vielfältige Einsatzfähigkeit erlangen die wenigen Platinzytostatika durch ihr unterschiedliches Ligandenumfeld und durch Kombination mit anderen Wirkstoffen und Behandlungsmethoden. Dennoch bleibt der Wirkmechanismus bei allen Platinkomplexen im Wesentlichen gleich. Sie binden an die DNA der Krebszelle

und verändern dessen Struktur in einem Maße, welches zur Apoptose und damit zum Zelltod führt. Leider geht dieser Wirkmechanismus mit schweren Nebenwirkungen einher, die auf der fehlenden Selektivität der Platinkomplexe beruhen.[30]

Die pharmakologischen Prozesse sind für Cisplatin (**3**) am besten untersucht, weshalb dieses im Folgenden exemplarisch im Detail besprochen werden soll. Cisplatin (**3**) wird wie sämtliche zugelassenen Platinkomplexe als Infusion i.v. appliziert, wobei es in chloridhaltiger Lösung eingesetzt wird. Aufgrund der hohen Chloridkonzentration im Blut wird es zunächst nicht hydrolysiert, bindet aber bereits zu großen Teilen an Serumproteine (z. B. Albumin) und wird rasch über die Nieren eliminiert.[16,31] Die dadurch stark erhöhte Konzentration an Cisplatin in diesem Organ macht die Nephrotoxizität zur dosislimitierenden Nebenwirkung. Eine Anreicherung ist zudem auch in anderen Organen wie der Leber, Milz, Prostata, Blase, Hoden und Pankreas, aber auch in Tumorgewebe nachweisbar.

Cisplatin wird hauptsächlich durch passive Diffusion, aber auch aktiv durch den Kupfertransporter CTR1 in Zellen aufgenommen.[17] Der Platinkomplex wird fast ausschließlich wegen des erhöhten Nährstoffbedarfs der sich schnell teilenden Krebszellen verstärkt in diese aufgenommen. In der Zelle wird Cisplatin (**3**) im Zytoplasma, bei deutlich geringerer Chlorid-Konzentration, zu den reaktiven Aqua-Komplexen **14** und **15** hydrolysiert, die stark elektrophil sind und somit nun an die negativ geladene DNA binden können. Vor allem über Koordination der *N*-7 Positionen der Purin-Basen werden verschiedene DNA-Addukte gebildet.

Um Apoptose auszulösen reichen allerdings nicht alle Verknüpfungen von Cisplatin mit der DNA aus. Besonders stark wird diese durch Quervernetzung zweier benachbarter Basen desselben DNA-Strangs deformiert, im Falle des Cisplatins vornehmlich über zwei Guanin-Basen zu 1,2-intrastrang-d(GpG)-Quervernetzungen (60% - 65%).[32] Dadurch wird die DNA-Helix bis zu 23° entwunden und um 30° bis 60° geknickt.[33] Eine solche Entartung behindert die Transkription und Replikation der Nukleinsäuren, wodurch die Zelle in einen Zellzyklusarrest eintritt und unter anderem über die Phosphorylierung des Tumor-Suppressor-Proteins p53 die Apoptosekaskade ausgelöst wird. Zudem werden einige weitere Mechanismen diskutiert.[18,30]

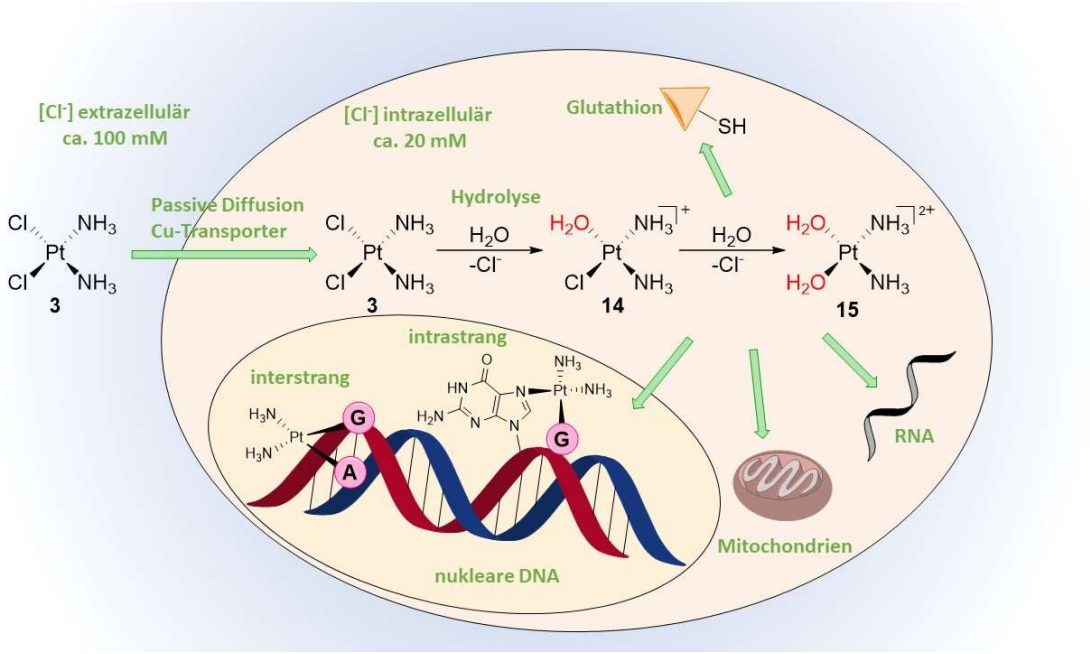

Abbildung 5: Aufnahme und Hydrolyse von Cisplatin (**3**) sowie Reaktionsmöglichkeiten der reaktiven Aqua-Komplexe **14** und **15** innerhalb einer Zelle mit z. B. Glutathion, RNA, mitochondrialer DNA sowie exemplarische intra- und interstrang Platinierungen an den Nukleinsäuren Guanin und Adenin der DNA im Zellkern.

Platinierungsreaktionen finden nicht nur im Zellkern statt, sondern betreffen auch die mitochondriale DNA sowie die im Zytosol befindliche RNA. Über den Beitrag dieser Platinierungen zur Zytotoxizität wird ebenfalls diskutiert.[18,34] Allerdings reagieren auch schwefelhaltige Proteine und Peptide wie das Glutathion sehr schnell mit diesen stark elektrophilen Aqua-Platinspezies **14** und **15**, was zu deren Desaktivierung führt.[18,35,36]

Wird das Ablesen der Erbgutinformationen gestört, so behilft sich die Zelle mit verschiedenen DNA-Reparaturmechanismen, welche die Apoptose jedoch nur bis zu einem bestimmten Platinierungsgrad verhindern können. Cisplatin-Resistenz geht daher zwar meist mit einer verstärkten DNA-Reparatur einher, kann aber auch durch verringerte Wirkstoffaufnahme bzw. verstärktem Ausstoß, erhöhter Glutathion-Konzentration oder Unterdrückung der Apoptose-Kaskade erworben werden.[12,18,30]

Um die Ausbildung von Resistenzen zu verhindern und bereits existierende zu brechen, wurden strukturell anspruchsvollere Platinverbindungen sowie Kombinationstherapien entwickelt. Durch den Austausch der Chlorido-Liganden gegen chelatisierende Abgangsgruppen wird sowohl die Hydrolysegeschwindigkeit als auch die Plasmaeiweißbindung der Platinkomplexe Carboplatin (**4**) und Nedaplatin (**6**) und damit

deren Toxizität herabgesetzt, während deren Aktivität erhalten bleibt. In Kombination mit einer erhöhten Wasserlöslichkeit lassen sich somit höhere Dosen als bei Cisplatin (**3**) verabreichen. Nach der Hydrolyse der Komplexe in der Zelle werden jedoch dieselben DNA-Addukte wie beim Cisplatin (**3**) ausgebildet, wodurch eine hohe Kreuzresistenz zwischen den drei Zytostatika besteht.[22,37]

Ein Austausch der Neutralliganden gegen sterisch anspruchsvolle Diamine kann diese Kreuzresistenzen brechen. Bei Oxaliplatin (**5**) mit dem (1*R*,2*R*)-Cyclohexyldiamin-Liganden verändern sich im Vergleich zu **3**, **4** und **6** die DNA-Addukte. Der Ligand verhindert die Anlagerung der Reparaturproteine, wodurch die Verbindung auch gegen Cisplatin-resistente Dickdarmkarzinome im FOLFOX-Therapieschema eingesetzt werden kann. Durch den Einsatz des Diaminoliganden bilden sich die Platin-DNA-Addukte zudem schneller aus und sind für die betroffene Zelle toxischer als die des Cisplatin. Auch wird **5** eine zusätzliche Toxizität durch ribosomalen Stress zugeschrieben.[38] Lobaplatin (**7**) hingegen weist keine Kreuzresistenz in Leukämiezellen auf und wird in China bei Leukämie, als auch Brust- und Lungenkrebs angewendet.[22,36]

Trotz aller Verbesserungen hinsichtlich Nebenwirkungen und Resistenzen, welche die Weiterentwicklung der Platinzytostatika mit sich brachte, besitzen **3**-**9** noch immer teils gravierende Toxizität, die deren Einsatz begrenzt. Weitere Einschränkungen sind die mangelnde Löslichkeit und Stabilität dieser Komplexe in biologischem Medium. Um die pharmakologischen Eigenschaften weiter optimieren zu können, entfernt man sich mittlerweile mehr und mehr von der Leitstruktur *cis*-$[Pt^{II}(NH_2R)_2X_2]$, die CLEARE und HOESCHELE 1973 für Platinzytostatika vorschlugen.[19] Neue Liganden wie z.B. NHCs und die Oxidationsstufe IV – wie bei Satraplatin mit zusätzlichen axialen Verlustliganden – werden heute aufgrund ihrer höheren Strukturvielfalt bevorzugt erforscht.

1.2.3 SYNTHESESTRATEGIEN ZU VERSCHIEDENEN PLATINKOMPLEXEN

Sämtliche zugelassenen Platin-Wirkstoffe lassen sich ausgehend von den Salzen des Tetrachloroplatinats synthetisieren, welche in nur zwei Schritten aus elementarem Platin zugänglich sind.[39] Cisplatin (**3**) wurde zunächst aus K_2PtCl_4 und Ammoniak in NH_4Cl-Lösung hergestellt. Aufgrund des *trans*-Effekts von Chlor entsteht dabei überwiegend das gewünschte *cis*-Isomer, jedoch ist dieser nicht stark genug, um die Bildung von

trans-[Pt(NH$_3$)$_2$Cl$_2$], sowie Magnus‘ grünes Salz ([Pt(NH$_3$)$_4$] · [PtCl$_4$]) als Nebenprodukte zu verhindern, die aufwendig abgetrennt werden müssen.[40] Daher geht die wohl am häufigsten genutzte Route nach DHARA *et al.*[41] über eine Tetraiodoplatinat-Zwischenstufe, womit man sich den deutlich stärkeren *trans*-Effekt des Iods zu Nutze macht. Beim Versetzen mit Ammoniak wird einer der Iodo-Liganden gegen ein erstes NH$_3$ ausgetauscht. Dieses Intermediat dirigiert nun den zweiten Ammin-Liganden zuverlässig in *cis*-Position. Das gebildete *cis*-Diammindiiodidoplatin(II) wird anschließend mit Silbernitrat behandelt und der entstandene Diaquakomplex mit einem Überschuss Kaliumchlorid in reines Cisplatin (**3**) überführt. Zuletzt wurde auch von einer Mikrowellenreaktion berichtet, mittels derer direkt aus K$_2$PtCl$_4$ (**16**) und Ammoniumacetat reines Cisplatin (**3**) gewonnen werden kann.[42]

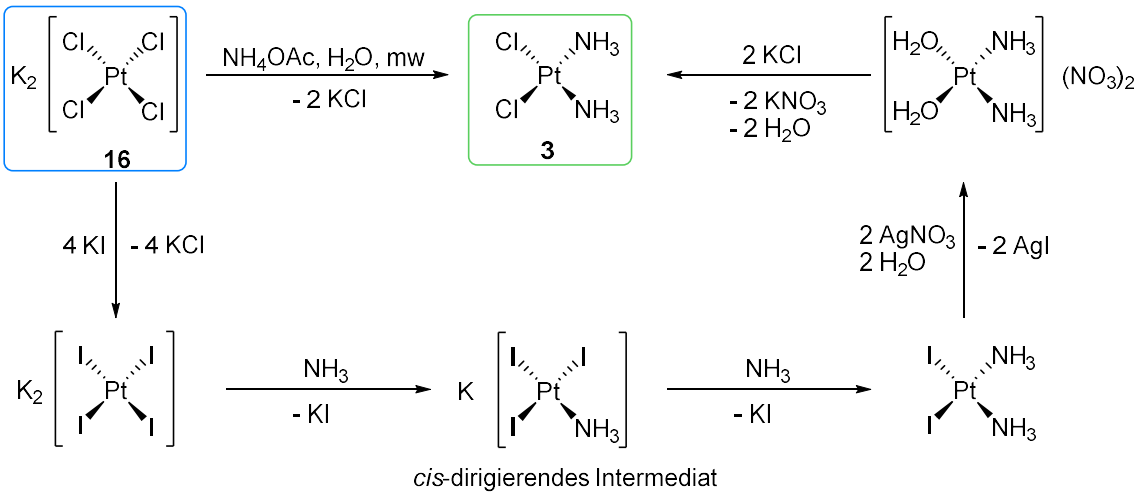

Schema 1: Synthesemethoden von Cisplatin (**3**) ausgehend von K$_2$PtCl$_4$ (**16**) über die Route nach DHARA *et al.*[41] oder direkt mittels Mikrowellenreaktion.

Die Synthese von Komplexen mit einem chelatisierenden Diamino-Liganden – wie es bei Oxaliplatin (**5**), Lobaplatin (**7**), Heptaplatin (**8**) und Miriplatin (**9**) der Fall ist – gestaltet sich insgesamt einfacher. Da die Ausbildung eines *trans*-Komplexes, je nach Diamin, sterisch sehr ungünstig bis unmöglich ist, kann hier K$_2$PtCl$_4$ (**16**) direkt umgesetzt werden und ein Umweg über einen Tetraiodo-Komplex ist nicht nötig. Um die entstandenen Chelatkomplexe **17** im Anschluss noch mit zweizähnigen Dicarboxylato- oder α-Hydroxycarboxylato-Liganden versehen zu können, müssen die Chloro-Liganden durch die entsprechende Dicarbonsäure/α-Hydroxycarbonsäure ausgetauscht werden. Im Falle von Dicarbonsäuren werden dazu meist deren Silbersalze eingesetzt, wodurch die Chloro-

Liganden als Silberchlorid aus der Reaktion ausgefällt werden und Komplextyp **18** entsteht.[25] Auch Carboplatin (**4**) ist auf diese Weise direkt aus Cisplatin (**3**) synthetisierbar.

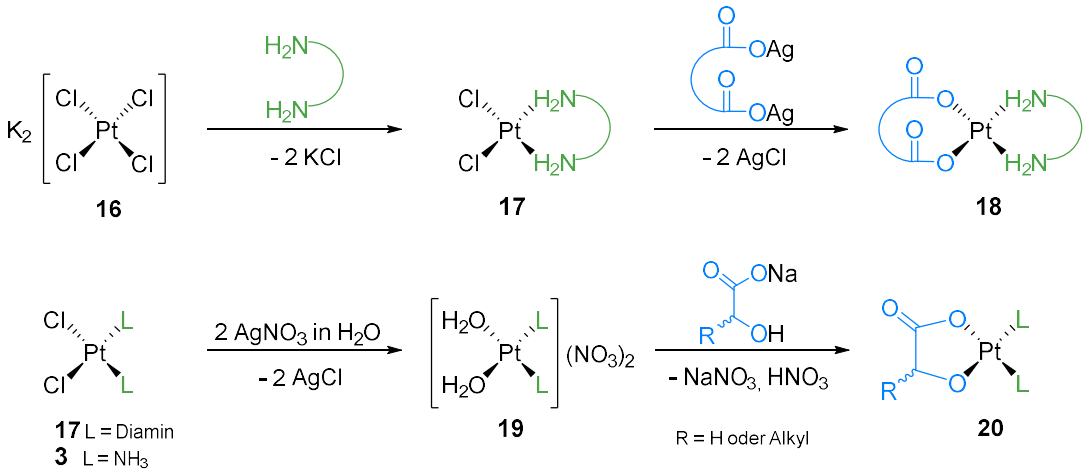

Schema 2: Synthesestrategien für die gängigen Platinzytostatika mit Diamin- und/oder Carboxylat-Liganden.

Eine universellere Methode, mit der verschiedenste Nukleophile als Liganden am Platin eingebracht werden können, ist die Fällung der Chloridionen mittels Silbernitrat in Wasser und der damit einhergehenden Bildung eines substitutionslabilen Diaquakomplexes **19**. Dieser kann anschließend im leicht Sauren mit verschiedenen anionischen Nukleophilen zu *cis*-[PtL_2Nu_2]-Komplexen oder mit α-Hydroxycarbonsäuren zu den entsprechenden Chelatkomplexen **20** wie z. B. auch Neda- (**6**) und Lobaplatin (**7**) abreagieren.[43,44]

Nach erfolgreicher Synthese eines Pt^{II}-Wirkstoffs erfolgt in der heutigen Entwicklung von neuen Platinzytostatika häufig noch eine Oxidation zu einem entsprechenden Pt^{IV}-Prodrug. Die zusätzlichen axialen Liganden mögen dabei lediglich zur Maskierung des aktiven Pt^{II}-Komplexes dienen, können aber auch aufwendigere Strukturen tragen, welche die Pharmakologie verbessern und das Wirkspektrum erweitern. Daher existieren mittlerweile einige Methoden, um Cisplatin-Analoga **21** zu Pt^{IV}-Komplexen mit verschiedenen axialen Liganden zu oxidieren.[44]

Als häufigstes Oxidationsmittel wird Wasserstoffperoxid verwendet, was in Wasser zur oxidativen Addition zweier axialer Hydroxo-Liganden wie bei **22** führt. Wird als Lösungsmittel jedoch ein Alkohol verwendet, so erhält man einen gemischten Pt^{IV}-Komplex **23** mit einem Hydroxo- und einem Alkoxo-Liganden.[45] Während dieselbe Reaktion in Carbonsäuren unerwünschte *cis*-Dicarboxylato-Pt^{IV}-Komplexe generiert, erhält man mit Carbonsäureanhydriden hingegen zuverlässig *trans*-Komplexe wie **24**.[46]

Eine alternative Methode, um sowohl einen Hydroxo- als auch einen Carboxylato-Liganden *trans*-ständig einzuführen, bietet das organische Peroxid ^{t}BuOOH, das in Gegenwart von Essigsäure und DMF in CH_2Cl_2 zur Bildung von Komplex **25** führt.[47,48]

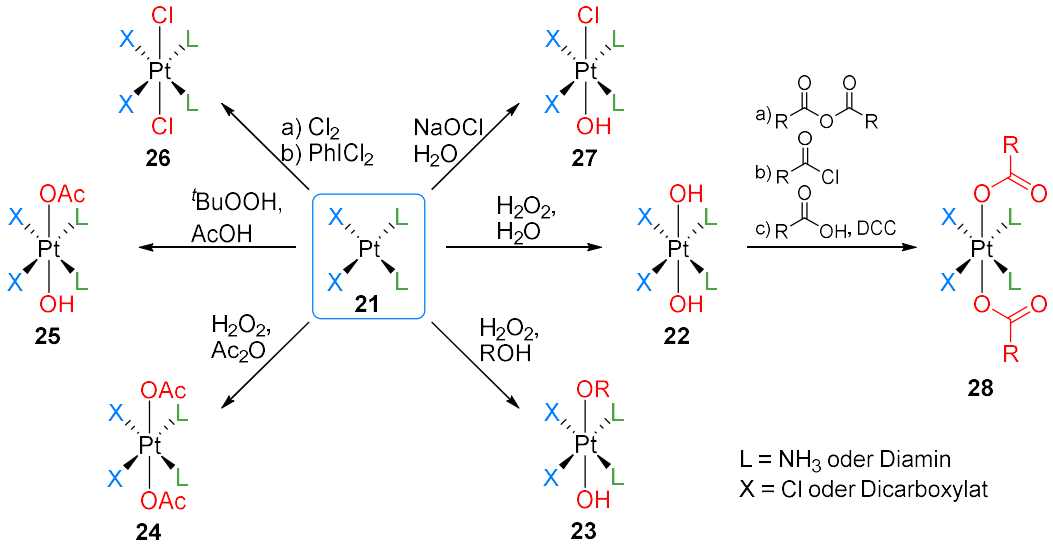

Schema 3: Synthesemethoden von Pt^{IV}-Verbindungen durch Oxidation von Pt^{II}-Komplexen und anschließender Derivatisierung.

Ebenfalls beliebt ist die Oxidation mit Halogenen wie Chlor, Brom und Iod.[49] Zur Synthese einer Pt^{IV}-Verbindung wie **26** wird der entsprechende Pt^{II}-Komplex in Lösung mit Chlorgas versetzt. Alternativ kann dazu auch das einfacher zu handhabende und in organischen Lösungsmitteln lösliche Iodbenzoldichlorid ($PhICl_2$) verwendet werden.[50-52] Auch lassen sich mit Hilfe von Natriumhypochlorit die gemischten Komplexe **27** herstellen, welche neben einem Chloro- auch einen Hydroxo-Liganden besitzen.[53]

Solche Pt^{IV}-Verbindungen mit axialen Hydroxo-Liganden eignen sich hervorragend für eine weitere Derivatisierung, um verschiedene Nukleophile an den Wirkstoff zu binden. Mittels Reaktion mit entsprechenden Carbonsäuren, bzw. deren Anhydriden oder Säurechloriden lassen sich Pt^{IV}-Carboxylate, Carbonate und Carbamate vom Typ **28** synthetisieren.[44,48,54]

1.3 Aktuelle Forschung nach antitumoralen Metallkomplexen

1.3.1 Platinkomplexe

Bei der aktuellen Forschung nach neuen Platinzytostatika wird in den meisten Fällen versucht, die klassischen platinbasierten Wirkstoffe durch zusätzliche Funktionalisierungen zu derivatisieren. Dadurch sollen Komplexe erhalten werden, die

bislang unempfängliche Tumorentitäten erreichen, sich noch gezielter in Tumorgewebe anreichern und/oder deren Nebenwirkungen verringern. Eine Möglichkeit dies zu erlangen, ist die Kopplung eines Platinkomplexes mit einem Substrat für spezifisch in Krebszellen überexprimierte Rezeptoren und Transporter.[55,56]

Die stark erhöhte Proliferationsrate von Krebszellen führt zu einem deutlich höheren Energie- und damit einhergehenden Glucosebedarf gegenüber gesunden Zellen, was eine Überexpression von Glucosetransportern auf der Zellmembran zur Folge hat. Durch Bindung verschiedener Kohlenhydrate an die Liganden klassischer Platinkomplexe, wie im Beispiel **29**, werden diese verstärkt von Krebszellen aufgenommen.[57,58] Etwas spezifischer als mit Glucose können hormonabhängige Krebsentitäten über ihre Steroidrezeptoren anvisiert werden. So findet man z. B. insbesondere auf den geschlechtsspezifischen Brust- und Prostatakarzinomen viele Estrogen- bzw. Androgenrezeptoren, die ein beliebter Angriffspunkt für gezielte Therapien sind. Durch die Kopplung entsprechender Rezeptoragonisten bzw. -antagonisten wirken Platinverbindungen wie **30** nicht nur selektiver, sondern haben auch das Potential, wichtige Signalkaskaden auszulösen oder zu unterbinden.[59] Neben Sacchariden und Steroiden können auch komplexere Peptide eingesetzt werden, um an tumorspezifische Rezeptoren zu binden. Dabei ist vor allem die NGR-Sequenz (Asn-Gly-Arg) zu erwähnen, die an das Oberflächenprotein CD13 bindet. Dieses wird hauptsächlich in Endothelzellen während der Angiogenese und in Tumor-Blutgefäßen exprimiert. Somit können über einen Linker an das zyklische CNGRC-Peptid gebundene Platinkomplexe selektiv und effektiv in Tumorzellen dirigiert werden.[60]

Ursprünglich nur dazu entwickelt, die Toxizität der klassischen Pt^{II}-Komplexe zu verringern, haben Pt^{IV}-Prodrugs in den letzten Jahren weitere positive Eigenschaften gezeigt. Die erste Generation dieser Prodrugs, wie das bereits erwähnte Satraplatin (**13**), besitzen neben der bewährten Leitstruktur *cis*-$[Pt^{II}(NH_2R)_2X_2]$ zwei zusätzliche axiale Liganden ohne bestimmte Funktion. Die somit erhaltenen Pt^{IV}-Prodrugs sind dank ihrer oktaedrischen Koordinationssphäre deutlich inerter und weniger anfällig gegen Ligandenaustausch als die entsprechenden quadratisch-planaren Pt^{II}-Komplexe. Deshalb werden Pt^{IV}-Prodrugs generell als deutlich weniger toxisch eingestuft, da unerwünschte Nebenreaktionen mit Biomolekülen reduziert werden. Dank einer damit einhergehend geringeren Wirkstoffeliminierung, sollte zudem die Bioverfügbarkeit erhöht sein. Beides

hängt jedoch stark von der Art und insbesondere dem Reduktionspotential der axialen Liganden ab.

Um ihr zytotoxisches Potential zu entfalten, muss die reaktivere Pt^{II}-Spezies – bislang meist Cisplatin (**3**) – durch reduktive Eliminierung der axialen Liganden freigesetzt werden.[63] Der Wirkmechanismus der freigesetzten Verbindung unterscheidet sich anschließend nicht weiter von dem der etablierten Platinkomplexe wie **3**. Da Krebszellen durch ihren erhöhten Energieverbrauch aber ein reduktiveres Milieu als gesundes Gewebe besitzen, sollten Pt^{IV}-Prodrugs im Tumorgewebe verstärkt reduziert werden.[28,56,64]

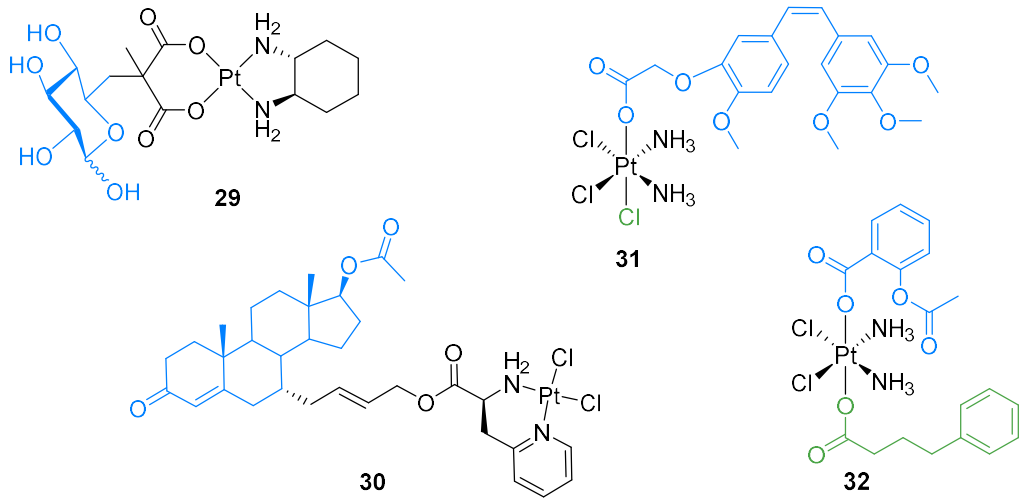

Abbildung 6: Drug-Targeting Pt^{II}-Komplexe mit Glucose-[57,58] bzw. Testosteron-Derivaten[59] (**29** bzw. **30**), sowie pleiotrope *Dual-* bzw. *Tripple-Threat*-Pt^{IV}-Komplexe **31** mit Combretastatin A-4 (Tubulinbinder)[61] bzw. **32** mit Acetylsalicylsäure (COX-Inhibitor) und 4-Phenylbuttersäure (HDAC-Inhibitor)[62] an Cisplatin.

Die Weiterentwicklungen der Pt^{IV}-Komplexe konzentrierten sich in der jüngsten Vergangenheit größtenteils auf die Funktionalität der axialen Liganden. Neben einer oralen Verfügbarkeit der stabilen Verbindungen lassen sich auch weitere pharmakologische Faktoren über die zusätzlichen Liganden justieren. Eine Variation der axialen Position hat direkten Einfluss auf die Lipophilie und Redox-Stabilität der Komplexe. Zudem können komplementäre Wirkstoffe an das Metallzentrum gebunden werden, wodurch pleiotrope Komplexe erhalten werden, die bei Reduktion in der Zelle gleich mehrere aktive Substanzen freisetzen. Die Beispiele **31** und **32** besitzen als Verlustliganden ein Combretastatin A-4 Derivat, beziehungsweise Acetylsalicylsäure und 4-Phenylbuttersäure, die als Tubulinbinder, COX-Inhibitor, respektive HDAC-Inhibitor bekannt sind.[61,62] In solchen Fällen spricht man von *Dual-*, *Triple-* oder mittlerweile gar

Quadruple-Action Pt^{IV}-Prodrugs.[65] Die schon für Pt^{II}-Komplexe erwähnten Methoden zur gezielten Krebstherapie mittels spezifischer Rezeptoren und Transporter (*Drug-Targeting*) lassen sich ebenfalls hervorragend mit den axialen Liganden der Pt^{IV}-Prodrugs umsetzen, um nun direkt die bewährten Platinzytostatika wie **3**-**9** in die Krebszelle zu dirigieren.[66]

1.3.2 KOMPLEXE ANDERER METALLE

Angetrieben vom Erfolg der Platinzytostatika wurden auch Komplexe anderer Metalle auf ihre antitumorale Wirkung untersucht. Dabei stehen mittlerweile Verbindungen von Eisen, Titan, Kupfer aber vor allem Ruthenium und Gold im besonderen Interesse, die ihr Potential bereits unter Beweis stellen konnten.

Mit NAMI-A (**33**) und KP1339 (**34**) stellen zwei geladene, oktaedrische Ru^{III}-Verbindungen mit Imidazol- bzw. Indazol-Liganden die wohl bekanntesten Vertreter dar. Beide Komplexe haben trotz der starken strukturellen Ähnlichkeit unterschiedliche Wirkweisen und wurden bereits in klinischen Studien der Phase I und II untersucht. Während NAMI-A (**33**) keine nennenswerte Zytotoxizität aufweist, wirkt es über antiangiogene Effekte und die Inhibierung von Metalloproteasen antimetastatisch. KP1339 (**34**) hingegen wirkt auch auf den Primärtumor und erzeugt dort reaktive Sauerstoffspezies (ROS), wodurch über die mitochondriale Caspase-Signalkaskade Apoptose induziert wird.[67,68]

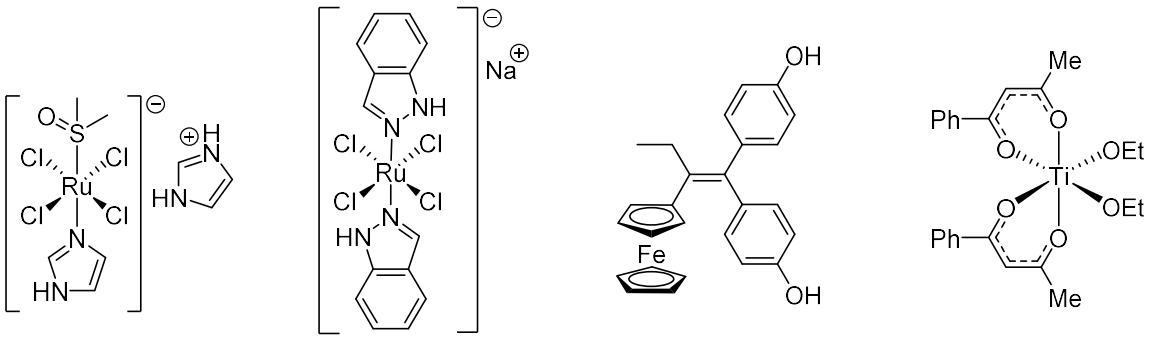

33 **34** **35** **36**

Abbildung 7: Ruthenium-, Eisen- und Titankomplexe mit antitumoraler Wirkung. NAMI-A (**33**), KP1339 (**34**), Ferrocifenol (**35**) und Budotitan (**36**).[68,73,74]

Schon kurze Zeit nach der Zulassung von Cisplatin wurde auch das bereits gegen rheumatoide Arthritis eingesetzte Auranofin (**2**) an Krebszellen getestet.[69] Der Gold(I)-Komplex zeigte *in vitro* eine zytotoxische Wirkung, woraufhin weitere Goldverbindungen synthetisiert und untersucht wurden. Über die Jahre wurde bekannt, dass insbesondere Gold-Phosphin-Komplexe antitumorale Effekte zeigen und meist eine Wechselwirkung

mit dem Selenoenzym Thioredoxin Reduktase (TrxR) für die Zytotoxizität verantwortlich zu sein scheint.[70,71] Allerdings sind auch andere Wirkmechanismen für Goldkomplexe bekannt, wie beispielsweise eine DNA-Bindung von Cisplatin-Mimics basierend auf Gold(III).[72,73]

Eisen, das im menschlichen Körper in großen Mengen vorkommt und daher potentiell verträglicher als nichtessentielle Metalle ist, zeigt vor allem in Form von Ferroceniumsalzen eine antiproliferative Wirkung. Durch den Austausch eines Benzols gegen Ferrocen an Tamoxifen, einem selektiven Östrogenrezeptor-Modulator, wurde die Klasse der Ferrocifene begründet, die großes Potential gegen hormonabhängigen Brustkrebs zeigt.[74] Der wohl bekannteste Vertreter ist das Ferrocifenol (**35**). Ebenfalls vielversprechend zeigen sich Nukleoside mit Ferrocen oder Eisencarbonyl Funktionalisierung.[75] Ein weiterer Metallocenkomplex mit zytotoxischer Wirkung ist das Titanocendichlorid, das wie der Ti^{IV}-Komplex Budotitan (**36**) bereits in klinischen Studien eingesetzt wurde. Das Potential von Titanverbindungen in der Chemotherapie wird jedoch durch eine schlechte Wasserlöslichkeit und Instabilität gegenüber Hydrolyse beeinträchtigt.[72,73] Als essentielles Element für viele Zellfunktionen wurde auch Kupfer in verschiedensten Komplexformen getestet. Ebenso vielfältig wie die Strukturmotive sind die Wirkmechanismen dieser Komplexe, die meist im Zusammenhang mit der Redoxaktivität des Metalls stehen.[73,76]

1.4 *N*-HETEROZYKLISCHE CARBENE UND IHRE KOMPLEXVERBINDUNGEN

1.4.1 EIGENSCHAFTEN UND VERWENDUNG VON NHCS

Allgemein als Carben bezeichnet werden neutrale Verbindungen des zweiwertigen Kohlenstoffs mit sechs Valenzelektronen. Diese reaktiven Elektronenmangel-verbindungen können in zwei quantenmechanischen Grundzuständen auftreten. Im Triplettzustand befinden sich die beiden ungebundenen Elektronen mit parallelem Spin in zwei p-Orbitalen eines sp-hybridisierten Kohlenstoffs, während sie bei Singulett-Carbenen gepaart in einem sp^2-Hybridorbital vorliegen und ein unbesetztes p-Orbital zurückbleibt.[77,78]

Eine besondere Form bilden die *N*-heterozyklischen Carbene (NHC), bei denen ein *N*-Heterozyklus den Singulettzustand und damit das gesamte Carben stabilisiert. Durch den benachbarten elektrophileren Stickstoff wird Elektronendichte vom freien Elektronenpaar am Carben abgezogen. Das unbesetzte p-Orbital wird gleichzeitig durch π-Orbitalinteraktion mit den freien Elektronenpaaren der Heteroatome teilweise gefüllt (Push-Pull-Effekt). Zudem zwängt die Ringstruktur des Heterozyklus den Carbenkohlenstoff in eine gewinkelte Orbitalanordnung, was den sp^2-Singulettzustand begünstigt. Durch die mesomeren Effekte kommt es bei Imidazol-2-yliden zudem zur Ausbildung eines vier-Elektronen-drei-Zentren-π-Systems, wodurch die *N*-*C*-Bindungen einen teilweisen Doppelbindungs- und der Heterozyklus einen aromatischen Charakter aufweisen.[77-79]

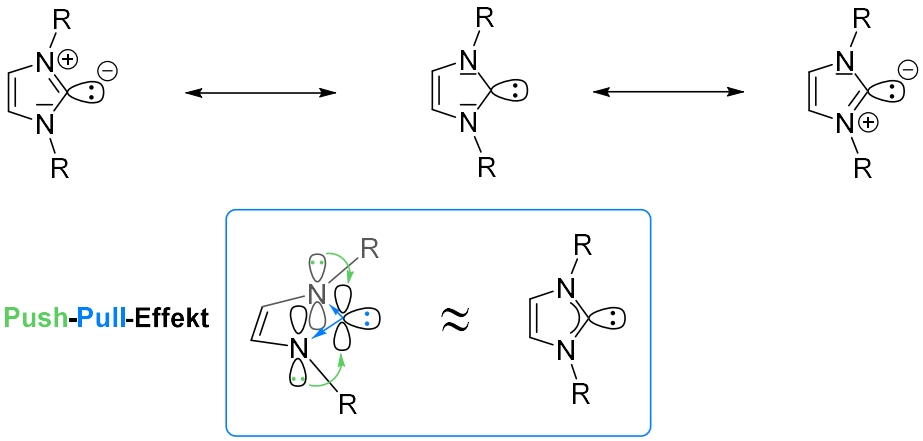

Abbildung 8: Grenzstrukturen von NHCs am Beispiel von Imidazol-2-ylidenen.

Im Gegensatz zu anderen Carbenen sind NHCs, insbesondere Imidazol-2-ylidene, als Liganden nahezu reine σ-Donoren während eine π-Rückbindung vom Metall durch die Mesomerie zwischen Heteroatomen und Carben-p-Orbital eine geringere Rolle spielt.[80,81] Zudem einen hohen Transeffekt besitzend, ähneln sie den Phosphin-Liganden, wobei die meisten NHCs die besseren Donoren sind.[82] Im Vergleich sind NHC-Metallkomplexe meist stabiler gegenüber Hitze, Luft und Feuchtigkeit als Phosphinkomplexe, außerdem lassen sich sterische und elektronische Eigenschaften der NHCs unabhängiger modifizieren. Ihre Stabilität, einfache Synthese und die damit einhergehende Variabilität machen die NHCs zu hervorragend anpassbaren Liganden, die dank ihrer σ-Donorstärke Komplexe mit nahezu allen Metallen ausbilden können.[83]

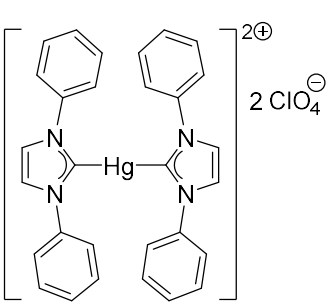

37

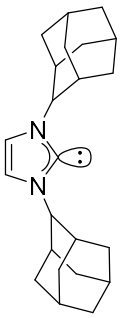

38

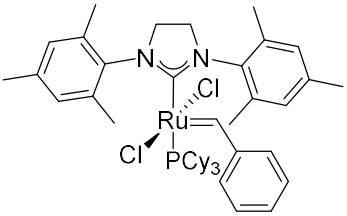

39

Abbildung 9: 37 einer der ersten NHC-Komplexe von WANZLICK *et al*.,[84] **38** das erste isolierte *N*-heterozyklische Carben von ARDUENGO *et al*.[85] und **39** ein Grubbs-Katalysator[86] der zweiten Generation.

Die Synthesen der ersten *N*-heterozyklischen Carbene erfolgte zunächst nur in Form ihrer Metallkomplexe 1968 durch WANZLICK *et al*.[84] sowie ÖFELE *et al*.,[87] da unkoordinierte NHCs zur Dimerisierung neigen. Die ersten freien NHCs konnten erst über 20 Jahre später von ARDUENGO *et al*.[85] durch den Einsatz sterisch anspruchsvoller und elektronisch günstiger Substituenten isoliert werden. Seitdem fanden die organischen Liganden immer neue Anwendungen und sind heute ein fester Bestandteil der Koordinationschemie. Vor allem in der Katalyse werden NHCs in der Organokatalyse[88] oder als Liganden wie bei den bekannten Grubbs-Katalysatoren[86,89] eingesetzt. Neben den Rutheniumkomplexen zur Olefinmetathese werden mittlerweile auch viele Palladium-NHC-Komplexe für C-C und C-Heteroatom Kreuzkupplungen wie der Heck-Reaktion, Suzuki- oder Buchwald-Hartwig-Kupplung verwendet.[90,91] Aufgrund der Stabilität und Vielseitigkeit, die NHC-Liganden bei der Katalyse zeigten, werden sie in den letzten Jahren auch verstärkt in der medizinischen Chemie untersucht.[81,91,92]

1.4.2 SYNTHESE VERSCHIEDENER NHC-STRUKTURMOTIVE UND METALLKOMPLEXE

Die elektronischen und sterischen Eigenschaften eines *N*-heterozyklischen Carbens werden durch die Art des Heterozyklus sowie von dessen Substituenten bestimmt. Als Grundgerüst können verschiedene Heterozyklen mit mindestens einem Stickstoffatom im Ring dienen. Die Ringgröße, die Substituenten als auch die Art und Anzahl weiterer Heteroatome wurde in den vergangenen Jahren stark variiert. Die bekanntesten Vertreter unter den NHCs sind Imidazol- (**40**), 2-Imidazolin- (**41**), Benzimidazol- (**42**), 1,2,4-Triazol- (**43**), Oxazol- (**44**) und Thiazolylidene (**45**). Die Synthesemethoden für diese und weitere NHC-Typen sind bereits in einigen vorangegangenen Arbeiten

zusammengefasst.[77,93,94] Diese Arbeit fokussiert sich daher lediglich auf die verwendeten Imidazol- und Benzimidazol-2-ylidene.

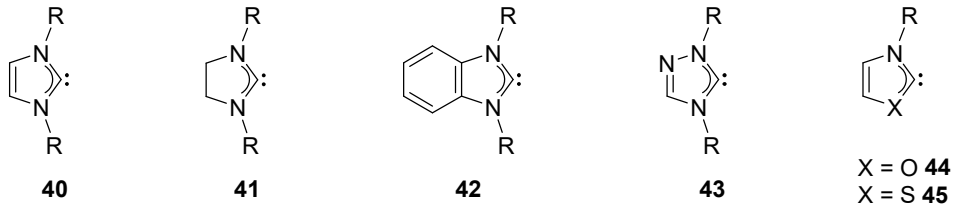

Abbildung 10: Carben-Strukturen verschiedener Heterozyklen, Imidazol-2-yliden (**40**), 2-Imidazolin-2-yliden (**41**), Benzimidazol-2-yliden (**42**), 1,2,4-Triazol-2-yliden (**43**), Oxazol-2-yliden (**44**) und Thiazol-2-yliden (**45**).

Bevor das Carben erzeugt und an ein Metallzentrum koordiniert werden kann, muss zunächst der entsprechend substituierte Heterozyklus in Form des Imidazolium- bzw. Benzimidazoliumsalzes synthetisiert werden. Bei einem lediglich *N*,*N*'-substituierten Zielmolekül kann meist vom kommerziell erhältlichen Imidazol bzw. Benzimidazol ausgegangen werden. Symmetrische (Benz-)Imidazoliumsalze können durch Alkylierung mit mindestens zwei Äquivalenten Alkylhalogenid erhalten werden, während mit nur einem Äquivalent das einfach substituierte Zwischenprodukt isoliert und zu einem unsymmetrischen (Benz-)Imidazoliumsalz weiter umgesetzt werden kann.[71,95] *N*-arylierte Spezies lassen sich mit Hilfe von entsprechenden Iodoniumsalzen[96] oder Boronsäuren[97] synthetisieren.

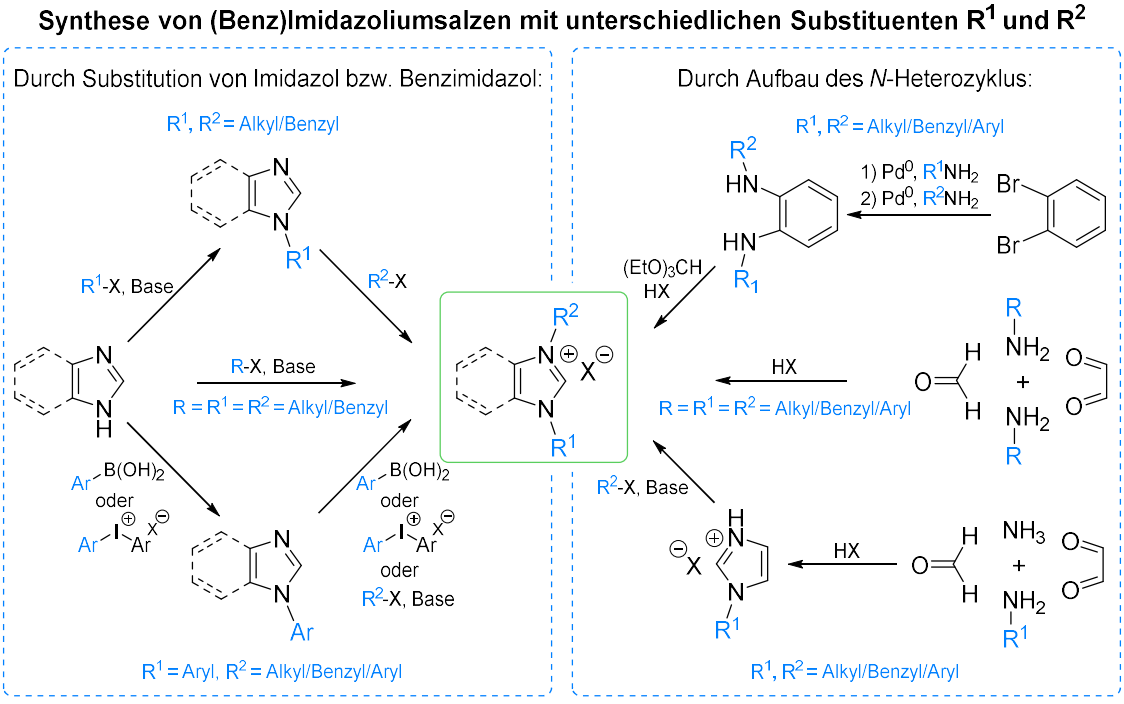

Schema 4: Synthesestrategien für unterschiedliche Imidazolium- und Benzimidazoliumsalze.

Eine weitere Möglichkeit, Imidazoliumsalze mit Arylen aber auch sterisch anspruchsvollen Alkylen zu erhalten, ist eine Mehrkomponentenreaktion, bei welcher der *N*-Heterozyklus aus Glyoxal, Formaldehyd und den entsprechenden Aminen aufgebaut wird. Zum Aufbau eines Benzimidazols kann 1,2-Dibromobenzol in zwei aufeinanderfolgenden Buchwald-Hartwig-Kreuzkupplungen zunächst mit den gewünschten *N*-Substituenten versehen und anschließend der Ring mit Triethoxymethan im Sauren zum Heterozyklus geschlossen werden.[93,98]

Um hochsubstituierte Imidazole zu erhalten, eignet sich besonders die van Leusen-Imidazolsynthese bei der auch an den Positionen 4 und 5 des Grundgerüstes unterschiedliche Reste eingebracht werden können. In dieser 2-Stufen-Synthese wird zunächst aus einem Aldehyd **46** und einem Amin **47** ein Aldimin **48** generiert, welches dann mit einem sogenannten TosMIC-Reagenz (**49**, Tosylmethylisocyanid) umgesetzt wird, um das 1,4,5-trisubstituierte Imidazol **50** zu erhalten.[99] Mit den bereits genannten Methoden lassen sich daraus im Anschluss Imidazoliumsalze mit bis zu vier unterschiedlichen Substituenten wie **51** generieren.

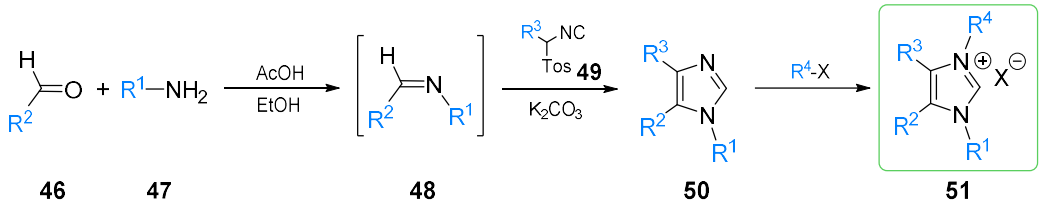

Schema 5: Syntheseweg über die van Leusen-Imidazolsynthese, hin zu hoch substituierten Imidazoliumsalzen.

Die damit schier unendliche Zahl an potenziellen NHC-Liganden kann nun mit unterschiedlichen Methoden an verschiedenste Metalle koordiniert werden. Die direkteste Variante zur Komplexierung ist der Austausch schwächerer Liganden gegen freie NHCs. Dazu wird das freie Carben **52** klassischer Weise durch Deprotonierung mit entsprechend starken Basen, wie z.B. KO^{t}Bu oder Alkalihydriden, generiert.[85] Ebenfalls bekannte Methoden zur Generierung von freien Carbenen sind die Reduktion von Thioharnstoffen[100] oder die α-Eliminierung von Abgangsgruppen[101] in Position 2 des Heterozyklus.

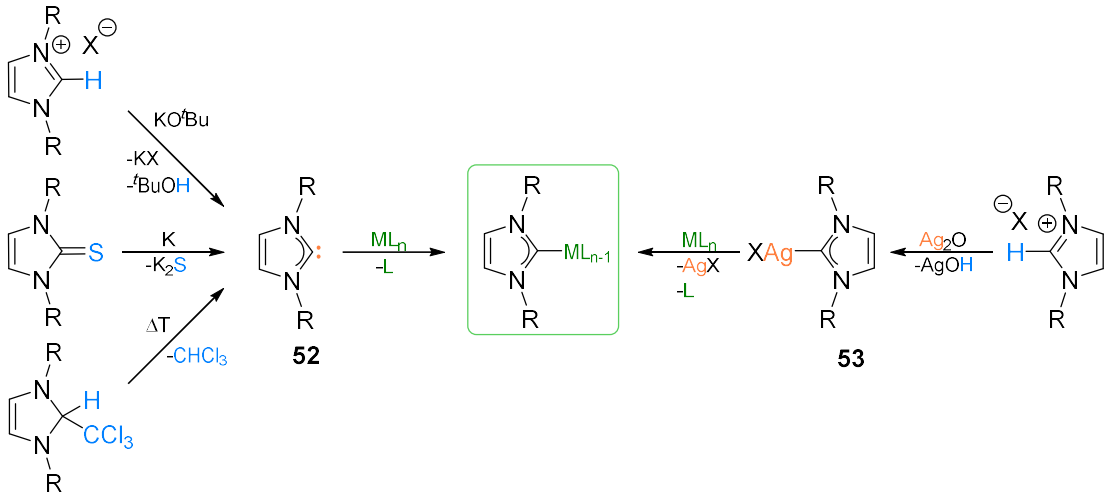

Schema 6: Verschiedene Methoden zur Darstellung unterschiedlichster NHC-Metallkomplexe über freie Imidazol-2-ylidene **52** oder die Carben-Transfer-Route nach WANG *et al.*[102]

Die mittlerweile wohl am häufigsten verwendete Methode zur Komplexierung von (Benz-)Imidazoliumsalzen stellt die von WANG *et al.*[102] entwickelte Carben-Transfer-Route dar, bei der die Deprotonierung zum Carben durch die Metallvorstufe selbst ausgelöst wird. In Anwesenheit von basischem Silberoxid lassen sich so (Benz-)Imidazoliumsalze in semi-labile NHC-Silberkomplexe **53** überführen, welche anschließend als Carben-Transferreagenz verwendet werden können, um NHCs unter sehr milden Bedingungen an eine Vielzahl von Metallen zu komplexieren.[103]

1.4.3 NHC-METALLKOMPLEXE IN DER MEDIZINISCHEN CHEMIE

Nachdem die klinische Forschung mit verschiedenen Metallkomplexen seit dem Durchbruch von Cisplatin immer wieder deren Potenzial aufzeigen konnte, aber nur in wenigen Fällen neue zugelassene Medikamente zum Vorschein brachte, verschob man den Fokus in den letzten zehn Jahren auf Komplexe mit den außerordentlich vielseitigen *N*-heterozyklischen Carben-Liganden. Dank der umfangreichen Substitutions-möglichkeiten und der guten Komplexierbarkeit lässt sich die Wirkung über die Reaktivität, Lipophilie, Sterik und zusätzliche Pharmakophore der NHC-Komplexe besser steuern, was dieser Wirkstoffklasse viel Aufmerksamkeit bescherte. Findet man bis ins Jahr 2008 hinein noch lediglich sechs wissenschaftliche Veröffentlichungen unter dem Suchbegriff "*N*-heterocyclic carbene + cancer" bei scifinder.cas.org,[104] sind es von 2009 bis 2018 bereits 145 Publikationen zu diesem Thema.

Neben einer Vielzahl an komplexierten Metallen wie u.a. Silber, Gold, Platin und Ruthenium, wurden dabei auch unterschiedliche Indikationen untersucht. Da in dieser Arbeit nur auf einige, vielversprechende Beispiele eingegangen werden kann, wird an dieser Stelle auf einige ausgezeichnete Übersichtsartikel verwiesen, die das Bild vervollständigen.[105-107]

Als die wohl ersten NHC-Metallkomplexe mit biologischer Wirkung wurden von CETINKAYA *et al*.[108] 1996 antimikrobielle Rhodium- und Ruthenium-Komplexe veröffentlicht. Mittlerweile übertreffen auf diesem Feld die NHC-Komplexe von Silber die aller anderen Metalle und zeigen selbst bei multiresistenten Keimen vielversprechende Wirkung. Der antibakterielle Effekt von Silber, z. B. in Form von $AgNO_3$, ist zwar schon seit langem bekannt, allerdings erhöhen die NHC-Komplexe wie **54** die Bioverfügbarkeit und geben die Silberionen über einen längeren Zeitraum ab.[109]

In der Krebsforschung hingegen spielen Silberkomplexe keine große Rolle. Hier liegt die größte Aufmerksamkeit der Wissenschaftler bei NHC-Platin(II) aber vor allem NHC-Gold(I)-Komplexen. Während Goldkomplexe ohne NHC-Liganden wie Auranofin eher als Antirheumatikum bekannt sind, zeigen viele NHC-Goldkomplexe neben einer antibakteriellen[110] auch eine antitumorale [111] Wirkung.

Das Design der NHC-Liganden schließt dabei einfache (Benz-)Imidazolliganden aber auch Naturstoffderivate ein. So synthetisierten CASINI *et al*.[112] den zytotoxischen Au^{I}-Komplex **55** mit zwei methylierten Koffein-2-ylidenen als NHC-Liganden, während Biersack *et al*.[113] bis-NHC-Au^{I}-Komplexe **56** mit Imidazol-verbrückten Combretastatin A-4 Derivaten entwickelten, die ähnlich dem CA-4 selbst eine antivaskulare Wirkung beibehielten.

TACKE *et al*.[114] paarten bei den Komplexen **57a-c** einen NHC mit je einem Chlorido-, Acetato- bzw. Thioglucopyranose-Liganden – analog dem Auranofin – am Goldzentrum und konnten dabei aufzeigen, dass das Zuckerderivat vermutlich durch bessere Löslichkeit und erhöhte Aufnahme positiv zur Wirkung beiträgt. Mit zwei neutralen Liganden entstehende lipophile, kationische Komplexe, wie bei NHC-Phosphin- und bis-NHC-Gold(I)komplexen, werden von Zellen meist besser aufgenommen und verstärkt in den Mitochondrien akkumuliert.[115] Genau dort befindet sich auch das vermeintliche Haupt-Target der Goldverbindungen: Das Selenoenzym Thioredoxin-Reduktase 2.[70,71,116] Einige

NHC-Gold(III)-Verbindungen zeigen zudem Topoisomerase I Inhibition, oder initiierten die Ausbildung von DNA-Strangbrüchen.[117]

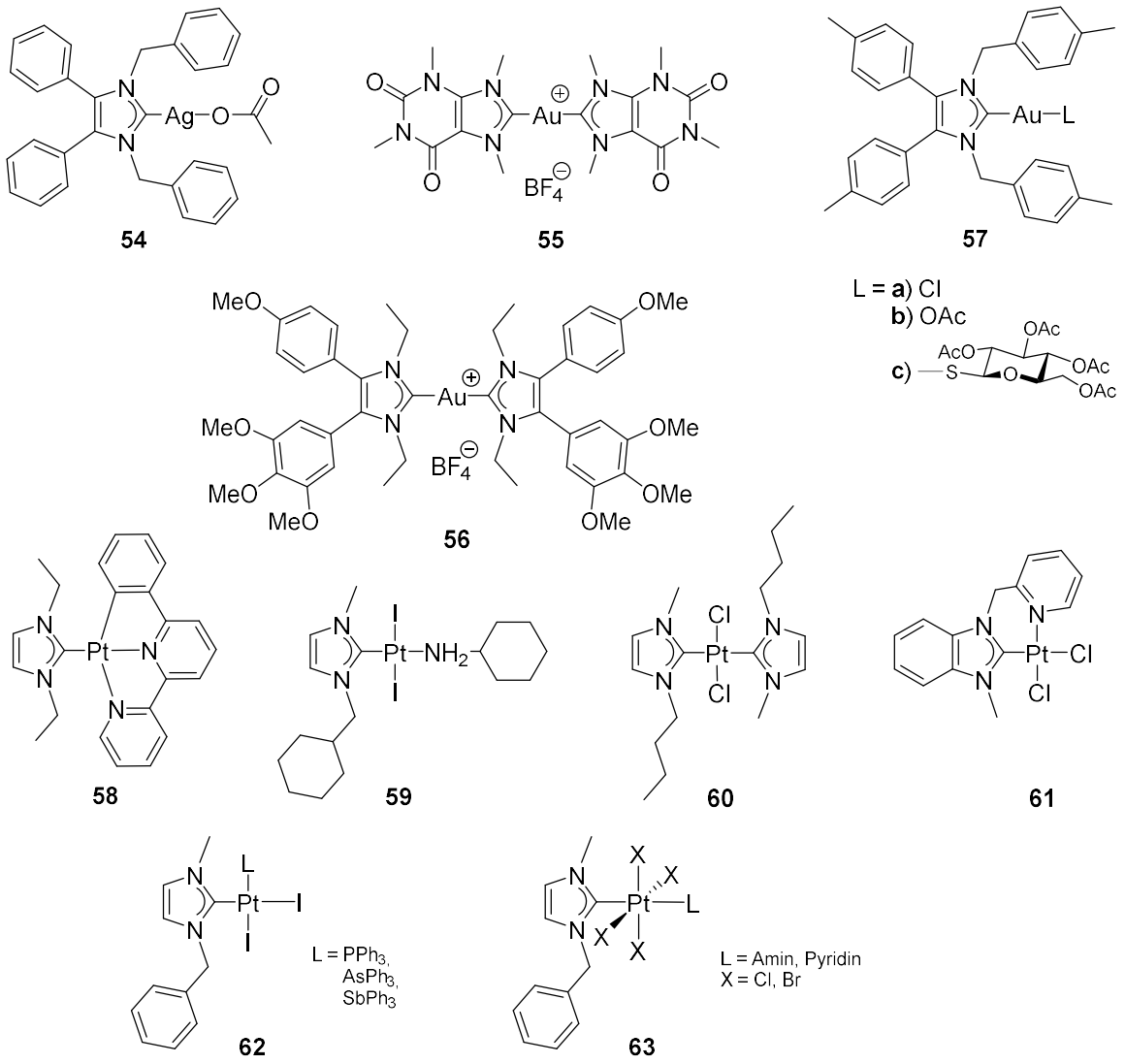

Abbildung 11: Strukturen von biologisch aktiven Ag^{I}-, Au^{I}-, Pt^{II}- und Pt^{IV}-Komplexen mit *N*-heterozyklischen Carbenliganden.

Gemessen am Erfolg von Cisplatin und seinen Derivaten macht die Forschung mit Platinkomplexen von *N*-heterozyklischen Carbenen als neue Wirkstoffe im Vergleich zu Gold-NHC-Komplexen bisher einen relativ kleinen Teil aus.[105-107,118] Viele Veröffentlichungen über neue NHC-Pt-Komplexe beziehen sich meist auf deren katalytische[119] oder photophysikalische[120] Eigenschaften. Einige dieser photoaktiven Komplexe mit 6-Phenyl-2,2‘-bipyridin-Liganden wie **58** besitzen bereits starke zytotoxische Aktivität, wobei zwar keine DNA-Interaktion aber eine verringerte Survivin Expression zu beobachten ist.[121] Als einer der ersten unter den NHC-Pt-Komplexen mit

anti-tumoralen Eigenschaften zeigte 2010 der Komplex **59** von MARINETTI *et al*.[122] stärkere anitiproliverative Aktivität als Cisplatin gegen eine Reihe von Krebszelllinien, darunter auch multiresistente, mit mittleren inhibitorischen Konzentrationen (IC_{50}) im niedrigen mikromolaren-Bereich. Dabei bindet dieser *trans*-Pt^{II}-Komplex ebenfalls an DNA, löst Apoptose jedoch über einen anderen Signalweg als Cisplatin aus.[123] Während das *trans*-Isomer von Cisplatin keine Wirkung zeigt, konnten unter den NHC-Komplexen besonders solche *trans*-[Pt^{II}(Amin)(NHC)X_2] Verbindungen überzeugen. Mit einem zweiten NHC in *trans*-Position besitzt Komplex **60** im Gegensatz zu Goldkomplexen mit demselben Ligandenumfeld keine antitumorale Wirkung.[124] Ein cyclometallierter *cis*-Pt^{II}-NHC-Komplex **61** von DINDA *et al*. zeigte im Vergleich zu Cisplatin und einem Gold-Analoga ebenfalls nur moderate Zytotoxizität.[125] Bessere Ergebnisse erzielten erst 2016 die Komplexe **62** von BELLEMIN-LAPONAZ *et al*.[126] mit *cis*-ständigen PPh_3-, $AsPh_3$- und $SbPh_3$-Liganden und ebenfalls IC_{50}-Werten im einstelligen µM-Bereich.

Pt^{IV}-Komplexe in Kombination mit NHC-Liganden sind bislang spärlich zu finden und wurden auf ihre mögliche Anwendbarkeit als Prodrugs lediglich von BELLMIN-LAPONNAZ *et al*.[50,127] untersucht, z. B. an Komplexen vom Typ **63**. Auch Ruthenium-NHC-Komplexe stehen bislang noch im Schatten ihrer bekannten Verwandten wie NAMI-A. Etliche NHC-Komplexe sind auch von Kupfer, Palladium, Rhodium und Iridium bekannt.[105-107,118,128]

2 SYNOPSIS

2.1 ZIELSETZUNG UND ÜBERBLICK ÜBER DIE TEILPROJEKTE

Nach mittlerweile über 45 Jahren stetiger Weiterentwicklung der erfolgreichen, aber mit schweren Nebenwirkungen behafteten Platinzytostatika, steht nun die von CLEARE und HOESCHELE[19] postulierte Leitstruktur, die aussichtsreiche Verbindungen als neutrale, planare Pt^{II}-Komplexe mit zwei *cis*-ständigen Aminliganden beschreibt, auf dem Prüfstand. Insbesondere *N*-heterozyklische Carbene, die zuletzt bereits als Liganden in Goldkomplexen ihr Potential aufgezeigt haben, bieten gänzlich neue und vielfältige Möglichkeiten zur Entwicklung von Metallotherapeutika für die Behandlung von Tumorerkrankungen. Eine weitergehende Evaluierung dieser Liganden und die Entwicklung neuer Synthesemethoden für antitumorale Platinkomplexe mit NHC-Liganden sowie deren Wirkoptimierung waren die Ziele dieser Arbeit.

Aufgeteilt in vier wissenschaftliche Publikationen, welche in Kapitel 4 zu finden sind, ist dies in der vorliegenden kumulativen Dissertationsschrift dargestellt. In den Publikationen I und II wurden überwiegend Pt^{II}-Komplexe mit unterschiedlichen NHC-Liganden in *cis*-Position zu Phosphinen synthetisiert und deren Struktur-Wirkungs-Beziehung untersucht.[129,130] Im Weiteren wurde daraufhin eine neue Methode entwickelt, welche die Synthese von Cisplatin-analogen *cis*-$[Pt^{II}Cl_2(NHC^1)(NHC^2)]$-Komplexen mit zwei unterschiedlichen NHC-Liganden ermöglicht.[131] Die Synthese von *cis*-$[Pt^{II}Cl_2(NHC)_2]$-Komplexen mit Benzimidazol-2-yliden-Liganden und darauffolgende Oxidationsversuche hin zu Pt^{IV}-Prodrugs sind in Publikation IV beschrieben. Weitere in diesem Zusammenhang erarbeitete Publikationen mit Beiträgen zur Synthese von Übergangsmetallkomplexen, die nicht Teil dieser Dissertationsschrift sind, werden in Kapitel 5 aufgelistet.

2.2 SYNTHESE VON (BENZ-)IMIDAZOL-Pt^{II}-KOMPLEXEN MIT PHOSPHINLIGANDEN

Das bekannteste Platinzytostatikum Cisplatin (**3**), mit der Struktur *cis*-$[Pt^{II}Cl_2(NH_3)_2]$, verdankt seinen Wirkmechanismus, eine besonders starke Hemmung der DNA-Replikation, unter anderem der *cis*-Anordnung seiner Liganden. Um diesen Aufbau bei der Entwicklung Cisplatin-analoger Pt^{II}-Komplexe mit NHC-Liganden beibehalten zu können, lieferten NEWMAN *et al.*[132] einen synthetischen Ansatz: Die Entdeckung, dass die

Carbentransfer-Reaktion eines NHC-Silberkomplexes, die mit Kaliumtetrachloroplatinat(II) (**16**) in CH_2Cl_2 zu *trans*-[$Pt^{II}Cl_2(NHC)_2$] führt, in DMSO hingegen ein Lösungsmittelmolekül als Ligand in *cis*-Stellung zum NHC koordiniert, eröffnet einen Zugang zum selektiven Ligandenaustausch in dieser Position.

Aufbauend auf diesem Prinzip wurde ein solcher *cis*-[$Pt^{II}Cl_2$(DMSO)(NHC)]-Komplex **65** über die Silbercarben-Transfer-Route, ausgehend von zuvor synthetisiertem Imidazoliumsalz **64**, hergestellt. Dieser diente anschließend aufgrund der Labilität des *cis*-ständigen DMSO-Liganden als Ausgangsstoff für die Synthese unterschiedlicher Phosphinkomplexe. So konnte durch Zugabe eines Äquivalents Triphenylphosphin der neutrale Komplex **66** beziehungsweise durch Zugabe eines Überschusses an PPh_3 sogar der kationische Komplex **67** erhalten werden. Versuche, den DMSO-Liganden mit Pyridinen wie 2-Picolin auszutauschen, um eine Verbindung analog zu Picoplatin (**10**) zu erhalten, lieferten nicht wie mit den Phosphinen einen Austausch in *cis*-Position zum NHC, sondern *trans*-Komplexe. So wurde der Komplex **68**, wie der ebenso synthetisierte *trans*-[$Pt^{II}Cl_2(NHC)_2$]-Komplex **69**, zur weiteren Untersuchung als Vergleichssubstanzen herangezogen.

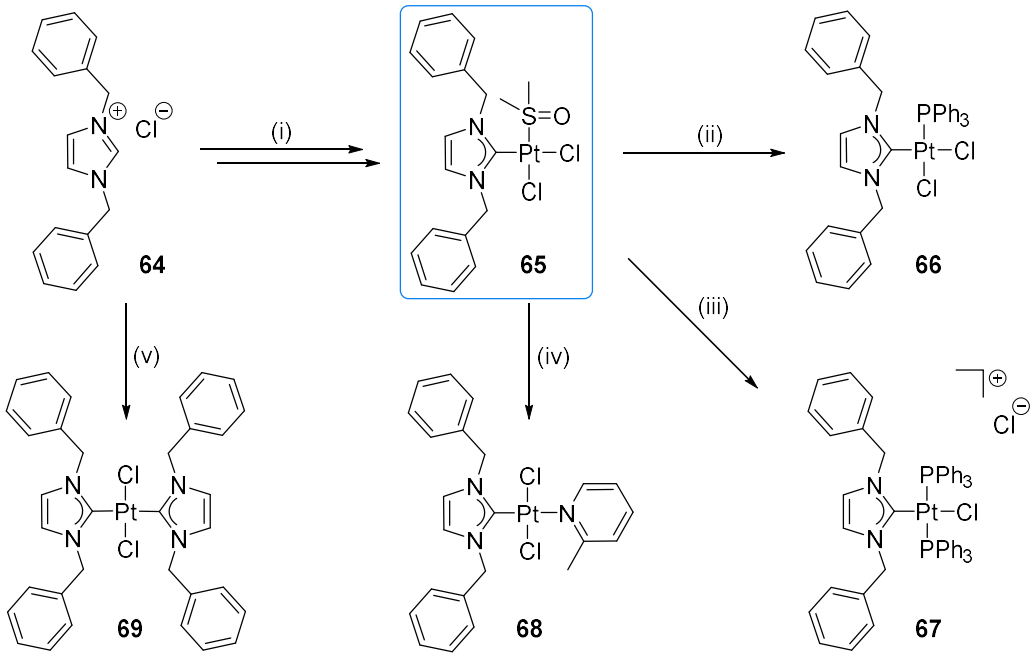

Schema 7: Synthese der NHC-Platinkomplexe **65**-**69**. Reagenzien und Bedingungen: (i) 1.) Ag_2O, CH_2Cl_2, rt, 2.) K_2PtCl_4, DMSO, 60 °C; (ii) 1 eq PPh_3, CH_2Cl_2, rt; (iii) 5 eq PPh_3, CH_2Cl_2, rt; (iv) 2-Picolin, CH_2Cl_2, rt; (v) 0,5 eq K_2PtCl_4, CH_2Cl_2, rt.

Bei den Untersuchungen der erhaltenen Komplexe auf ihre Zytotoxizität und mögliche Wirkmechanismen – in Zusammenarbeit mit einigen Kooperationspartnern – wurden im

Hinblick auf eine weitere Entwicklung von NHC-Platinkomplexen einige interessante Beobachtungen gemacht: So interagierten lediglich die Komplexe mit der guten Abgangsgruppe Chlorid *trans* zum NHC-Liganden mit DNA. Dabei zeigte der sterisch gut zugängliche Komplex **65** ähnliche Eigenschafften wie Cisplatin auf, die Komplexe **66** und **67** führten mit zunehmender sterischer Abschirmung des Metalls hingegen zur Ausbildung von ungewöhnlichen DNA-Aggregaten. Entgegen der Theorie von CLEARE und HOESCHELE,[19] dass geladene Verbindungen generell inaktiv und kaum toxisch sind, zeigte der kationische Komplex **67** in MTT-Assays die mit Abstand stärkste Zytotoxizität mit meist nanomolaren IC_{50}-Werten an verschiedenen Krebszelllinien.

Aufbauend auf diesen Ergebnissen wurden nachfolgend zwei Strategien verfolgt, um die sterische Abschirmung und weitere physikochemische Eigenschafften von NHC-Platin-Verbindungen feiner justieren sowie den Einfluss auf deren Wirkung besser verstehen zu können. Eine naheliegende Möglichkeit dazu war eine Variation der an den NHC-Stickstoffen befindlichen Substituenten, die in direkter Nachbarschaft zum Platinzentrum liegen. Ein Austausch der Benzylgruppen am Imidazol durch kurzkettige Alkyle ging allerdings mit schlechten Löslichkeiten einher, weshalb lipophilere Benzimidazole als NHC-Grundgerüst herangezogen wurden.

Mit jeweils verdoppelnder Kettenlänge der *N*-Alkylsubstituenten wurden die Benzimidazol-Liganden **70a**-**d** mit *N*-methyl, -ethyl, -butyl und -octyl Substituenten synthetisiert. Diese wurden anschließend analog der Verbindung **64** in die *cis*-[$Pt^{II}Cl_2$(DMSO)(NHC)]-Komplexe **71a**-**d** überführt. Dabei waren durch die verschieden langen Seitenketten bereits Unterschiede bezüglich der Reaktionszeiten und Löslichkeiten zu beobachten, die sich bei der anschließenden Synthese der Phosphinkomplexe besonders stark bemerkbar machten: So gelang die Umsetzung vom Methyl-substituierten **71a** zu **72a** nur in hoher Verdünnung und mit geringer Ausbeute, da selbst mit lediglich 1 eq PPh_3 überwiegend der bis-Phosphin-Komplex **73a** entstand und viel unverbrauchtes **71a** zurückblieb. Mit längeren Seitenketten hingegen bildete sich auch mit größeren Mengen Phosphin kaum das entsprechende bis-PPh_3-Produkt **73**. Um die *trans*-[Pt^{II}Cl(NHC)(PPh_3)$_2$]Cl-Komplexe dennoch zu erhalten, mussten im Gegensatz zur Synthese der Komplexe **67** deutlich drastischere Reaktionsbedingungen gewählt werden. Die sterisch anspruchsvollste kationische Verbindung **73d** erwies sich sogar als instabil

und konnte, obwohl laut ^{31}P-NMR in Lösung nahezu rein vorhanden, immer nur als Mischung mit **72d** und PPh_3 isoliert werden.

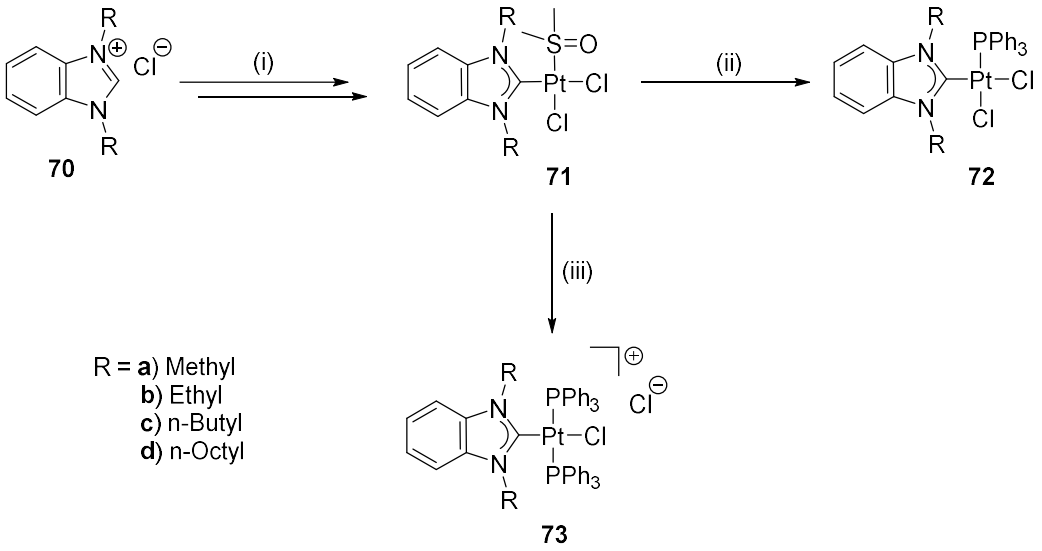

70 71 72 73

Schema 8: Synthese der Komplextypen **71**-**73** mit Benzimidazol-2-yliden-Liganden. Reagenzien und Bedingungen: (i) 1.) Ag_2O, CH_2Cl_2, rt, 2.) K_2PtCl_4, DMSO, 60 °C; (ii) PPh_3, CH_2Cl_2 rt; (iii) Üs. PPh_3, CH_2Cl_2, rt; **73c**: 10 eq PPh_3, CH_3CN, 60 °C; **73d**: instabil, Zersetzung bei Aufreinigung.

Die elf hieraus neu synthetisierten Benzimidazol-2-yliden-Platinkomplexe zeigten mit zunehmender Größe und Lipophilie eine klare strukturelle Abhängigkeit ihrer zytotoxischen Eigenschaften. Besonders auffällig war die Aufnahme der Komplexe, die an HCT116 Kolonkarzinomzellen untersucht wurde. Hierbei konnte eine erhöhte Wirkstoffaufnahme von **71a**-**d**, **72a**-**d** und **73a**-**c** sowohl mit jeweils zunehmender Kettenlänge als auch mit steigender Anzahl der Phosphinliganden beobachtet werden. Lediglich **72d** mit *n*-Octyl-Substituenten und einem Phosphin-Liganden war zu groß oder zu lipophil, um von der Zelle in größeren Mengen aufgenommen werden zu können. In Korrelation dazu steht auch die Zytotoxizität der Komplexe, von den inaktiven **71a** und **72a** bis hin zu niedrigen nanomolaren IC_{50}-Werten für **73a** und **b** an sechs von sieben getesteten Krebszelllinien. Zudem konnte die Erkenntnis gewonnen werden, dass selbst die DNA-Interaktion nicht nur von der Art der Liganden des Komplexes abhängt, sondern tatsächlich auch stark durch die Substituenten am NHC beeinflusst wird: Unter den neutralen Verbindungen **72** zeigte im Ethidiumbromid-Assay lediglich das *n*-Butyl substituierte **72c** einen Effekt auf DNA, dieser war vergleichbar stark wie der der geladenen Komplexe **73**.

2.3 ENTWICKLUNG NEUARTIGER *CIS*-[$Pt^{II}Cl_2(NHC)^1(NHC)^2$]-KOMPLEXE

Da also nicht nur Art und Größe der *cis*-ständigen Liganden, sondern auch der NHC-Ligand selbst großen Einfluss auf das Wirkungsprofil der Platin-Komplexe hat, besteht eine weitere Möglichkeit dieses noch besser steuern zu können in der Variation zweier zueinander *cis*-stehender NHC-Liganden am Platinzentrum. Solche Cisplatin-analoge Verbindungen konnten bislang mittels der Methoden von NOLAN *et al.*[133] und RÖSCHENTHALER *et al.*[134] lediglich als symmetrische *cis*-[$Pt^{II}Cl_2(NHC)_2$]-Komplexe mit identischen NHC-Liganden synthetisiert werden.

Um jedoch zwei unterschiedliche NHC-Liganden sukzessive in *cis*-Konfiguration an ein Platinzentrum zu koordinieren, musste eine neue Methode entwickelt werden. Nach einigen Versuchen stellten sich dafür erneut die DMSO Komplexe vom Typ **74** als ideale Ausgangsverbindungen heraus. Während zusammen mit den als Carbentransfer-reagenzien bekannten Silberkomplexen keine Reaktion stattfand, waren freie Carbene in der Lage den DMSO-Liganden in *cis*-Position zum bereits vorhandenen NHC zu substituieren. In trockenem CH_2Cl_2 kann ein Imidazoliumsalz **NHC^1**xHCl **75** in Anwesenheit von KO^{t}Bu *in situ* zum freien Carben **NHC^1** deprotoniert werden, welches dann mit der DMSO-Vorstufe *cis*-[$Pt^{II}Cl_2$(DMSO)(**NHC**)^2] **74** durch Ligandenaustausch reagiert. Im Gegensatz zu den bisherigen Methoden lassen sich auf diese Weise nun auch unsymmetrische *cis*-[$Pt^{II}Cl_2$(**NHC**)^1(**NHC**)^2]-Komplexe **76** mit einer Vielzahl von Kombinationsmöglichkeiten generieren.

Zunächst wurden so die Komplexe **76a**-**h** mit verschiedenen imidazolbasierten NHC-Liganden hergestellt, wobei sämtliche Kombinationen in guten bis sehr guten Ausbeuten von bis zu 93% erhalten wurden. Um ausgehend von diesen Verbindungen erneut kationische Komplexe zu erhalten, die bei den zuvor untersuchten Komplextypen die jeweils stärkste Zytotoxizität aufwiesen, wurden auch die *cis*-[$Pt^{II}Cl_2(NHC)^1(NHC)^2$]-Komplexe mit PPh_3 umgesetzt. Unsymmetrische Komplexe wie **76c** und **76d** ergaben erwartungsgemäß untrennbare Gemische der beiden möglichen Stereoisomere, weshalb nur die symmetrischen Verbindungen **76a** und **76b** zu den geladenen Komplexen **77** umgesetzt wurden.

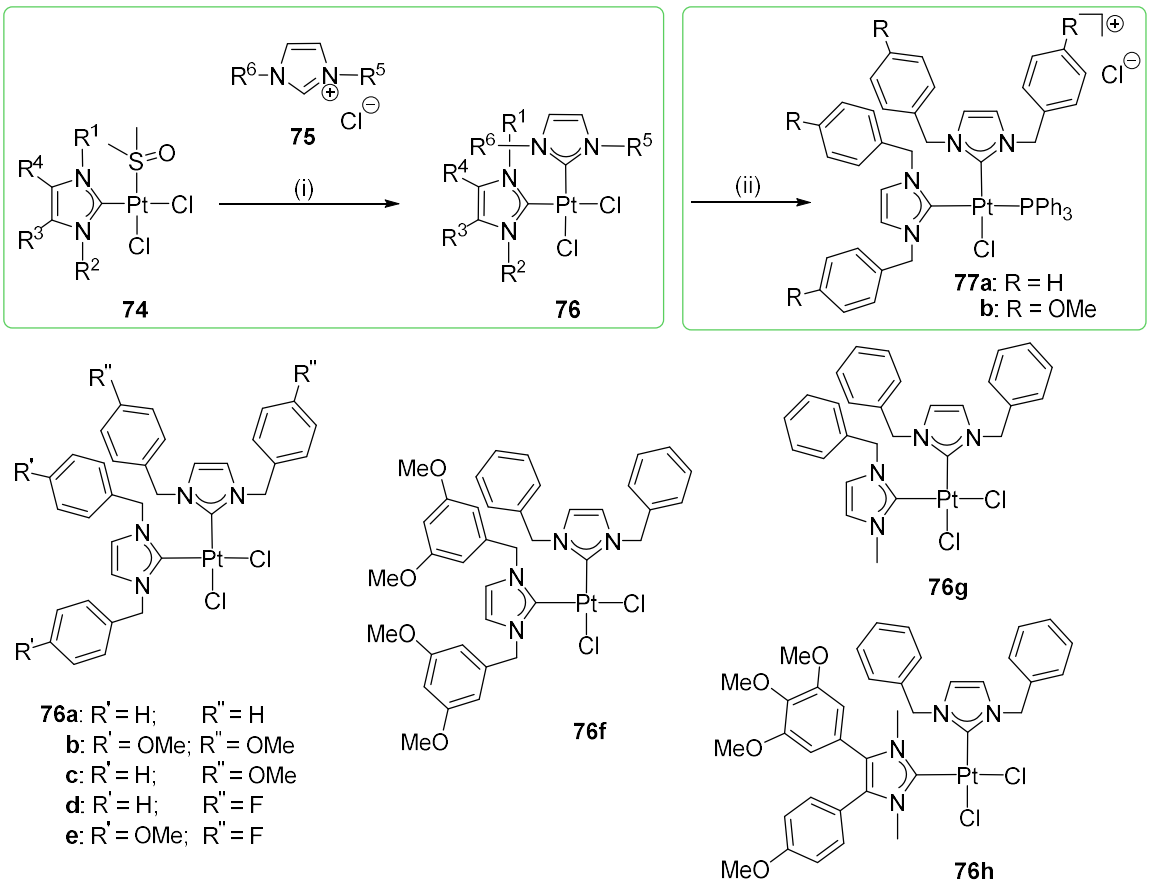

Schema 9: Neue Methode zur Darstellung neuartiger *cis*-[$Pt^{II}Cl_2(NHC)^1(NHC)^2$]-Komplexe **76a**-**h** und deren weitere Umsetzung zu geladenen *cis*-[$Pt^{II}Cl(NHC)_2(PPh_3)$]Cl-Komplexen **77a** und **b**. Reagenzien und Bedingungen: (i) **75**, KO^{t}Bu, CH_2Cl_2 (trocken), Ar-Atmosphäre, rt; (ii) PPh_3, CH_2Cl_2, rt.

Die zehn neuartigen Komplexe wurden auf ihre antiproliferativen Eigenschaften untersucht, wobei in MTT-Tests niedrige mikromolare, für die kationischen sogar nanomolare, IC_{50}-Werte ermittelt wurden. Besonders interessant war dabei die enorme Abhängigkeit der Zytotoxizität von den eingesetzten NHC-Liganden. Während die durchweg benzylsubstituierten Komplexe **76a-f** ähnliche IC_{50}-Werte aufwiesen, sorgte der Austausch eines Benzylrestes gegen Methyl bei **76g** für einen erheblich schwächeren Effekt des Platinkomplexes auf die getesteten Krebszellen. Mit einem hochsubstituierten, Combretastatin A-4-abgeleiteten NHC^2-Liganden erlangte **76h** eine auffallend hohe Selektivität gegenüber einigen Zelllinien, die wohl auf die Struktur des Naturstoffs zurückzuführen ist. Durch solche pleiotrope Effekte könnten Verbindungen dieser neuen Komplexart als *multi-targeted Drugs* entwickelt werden.[135] In Wechselwirkung mit DNA konnte *in vitro* erneut eine Aggregation durch die Komplexe **76b** und **77b** beobachtet werden, während der als Vergleichssubstanz synthetisierte Komplex ***trans*-76b** keinen Effekt zeigte.

Als Beleg für die breite Anwendbarkeit der neuentwickelten Synthesemethode und um gegenüber oxidativen Bedingungen stabilere Komplexe zu erhalten, wurden im weiteren Verlauf auch Benzimidazol-Liganden über diese Route umgesetzt. Da von den entsprechenden *cis*-[$Pt^{II}Cl_2$(NHC)(PPh_3)]-Komplexen der erhebliche Einfluss der Substituenten am NHC bereits bekannt war, wurde erneut die Spanne von *N,N*-dimethyl- über diethyl- und dibutyl- bis hin zu *N,N*-dioctyl-Benzimidazolliganden abgedeckt. Die Synthese verlief gemäß der zuvor ausgearbeiteten Methodik und lieferte die stark unterschiedlich abgeschirmten Komplexe **79a-d** (Schema 10). Als Vergleichssubstanzen für die biologische Aktivität der Komplexe sowie für geplante Oxidationsversuche, wurde die zuvor synthetisierte Verbindung **76a** herangezogen und zudem der *trans*-Komplex ***trans*-79c** synthetisiert. Sämtliche Reaktionen mit den Benzimidazolliganden verliefen problemlos unter denselben Bedingungen wie mit Imidazolliganden, allerdings mit geringeren Ausbeuten für die beiden Extrema **79a** und **d**. Auf die Ergebnisse der Zytotoxizitätsuntersuchungen wird im direkten Vergleich mit den analogen Pt^{IV}-Verbindungen im folgenden Kapitel eingegangen.

2.4 OXIDATIONSVERSUCHE ZU Pt^{IV}-KOMPLEXEN

Die sechs zuvor synthetisierten Pt^{II}-Komplexe **79a-d**, ***trans*-79c** und **76a** wurden anschließend ausführlichen Oxidationsexperimenten unterzogen, um potenzielle Pt^{IV}-Prodrugs zu erhalten. Mit Iodbenzoldichlorid ($PhICl_2$), welches gewonnen aus Iodbenzol, HCl und NaOCl,[52] als leichter handhabbare Alternative zu Chlorgas eingesetzt werden kann, wurde zu den entsprechenden *cis*-[$Pt^{IV}Cl_4(NHC)_2$]-Komplexen **80a-d**, ***trans*-80c** und **81** oxidiert. Die stabilen, neuartigen Komplexe konnten dabei mit Ausbeuten von mindestens 88% gewonnen werden. Weitere Versuche *cis,cis,trans*-[$Pt^{IV}Cl_2(NHC)_2(OH)_2$] bzw. [$Pt^{IV}Cl_3(NHC)_2(OH)$]-Komplexe, die zusätzliche Funktionalisierungen an den axialen Hydroxo-Liganden ermöglichen würden,[44,61,62] zu synthetisieren, scheiterten an einer intrinsischen Instabilität solcher Komplexe mit den hier eingesetzten Liganden.

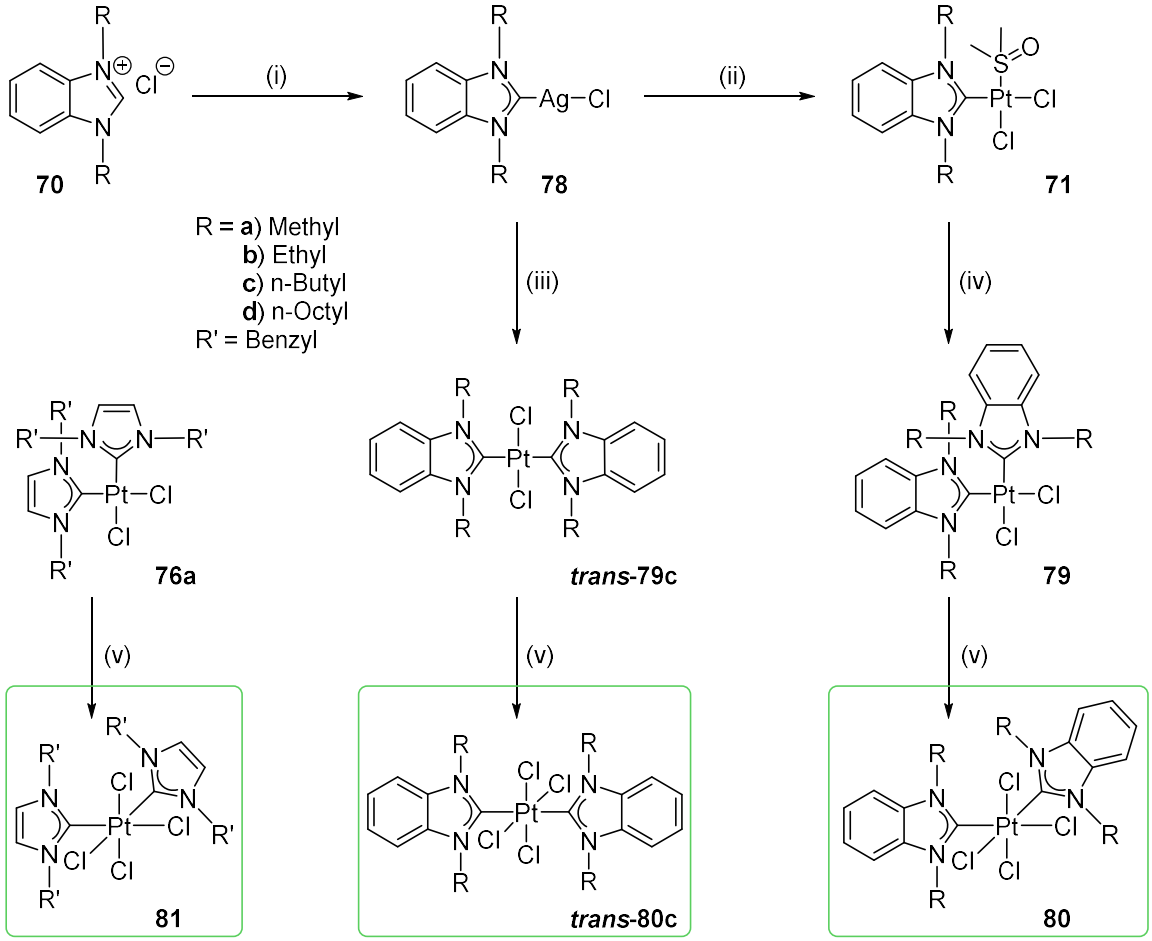

Schema 10: Synthese von *cis*- und *trans*-[$Pt^{II}Cl_2$(dialkylbenzimidazol-2-yliden)$_2$]-Komplexen sowie deren Oxidation zu [$Pt^{IV}Cl_4$(dialkylbenzimidazol-2-yliden)$_2$]-Komplexen und die analoge Synthese von **81**.
Reagenzien und Bedingungen: (i) Ag_2O, CH_2Cl_2, rt; (ii) K_2PtCl_4, DMSO, 60 °C; (iii) K_2PtCl_4, CH_2Cl_2, rt; (iv) **70**, KO^{t}Bu, CH_2Cl_2 (trocken), Ar-Atmosphäre, rt; (v) $PhICl_2$, CH_2Cl_2, rt.

Umsetzungen der Komplexe **79** mit H_2O_2, ^{t}BuOOH, NaOCl oder KOCl in verschiedenen Lösungsmitteln – u.a. Alkohole und Carbonsäurederivate – zeigten bei Reaktionskontrollen wiederholt Anzeichen von Pt^{IV}-Verbindungen, welche jedoch nicht isoliert werden konnten. Erst durch die Kristallisation einer kleinen Menge *cis*-[$Pt^{IV}Cl_3$(*N*,*N*-diethylbenzimidazol-2-yliden)$_2$(OH)] (**82**) aus einer NMR-Probe der Reaktion von **79b** mit NaOCl in Acetonitril/H_2O konnte die Existenz eines solchen Komplexes in NMR-Spektren nachgewiesen werden. Allerdings zeigte dieselbe Probe bei erneuter Messung nach fünf Tagen die Signale des reinen Startmaterials **79b**, was in Kombination mit den Ergebnissen aus Ligandenaustausch-Versuchen auf eine rasche Zersetzung der Pt^{IV}-Hydroxokomplexe schließen lässt.

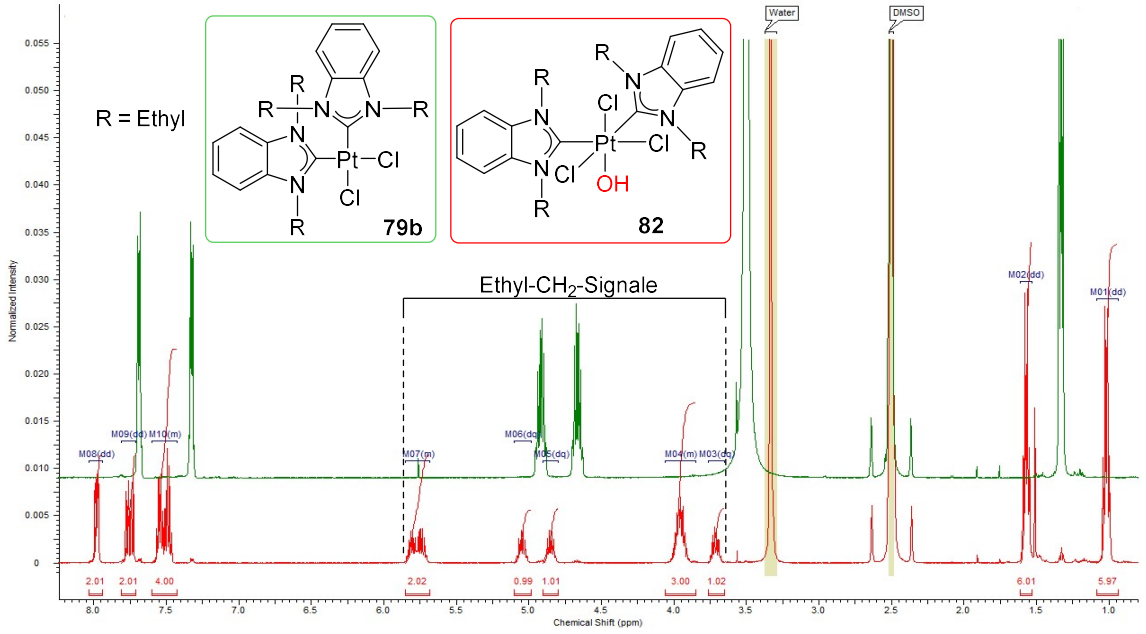

Abbildung 12: rot: ^{1}H-NMR von Kristallen aus einer Reaktion von **79b** mit NaOCl, entspricht Pt^{IV}-Hydroxo-Komplex **82**; **grün:** ^{1}H-NMR derselben Probe fünf Tage später, entspricht reinem Edukt **79b**.

Bei der zytotoxischen Wirkung der Komplexe war erneut ein sehr starker Einfluss durch die Substituenten der Benzimidazol-Liganden zu erkennen: Während **79c** und sein *trans*-Isomer als einzige der neuen Pt^{II}-Komplexe Aktivität zeigten, waren **80a** und **d** nicht löslich genug, um überhaupt getestet werden zu können. Die aktiven Pt^{IV}-Komplexe **80b** und **c**, sowie ***trans*-80c** und **81** hingegen besitzen eine gewisse Selektivität gegenüber Krebszellen im Vergleich zu nicht-malignen Fibroblasten und scheinen trotz beachtlicher Zytotoxizität deutlich schwächer mit DNA zu interagieren als die Pt^{II}-Komplexe **76a** und Cisplatin (**3**). Ob die beobachteten Effekte auf einer Reduktion der Pt^{IV}-Prodrugs, einem eigenständigen Wirkmechanismus oder einer verstärkten Aufnahme dieser Komplexe beruhen, muss in künftigen Experimenten untersucht werden.

3 LITERATURVERZEICHNIS

[1] C. J. Jones, J. R. Thornback, *Medicinal Applications of Coordination Chemistry;* Royal Society of Chemistry, Cambridge **2007**.

[2] J. Almkvist, *Syphilis-Therapie;* Springer Verlag Berlin, Heidelberg **1928**. DOI: 10.1007/978-3-642-47826-0

[3] Paracelsus, *Das Buch Paragranum: Septem Defensiones;* CreateSpace Independent Publishing Platform, Berlin **2013**.

[4] P. Ehrlich, A. Bertheim, *Ber. Dtsch. Chem. Ges.* **1912**, *45*, 756–766. DOI: 10.1002/cber.191204501110.

[5] a) N. C. Lloyd, H. W. Morgan, B. K. Nicholson, R. S. Ronimus, S. Riethmiller, *Chemistry in New Zealand* **2005**, *69*, 24–27; b) I.Ott, *Nachr. Chem.* **2009**, *57*, 628–631. DOI: 10.1002/nadc.200964895.

[6] J. Forestier, *The Lancet* **1934**, *224*, 646–648. DOI: 10.1016/S0140-6736(00)82169-8.

[7] I. Bertini, H. B. Gray, S. Lippard, J. Valentine, *Bioinorganic chemistry;* University Science Books, Mill Valley, California **1994**.

[8] A. Wasmus, P. Kindel, S. Mattussek, H.-H. Raspe, *Scan. J. Rheumatology* **1989**, *18*, 33–44. DOI: 10.3109/03009748909092611.

[9] B. Rosenberg, L. van Camp, T. Krigas, *Nature* **1965**, *205*, 698–699. DOI: 10.1038/205698a0.

[10] B. Rosenberg, *Interdiscip. Sci. Rev.* **1978**, *3*, 134–147. DOI: 10.1179/030801878791926119.

[11] B. Rosenberg, L. van Camp, J. E. Trosko, V. H. Mansour, *Nature* **1969**, *222*, 385–386. DOI: 10.1038/222385a0.

[12] B. Lippert. *Cisplatin: Chemistry and biochemistry of a leading anticancer drug;* Verlag Helvetica Chimica Acta; Wiley-VCH, Zürich, **1999**.

[13] a) Z. Guo, P. J. Sadler, *Angew. Chem. Int. Ed.* **1999**, *38*, 1512–1531. DOI: 10.1002/(SICI)1521-3773(19990601)38:11<1512::AID-ANIE1512>3.0.CO;2-Y;

b) N. P. E. Barry, P. J. Sadler, *Chem. Commun.* **2013**, *49*, 5106–5131. DOI: 10.1039/c3cc41143e.

[14] A. Brayfield, W. Martindale. *Martindale: The complete drug reference;* Pharmaceutical Press, London **2014**.

[15] M. Galanski, M. Jakupec, B. Keppler, *Curr. Med. Chem.* **2005**, *12*, 2075–2094. DOI: 10.2174/0929867054637626.

[16] R. Oun, Y. E. Moussa, N. J. Wheate, *Dalton Trans.* **2018**, *47*, 6645–6653. DOI: 10.1039/c8dt00838h.

[17] K. O. Alfarouk, C.-M. Stock, S. Taylor, M. Walsh, A. K. Muddathir, D. Verduzco, A. H. H. Bashir, O. Y. Mohammed, G. O. Elhassan, S. Harguindey, S. J. Reshkin, M. E. Ibrahim, C. Rauch, *Cancer Cell Int.* **2015**, *15*, 71. DOI: 10.1186/s12935-015-0221-1.

[18] S. Dasari, P. B. Tchounwou, *Eur. J. Pharm.* **2014**, *740*, 364–378. DOI: 10.1016/j.ejphar.2014.07.025.

[19] M. J. Cleare, J. D. Hoeschele, *Bioinorg.Chem.* **1973**, *2*, 187–210. DOI: 10.1016/S0006-3061(00)80249-5.

[20] K. M. Deo, D. L. Ang, B. McGhie, A. Rajamanickam, A. Dhiman, A. Khoury, J. Holland, A. Bjelosevic, B. Pages, C. Gordon, J. R. Aldrich-Wright, *Coordination Chem. Rev.* **2017**, *375*, 148-163. DOI: 10.1016/j.ccr.2017.11.014.

[21] W. Voigt, A. Dietrich, H.-J. Schmoll, *Pharm. Unserer Zeit* **2006**, *35*, 134–143. DOI: 10.1002/pauz.200500162.

[22] N. J. Wheate, S. Walker, G. E. Craig, R. Oun, *Dalton Trans.* **2010**, *39*, 8113–8127. DOI: 10.1039/c0dt00292e.

[23] S. Kaneko, J. Furuse, M. Kudo, K. Ikeda, M. Honda, Y. Nakamoto, M. Onchi, G. Shiota, O. Yokosuka, I. Sakaida, T. Takehara, Y. Ueno, K. Hiroishi, S. Nishiguchi, H. Moriwaki, K. Yamamoto, M. Sata, S. Obi, S. Miyayama, Y. Imai, *Hepatology research : the official journal of the Japan Society of Hepatology* **2012**, *42*, 523–542. DOI: 10.1111/j.1872-034X.2012.00981.x.

[24] K. R. Harrap, *Canc. Treat. Rev.* **1985**, *12*, 21–33. DOI: 10.1016/0305-7372(85)90015-5.

[25] Y. Kidani, K. Inagaki, M. Iigo, A. Hoshi, K. Kuretani, *J. Med. Chem.* **1978**, *21*, 1315–1318. DOI: 10.1021/jm00210a029.

[26] a) T. Okusaka, S. Okada, T. Nakanishi, S. Fujiyama, Y. Kubo, *Investigational new drugs* **2004**, *22*, 169–176. DOI: 10.1023/B:DRUG.0000011793.72775.d1; b) K. Tanaka, T. Kunimatsu, J. Shimakura, M. Hanada, *Development of Miriplatin, a Novel Antitumor Platinum for Hepatocellular Carcinoma, Sumitomo Kagaku* **2011**, *1*, 1-11.

[27] Webseite: Abgerufen am 26 Juli 2018, von clinicaltrials.gov

[28] D. Gibson, *Dalton Trans.* **2016**, *45*, 12983–12991. DOI: 10.1039/c6dt01414c.

[29] H. Choy, *Expert review of anticancer therapy* **2006**, *6*, 973–982. DOI: 10.1586/14737140.6.7.973.

[30] A.-M. Florea, D. Büsselberg, *Cancers* **2011**, *3*, 1351–1371. DOI: 10.3390/cancers3011351.

[31] G. Ferraro, L. Massai, L. Messori, A. Merlino, *Chem. Commun.* **2015**, *51*, 9436–9439. DOI: 10.1039/c5cc01751c.

[32] A. M. J. Fichtinger-Schepman, J. L. van der Veer, J. H. J. Den Hartog, P. H. M. Lohman, J. Reedijk, *Biochem.* **1985**, *24*, 707–713. DOI: 10.1021/bi00324a025.

[33] a) E. R. Jamieson, S. J. Lippard, *Chem. Rev.* **1999**, *99*, 2467–2498. DOI: 10.1021/cr980421n; b) J. Reedijk, *Chem. Commun.* **1996**, 801-806. DOI: 10.1039/cc9960000801.

[34] a) A. A. Hostetter, E. G. Chapman, V. J. DeRose, *J. Am. Chem. Soc.* **2009**, *131*, 9250–9257. DOI: 10.1021/ja809637e; b) E. G. Chapman, V. J. DeRose, *J. Am. Chem. Soc.* **2010**, *132*, 1946–1952. DOI: 10.1021/ja908419j; c) J. L. Podratz, A. M. Knight, L. E. Ta, N. P. Staff, J. M. Gass, K. Genelin, A. Schlattau, L. Lathroum, A. J. Windebank, *Neurobiol Dis.* **2011**, *41*, 661–668. DOI: 10.1016/j.nbd.2010.11.017; d) Z. Yang, L. M. Schumaker, M. J. Egorin, E. G. Zuhowski, Z. Guo, K. J. Cullen, Clin. Cancer. Res. **2006**, *12*, 5817–5825. DOI: 10.1158/1078-0432.CCR-06-1037.

[35] a) D. Wang, S. J. Lippard, *Nature reviews Drug discovery* **2005**, *4*, 307–320. DOI: 10.1038/nrd1691; b) A. Basu, S. Krishnamurthy, *Journal of Nucleic Acids* **2010**, *2010*. DOI: 10.4061/2010/201367.

[36] P. J. O'Dwyer, J. P. Stevenson, S. W. Johnson, *Drugs* **2000**, *59*, 19–27. DOI: 10.2165/00003495-200059004-00003.

[37] a) I. Ott, R. Gust, *Pharm. Unserer Zeit* **2006**, *35*, 124–133. DOI: 10.1002/pauz.200500161; b) K. J. Barnham, M. I. Djuran, P. d. S. Murdoch, J. D. Ranford, P. J. Sadler, *Inorg. Chem.* **1996**, *35*, 1065–1072. DOI: 10.1021/ic950973d; c) U. Frey, J. D. Ranford, P. J. Sadler, *Inorg. Chem.* **1993**, *32*, 1333–1340. DOI: 10.1021/ic00060a005.

[38] P. M. Bruno, Y. Liu, G. Y. Park, J. Murai, C. E. Koch, T. J. Eisen, J. R. Pritchard, Y. Pommier, S. J. Lippard, M. T. Hemann, *Nat. Med.* **2017**, *23*, 461–471. DOI: 10.1038/nm.4291.

[39] Fernelius, W. C., *Inorganic Synthesis, Volume II;* McGraw-Hill Book Company, New York **1946**.

[40] G. B. Kauffman, D. O. Cowan, *Inorg. Synth.* **1963**, 239-245.

[41] S. C. Dhara, *Indian J. Chem.* **1970**, *8*, 193-194.

[42] E. A. Pedrick, N. E. Leadbeater, *Inorg. Chem. Comm.* **2011**, *14*, 481–483. DOI: 10.1016/j.inoche.2011.01.005.

[43] A. Pasini, C. Caldiroia, S. Spinelli, M. Valsecchi, *Synth. React. Inorg. M.* **1993**, *23*, 1021–1060. DOI: 10.1080/15533179308016879.

[44] J. J. Wilson, S. J. Lippard, *Chem. Rev.* **2014**, *114*, 4470–4495. DOI: 10.1021/cr4004314.

[45] T. S. Chung, Y. M. Na, S. W. Kang, O.-S. Jung, Y.-A. Lee, *Transit. Met. Chem.* **2005**, *30*, 541–545. DOI: 10.1007/s11243-005-2653-2.

[46] Y.-A. Lee, K. H. Yoo, O.-S. Jung, *Bull. Chem. Soc. Jpn.* **2003**, *76*, 107–110. DOI: 10.1246/bcsj.76.107.

[47] J. Z. Zhang, E. Wexselblatt, T. W. Hambley, D. Gibson, *Chem. Commun.* **2012**, *48*, 847–849. DOI: 10.1039/c1cc16647f.

[48] J. Z. Zhang, P. Bonnitcha, E. Wexselblatt, A. V. Klein, Y. Najajreh, D. Gibson, T. W. Hambley, *Chemistry* **2013**, *19*, 1672–1676. DOI: 10.1002/chem.201203159.

[49] a) T. C. Johnstone, S. M. Alexander, J. J. Wilson, S. J. Lippard, *Dalton Trans.* **2015**, *44*, 119–129. DOI: 10.1039/c4dt02627f; b) R. J. Brandon, J. C. Dabrowiak, *J. Med. Chem.* **1984**, *27*, 861–865. DOI: 10.1021/jm00373a009.

[50] M. Bouché, G. Dahm, M. Wantz, S. Fournel, T. Achard, S. Bellemin-Laponnaz, *Dalton Trans.* **2016**, *45*, 11362–11368. DOI: 10.1039/c6dt01846g.

[51] S.-X. Guo, D. N. Mason, S. A. Turland, E. T. Lawrenz, L. C. Kelly, G. D. Fallon, B. M. Gatehouse, A. M. Bond, G. B. Deacon, A. R. Battle, T. W. Hambley, S. Rainone, L. K. Webster, C. Cullinane, *J. Inorg. Biochem.* **2012**, *115*, 226–239. DOI: 10.1016/j.jinorgbio.2012.07.016.

[52] M. S. Carle, G. K. Shimokura, G. K. Murphy, *Eur. J. Org. Chem.* **2016**, *2016*, 3930–3933. DOI: 10.1002/ejoc.201600714.

[53] F. Liu, W. Chen, *Eur. J. Inorg. Chem.* **2006**, *2006*, 1168–1173. DOI: 10.1002/ejic.200500878.

[54] a) R. Kizu, T. Nakanishi, K. Hayakawa, A. Matsuzawa, M. Eriguchi, Y. Takeda, N. Akiyama, T. Tashiro, Y. Kidani, *Cancer Chemother. Pharmacol.* **1999**, *43*, 97–105. DOI: 10.1007/s002800050869; b) C. M. Giandomenico, M. J. Abrams, B. A. Murrer, J. F. Vollano, M. I. Rheinheimer, S. B. Wyer, G. E. Bossard, J. D. Higgins, *Inorg. Chem.* **1995**, *34*, 1015–1021. DOI: 10.1021/ic00109a004.

[55] a) E. Gabano, M. Ravera, D. Osella, *Curr. Med. Chem.* **2009**, *16*, 4544–4580. DOI: 10.2174/092986709789760661; b) X. Wang, Z. Guo, *Chem. Soc. Rev.* **2013**, *42*, 202–224. DOI: 10.1039/c2cs35259a; c) J. S. Butler, P. J. Sadler, *Curr. Opin. Chem. Biol.* **2013**, *17*, 175–188. DOI: 10.1016/j.cbpa.2013.01.004.

[56] T. C. Johnstone, K. Suntharalingam, S. J. Lippard, *Chem. Rev.* **2016**, *116*, 3436–3486. DOI: 10.1021/acs.chemrev.5b00597.

[57] P. Liu, Y. Lu, X. Gao, R. Liu, D. Zhang-Negrerie, Y. Shi, Y. Wang, S. Wang, Q. Gao, *Chem. Commun.* **2013**, *49*, 2421–2423. DOI: 10.1039/c3cc38589b.

[58] M. Patra, T. C. Johnstone, K. Suntharalingam, S. J. Lippard, *Angew. Chem.* **2016**, *128*, 2596–2600. DOI: 10.1002/ange.201510551.

[59] a) S. Fortin, K. Brasseur, N. Morin, É. Asselin, G. Bérubé, *Eur. J. Med. Chem.* **2013**, *68*, 433–443. DOI: 10.1016/j.ejmech.2013.08.011; b) R. Gust, K. Niebler, H. Schönenberger, *J. Med. Chem.* **2005**, *48*, 7132–7144. DOI: 10.1021/jm050186i.

[60] M. W. Ndinguri, R. Solipuram, R. P. Gambrell, S. Aggarwal, R. P. Hammer, *Bioconjug. Chem.* **2009**, *20*, 1869–1878. DOI: 10.1021/bc900065r.

[61] X. Huang, R. Huang, S. Gou, Z. Wang, Z. Liao, H. Wang, *Bioconjug. Chem.* **2016**, *27*, 2132–2148. DOI: 10.1021/acs.bioconjchem.6b00353.

[62] E. Petruzzella, R. Sirota, I. Solazzo, V. Gandin, D. Gibson, *Chem. Sci.* **2018**, *9*, 4299–4307. DOI: 10.1039/c8sc00428e.

[63] E. E. Blatter, J. F. Vollano, B. S. Krishnan, J. C. Dabrowiak, *Biochem.* **1984**, *23*, 4817–4820. DOI: 10.1021/bi00316a001.

[64] a) M. D. Hall, H. R. Mellor, R. Callaghan, T. W. Hambley, *J. Med. Chem.* **2007**, *50*, 3403–3411. DOI: 10.1021/jm070280u; b) M. D. Hall, T. W. Hambley, *Coord. Chem. Rev.* **2002**, *232*, 49–67. DOI: 10.1016/S0010-8545(02)00026-7; c) E. Wexselblatt, D. Gibson, *J. Inorg. Biochem.* **2012**, *117*, 220–229. DOI: 10.1016/j.jinorgbio.2012.06.013.

[65] a) E. Petruzzella, J. P. Braude, J. R. Aldrich-Wright, V. Gandin, D. Gibson, *Angew. Chem. Int. Ed.* **2017**, *56*, 11539–11544. DOI: 10.1002/anie.201706739; b) J. Yang, X. Sun, W. Mao, M. Sui, J. Tang, Y. Shen, *Mol. Pharmaceutics* **2012**, *9*, 2793–2800. DOI: 10.1021/mp200597r; c) W. H. Ang, I. Khalaila, C. S. Allardyce, L. Juillerat-Jeanneret, P. J. Dyson, *J. Am. Chem. Soc.* **2005**, *127*, 1382–1383. DOI: 10.1021/ja0432618.

[66] S. Mukhopadhyay, C. M. Barnés, A. Haskel, S. M. Short, K. R. Barnes, S. J. Lippard, *Bioconjug. Chem.* **2008**, *19*, 39–49. DOI: 10.1021/bc070031k.

[67] S. Thota, D. A. Rodrigues, D. C. Crans, E. J. Barreiro, *J. Med. Chem.* **2018**. DOI: 10.1021/acs.jmedchem.7b01689.

[68] M. Adams, M. Hanif, C. G. Hartinger. In *Encyclopedia of Inorganic and Bioinorganic Chemistry*. Scott, Robert A. (Ed.); John Wiley & Sons, Chichester UK, **2011**; Vol. 4; pp 1–21.

[69] C. Roder, M. J. Thomson, *Drugs in R&D* **2015**, *15*, 13–20. DOI: 10.1007/s40268-015-0083-y.

[70] T. Tanaka, F. Hosoi, Y. Yamaguchi-Iwai, H. Nakamura, H. Masutani, S. Ueda, A. Nishiyama, S. Takeda, H. Wada, G. Spyrou, J. Yodoi, *EMBO J.* **2002**, *21*, 1695–1703. DOI: 10.1093/emboj/21.7.1695.

[71] R. Rubbiani, I. Kitanovic, H. Alborzinia, S. Can, A. Kitanovic, L. A. Onambele, M. Stefanopoulou, Y. Geldmacher, W. S. Sheldrick, G. Wolber, A. Prokop, S. Wölfl, I. Ott, *J. Med. Chem.* **2010**, *53*, 8608–8618. DOI: 10.1021/jm100801e.

[72] a) E. R. T. Tiekink, *Inflammopharmacology* **2008**, *16*, 138–142. DOI: 10.1007/s10787-007-0018-5; b) T. Lazarević, A. Rilak, Ž. D. Bugarčić, *Eur. J. Med. Chem.* **2017**, *142*, 8–31. DOI: 10.1016/j.ejmech.2017.04.007; c) C. I. Yeo, K. K. Ooi, E. R. T. Tiekink, *Molecules* **2018**, *23*, 1410-1436. DOI: 10.3390/molecules23061410.

[73] I. Ott, R. Gust, *Archiv der Pharmazie* **2007**, *340*, 117–126. DOI: 10.1002/ardp.200600151.

[74] G. Jaouen, A. Vessières, S. Top, *Chem. Soc. Rev.* **2015**, *44*, 8802–8817. DOI: 10.1039/c5cs00486a.

[75] D. Schlawe, A. Majdalani, J. Velcicky, E. Heßler, T. Wieder, A. Prokop, H.-G. Schmalz, *Angew. Chem.* **2004**, *116*, 1763–1766. DOI: 10.1002/ange.200353132.

[76] a) U. Ndagi, N. Mhlongo, M. E. Soliman, Drug Des. Devel. Ther. **2017**, *11*, 599–616. DOI: 10.2147/DDDT.S119488; b) S. Tardito, L. Marchio, *Curr. Med. Chem.* **2009**, *16*, 1325–1348. DOI: 10.2174/092986709787846532.

[77] F. E. Hahn, M. C. Jahnke, *Angew. Chem.* **2008**, *120*, 3166–3216. DOI: 10.1002/ange.200703883.

[78] K. M. Hindi, M. J. Panzner, C. A. Tessier, C. L. Cannon, W. J. Youngs, *Chem. Rev.* **2009**, *109*, 3859–3884. DOI: 10.1021/cr800500u.

[79] C. Boehme, G. Frenking, *J. Am. Chem. Soc.* **1996**, *118*, 2039–2046. DOI: 10.1021/ja9527075.

[80] D. Nemcsok, K. Wichmann, G. Frenking, *Organometallics* **2004**, *23*, 3640–3646. DOI: 10.1021/om049802j.

[81] W. A. Herrmann, *Angew. Chem. Int. Ed.* **2002**, *41*, 1290–1309. DOI: 10.1002/1521-3773(20020415)41:8<1290::AID-ANIE1290>3.0.CO;2-Y.

[82] a) R. H. Crabtree, *J. Organomet. Chem.* **2005**, *690*, 5451–5457. DOI: 10.1016/j.jorganchem.2005.07.099; b) C. M. Crudden, D. P. Allen, *Coord. Chem. Rev.* **2004**, *248*, 2247–2273. DOI: 10.1016/j.ccr.2004.05.013.

[83] a) N. Kuhn, A. Alsheikh, *Coord. Chem. Rev.* **2005**, *249*, 829–857. DOI: 10.1016/j.ccr.2004.10.003; b) P. L. Arnold, I. J. Casely, *Chem. Rev.* **2009**, *109*, 3599–3611. DOI: 10.1021/cr8005203; c) J. Huang, H.-J. Schanz, E. D. Stevens, S. P. Nolan, *Organometallics* **1999**, *18*, 2370–2375. DOI: 10.1021/om990054l.

[84] H.-W. Wanzlick, H.-J. Schönherr, *Angew. Chem. Int. Ed.* **1968**, *7*, 141–142. DOI: 10.1002/anie.196801412.

[85] A. J. Arduengo, R. L. Harlow, M. Kline, *J. Am. Chem. Soc.* **1991**, *113*, 361–363. DOI: 10.1021/ja00001a054.

[86] M. Scholl, S. Ding, C. W. Lee, R. H. Grubbs, *Org. Lett.* **1999**, *1*, 953–956. DOI: 10.1021/ol990909q.

[87] K. Öfele, *J. Organomet. Chem.* **1968**, *12*, 42-43. DOI: 10.1016/S0022-328X(00)88691-X.

[88] D. Enders, O. Niemeier, A. Henseler, *Chem. Rev.* **2007**, *107*, 5606–5655. DOI: 10.1021/cr068372z.

[89] G. C. Vougioukalakis, R. H. Grubbs, *Chem. Rev.* **2010**, *110*, 1746–1787. DOI: 10.1021/cr9002424.

[90] W. A. Herrmann, M. Elison, J. Fischer, C. Köcher, Artus, Georg R. J., *Angew. Chem. Int. Ed.* **1995**, *34*, 2371–2374. DOI: 10.1002/anie.199523711.

[91] E. A. B. Kantchev, C. J. O'Brien, M. G. Organ, *Angew. Chem. Int. Ed.* **2007**, *46*, 2768–2813. DOI: 10.1002/anie.200601663.

[92] a) V. Nair, S. Bindu, V. Sreekumar, *Angew. Chem.* **2004**, *116*, 5240–5245. DOI: 10.1002/ange.200301714; b) O. Navarro, N. Marion, J. Mei, S. P. Nolan, *Chemistry*, **2006**, *12*, 5142–5148. DOI: 10.1002/chem.200600283.

[93] L. Hintermann, *Beilstein J. Org. Chem.* **2007**, *3*, 1-5. DOI: 10.1186/1860-5397-3-22.

[94] N. R. Candeias, L. C. Branco, P. M. P. Gois, C. A. M. Afonso, A. F. Trindade, *Chem. Rev.* **2009**, *109*, 2703–2802. DOI: 10.1021/cr800462w.

[95] P. Fournari, P. d. Cointet, E. Laviron, *Bull. Soc. Chim. Fr.* **1968**, 2438–2446.

[96] a) Tai-Yong Lv, Lei Yang, Yin-Song Zhao, Fei-Jie Song, Jing-Bo Lan, Jing-Song You, Ge Gao, *Chinese Chemical Letters* **2013**, *24*, 773–776; b) E. A. Merritt, B. Olofsson, *Angew. Chem. Int. Ed.* **2009**, *48*, 9052–9070. DOI: 10.1002/anie.200904689.

[97] E. Alcalde, I. Dinarès, S. Rodríguez, C. Garcia de Miguel, *Eur. J. Org. Chem.* **2005**, *2005*, 1637–1643. DOI: 10.1002/ejoc.200400453.

[98] a) J. Liu, J. Chen, J. Zhao, Y. Zhao, L. Li, H. Zhang, *Synthesis* **2003**, 2661–2666. DOI: 10.1055/s-2003-42444; b) L. Benhamou, E. Chardon, G. Lavigne, S. Bellemin-Laponnaz, V. César, *Chem. Rev.* **2011**, *111*, 2705–2733. DOI: 10.1021/cr100328e; c) F. M. Rivas, U. Riaz, A. Giessert, J. A. Smulik, S. T. Diver, *Org. Lett.* **2001**, *3*, 2673-2676. DOI: 10.1021/ol016254m.

[99] A. M. van Leusen, J. Wildeman, O. H. Oldenziel, *J. Org. Chem.* **1977**, *42*, 1153–1159. DOI: 10.1021/jo00427a012.

[100] N. Kuhn, T. Kratz, *Synthesis* **1993**, *6*, 561–562. DOI: 10.1055/s-1993-25902.

[101] H.-W. Wanzlick, F. Esser, H.-J. Kleiner, *Chem. Ber.* **1963**, *96*, 1208–1212. DOI: 10.1002/cber.19630960505.

[102] H. M. J. Wang, I. J. B. Lin, *Organometallics* **1998**, *17*, 972–975. DOI: 10.1021/om9709704.

[103] a) J. C. Garrison, W. J. Youngs, *Chem. Rev.* **2005**, *105*, 3978–4008. DOI: 10.1021/cr050004s; b) I. J. B. Lin, C. S. Vasam, *Comm. Inorg. Chem.* **2004**, *25*, 75–129. DOI: 10.1080/02603590490883652.

[104] Webseite: Abgerufen 27. Januar 2019, von scifinder.cas.org.

[105] L. Oehninger, R. Rubbiani, I. Ott, *Dalton Trans.* **2013**, *42*, 3269–3284. DOI: 10.1039/c2dt32617e.

[106] T. Zou, C.-N. Lok, P.-K. Wan, Z.-F. Zhang, S.-K. Fung, C.-M. Che, *Curr. Opin. Chem. Biol.* **2018**, *43*, 30–36. DOI: 10.1016/j.cbpa.2017.10.014.

[107] W. Liu, R. Gust, *Coord. Chem. Rev.* **2016**, *329*, 191–213. DOI: 10.1016/j.ccr.2016.09.004.

[108] B. Cetinkaya, E. Cetinkaya, H. Küçükbay, R. Durmaz, *Arzneim.-Forsch./ Drug Res.* **1996**, *46*, 821–823.

[109] a) A. Kascatan-Nebioglu, A. Melaiye, K. Hindi, S. Durmus, M. J. Panzner, L. A. Hogue, R. J. Mallett, C. E. Hovis, M. Coughenour, S. D. Crosby, A. Milsted, D. L. Ely, C. A. Tessier, C. L. Cannon, W. J. Youngs, *J. Med. Chem.* **2006**, *49*, 6811–6818. DOI: 10.1021/jm060711t; b) S. Roland, C. Jolivalt, T. Cresteil, L. Eloy, P. Bouhours, A. Hequet, V. Mansuy, C. Vanucci, J.-M. Paris, *Chemistry* **2011**, *17*, 1442–1446. DOI: 10.1002/chem.201002812; c) P. O. Asekunowo, R. A. Haque, M. R. Razali, *Rev.Inorg.Chem.* **2017**, *37*, 29-50. DOI: 10.1515/revic-2016-0007.

[110] a) İ. Özdemir, A. Denizci, H. T. Öztürk, B. Çetinkaya, *Appl. Organometal. Chem.* **2004**, *18*, 318–322. DOI: 10.1002/aoc.668; b) I. Ozdemir, N. Temelli, S. Günal, S. Demir, *Molecules* **2010**, *15*, 2203–2210. DOI: 10.3390/molecules15042203.

[111] S. A. Patil, S. A. Patil, R. Patil, R. S. Keri, S. Budagumpi, G. R. Balakrishna, M. Tacke, *Future Med. Chem.* **2015**, *7*, 1305–1333. DOI: 10.4155/fmc.15.61.

[112] B. Bertrand, L. Stefan, M. Pirrotta, D. Monchaud, E. Bodio, P. Richard, P. Le Gendre, E. Warmerdam, M. H. de Jager, G. M. M. Groothuis, M. Picquet, A. Casini, *Inorg. Chem.* **2014**, *53*, 2296–2303. DOI: 10.1021/ic403011h.

[113] J. K. Muenzner, B. Biersack, H. Kalie, I. C. Andronache, L. Kaps, D. Schuppan, F. Sasse, R. Schobert, *ChemMedChem* **2014**, *9*, 1195–1204. DOI: 10.1002/cmdc.201400049.

[114] F. Hackenberg, H. Müller-Bunz, R. Smith, W. Streciwilk, X. Zhu, M. Tacke, *Organometallics* **2013**, *32*, 5551–5560. DOI: 10.1021/om400819p.

[115] R. Rubbiani, S. Can, I. Kitanovic, H. Alborzinia, M. Stefanopoulou, M. Kokoschka, S. Mönchgesang, W. S. Sheldrick, S. Wölfl, I. Ott, *J. Med. Chem.* **2011**, *54*, 8646–8657. DOI: 10.1021/jm201220n.

[116] I. Ott, *Coord. Chem. Rev.* **2009**, *253*, 1670–1681. DOI: 10.1016/j.ccr.2009.02.019.

[117] a) B. Bertrand, A. Casini, *Dalton Trans.* **2014**, *43*, 4209–4219. DOI: 10.1039/C3DT52524D; b) J. J. Yan, A. L.-F. Chow, C.-H. Leung, R. W.-Y. Sun, D.-L. Ma, C.-M. Che, *Chem. Commun.* **2010**, *46*, 3893–3895. DOI: 10.1039/C001216E;

[118] S. B. Aher, P. N. Muskawar, K. Thenmozhi, P. R. Bhagat, *Eur.n J. Med. Chem.* **2014**, *81*, 408–419. DOI: 10.1016/j.ejmech.2014.05.036.

[119] a) D. Brissy, M. Skander, H. Jullien, P. Retailleau, A. Marinetti, *Org. Lett.* **2009**, *11*, 2137–2139. DOI: 10.1021/ol900724z; b) K. Cavell, *Dalton Trans.* **2008**, 6676–6685. DOI: 10.1039/b811449h.

[120] T. Strassner, *Acc. Chem. Res.* **2016**, *49*, 2680–2689. DOI: 10.1021/acs.accounts.6b00240.

[121] R. Wai-Yin Sun, A. Lok-Fung Chow, X.-H. Li, J. J. Yan, S. Sin-Yin Chui, C.-M. Che, *Chem. Sci.* **2011**, *2*, 728. DOI: 10.1039/c0sc00593b.

[122] M. Skander, P. Retailleau, B. Bourrié, L. Schio, P. Mailliet, A. Marinetti, *J. Med. Chem.* **2010**, *53*, 2146–2154. DOI: 10.1021/jm901693m.

[123] M. Chtchigrovsky, L. Eloy, H. Jullien, L. Saker, E. Ségal-Bendirdjian, J. Poupon, S. Bombard, T. Cresteil, P. Retailleau, A. Marinetti, *J. Med. Chem.* **2013**, *56*, 2074–2086. DOI: 10.1021/jm301780s.

[124] N. Estrada-Ortiz, F. Guarra, I. A. M. de Graaf, L. Marchetti, M. H. de Jager, G. M. M. Groothuis, C. Gabbiani, A. Casini, *ChemMedChem* **2017**, *12*, 1429–1435. DOI: 10.1002/cmdc.201700316.

[125] S. D. Adhikary, D. Bose, P. Mitra, K. D. Saha, V. Bertolasi, J. Dinda, *New J. Chem.* **2012**, *36*, 759. DOI: 10.1039/c2nj20928d.

[126] M. Bouché, G. Dahm, A. Maisse-François, T. Achard, S. Bellemin-Laponnaz, *Eur. J. Inorg. Chem.* **2016**, *2016*, 2828–2836. DOI: 10.1002/ejic.201600296.

[127] M. Bouché, A. Bonnefont, T. Achard, S. Bellemin-Laponnaz, *Dalton Trans.* **2018**, *47*, 11491–11502. DOI: 10.1039/c8dt02113a.

[128] a) L. Oehninger, M. Stefanopoulou, H. Alborzinia, J. Schur, S. Ludewig, K. Namikawa, A. Muñoz-Castro, R. W. Köster, K. Baumann, S. Wölfl, W. S. Sheldrick, I. Ott, *Dalton Trans.* **2013**, *42*, 1657–1666. DOI: 10.1039/C2DT32319B; b) S. Ray, R. Mohan, J. K.

Singh, M. K. Samantaray, M. M. Shaikh, D. Panda, P. Ghosh, *J. Am. Chem. Soc.* **2007**, *129*, 15042–15053. DOI: 10.1021/ja075889z; c) Y. Gothe, T. Marzo, L. Messori, N. Metzler-Nolte, *Chem. Commun.* **2015**, *51*, 3151–3153. DOI: 10.1039/C4CC10014J.

[129] J. K. Muenzner, T. Rehm, B. Biersack, A. Casini, I. A. M. de Graaf, P. Worawutputtapong, A. Noor, R. Kempe, V. Brabec, J. Kasparkova, R. Schobert, *J. Med. Chem.* **2015**, *58*, 6283–6292. DOI: 10.1021/acs.jmedchem.5b00896.

[130] T. Rehm, M. Rothemund, A. Bär, T. Dietel, R. Kempe, H. Kostrhunova, V. Brabec, J. Kasparkova, R. Schobert, *Dalton Trans.* **2018**, *47*, 17367–17381. DOI: 10.1039/c8dt03360a.

[131] T. Rehm, M. Rothemund, J. K. Muenzner, A. Noor, R. Kempe, R. Schobert, *Dalton Trans.* **2016**, *45*, 15390–15398. DOI: 10.1039/c6dt02350a.

[132] C. P. Newman, R. J. Deeth, G. J. Clarkson, J. P. Rourke, *Organometallics* **2007**, *26*, 6225–6233. DOI: 10.1021/om700671y.

[133] S. Fantasia, A. Pasini, S. P. Nolan, *Dalton Trans.* **2009**, 8107–8110. DOI: 10.1039/B911164F.

[134] L. C. Lewis-Alleyne, B. S. Bassil, T. Böttcher, G.-V. Röschenthaler, *Dalton Trans.* **2014**, *43*, 15700–15703. DOI: 10.1039/C4DT02214A.

[135] R. G. Kenny, C. J. Marmion, *Chem. Rev.* **2019**, *119*, 1058-1137. DOI: 10.1021/acs.chemrev.8b00271.

[136] T. Rehm, M. Rothemund, T. Dietel, R. Kempe, R. Schobert, *Dalton Trans.* **2019**, , 48, 16358-16365. DOI: 10.1039/c9dt02438g.

4 PUBLIKATIONEN

4.1 DARSTELLUNG DES EIGENANTEILS

Die in dieser Arbeit vorgestellten Publikationen wurden in Kooperation mit anderen Mitarbeitern der Universität Bayreuth, sowie mit Wissenschaftlern anderer Institutionen erarbeitet. Im folgenden Kapitel sollen die jeweiligen Anteile an den einzelnen Veröffentlichungen genauer beschrieben werden.

4.1.1 ZU PUBLIKATION I

Veröffentlicht im *Journal of Medicinal Chemistry* **2015**, *58*, 6283−6292 (DOI: 10.1021/acs.jmedchem.5b00896) unter dem Titel:

„Adjusting the DNA Interaction and Anticancer Activity of Pt(II) N-Heterocyclic Carbene Complexes by Steric Shielding of the Trans Leaving Group“

Von den Autoren:
Julienne K. Münzner, Tobias Rehm, Bernhard Biersack, Angela Casini, Inge A. M. de Graaf, Pawida Worawutputtapong, Awal Noor, Rhett Kempe, Viktor Brabec, Jana Kasparkova und *Rainer Schobert*

Zu dieser Arbeit wurden die Komplexe **3a**-**d** von mir synthetisiert, aufgereinigt sowie charakterisiert. Die Synthese von Verbindung **2** wurde erstmals von Dr. Bernhard Biersack durchgeführt, der zusammen mit Prof. Rainer Schobert auch bei Planung der Synthese unterstützt hat sowie bei der Verfassung der Publikation involviert war. Die Erstellung des Manuskripts erfolgte in Zusammenarbeit mit Dr. Julienne Münzner, auf die auch der größte Teil der biologischer Assays zurück geht. Die Arbeitsgruppen um Prof. Viktor Brabec, Prof. Jana Kasparkova und Prof. Angela Casini untersuchten die detaillierte DNA-Bindung bzw. Nephrotoxizität, während Dr. Awal Noor und Prof. Rhett Kempe die Kristallstrukturen beisteuerten.

4.1.2 ZU PUBLIKATION II

Veröffentlicht in *Dalton Transactions* **2018**, *47*, 17367 (DOI: 10.1039/c8dt03360a) unter dem Titel:

„N,N-Dialkylbenzimidazol-2-ylidene platinum complexes – effects of alkyl residues and ancillary cis-ligands on anticancer activity“

Von den Autoren:

Tobias Rehm, Matthias Rothemund, Alexander Bär, Thomas Dietel, Rhett Kempe, Hana Kostrhunova, Viktor Brabec, Jana Kasparkova und *Rainer Schobert*

Diese Publikation wurde gemeinsam mit Matthias Rothemund verfasst, der zudem die biochemischen Untersuchungen federführend übernahm. Unterstützung dazu kam von Dr. Hana Kostrhunova, Prof. Jana Kasparkova und Prof. Viktor Brabec, welche die Aufnahme der Komplexe sowie Art und Kinetik der DNA-Bindung weitergehend untersuchten. Planung und Durchführung sämtlicher Synthesen wurden von mir durchgeführt, ebenso wie die spektroskopische Untersuchung und Charakterisierung der zwölf neuen Verbindungen. Um für ausführlichere Untersuchungen genügend Substanz zur Verfügung zu haben, wurden einige der Komplexe von Alexander Bär nachträglich erneut synthetisiert. Kristallstrukturen aller drei Komplextypen konnten dank Dr. Thomas Dietel und Prof. Rhett Kempe gewonnen werden. Prof. Rainer Schobert war in stetigen wissenschaftlichen Diskussionen, sowie bei der Verfassung, Korrektur und Revision der Publikation involviert.

4.1.3 ZU PUBLIKATION III

Veröffentlicht in *Dalton Transactions* **2016**, *45*, 15390 (DOI: 10.1039/c6dt02350a) unter dem Titel:

„Novel cis-[(NHC)^1(NHC)^2(L)Cl]platinum(II) complexes – synthesis, structures, and anticancer activities“

Von den Autoren:

Tobias Rehm, Matthias Rothemund, Julienne K. Münzner, Awal Noor, Rhett Kempe und *Rainer Schobert*

Die Synthesestrategie hin zu neuartigen *cis*-[Pt^{II}Cl$_2$(NHC)^1(NHC)^2]-Komplexen wurde von mir entwickelt. Ebenso wurden sämtliche Synthesen, die spektroskopischen Untersuchungen und die Charakterisierung der zehn neuen Verbindungen von mir durchgeführt. Die Untersuchung der zytotoxischen Eigenschaften und DNA-Interaktionen stammen von Matthias Rothemund und Dr. Julienne Münzner. Kristallstrukturen wurden erneut von Dr. Awal Noor und Prof. Rhett Kempe beigesteuert. Prof. Rainer Schobert war in stetigen wissenschaftlichen Diskussionen, sowie bei der Verfassung, Korrektur und Revision der Publikation involviert.

4.1.4 ZU PUBLIKATION IV

Angenommen von *Dalton Transactions* **2019**, 48, 16358-16365 (DOI: 10.1039/c9dt02438g) unter dem Titel:

„Synthesis, structures and cytotoxic effects in vitro of cis- and trans-[$Pt^{IV}Cl_4(NHC)_2$] complexes and their Pt^{II} precursors“

Von den Autoren:

Tobias Rehm, Matthias Rothemund, Thomas Dietel, Rhett Kempe und *Rainer Schobert*

Die Synthese der Pt^{II} und Pt^{IV}-Komplexe wurde, ebenso wie die weiterführenden Oxidationsversuche, spektroskopische Untersuchungen und Charakterisierung der elf neuen Verbindungen, von mir durchgeführt. Die Untersuchung der zytotoxischen Eigenschaften stammen von Matthias Rothemund. Kristallstrukturen wurden von Dr. Thomas Dietel und Prof. Rhett Kempe beigesteuert. Prof. Rainer Schobert war an den stetigen wissenschaftlichen Diskussionen, sowie bei der Verfassung, Korrektur und Revision der der Publikation beteiligt.

4.2 PUBLIKATION I

„Adjusting the DNA Interaction and Anticancer Activity of Pt(II) N-Heterocyclic Carbene Complexes by Steric Shielding of the Trans Leaving Group“

Journal of Medicinal Chemistry **2015**, *58*, 6283−6292

Julienne K. Muenzner,[†] Tobias Rehm,[†] Bernhard Biersack,[†] Angela Casini,[‡] Inge A. M. de Graaf,[‡] Pawida Worawutputtapong,[‡] Awal Noor,[§] Rhett Kempe,[§] Viktor Brabec,[∥] Jana Kasparkova,[⊥] and Rainer Schobert[*,†]

[†]Organic Chemistry Laboratory, [§]Lehrstuhl für Anorganische Chemie II (Catalyst Design), University Bayreuth, Universitaetsstrasse 30, 95440 Bayreuth, Germany

[‡]Department of Pharmacokinetics, Toxicology and Targeting, Research Institute of Pharmacy, University of Groningen, Antonius Deusinglaan 1, 9713 AV Groningen, The Netherlands

[∥]Institute of Biophysics, Academy of Sciences of the Czech Republic, CZ-61265 Brno, Czech Republic

[⊥]Department of Biophysics, Faculty of Science, Palacky University, 17. listopadu 12, CZ-77146 Olomouc, Czech Republic

Corresponding Author

*E-mail: Rainer.Schobert@uni-bayreuth.de. Fax: +49 (0)921552671. Phone: +49 (0)921 552679.

Journal of Medicinal Chemistry

Article

pubs.acs.org/jmc

Adjusting the DNA Interaction and Anticancer Activity of Pt(II) N-Heterocyclic Carbene Complexes by Steric Shielding of the Trans Leaving Group

Julienne K. Muenzner,[†] Tobias Rehm,[†] Bernhard Biersack,[†] Angela Casini,[‡] Inge A. M. de Graaf,[‡] Pawida Worawutputtapong,[‡] Awal Noor,[§] Rhett Kempe,[§] Viktor Brabec,[∥] Jana Kasparkova,[⊥] and Rainer Schobert*[,†]

[†]Organic Chemistry Laboratory, [§]Lehrstuhl fuer Anorganische Chemie II (Catalyst Design), University Bayreuth, Universitaetsstrasse 30, 95440 Bayreuth, Germany

[‡]Department of Pharmacokinetics, Toxicology and Targeting, Research Institute of Pharmacy, University of Groningen, Antonius Deusinglaan 1, 9713 AV Groningen, The Netherlands

[∥]Institute of Biophysics, Academy of Sciences of the Czech Republic, CZ-61265 Brno, Czech Republic

[⊥]Department of Biophysics, Faculty of Science, Palacky University, 17. listopadu 12, CZ-77146 Olomouc, Czech Republic

Supporting Information

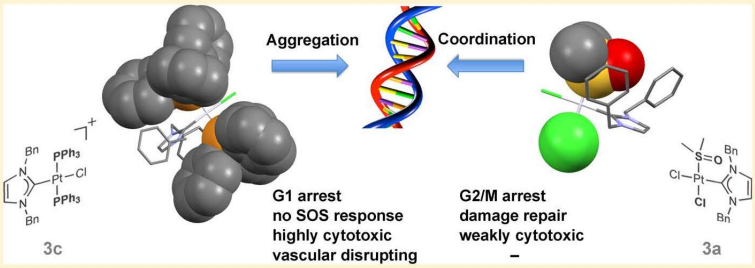

ABSTRACT: Five platinum(II) complexes bearing a (1,3-dibenzyl)imidazol-2-ylidene ligand but different leaving groups trans to it were examined for cytotoxicity, DNA and cell cycle interference, vascular disrupting properties, and nephrotoxicity. The cytotoxicity of complexes **3a–c** increased with the steric shielding of their leaving chloride ligand, and complex **3c**, featuring two triphenylphosphanes, was the most efficacious, with submicromolar IC_{50} concentrations. Complexes **3a–c** interacted with DNA in electrophoretic mobility shift and ethidium bromide binding assays. The cationic complex **3c** did not bind coordinatively to DNA but led to its aggregation, damage that is not amenable to the usual repair mechanisms. Accordingly, it arrested the cell cycle of melanoma cells in G1 phase, whereas *cis*-dichlorido[(1,3-dibenzyl)imidazol-2-ylidene](dimethyl sulfoxide) platinum(II) **3a** induced G2/M phase arrest. Complex **3c** also disrupted the blood vessels in the chorioallantoic membrane of fertilized chicken eggs. *Ex vivo* studies using precision-cut tissue slices suggested the nephrotoxicities of **3a–c** to be clinically manageable.

INTRODUCTION

Since the discovery of its antitumor activity in the late 1960s by Rosenberg et al.,[1] cisplatin has become one of the leading drugs in cancer chemotherapy. Only two additional platinum(II) drugs, carboplatin and oxaliplatin, have been approved in the US and EU for the treatment of certain forms of cancer.[2−4] These complexes are known to interact with DNA as their main cellular target and to form DNA adducts by coordination of the *cis*-$[Pt(R\text{-}NH_2)_2]$ fragment to the N-7 atom of purine bases, preferentially guanine.[2,4] The formation of intra- or interstrand cross-links leads to an impairment of DNA replication and transcription, G2/M phase cell cycle arrest, and, eventually, cancer cell apoptosis. However, the clinical application of platinum drugs is associated with unwanted side effects such as nephrotoxicity, ototoxicity, and neurotoxicity.[4−6] Resistance, both inherent and acquired, is another common problem.[3,4] A host of further platinum complexes was synthesized with the intention of overcoming or at least ameliorating the negative aspects of platinum chemotherapy, among them are compounds with trans coordination at the platinum center, complexes of platinum(IV), and heteronuclear complexes. In recent years, antitumoral complexes of other transition metals, including gold, silver, palladium, copper, rhodium, and ruthenium, bearing N-heterocyclic carbene (NHC) ligands have come to the fore.[7−11] This is, in part, owed to the stability of these Wanzlick-type carbenes and to the possibility of varying their substituents for pharmacological optimization. Various modes of action were

Received: June 10, 2015
Published: July 16, 2015

DOI: 10.1021/acs.jmedchem.5b00896
J. Med. Chem. 2015, 58, 6283−6292

identified such as interference with cell cycle progression, mitochondrial function, or DNA repair.[7−13] DNA is not necessarily a target any more, not even for platinum(II) complexes.[14,15] Herein, we report five new Pt(II) NHC complexes, their crystal structures, the dependency of their DNA interactions and anticancer/antivascular properties on the nature and position of their ligands, and their nephrotoxicities in an *ex vivo* rat model.

RESULTS AND DISCUSSION

Complex Syntheses and Structures. On the basis of protocols by Newman et al.,[16] we prepared five new [(1,3-dibenzyl)imidazol-2-yl]platinum(II) carbene complexes (Scheme 1). The known silver carbene complex **1**[17,18] was

Scheme 1. Synthesis of Platinum(II) NHC Complexes 2 and 3a−d[a]

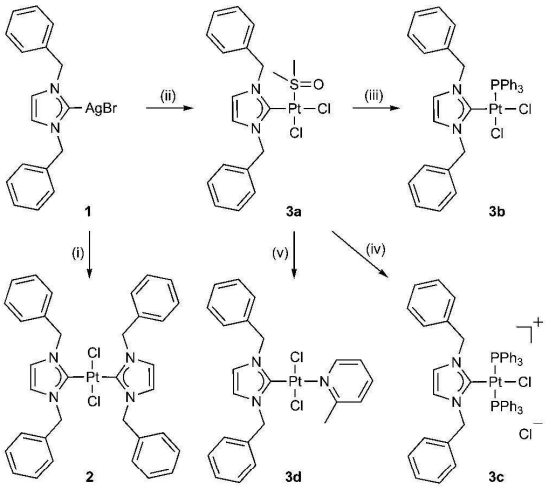

[a]Reagents and conditions: (i) 0.5 equiv K_2PtCl_4, CH_2Cl_2, rt, 24 h; (ii) K_2PtCl_4, DMSO, 60 °C, 24 h; (iii) 1 equiv PPh_3, CH_2Cl_2, rt, 1.5 h; (iv) 5 equiv PPh_3, CH_2Cl_2, rt, 30 min; (v) 2-picoline, CH_2Cl_2, rt, 6 days.

reacted with one-half an equivalent of K_2PtCl_4 in dichloromethane to give *trans*-$(NHC)_2PtCl_2$ complex **2**. The completion of this transmetalation was monitored by the upfield shift of the ^{13}C NMR signal of the carbene C atom from 181.3 ppm in complex **1** to 166.0 ppm in complex **2**. *cis*-(NHC)(DMSO)$PtCl_2$ complex **3a** was obtained from reaction of complex **1** with one equivalent of K_2PtCl_4 in DMSO at 60 °C. Its ^1H NMR spectrum showed equivalent imidazole and DMSO signals, whereas the benzyl protons were inequivalent and split into two doublets, 0.06 ppm apart and coupling with $^2J_{AB}$ = 15 Hz. This confirms the cis configuration of NHC and DMSO ligands as well as a perpendicular orientation of the imidazole ring relative to the plane spanned by the $PtCl_2$(DMSO) fragment (Figure 1). The ^{13}C NMR resonance of the carbene C atom of **3a** lay at 144.9 ppm, and the ^{195}Pt spectrum showed a signal at 962 ppm. The DMSO ligand of **3a** was readily replaced upon reaction with one equivalent of triphenylphosphane in dichloromethane at room temperature to afford *cis*-(NHC)$(PPh_3)PtCl_2$ complex **3b**, which was precipitated by addition of *n*-hexane. Its ^1H NMR spectrum showed the benzylic protons as two doublets, 1.32 ppm apart and coupling with $^2J_{AB}$ = 14 Hz. The ^{13}C NMR signal of the carbene C atom appeared as a doublet at 149.9 ppm with $^2J_{CP}$ = 8.1 Hz; the ^{195}Pt spectrum revealed a doublet at 504 ppm with $^1J_{PtP}$ = 3915 Hz. This $^{31}P-^{195}Pt$ coupling was also visible in the ^{31}P NMR for the signal at 8.49 ppm with $^1J_{PPt}$ = 3894 Hz. The ionic bis(triphenylphosphane) complex **3c** was obtained by adding a 5-fold excess of PPh_3 to the DMSO precursor **3a** in dichloromethane. After 30 min at room temperature, *n*-hexane was added to precipitate the pure product complex **3c**. Extended reaction periods (>5 h) led to formation of *cis*-dichloridobis(triphenylphosphane)platinum(II).

The benzylic protons gave rise to a singlet in the ^1H NMR spectrum of **3c**, which proves that the two phosphane ligands stand trans to each other. Their presence is also indicated by triplets in the ^{13}C NMR spectrum for the carbene C atom at 145.0 ppm with $^2J_{CP}$ = 10 Hz and for the platinum in the ^{195}Pt NMR spectrum at 159.9 ppm with $^1J_{PtP}$ = 2503 Hz. The corresponding $^{31}P-^{195}Pt$ coupling in the ^{31}P NMR for the signal at 17.5 ppm was $^1J_{PPt}$ = 2503 Hz. Complex **3d** was obtained from reaction of **3a** with 2-picoline. Integrations and the singlet signal for the benzylic hydrogens in the ^1H NMR spectrum confirm **3d** to be the *trans*-(NHC)(2-picoline)$PtCl_2$ complex. Figure 1 depicts the benzylic proton signals in the ^1H NMR spectra of complexes **1** and **3a−c**.

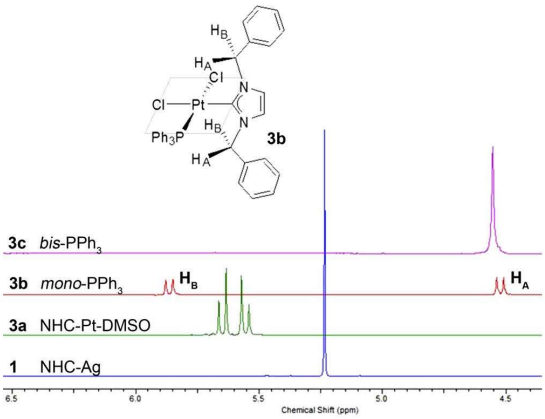

Figure 1. Benzylic proton signals in ^1H NMR spectra of complexes **1** and **3a−c**.

Crystals suitable for X-ray diffraction analyses were grown by slow infusion of hexane into saturated solutions of **3a** or **3b** in dichloromethane and **3c** in chloroform kept at 0 °C. Figure 2 shows the molecular structures. The characteristic bond lengths and angles were quite similar for all three complexes. The distances between the metal and the carbene carbon atoms C1 were in the range of 1.95−1.97 Å, and those between the metal and the leaving chloride Cl1 were about 2.35 Å. The C1−Pt−Cl1 angles were in the range of 174° (**3b**) to 177° (**3a**, **3c**). However, the potential leaving chloride Cl1 gets distinctly more shielded when going from **3a** to **3b** to **3c**.

Biological Evaluation: Cancer Cell Growth Inhibition. Complexes **2** and **3a−d** were screened for antiproliferative activity against a panel of seven cancer cell lines using the MTT assay.[19] All compounds showed dose-dependent inhibition of cell growth, with IC_{50} values mainly in the low micromolar range even against cisplatin-resistant cell lines such as HT-29 colon carcinoma.[20,21] Table 1 summarizes the IC_{50} values calculated

DOI: 10.1021/acs.jmedchem.5b00896
J. Med. Chem. 2015, 58, 6283−6292

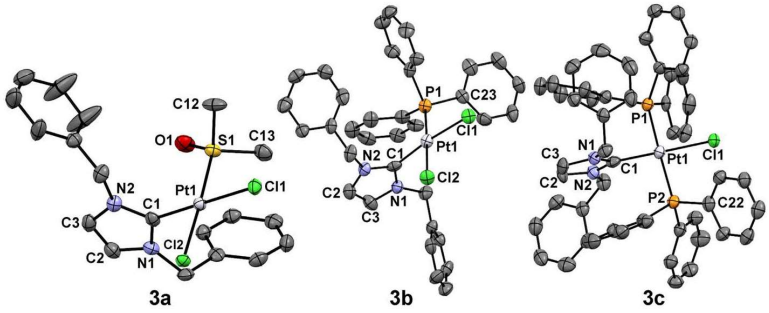

Figure 2. Molecular structures of chloridoplatinum(II) carbene complexes **3a–c** (cation only) as thermal ellipsoid representations at 50% probability level showing the atomic numbering schemes (H atoms omitted). Selected bond lengths [Å] and angles [deg]: **3a**: Pt1–C1 1.972(8), Pt1–Cl1 2.357(2), Pt1–Cl2 2.339(2), Pt1–S1 2.205(2), C1–N1 1.35(1), C1–N2 1.34(1), C2–N1 1.36(1), C3–N2 1.38(1), C1–Pt1–Cl1 177.6(2), S1–Pt1–Cl2 177.58(6), C1–Pt1–S1 90.3(2); **3b**: Pt1–C1 1.95(1), Pt1–Cl1 2.349(3), Pt1–Cl2 2.360(3), Pt1–P1 2.236(3), C1–N1 1.35(1), C1–N2 1.37(1), C2–N2 1.39(1), C3–N1 1.39(1), P1–C23 1.81(1), C1–Pt1–Cl1 173.5(3), P1–Pt1–Cl2 178.0(1), C1–Pt1–P1 94.0(3); **3c**: Pt1–C1 1.975(6), Pt1–Cl1 2.350(1), Pt1–P1 2.326(1), Pt1–P2 2.324(2), C1–N1 1.35(1), C1–N2 1.358(8), C2–N2 1.377(9), C3–N1 1.388(7), P2–C22 1.808(7), C1–Pt1–Cl1 177.3(2), P1–Pt1–P2 174.06(6), C1–Pt1–P1 87.59(6), C1–Pt1–P2 89.90(6).

Table 1. Inhibitory Concentrations[a] IC_{50} [μM] of Cisplatin and Complexes 2 and 3a–d when Applied to Human Cancer Cell Lines and Fibroblasts

compound/cell line	2	3a	3b	3c	3d	cisplatin
518A2	12.0 ± 0.3	27.7 ± 1.2	7.5 ± 0.4	0.32 ± 0.02	11.4 ± 0.5	5.3 ± 0.4
Panc-1	20.4 ± 1.3	20.6 ± 0.3	7.7 ± 0.5	0.32 ± 0.01	5.1 ± 0.3	4.8 ± 0.7
MCF-7/Topo	7.7 ± 0.7	31.2 ± 1.2	3.9 ± 0.3	0.15 ± 0.01	5.1 ± 0.2	10.6 ± 0.7
KB-V1/Vbl	>50	>50	4.5 ± 0.5	2.1 ± 0.2	8.6 ± 1.4	>100
HCT-116	11.3 ± 0.7	18.0 ± 1.4	6.7 ± 0.4	0.28 ± 0.06	5.9 ± 1.1	5.0 ± 0.6
HT-29	8.4 ± 0.3	22.7 ± 0.7	9.6 ± 0.4	0.85 ± 0.05	42.2 ± 4.8	>100
DLD-1	14.7 ± 3.4	27.0 ± 1.6	2.5 ± 0.4	0.92 ± 0.09	32.3 ± 3.4	32.6 ± 2.4
CCD18Co	35.8 ± 11.4	>50	14.5 ± 2.1	2.8 ± 0.1	>50	>100

[a]Values derived from dose–response curves obtained by measuring the percentage of viable cells relative to that of untreated controls after 72 h of incubation using the MTT assay; human cancer cell lines: 518A2 melanoma, Panc-1 pancreatic ductular adenocarcinoma, MCF-7/Topo breast adenocarcinoma, KB-V1/Vbl cervix carcinoma, HCT-116 and HT-29 colon carcinoma, and DLD-1 colorectal adenocarcinoma; nonmalignant cell line: CCD18Co human colon fibroblasts. Values represent means of four experiments ± SD.

from dose–response curves. The antiproliferative effects were dependent on the nature and configuration of the auxiliary non-NHC ligands. Biscarbene complex **2** was active, with low-double-digit micromolar IC_{50} values across the panel. *cis*-Dichlorido-(monophosphane) complex **3b** and *trans*-dichlorido(2-picoline) complex **3d** were of similar efficacy against the cisplatin-sensitive cancer cell lines, with single-digit IC_{50} figures. While complex **3b** was also efficacious against the cisplatin-resistant HT-29 and DLD-1 colon carcinoma cells, complex **3d** was virtually inactive against these cell lines. *cis*-Dichlorido(DMSO) complex **3a** was least active, on average. Strikingly, *trans*-bisphosphane complex **3c** reached nanomolar IC_{50} values against all but one cancer cell line. In principle, this could be due to its ionic nature enabling its cellular uptake via cation transporters that are frequently overexpressed in cancer cells.[22−26] However, when we measured the lipophilicities (i.e., log P values) and the platinum content of treated HCT-116 colon carcinoma cells, we found that both increased like the cytotoxicities when going from **3a** to **3b** to **3c** (cf. Supporting Information, Table S2), presumably because of the large organic PPh_3 groups.

DNA Interaction. Complexes **2** and **3a–d** were incubated with circular pBR322 plasmid DNA, and the resulting changes in the electrophoretic mobility of the plasmids' topological forms were monitored (Figure 3). The observed band shifts did not correlate with the cytotoxicities of the complexes. Complexes **2** and **3d**, both featuring a poor leaving ligand trans to the NHC ligand, did not alter the electrophoretic mobility of the DNA. In contrast, complexes **3a–c**, all featuring the good leaving ligand

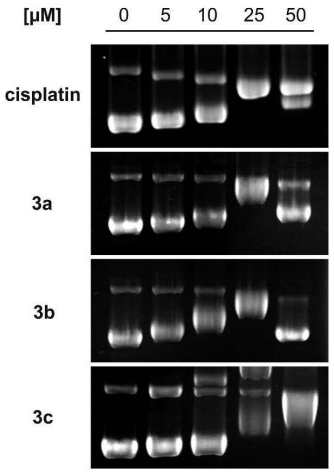

Figure 3. Interaction of cisplatin and complexes **3a–c** with circular pBR322 plasmid DNA, as observed by electrophoretic mobility shift assays (EMSA), after 24 h of incubation. Pictures are representative of at least two independent experiments.

DOI: 10.1021/acs.jmedchem.5b00896
J. Med. Chem. 2015, 58, 6283−6292

Cl, induced a concentration-dependent band shift. At higher complex concentrations (25 and 50 μM), a rewinding of the plasmid DNA occurred with renewed increase of the electrophoretic mobility. For the most cytotoxic complex **3c**, additional bands with even less electrophoretic mobility than that of the plasmid's open-circular (oc) form appeared for concentrations $\geq$10 μM. When 25 or 50 μM **3c** was applied, large amounts of plasmid DNA remained in the wells of the gel, suggesting that bigger DNA adducts had formed that cannot penetrate the pores of the agarose gel (for a full picture of EMSA gel with complex **3c**, cf. Supporting Information, Figure S1). Cisplatin accelerated the mobility of the relaxed form due to its bifunctional binding to DNA, which shortens and condenses the DNA helix.[27,28] In contrast, complexes **3a**–**c** accelerated the mobility of the relaxed form only marginally, indicating that they interact with DNA in a way fundamentally different from that of cisplatin.

In a fluorescence-based staining assay,[29,30] high-molecular-mass salmon sperm DNA (SS DNA) was incubated with cisplatin or complexes **3a**–**c** and was then stained with ethidium bromide (EtdBr), and the fluorescence of EtdBr–DNA adducts was measured (Figure 4). While complexes **3a** and **3b** reduced the

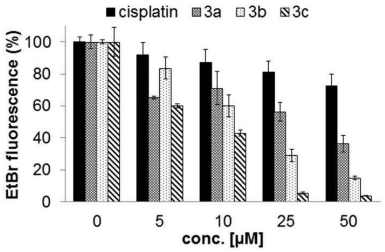

Figure 4. Relative ethidium bromide–DNA adduct fluorescence after preincubation with vehicle (set to 100%), cisplatin, or complexes **3a**–**c** (5, 10, 25, and 50 μM) for 2 h. Decreased fluorescence is indicative of inhibition of ethidium bromide intercalation into DNA.

EtdBr fluorescence to 36 and 15%, respectively, complex **3c** at the highest concentration prevented the intercalation of the fluorescent dye, leaving a residual fluorescence of only 4%.

In order to decide whether the effects observed in the EMSA and EtdBr staining studies originated from different amounts of Pt coordinatively bound to DNA or from an altogether different binding mode, more experiments were performed. Solutions of double-helical high-molecular-mass calf thymus (CT) DNA were incubated with compounds **3a**–**c** at an r_i of 0.05 in $NaClO_4$ (10 mM) at 37 °C (r_i is defined as the molar ratio of free platinum complex to nucleotide phosphates at the onset of incubation with DNA). At regular time intervals, aliquots of the reaction mixture were withdrawn, dialyzed against 1 M NaCl to remove all unbound platinum complex along with platinum complex fragments noncoordinatively bound to DNA, and assayed by flame atomic absorption spectrometry (FAAS) for platinum irreversibly (coordinatively) bound to DNA. Its amount increased with time (Figure 5A). $T_{50\%}$, the time by which half of the maximum amount of Pt was bound, was ca. 0.5 and 5.2 h for complexes **3a** and **3b**, respectively. Compound **3c** bound to DNA markedly slower. Essentially the same binding rates were observed in experiments with compounds **3a**–**c** at r_i = 0.1 (not shown). In addition, DNA was incubated with **3a**–**c** or cisplatin for 24 h, and then the samples were centrifuged through a Sephadex G50 column to remove free or noncovalently bound

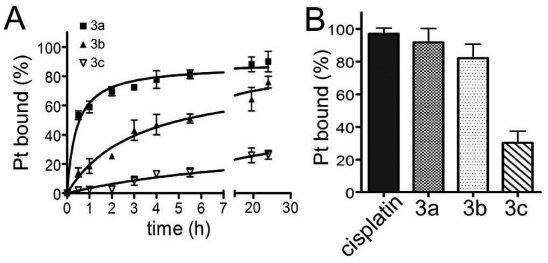

Figure 5. (A) Kinetics of the reaction of **3a**–**c** with double-helical CT DNA at r_i = 0.05 in $NaClO_4$ (10 mM) at 37 °C. Data represent mean ± SD values from three independent experiments. (B) The relative amount of Pt bound to DNA after 24 h of incubation with **3a**–**c** or cisplatin at 37 °C. Data represent mean ± SD values.

platinum and assayed by FAAS. Figure 5B shows that the ability of complexes **3a**–**c** to bind coordinatively to DNA decreased with increasing numbers of PPh_3 ligands, which might sterically restrict the contact with DNA or the hydrolysis of the leaving chloride. The upshot is that the amount of fragments of **3a**–**c** coordinatively bound to DNA correlates inversely with the cytotoxicity of these complexes against tumor cells.

These results, together with those of the EMSA and EtdBr studies, support the hypothesis that **3c** might interact with DNA predominantly via noncovalent interactions, facilitated by its positive charge. A similar behavior had already been described for compounds that effectively condense or aggregate DNA.[31−33] Moreover, when the blockage of EtdBr intercalation into CT DNA was assessed, the formation of aggregated DNA fibers in the solution was observed, especially at higher concentrations of compound **3c** (25 and 50 μM) and, to a lesser extent, also of compound **3b**. Therefore, the ability of complexes **3a**–**c** to initiate the condensation or aggregation of DNA was assessed by a light scattering assay[34] that measures the intensity of light scattered by a diluted DNA solution at a 90° angle with respect to the incident beam. This intensity increases in a concentration-dependent manner in the presence of condensing agents due to the formation of condensed DNA particles. The EC_{50} value represents the concentration of the test compound at which 50% of the total amount of DNA is condensed (Figure 6A). In keeping with the EMSA data, complex **3c** was the most efficient inducer of DNA aggregation, with an EC_{50} value of 0.51 ± 0.04 μM, whereas complex **3b** exhibited an EC_{50} value of 1.00 ± 0.02 μM, and complex **3a** failed to induce DNA condensation. The turbidity of the solutions was also determined UV/vis spectrophotometrically by monitoring the absorbance of CT

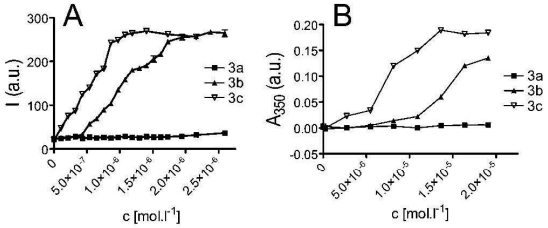

Figure 6. (A) Intensity of light scattered by CT DNA (1.5×10^{-6} M; 10 mM cacodylate, pH 7.2, 25 °C) in the presence various concentrations of **3a**–**c**. (B) Absorption of CT DNA (1×10^{-4} M; 10 mM NaCl, 10 mM TrisCl, pH 7.4, 25 °C) in the presence of **3a**–**c** at 350 nm.

DOI: 10.1021/acs.jmedchem.5b00896
J. Med. Chem. 2015, 58, 6283−6292

DNA at 350 nm (Figure 6B), which rose upon addition of **3b** or **3c**, indicating the onset of the condensation process,[35] and which kept increasing with growing concentration. Once more, complex **3a** did not lead to turbidity changes up to concentrations of ca. 20 μM.

Considering these results, the observed decrease of EtdBr fluorescence induced by complexes **3b** and **3c** (Figure 4) is likely the consequence of a reduced concentration of DNA amenable to EtdBr intercalation. The data indicate that the cytotoxicity against cancer cells of **3a**–**c** correlates with their ability to condense/aggregate DNA rather than with their ability to coordinatively bind to DNA. Taken together, the DNA interactions of (NHC)Pt(II) complexes bearing one or two triphenylphosphane ligands are significantly different from those of cisplatin. This was further corroborated by their effects on the morphology of growing *Escherichia coli*. Unlike cisplatin, complexes **3b** and **3c** did not induce filamentation and growth of the bacteria to a size 15 times longer than normal.[36,37] However, complex **3a** induced filamentous growth of some of the bacteria, albeit to a lesser extent than that with cisplatin (cf. Supporting Information, Figure S2). A final experiment demonstrating the peculiar DNA interaction of complexes **3a**–**c** as opposed to that of cisplatin was their failure to induce lysis in *E. coli* infected with bacteriophage λ,[38] which also proves that DNA damage caused by these complexes does not elicit the usual SOS repair machinery (cf. Supporting Information, Figure S3).

Cell Cycle Interference. The influence of the complexes **3a**–**c** on the cell cycle progression of 518A2 melanoma cells was analyzed using propidium iodide staining and flow cytometry (Figure 7). Cisplatin was used as a reference since a G2/M phase

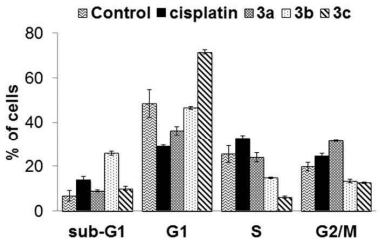

Figure 7. Effects of cisplatin and complexes **3a**–**c** on the cell cycle progression of 518A2 melanoma cells. Shown are the percentages of cells in G1, S, and G2/M phases and apoptotic cells (sub-G1), as obtained by flow cytometry after DNA staining with propidium iodide. Cells were treated with 50 μM cisplatin, 30 μM **3a**, 5 μM **3b**, or 500 nM **3c** for 24 h. Values represent means ± SD of three experiments.

arrest has already been reported as an essential step in its mechanism of action.[2,4,39,40] When 518A2 melanoma cells were treated with 50 μM of cisplatin for 24 h, a moderate accumulation of cells in the G2/M and S phases of the cell cycle as well as an increase of apoptotic cells was observed. Complex **3a** also arrested 518A2 cells in the G2/M phase of the cell cycle; however, it did so to a greater extent than cisplatin. Both cisplatin and complex **3a** reduced the number of cells in the G1 phase of the cell cycle. In contrast, complex **3b** did not induce any kind of cell cycle arrest but directly led to cell death at a concentration as low as 5 μM. Complex **3c** showed a completely different effect, namely, a marked accumulation of 518A2 cells in the G1 phase and a decrease of cells in the S phase. This is in line with the particular mode of interaction of **3c** with DNA, which probably prevents 518A2 melanoma cells from proceeding to S phase due to an impairment of DNA transcription and replication.

Vascular Disrupting Properties. Since we had found certain metal NHC complexes to be vascular disrupting,[10,11] we analyzed the effects of complexes **3a**–**c** on developing blood vessels in the chorioallantoic membrane (CAM) of fertilized chicken eggs as an *in vivo* model.[11,41,42] While complex **3b** showed only moderate vascular disrupting effects after 24 h, complexes **3a** and **3c** were highly effective as early as 6 h post treatment, disrupting the capillary reticulation and degrading even big blood vessels. Complex **3c** was the most effective compound and led to a complete destruction of blood vessels in the treated area of the CAM after 24 h. Cisplatin displayed a negligible effect on the developing vasculature, although it penetrated into the CAM rather deeply (Figure 8).

Nephrotoxicity. The organ toxicity of complexes **3a**–**c** in comparison to the nephrotoxic[5,6] cisplatin was studied using precision-cut tissue slices (PCTS) of rat kidneys that can be cultured *ex vivo* (Figure 9).[43,44] These slices represent viable explants with all cell types in their natural environment, thereby maintaining intercellular and cell–matrix interactions. They constitute a meaningful organ model that was previously applied for the toxicity assessment of cisplatin (kidney),[45] experimental gold compounds (liver, kidney, and colon),[46] and amino-ferrocenyl prodrugs (liver).[47]

Different concentrations of complexes **3a**–**c** were incubated with kidney slices (PCKS) for 24 h, and the tissue viability was determined by measuring the ATP content. Complexes **3a** and **3b** showed a moderate effect on the PCKS viability when compared to that with cisplatin, which reduced it to 50% at concentrations of ca. 10–15 μM. In contrast, complex **3c** was more toxic and reduced the PCKS viability to ~30% at a concentration as low as 5 μM. It should be kept in mind, though, that complex **3c** was 15 times more efficacious than cisplatin against the cancer cell lines tested in the MTT assays and thus could possibly be administered to animals or patients at a correspondingly lower dosage.

The effects of different concentrations of complexes **3a** and **3c** on the histomorphology of PCKS were also assessed. The results confirm those of the ATP viability assay. Figure 10 shows representative pictures for the treatment with **3a**. The kidney slices were only slightly affected by 1 μM **3a**, although some toxic effects on tubular cells became apparent. More pronounced morphological alterations were observed upon treatment with 25 μM **3a**, whereas 100 μM of this compound led to outright kidney cell necrosis, indicated by the loss of nuclei. The strong impact of **3c** on the viability of PCKS shown in Figure 9 was mirrored by an induction of distinct cell necrosis in slices treated with concentrations as low as 1 μM (cf. Supporting Information, Figure S4).

■ CONCLUSIONS

This study showed that only NHC platinum(II) complexes with good leaving groups such as chloride trans to the NHC ligand, e.g., complexes **3a**–**c**, interact noticeably with DNA in electrophoretic mobility shift and ethidium bromide staining assays. However, this is not a prerequisite for high cytotoxicity against cancer cells, apparent from the efficacy of the nonbinders to DNA, complexes **2** and **3d**.

Within the series of *trans*-chlorido-[(1,3-dibenzyl)imidazol-2-ylidene]platinum(II) complexes **3a**–**c**, there is an increasing steric shielding of the leaving chloride by the two spectator ligands when going from **3a** (spectator ligands: chlorido and

DOI: 10.1021/acs.jmedchem.5b00896
J. Med. Chem. 2015, 58, 6283–6292

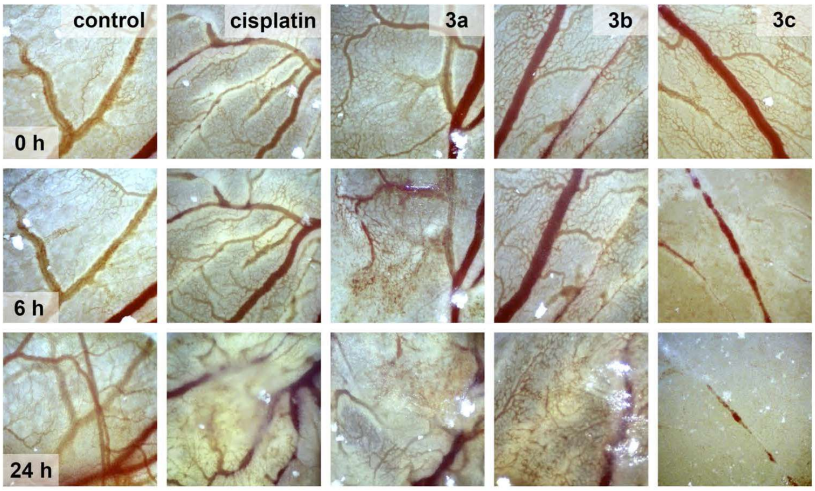

Figure 8. Effects of cisplatin and complexes **3a–c** when applied topically (10 nmol in 10 μL of H_2O) on developing vasculature in the chorioallantoic membrane of fertilized chicken eggs after 6 and 24 h of incubation. Control, respective amount of DMF (in a total volume of 10 μL of H_2O); images are representative of three independent experiments.

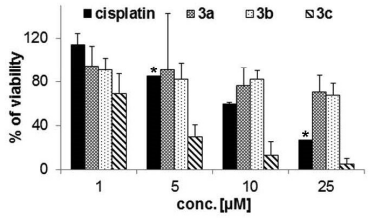

Figure 9. Viability of precision-cut kidney slices (PCKS) treated with different concentrations of cisplatin or complexes **3a–c** for 24 h, normalized by means of protein concentrations. The viability of control slices was set to 100%. Values represent means ± SD of at least two independent experiments performed in triplicate, except for starred bars, which were obtained from single experiments run in triplicate.

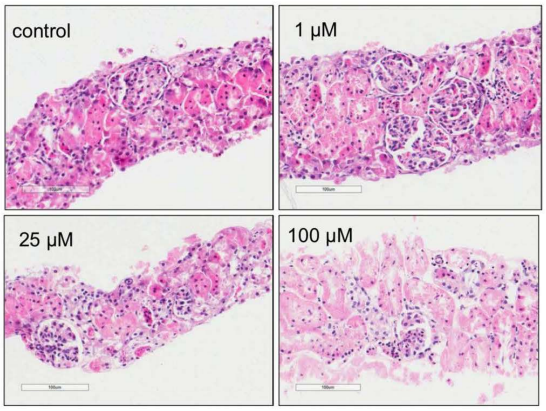

Figure 10. Morphology of PCKS treated with different concentrations of complex **3a** for 24 h; scale bars, 100 μm.

DMSO) to **3b** (chlorido and PPh_3) to **3c** (two PPh_3). Complex **3a** bound at the highest rate and to the greatest extent to double-helical CT DNA and resembled cisplatin most closely as to the pattern of the various DNA morphologies in the EMSA with circular pBR322 plasmid DNA. Like cisplatin, it led to a pronounced G2/M cell cycle arrest of 518A2 melanoma cells and to an SOS response in *E. coli* bacteria. In essence, complex **3a** most closely resembles cisplatin as to its effects on a cellular level and so is likely to bind to DNA also in a coordinating manner. Complex **3b** takes a middle position, resembling **3a** in terms of the effects in the EMSA yet differing in many other aspects. It bound less rapidly to CT DNA and in a way that generated light scattering adducts and turbidity in solution. It did not lead to G2/M cell cycle arrest in the melanoma cells but to an increased fraction of apoptotic cells, and it did not elicit an SOS response in *E. coli*. Complex **3c** binds to DNA predominantly by initiating its aggregation and precipitation to the effect of a G1 phase cell cycle arrest in the tested melanoma cells and a strong antiproliferative impact on all tested cancer cells avoiding the usual SOS response. It also showed a vascular disrupting effect, hitherto known only of NHC gold complexes. It remains to be shown whether a platinum center is altogether required or if effects similar to those of **3c** could also be induced by complexes of other central metals bearing sterically shielded leaving groups. Another issue to clarify in animal studies is whether the high organ toxicity of complexes that elicit DNA aggregation may be compensated by a reduction of the required dosage.

■ EXPERIMENTAL SECTION

Chemistry. *General.* Melting points are uncorrected; IR spectra were recorded on an FT-IR spectrophotometer with ATR sampling unit; NMR spectra were run on 300 and 500 MHz spectrometers; chemical shifts are given in ppm (δ) downfield from tetramethylsilane as internal standard, ^{195}Pt-NMR shifts are quoted relative to $\Xi(^{195}Pt)$ = 21.4 MHz; mass spectra: direct inlet, EI, 70 eV; HRMS: UPLC/Orbitrap MS system in ESI mode; microanalyses: Vario EL III elemental analyzer. The NHC ligand and its silver carbene complex **1** were prepared according to the literature.[17,18] All tested compounds were >95% pure by elemental analysis or UPLC/HRMS.

*trans-Dichlorido-bis(1,3-dibenzylimidazol-2-ylidene)platinum(II) (**2**).* A solution of 1,3-dibenzylimidazol-2-ylidene silver(I) bromide (50 mg, 0.115 mmol) in CH_2Cl_2 was treated with K_2PtCl_4 (23 mg, 0.057 mmol), and the resulting mixture was stirred at room temperature for 24

DOI: 10.1021/acs.jmedchem.5b00896
J. Med. Chem. 2015, 58, 6283–6292

h. The suspension was filtered, the filtrate was concentrated in vacuum, and the residue was recrystallized from CH_2Cl_2/hexane. Yield: 30 mg (0.039 mmol, 68%); off-white solid of mp 164−166 °C; ν_{max}/cm^{-1}: 3160, 3128, 3099, 3035, 2947, 1602, 1561, 1494, 1451, 1412, 1398, 1356, 1334, 1227, 1203, 1182, 1158, 1151, 1101, 1076, 1029, 960, 935, 918, 852, 825, 792, 770, 724, 704, 697, 662; ^{1}H NMR (300 MHz, $CDCl_3$) δ 5.27 (s, 8H), 6.8−6.9 (m, 4H), 7.3−7.4 (m, 20H); ^{13}C NMR (75.5 MHz, $CDCl_3$) δ 55.8, 121.5, 127.8, 128.7, 129.1, 135.3, 166.0; *m/z* (EI, %) 692 (3), 691 (4), 690 (4), 689 (2) [$M^+ - 2Cl$], 442 (2), 441 (2), 249 (10), 158 (23), 91 (100); HRMS: *m/z* calcd, 784.15496; found, 784.15338 [$C_{34}H_{32}PtN_4Cl_2Na^+$; $(M + Na)^+$].

*cis-Dichlorido-(1,3-dibenzylimidazol-2-ylidene)(dimethyl sufoxide)platinum(II) (**3a**).* A solution of 1,3-bis(benzyl)imidazol-2-ylidene silver(I) bromide (69 mg, 0.158 mmol) in DMSO was treated with K_2PtCl_4 (66 mg, 0.158 mmol), and the resulting mixture was stirred at 60 °C for 24 h. After adding CH_2Cl_2, the reaction mixture was filtered and the filtrate was washed with water and then dried over Na_2SO_4. The solvent was removed in vacuum, and the remainder ws recrystallized from CH_2Cl_2/hexane. Yield: 85 mg (0.143 mmol, 91%); colorless crystalline solid of mp 258 °C (dec.). Anal. Calcd for $C_{19}H_{22}Cl_2N_2OPtS$: C, 38.32; H, 4.23; N, 4.70. Found: C, 38.31; H, 3.91; N, 4.64. ν_{max}/cm^{-1}: 3091, 2933, 2836, 1611, 1585, 1511, 1455, 1441, 1350, 1303, 1245, 1175, 1111, 1028, 822, 773, 729, 702, 686, 658; ^{1}H NMR (500 MHz, $CDCl_3$) δ 3.16 (s, 6H), 5.70 (ABq, $\Delta\delta$ = 0.06, $^2J_{AB}$ = 15 Hz, 4H), 6.83 (s, 2H), 7.32−7.45 (m, 10H); ^{13}C NMR (125 MHz, $CDCl_3$) δ 45.5, 54.5, 121.4, 128.3, 128.6, 129.2, 135.1, 144.9; ^{195}Pt NMR ($CDCl_3$) δ 962 ppm; *m/z* (EI, %) 592 (15) [M^+], 556 (10) [$M^+ - Cl$], 521 (4) [$M^+ - Cl$], 441 (81), 349 (9), 247 (9), 157 (22), 91 (37), 78 (100), 63 (98); HRMS: *m/z* calcd, 556.07836; found, 556.07788 [$C_{19}H_{22}N_2OClPtS^+$; $(M - Cl)^+$]. Crystallographic data were deposited with The Cambridge Crystallographic Data Centre (CCDC) under no. 1062990.

*cis-Dichlorido-(1,3-dibenzylimidazol-2-ylidene)-(triphenylphosphane)platinum(II) (**3b**).* Triphenylphosphane (13 mg, 0.051 mmol) was slowly added to a solution of complex **3a** (30 mg, 0.051 mmol) in CH_2Cl_2, and the resulting mixture was stirred at room temperature for 90 min. The volatiles were removed in vacuum, and the remaining crude product was purified by recrystallization from CH_2Cl_2/hexane. Yield: 18 mg (0.023 mmol, 46%); colorless crystalline solid of mp 316 °C (dec.). Anal. Calcd for $C_{35}H_{31}Cl_2N_2PPt$: C, 54.13; H, 4.02; N, 3.61. Found: C, 53.52; H, 4.57; N, 3.47. ν_{max}/cm^{-1}: 3059, 3041, 1497, 1483, 1457, 1435, 1309, 1261, 1232, 1185, 1162, 1101, 1074, 1028, 999, 823, 726, 693, 617, 577; ^{1}H NMR (300 MHz, $CDCl_3$) δ 4.52 (d, $^2J_{AB}$ = 14.3 Hz, 2H), 5.84 (d, $^2J_{AB}$ = 14.3 Hz, 2H), 6.37 (s, 2H), 7.22−7.31 (m, 10H), 7.32−7.40 (m, 6H), 7.44−7.60 (m, 9H); ^{13}C NMR (75.5 MHz, $CDCl_3$) δ 54.3, 120.2, 128.4 (d, $^2J_{CP}$ = 11 Hz), 128.6, 128.8, 129.3, 129.5 (d, $^1J_{CP}$ = 63 Hz), 131.0 (d, $^3J_{CP}$ = 2.3 Hz), 134.1 (d, $^2J_{CP}$ = 11 Hz), 134.3, 149.9 (d, $^2J_{CP}$ = 8.1 Hz); ^{31}P NMR (121 MHz, $CDCl_3$) δ 8.49 ($^1J_{PPt}$ = 3894 Hz); ^{195}Pt NMR ($CDCl_3$) δ 504 ppm (d, $^1J_{PtP}$ = 3915 Hz); *m/z* (EI, %) 776 (6) [M^+], 740 (15) [$M^+ - Cl$], 703 (14) [$M^+ - 2Cl$], 689 (7), 456 (10), 442 (10), 337 (7), 297 (27), 262 (100), 247 (35), 183 (61), 91 (43); HRMS: *m/z* calcd, 740.15556; found, 740.15454 [$C_{35}H_{31}N_2ClPPt^+$; $(M - Cl)^+$]. Crystallographic data were deposited with The Cambridge Crystallographic Data Centre CCDC under no. 1062991.

*trans-Chlorido-(1,3-dibenzylimidazol-2-ylidene)bis-(triphenylphosphane)platinum(II) chloride (**3c**).* Triphenylphosphane (55 mg, 0.210 mmol) was slowly added to a solution of complex **3a** (25 mg, 0.042 mmol) in CH_2Cl_2, and the resulting mixture was stirred at room temperature for 30 min. The solvent was removed in vacuum, and the residue recrystallized from CH_2Cl_2/hexane. Yield: 23 mg (0.022 mmol, 53%); colorless crystalline solid of mp 117 °C. Anal. Calcd for $C_{53}H_{46}Cl_2N_2P_2Pt$: C, 61.27; H, 4.46; N, 2.70. Found: C, 59.54; H, 4.77; N, 2.74. ν_{max}/cm^{-1}: 3053, 2922, 2854, 1572, 1581, 1456, 1435, 1415, 1358, 1311, 1234, 1183, 1096, 1028, 999, 830, 744, 727, 689, 619; ^{1}H NMR (500 MHz, $CDCl_3$) δ 4.54 (s, 4H), 6.80 (d, $^3J_{HH}$ = 7.5 Hz, 4H), 6.94 (s, 2H), 6.98 (t, $^3J_{HH}$ = 7.5 Hz, 4H), 7.17 (t, $^3J_{HH}$ = 7.5 Hz, 2H), 7.28−7.68 (m, 30H); ^{13}C NMR (125 MHz, $CDCl_3$) δ 54.7, 122.9, 128.0 (t, $^1J_{CP}$ = 29 Hz), 128.5, 128.6, 128.7, 128.9, 129.2, 129.2 (t, $^3J_{CP}$ = 5.5 Hz), 129.5, 132.0, 132.3, 134.1, 145.0 (t, $^2J_{CP}$ = 10 Hz); ^{31}P NMR (202 MHz, $CDCl_3$) δ 17.5 ($^1J_{PPt}$ = 2503 Hz); ^{195}Pt NMR ($CDCl_3$) δ 159.9 ppm (t, $^1J_{PtP}$ = 2503 Hz); *m/z* (EI, %) 778 (6) [$M^+ - PPh_3$], 742 (10) [$M^+ - Cl - PPh_3$], 705 (10) [$M^+ - 2Cl - PPh_3$], 614 (2), 457 (7), 443 (6), 378 (5), 263 (100), 248 (25), 184 (45), 108 (21), 91 (27); HRMS: *m/z* calcd, 1002.24670; found, 1002.24280 [$C_{53}H_{46}N_2ClP_2Pt^+$; $(M - Cl)^+$]. Crystallographic data were deposited with The Cambridge Crystallographic Data Centre CCDC under no. 1062992.

*trans-Dichlorido-(1,3-dibenzylimidazol-2-ylidene)(2-picoline)-platinum(II) (**3d**).* 2-Picoline (100 μL, 1.01 mmol) was slowly added to a solution of complex **3a** (32 mg, 0.054 mmol) in CH_2Cl_2, and the resulting mixture was stirred at room temperature for 6 days. It was washed with water, the organic phase was dried over Na_2SO_4 and evaporated to leave a residue that was recrystallized from CH_2Cl_2/hexane. Yield: 18 mg (0.030 mmol, 55%); off-white solid of mp 226 °C (dec.); ν_{max}/cm^{-1}: 3166, 3055, 3030, 2836, 1610, 1571, 1489, 1455, 1421, 1349, 1294, 1226, 1208, 1157, 1112, 1030, 824, 764, 725, 702, 690, 595, 563; ^{1}H NMR (300 MHz, $CDCl_3$) δ 3.15 (s, 3H), 5.94 (s, 4H), 6.68 (s, 2H), 7.18−7.24 (m, 1H), 7.27 (d, $^3J_{HH}$ = 7.7 Hz, 1H), 7.32−7.44 (m, 6H), 7.51−7.59 (m, 4H), 7.63 (td, $^3J_{HH}$ = 7.7, 1.6 Hz, 1H), 8.85 (dt, $^3J_{HH}$ = 4.9, 0.8 Hz, 1H); ^{13}C NMR (75.5 MHz, $CDCl_3$) δ 25.3, 54.1, 120.6, 122.2, 126.2, 128.3, 128.6, 128.9, 135.8, 137.5, 141.3, 151.4, 160.0; *m/z* (EI, %) 607 (13) [M^+], 536 (4) [$M^+ - 2Cl$], 441 (28), 351 (4), 248 (2), 157 (6), 93 (100), 78 (14), 66 (34); HRMS: *m/z* calcd, 629.08146; found, 629.08081 [$C_{23}H_{23}N_3Cl_2PtNa^+$; $(M + Na)^+$].

Biological Studies. *Electrophoretic Mobility Shift Assay (EMSA).* Circular pBR322 plasmid DNA (1.5 μg, Thermo Scientific) was incubated with dilution series of cisplatin or complexes **2** and **3a−c** (5, 10, 25, 50 μM) in 1× TE buffer (10 mM Tris-HCl, 1 mM EDTA, pH 8.5) at 37 °C for 24 h (20 μL total sample volume). DNA samples without the addition of any test substance served as negative controls. Subsequent to the 24 h of incubation, samples were subjected to gel electrophoresis using 1% agarose gels in 0.5 TBE buffer (89 mM Tris, 89 mM boric acid, 25 mM EDTA, pH 8.3). Gels were stained with ethidium bromide, and DNA bands were visualized using UV excitation. Experiments were carried out at least in duplicate.

Ethidium Bromide Staining Assay. The extent of the Pt(II) complexes' DNA interaction was further assessed by a fluorescence-based ethidium bromide staining assay.[29,30] Salmon sperm DNA (SS DNA, Sigma-Aldrich) was pipetted into a black 96-well plate in 1× TE buffer to reach a final amount of 1 μg/100 μL assay volume and incubated with varying concentrations of cisplatin or complexes **3a−c** (5, 10, 25, or 50 μM, each concentration in triplicate) for 2 h at 37 °C. Afterward, 100 μL of a 10 μg/mL ethidium bromide solution in 1× TE buffer was added to each well. After 5 min of incubation, the fluorescence (λ_{ex} = 535 nm, λ_{em} = 595 nm) of each well was detected using a microplate reader (Tecan). Each fluorescence value was corrected by possible intrinsic compound and ethidium bromide background fluorescence (samples without DNA); the resulting values were then expressed as a percent of solvent controls (DMSO or DMF, 100% ethidium bromide binding = 100% fluorescence). Decreased fluorescence (%) is representative of impaired formation of ethidium bromide−DNA adducts due to DNA intercalation sites being blocked by the test compounds.

Quantitative Evaluation of Covalent Binding to Mammalian DNA in Cell-Free Medium. Solutions of double-helical CT DNA (42% G + C, mean molecular mass ca. 2×10^7) at a concentration of 0.32 mg mL^{-1} (1.0×10^{-3} M related to the phosphorus content) were incubated with compounds **3a**, **3b**, or **3c** (5×10^{-5} M) at a value of r_i = 0.05 in 0.1 mM NaCl at 37 °C. At regular intervals, aliquots of the reaction mixtures were withdrawn and exhaustively dialyzed first against 1 M NaCl (1 h, 4 °C) and then against ultrapure water. Subsequently, the samples were assayed by FAAS for platinum bound to DNA. DNA concentrations in the samples were verified by absorption spectrophotometry (ε_{260} = 6400 L mol^{-1} cm^{-1}).

Total Light Scattering. According to a literature procedure,[34] the experiments were carried out in cacodylate buffers (10 mM, pH 7.2), which, like the stock solutions of the test compounds in DMF, were filtered through 0.2 μm filters before use to avoid interference from dust particles. A solution of CT DNA (1.5 μM) was prepared in a 1 cm quartz cuvette in a total volume of 2.5 mL. Small volumes (1 μL) of compounds **3a**, **3b**, or **3c** were added to the CT DNA solution to obtain the desired

DOI: 10.1021/acs.jmedchem.5b00896
J. Med. Chem. 2015, 58, 6283−6292

concentration, and the solution was thoroughly mixed. The mixture was left undisturbed for 10 min at room temperature, and the total intensity light scattering was measured using a Varian Cary Eclipse spectrofluorophotometer with excitation and emission wavelengths set to 305 nm. The excitation and emission slit widths were 5 nm, and the integration time was set to 5 s. The scattered light was measured at a 90° angle relative to the incident beam.

Cell Cycle Analysis. 518A2 cells (5×10^4/mL) were grown on 6-well plates for 24 h and then treated with cisplatin or complexes **3a−c** for 24 h (cisplatin, 50 μM; **3a**, 30 μM; **3b**:, 5 μM; and **3c**, 500 nM). Solvent controls (DMSO or DMF) were treated identically. After fixation (70% EtOH, 4 °C), the cells were incubated with propidium iodide (PI, Roth) staining solution (50 μg/mL PI, 0.1% sodium citrate, 50 μg/mL RNase A in PBS) for 30 min at 37 °C. The fluorescence intensity of 10 000 single cells was measured at λ_{em} = 620 nm (λ_{ex} = 488 nm laser source) using a Beckman Coulter Cytomics FC 500 flow cytometer and analyzed (CXP Analysis, Beckman Coulter) for fractions of cells in G1, S, and G2/M phases. The percentage of apoptotic cells was assessed from sub-G1 peaks. The experiment for each sample was carried out in triplicate.

Chorioallantoic Membrane (CAM) Assay. Fertilized, specific pathogen-free (SPF) chicken eggs (VALO BioMedia) were bred in an incubator at 37 °C and a relative humidity of 60%. On day 5, windows (Ø 1.5−2 cm) were cut into the shell at the more rounded pole. The cavities were sealed with tape, and incubation was continued overnight. Rings of thin silicon foil (Ø 5 mm) were placed on the CAM with its developing blood vessels, and cisplatin or complexes **3a−c** (10 nmol in a volume of 10 μL of H_2O) were added. Solvent controls with respective amounts of DMSO or DMF were treated identically. The effects on the developing vasculature were documented after further incubation for 6 and 24 h using a light microscope (60× magnification, Traveler).[11,41,42] For each substance, the assay was performed at least in triplicate.

Ex Vivo Toxicity in Precision-Cut Kidney Slices..[43,44] Male Wistar rats (Charles River, Kissleg, Germany), 250−450 g, were housed under a 12 h dark/light cycle at constant humidity and temperature. Animals were permitted free access to tap water and standard lab chow. All experiments were approved by the Committee for Care and Use of Laboratory Animals of the University of Groningen and were performed according to strict governmental and international guidelines.

Fresh, viable rat kidneys were cut sagittally, and cylindrical cores of 7 mm diameter were prepared from the renal cortex with a manual tissue coring tool. Subsequently, PCKS with a wet weight of 5 mg were prepared in ice-cold Krebs−Henseleit buffer saturated with carbogen (95% O_2 and 5% CO_2) using a Krumdieck tissue slicer (Alabama R&D, Munford, AL, USA). The PCKS were preincubated at 37 °C for 1 h in Williams medium E supplemented with D-glucose monohydrate (275 mg/mL) and penicillin−streptomycin (100 U/mL and 100 μg/mL) and saturated with 80% O_2 and 20% CO_2 at pH 7.4. The slices were put in fresh medium, and incubation with cisplatin or complexes **3a−c** at different concentrations was continued for 24 h. Untreated kidney slices served as controls. The slices were transferred to 1 mL sonication solution (70% ethanol, 2 mM EDTA) in a safe-lock micro test tube containing glass MiniBeads, frozen in liquid nitrogen, and stored at −80 °C. Before analyzing the viability of the PCKS with the ATP bioluminescence assay kit CLS II (Roche), the samples were thawed and homogenized with a Mini-Beadbeater (Biospec Products) for 45 s. The ATP levels of the slices were normalized by means of protein concentrations determined by Lowry's method (Bio-Rad DC protein assay). The slices were dried overnight at 37 °C, 200 μL of 5 M NaOH was added, and incubation was continued at 37 °C for 30 min. The samples were diluted five times with Milli-Q water and homogenized with the Mini-Beadbeater for 40 s. The ATP content was corrected by the protein amount of each slice and expressed as pmol/μg protein. The protein content of the PCTS was determined by the Bio-Rad DC protein assay (Munich, Germany) using bovine serum albumin (BSA, Sigma-Aldrich, Steinheim, Germany) for the calibration curve. The viability of treated PCKS was expressed as a percent of the viability of controls set to 100%. For each test compound, at least two independent experiments were carried out in triplicate. Morphological changes induced in tissue sections by treatment with complexes **3a** or **3c** for 24 h were documented for three PCKS, which were incubated in 1 mL of buffered formalin at 4 °C overnight, followed by storage in 70% ethanol (4 °C). Dehydration of the PCKS, embedding in paraffin, sectioning, and staining with hematoxylin and eosin were carried out according to standard histological procedures.

■ ASSOCIATED CONTENT

Supporting Information

Instruments used; crystal structure determination and data of **3a−c**; cell lines and culture conditions; MTT assay; platinum accumulation (FAAS); partition coefficient; effect on bacterial morphology and on the induction of lysogenic bacteria; and histomorphology of PCKS treated with **3c**. The Supporting Information is available free of charge on the ACS Publications website at DOI: 10.1021/acs.jmedchem.5b00896.

■ AUTHOR INFORMATION

Corresponding Author

*E-mail: Rainer.Schobert@uni-bayreuth.de. Fax: +49 (0)921 552671. Phone: +49 (0)921 552679.

Notes

The authors declare no competing financial interest.

■ ACKNOWLEDGMENTS

We thank the COST Action CM1105 "Functional metal complexes that bind to biomolecules" for support and an STSM appropriation (J.K.M.). R.S. thanks the Deutsche Forschungsgemeinschaft for a grant (Scho 402/12-1), J.K. and V.B. thank the Czech Science Foundation for a grant (14-21053S), and J.K.M. thanks the Elite Study Program "Macromolecular Science", Elite Network of Bavaria, for its support.

■ ABBREVIATIONS USED

CAM, chorioallantoic membrane; EdtBr, ethidium bromide; EMSA, electrophoretic mobility shift assay; FAAS, flame atomic absorption spectrometry; MTT, 3-(4,5-dimethylthiazol-2-yl)-2,5-diphenyltetrazolium bromide; NHC, N-heterocyclic carbene; PCTS/PCKS, precision-cut tissue/kidney slices

■ REFERENCES

(1) Rosenberg, B.; VanCamp, L.; Trosko, J. E.; Mansour, V. H. Platinum compounds: a new class of potent antitumour agents. *Nature* **1969**, *222*, 385−386.

(2) Jamieson, E. R.; Lippard, S. J. Structure, Recognition, and processing of cisplatin-DNA adducts. *Chem. Rev.* **1999**, *99*, 2467−2498.

(3) Kartalou, M.; Essigmann, J. M. Mechanisms of resistance to cisplatin. *Mutat. Res., Fundam. Mol. Mech. Mutagen.* **2001**, *478*, 23−43.

(4) Wang, D.; Lippard, S. J. Cellular processing of platinum anticancer drugs. *Nat. Rev. Drug Discovery* **2005**, *4*, 307−320.

(5) Oh, G. S.; Kim, H. J.; Shen, A.; Lee, S. B.; Khadka, D.; Pandit, A.; So, H. S. Cisplatin-induced kidney dysfunction and perspectives on improving treatment strategies. *Electrolyte Blood Pressure* **2014**, *12*, 55−65.

(6) Dasari, S.; Tchounwou, P. B. Cisplatin in cancer therapy: molecular mechanisms of action. *Eur. J. Pharmacol.* **2014**, *740*, 364−378.

(7) Oehninger, L.; Rubbiani, R.; Ott, I. N-Heterocyclic carbene metal complexes in medicinal chemistry. *Dalton Trans.* **2013**, *42*, 3269−3284.

(8) Liu, W.; Gust, R. Metal N-heterocyclic carbene complexes as potential antitumor metallodrugs. *Chem. Soc. Rev.* **2013**, *42*, 755−773.

(9) Kaps, L.; Biersack, B.; Müller-Bunz, H.; Mahal, K.; Muenzner, J.; Tacke, M.; Mueller, T.; Schobert, R. Gold(I)-NHC complexes of antitumoral diarylimidazoles: structures, cellular uptake routes and anticancer activities. *J. Inorg. Biochem.* **2012**, *106*, 52−58.

(10) Muenzner, J.; Biersack, B.; Kaps, L.; Schobert, R.; Sasse, F. Synergistic "gold effects" of anti-vascular 4,5-diarylimidazol-2-ylidene

DOI: 10.1021/acs.jmedchem.5b00896
J. Med. Chem. 2015, 58, 6283−6292

gold(I) carbene complexes. *Int. J. Clin. Pharmacol. Ther.* **2013**, *51*, 44−46.
(11) Muenzner, J. K.; Biersack, B.; Kalie, H.; Andronache, I. C.; Kaps, L.; Schuppan, D.; Sasse, F.; Schobert, R. Gold(I) biscarbene complexes derived from vascular-disrupting combretastatin A-4 address different targets and show antimetastatic potential. *ChemMedChem* **2014**, *9*, 1195−1204.
(12) Mendes, F.; Groessl, M.; Nazarov, A. A.; Tsybin, Y. O.; Sava, G.; Santos, I.; Dyson, P. J.; Casini, A. Metal-based inhibition of poly(ADP-ribose) polymerase−the guardian angel of DNA. *J. Med. Chem.* **2011**, *54*, 2196−2206.
(13) Lease, N.; Vasilevski, V.; Carreira, M.; de Almeida, A.; Sanaú, M.; Hirva, P.; Casini, A.; Contel, M. Potential anticancer heterometallic Fe-Au and Fe-Pd agents: initial mechanistic insights. *J. Med. Chem.* **2013**, *56*, 5806−5818.
(14) Zhang, J.-J.; Che, C.-M.; Ott, I. Caffeine derived platinum(II) N-heterocyclic carbene complexes with multiple anti-cancer activities. *J. Organomet. Chem.* **2015**, *782*, 37−41.
(15) Zamora, A.; Pérez, S. A.; Rodríguez, V.; Janiak, C.; Yellol, G. S.; Ruiz, J. Dual antitumor and antiangiogenic activity of organoplatinum-(II) complexes. *J. Med. Chem.* **2015**, *58*, 1320−1336.
(16) Newman, C. P.; Deeth, R. J.; Clarkson, G. J.; Rourke, J. P. Synthesis of Mixed NHC/L Platinum(II) Complexes: Restricted rotation of the NHC group. *Organometallics* **2007**, *26*, 6225−6233.
(17) Patil, S.; Claffey, J.; Deally, A.; Hogan, M.; Gleeson, B.; Menéndez Méndez, L. M.; Müller-Bunz, H.; Paradisi, F.; Tacke, M. Synthesis, cytotoxicity and antibacterial studies of *p*-methoxybenzyl-substituted and benzyl-substituted N-heterocyclic carbene−silver complexes. *Eur. J. Inorg. Chem.* **2010**, *2010*, 1020−1031.
(18) Patil, S.; Deally, A.; Hackenberg, F.; Kaps, L.; Müller-Bunz, H.; Schobert, R.; Tacke, M. Novel benzyl- or 4-cyanobenzyl-substituted N-heterocyclic (bromo)(carbene)silver(I) and (carbene)(chloro)gold(I) complexes: synthesis and preliminary cytotoxicity studies. *Helv. Chim. Acta* **2011**, *94*, 1551−1562.
(19) Mosmann, T. Rapid colorimetric assay for cellular growth and survival: application to proliferation and cytotoxicity assays. *J. Immunol. Methods* **1983**, *65*, 55−63.
(20) Alvarez, M.; Robey, R.; Sandor, V.; Nishiyama, K.; Matsumoto, Y.; Paull, K.; Bates, S.; Fojo, T. Using the national cancer institute anticancer drug screen to assess the effect of MRP expression on drug sensitivity profiles. *Mol. Pharmacol.* **1998**, *54*, 802−814.
(21) Roundhill, E. A.; Burchill, S. A. Detection and characterisation of multi-drug resistance protein 1 (MRP-1) in human mitochondria. *Br. J. Cancer* **2012**, *106*, 1224−1233.
(22) Jong, N. N.; McKeage, M. J. Emerging roles of metal solute carriers in cancer mechanisms and treatment. *Biopharm. Drug Dispos.* **2014**, *35*, 450−462.
(23) Gupta, S.; Wulf, G.; Henjakovic, M.; Koepsell, H.; Burckhardt, G.; Hagos, Y. Human organic cation transporter 1 is expressed in lymphoma cells and increases susceptibility to irinotecan and paclitaxel. *J. Pharmacol. Exp. Ther.* **2012**, *341*, 16−23.
(24) Howell, S. B.; Safaei, R.; Larson, C. A.; Sailor, M. J. Copper transporters and the cellular pharmacology of the platinum-containing cancer drugs. *Mol. Pharmacol.* **2010**, *77*, 887−894.
(25) Zoldakova, M.; Kornyei, Z.; Brown, A.; Biersack, B.; Madarász, E.; Schobert, R. Effects of a combretastatin A4 analogous chalcone and its Pt-complex on cancer cells: a comparative study of uptake, cell cycle and damage to cellular compartments. *Biochem. Pharmacol.* **2010**, *80*, 1487−1496.
(26) Koepsell, H.; Lips, K.; Volk, C. Polyspecific organic cation transporters: structure, function, physiological roles, and biopharmaceutical implications. *Pharm. Res.* **2007**, *24*, 1227−1251.
(27) Cohen, G. L.; Bauer, W. R.; Barton, J. K.; Lippard, S. J. Binding of cis and trans dichlorodiammineplatinum(II) to DNA: evidence for unwinding and shortening of the double helix. *Science* **1979**, *203*, 1014−1016.
(28) Scovell, W. M.; Collart, F. Unwinding of supercoiled DNA by cis- and trans-diamminedichloroplatinum(II): influence of the torsional strain on DNA unwinding. *Nucleic Acids Res.* **1985**, *13*, 2881−2895.
(29) Spoerlein-Guettler, C.; Mahal, K.; Schobert, R.; Biersack, B. Ferrocene and (arene)ruthenium(II) complexes of the natural anticancer naphthoquinone plumbagin with enhanced efficacy against resistant cancer cells and a genuine mode of action. *J. Inorg. Biochem.* **2014**, *138*, 64−72.
(30) Di Salvo, A.; Dugois, P.; Tandeo, D.; Peltekian, M.; Kong Thoo Lin, P. Synthesis, cytotoxicity and DNA binding of oxoazabenzo[de]-anthracenes derivatives in colon cancer Caco-2 cells. *Eur. J. Med. Chem.* **2013**, *69*, 754−761.
(31) Sun, S.; Liu, W.; Cheng, N.; Zhang, B.; Cao, Z.; Yao, K.; Liang, D.; Zuo, A.; Guo, G.; Zhang, J. A thermoresponsive chitosan-NIPAAm/vinyl laurate copolymer vector for gene transfection. *Bioconjugate Chem.* **2005**, *16*, 972−980.
(32) Dong, X.; Wang, X.; He, Y.; Yu, Z.; Lin, M.; Zhang, C.; Wang, J.; Song, Y.; Zhang, Y.; Liu, Z.; Li, Y.; Guo, Z. Reversible DNA condensation induced by a tetranuclear nickel(II) complex. *Chem. - Eur. J.* **2010**, *16*, 14181−14189.
(33) Malina, J.; Farrell, N. P.; Brabec, V. DNA condensing effects and sequence selectivity of DNA binding of antitumor noncovalent polynuclear platinum complexes. *Inorg. Chem.* **2014**, *53*, 1662−1671.
(34) Vijayanathan, V.; Thomas, T.; Shirahata, A.; Thomas, T. J. DNA condensation by polyamines: a laser light scattering study of structural effects. *Biochemistry* **2001**, *40*, 13644−13651.
(35) Kankia, B. I.; Buckin, V.; Bloomfield, V. A. Hexamminecobalt-(III)-induced condensation of calf thymus DNA: circular dichroism and hydration measurements. *Nucleic Acids Res.* **2001**, *29*, 2795−2801.
(36) Rosenberg, B. Platinum complexes for the treatment of cancer. *Interdiscip. Sci. Rev.* **1978**, *3*, 134−147.
(37) Johnstone, T. C.; Alexander, S. M.; Lin, W.; Lippard, S. J. Effects of monofunctional platinum agents on bacterial growth: A retrospective study. *J. Am. Chem. Soc.* **2014**, *136*, 116−118.
(38) Reslova, S. The induction of lysogenic strains of Escherichia coli by cis-dichlorodiammineplatinum(II). *Chem.-Biol. Interact.* **1971**, *4*, 66−70.
(39) Sorenson, C. M.; Eastman, A. Mechanism of cis-diamminedichloroplatinum(II)-induced cytotoxicity: role of G2 arrest and DNA double-strand breaks. *Cancer Res.* **1988**, *48*, 4484−4488.
(40) Sorenson, C. M.; Eastman, A. Influence of cis-diamminedichloroplatinum(II) on DNA synthesis and cell cycle progression in excision repair proficient and deficient Chinese hamster ovary cells. *Cancer Res.* **1988**, *48*, 6703−6707.
(41) Norrby, K. In vivo models of angiogenesis. *J. Cell. Mol. Med.* **2006**, *10*, 588−612.
(42) Nitzsche, B.; Gloesenkamp, C.; Schrader, M.; Ocker, M.; Preissner, R.; Lein, M.; Zakrzewicz, A.; Hoffmann, B.; Höpfner, M. Novel compounds with antiangiogenic and antiproliferative potency for growth control of testicular germ cell tumours. *Br. J. Cancer* **2010**, *103*, 18−28.
(43) Parrish, A. R.; Gandolfi, A. J.; Brendel, K. Precision-cut tissue slices: applications in pharmacology and toxicology. *Life Sci.* **1995**, *57*, 1887−1901.
(44) de Graaf, I. A. M.; Olinga, P.; de Jager, M. H.; Merema, M. T.; de Kanter, R.; van de Kerkhof, E. G.; Groothuis, G. M. M. Preparation and incubation of precision-cut liver and intestinal slices for application in drug metabolism and toxicity studies. *Nat. Protoc.* **2010**, *5*, 1540−1551.
(45) Vickers, A. E.; Rose, K.; Fisher, R.; Saulnier, M.; Sahota, P.; Bentley, P. Kidney slices of human and rat to characterize cisplatin-induced injury on cellular pathways and morphology. *Toxicol. Pathol.* **2004**, *32*, 577−590.
(46) Bertrand, B.; Stefan, L.; Pirrotta, M.; Monchaud, D.; Bodio, E.; Richard, P.; Le Gendre, P.; Warmerdam, E.; de Jager, M. H.; Groothuis, G. M.; Picquet, M.; Casini, A. Caffeine-based gold(I) N-heterocyclic carbenes as possible anticancer agents: synthesis and biological properties. *Inorg. Chem.* **2014**, *53*, 2296−2303.
(47) Daum, S.; Chekhun, V. F.; Todor, I. N.; Lukianova, N. Y.; Shvets, Y. V.; Sellner, L.; Putzker, K.; Lewis, J.; Zenz, T.; de Graaf, I. A.; Groothuis, G. M.; Casini, A.; Zozulia, O.; Hampel, F.; Mokhir, A. Improved synthesis of N-benzylaminoferrocene-based prodrugs and

DOI: 10.1021/acs.jmedchem.5b00896
J. Med. Chem. 2015, 58, 6283−6292

evaluation of their toxicity and antileukemic activity. *J. Med. Chem.* **2015**, *58*, 2015−2024.

DOI: 10.1021/acs.jmedchem.5b00896
J. Med. Chem. 2015, 58, 6283−6292

Supporting Information

Adjusting the DNA interaction and anticancer activity of Pt(II) *N*-heterocyclic carbene complexes by steric shielding of the *trans* leaving group

Julienne K. Muenzner[†], Tobias Rehm[†], Bernhard Biersack[†], Angela Casini[‡], Inge A. M. de Graaf[‡], Pawida Worawutputtapong[‡], Awal Noor[§], Rhett Kempe[§], Viktor Brabec[¶], Jana Kasparkova[#], and Rainer Schobert*[,†]

[†]*Organic Chemistry Laboratory, University Bayreuth, Universitaetsstr. 30, 95440 Bayreuth, Germany*

[‡]*Dept. of Pharmacokinetics, Toxicology and Targeting, Research Institute of Pharmacy, University of Groningen, Antonius Deusinglaan 1, 9713 AV Groningen, The Netherlands*

[§]*Lehrstuhl fuer Anorganische Chemie II (Catalyst Design), Universitaet Bayreuth, Universitaetsstr. 30, 95440 Bayreuth*

[¶] *Institute of Biophysics, Academy of Sciences of the Czech Republic, CZ-61265 Brno, Czech Republic*

[#] *Department of Biophysics, Faculty of Science, Palacky University, 17. listopadu 12, CZ-77146 Olomouc, Czech Republic*

*Corresponding author. E-mail: Rainer.Schobert@uni-bayreuth.de

TOC

General remarks and instruments used

Melting points (uncorrected), Büchi Melting Point M-565; IR spectra, Perkin-Elmer Spectrum One FT-IR spectrophotometer with ATR sampling unit; NMR spectra, Bruker Avance 300 spectrometer (300MHz) and Bruker Avance III HD spectrometer (500 MHz); chemical shifts are given in ppm (δ) downfield from tetramethylsilane as internal standard, ^{195}Pt-NMR shifts quoted relative to $\Xi(^{195}Pt) = 21.4$ MHz; Mass spectra, Thermo Finnigan MAT 8500 (EI) and Thermo Scientific QExactive (HRMS); Microanalyses, Perkin-Elmer 2400 CHN elemental analyzer. Organic solvents were distilled prior to use, chemicals were purchased from the usual retailers and used without further purification. The NHC ligand and its silver carbene complex **1** were prepared according to the literature. [17,18] All tested compounds were > 98% pure by elemental analysis and/or HPLC.

Crystal structure determination and structural data of 3a-c

Diffractometer used: STOE-IPDS II; data collection by: X-AREA-STOE; cell refinement by: X-AREA-STOE. The three single crystal samples were measured with Mo-Kα and collected at 133K. The structures were solved by direct methods using SIR97 and refined by full matrix least-squares on F^2 for all data using SHELXL2014. All hydrogen atoms were added at calculated positions and refined using a riding model. Anisotropic thermal displacement parameters were used for all non-hydrogen atoms. Further details about the data collection are listed in Table S1 together with reliability factors. Supplementary crystallographic data were deposited with The Cambridge Crystallographic Data Centre CCDC at numbers 1062990 (**3a**), 1062991 (**3b**), and 1062992 (**3c**) and can be obtained free of charge at www.ccdc.cam.ac.uk/data_request/cif.

Table S1. X-ray structural data of platinum carbene complexes **3a-c**

	3a (CCDC1062990)	**3b** (CCDC1062991)	**3c** (CCDC1062992)
Empirical formula	$C_{19}H_{22}Cl_2N_2OPtS$	$C_{35}H_{31}Cl_2N_2PPt$	$C_{57}H_{50}Cl_{14}N_2P_2Pt$
Formula weight	592.43	776.58	1516.32
Temperature	133 K	133 K	133 K
Wavelength	0.71069 Å	0.71069 Å	0.71069 Å
Crystal system	orthorhombic	monoclinic	triclinic
Space group	$Pna2_1$	$P2_1/c$	P-1
Unit cell dimensions	a = 10.7580(4) Å b = 20.3260(8) Å c = 9.4100(4) Å α = β = γ = 90°	a = 15.7470(8) Å b = 11.1480(5) Å c = 17.9600(9) Å α = γ = 90° β = 97.023(4)°	a = 10.4580(4) Å b = 15.3410(5) Å c = 21.0210(8) Å α = 76.344(3)° β = 82.256(3)° γ = 71.766(3)°
Volume	2057.66(14) $Å^3$	3129.2(3) $Å^3$	3105.9(2) $Å^3$
Z	4	4	4
Density (calcd)	1.912 Mg/m^3	1.648 Mg/m^3	1.621 Mg/m^3
Absorption coefficient	7.191 mm^{-1}	4.73 mm^{-1}	2.95 mm^{-1}
F(000)	1144	1528	1504
Crystal size / mm^3	0.20 × 0.19 × 0.07	0.17 × 0.15 × 0.10	0.13 × 0.11 × 0.10
Theta range (data col.)	2.0 to 26.3°	1.3 to 26.3°	1.4 to 26.3°
Index ranges	$-13 \le h \le 13$	$-19 \le h \le 19$	$-12 \le h \le 13$
Index ranges	$-25 \le k \le 25$	$-13 \le k \le 13$	$-18 \le k \le 19$
Index ranges	$-11 \le l \le 11$	$-22 \le l \le 22$	$-25 \le l \le 26$
Reflections collected	27647	42874	43574
Independent reflexes	4084 [R_{int}=0.060]	6269 [R_{int}=0.224]	12393 [R_{int}=0.144]
Completeness to θmax	99.3 %	99.4 %	98.8 %
Absorption correction	numerical	numerical	numerical
Max / min transmission	0.6029 / 0.3122	0.480 / 0.618	0.8057 / 0.6436
Refinement method	Full–matrix least–squares on F^2	Full–matrix least–squares on F^2	Full–matrix least–squares on F^2
Data / restraints / param	4084 / 1 / 237	6269 / 0 / 370	12393 / 0 / 697
Goodness–of–fit on F^2	0.974	0.928	1.003
Final R indices	R_1 = 0.0227	R_1 = 0.0523	R_1 = 0.0541
[I>2σ(I)]	wR_2 = 0.0512	wR_2 = 0.1003	wR_2 = 0.1347
R indices	R_1 = 0.0305	R_1 = 0.1145	R_1 = 0.0683
(all data)	wR_2 = 0.0536	wR_2 = 0.1003	wR_2 = 0.1460
Largest diff. peak / hole	0.98/– 0.55 $eÅ^{-3}$	1.25/– 2.13 $eÅ^{-3}$	2.48/– 2.66 $eÅ^{-3}$

Cell lines and culture conditions

The human melanoma cell line 518A2 was obtained from the Department of Radiotherapy, Medical University of Vienna (Austria).[40-42] The Panc-1 pancreatic carcinoma cell line (CRL-1469™), the DLD-1 colorectal adenocarcinoma cells (CCL-221™), and the CCD-18Co human fibroblasts (CRL-1459™) were obtained from the American Type Culture Collection (ATCC). All other cancer cell lines were purchased from the German Centre of Biological Materials (DSMZ), Braunschweig, Germany. All cells were grown at 37 °C, 5% CO_2, 95% humidity in Dulbecco's Modified Eagle Medium (DMEM with 3.7 g/L $NaHCO_3$, 4.5 g/L D-glucose and 0.58 g/L stable glutamine (L-alanyl-L-glutamine), without sodium pyruvate; Biochrom) containing 10% fetal bovine serum (FBS), 1% Antibiotic-Antimycotic and 250 µg/mL gentamycine (all from Gibco), apart from the HT-29 cell line that was grown in RPMI-1640 medium (10% FBS, 1% Antibiotic-Antimycotic, 250 µg/mL gentamycine). To reach high expression levels of the breast cancer resistance protein (BCRP) in MCF-7/Topo cells and the P-glycoprotein (Pgp) in KB-V1/Vbl cells, the maximum tolerated dose of topotecan (Topo) or vinblastine(Vbl), respectively, was added to the cell culture medium 24 h after every cell passage over several weeks. Only mycoplasma-free cell cultures were used.

Growth inhibition (MTT) assay

3-(4,5-Dimethylthiazol-2-yl)-2,5-diphenyl-tetrazolium bromide (MTT; ABCR) was used to identify viable cells that reduce it to a violet formazan.[19] The adherent 518A2 melanoma, Panc-1 pancreatic carcinoma, the MCF-7/Topo breast adenocarcinoma, the KB-V1/Vbl cervix carcinoma, the HCT-116 and HT-29 colon carcinoma cells as well as the DLD-1 colorectal adenocarcinoma cells (5000 cells per well) were seeded and cultured for 24 h on 96-well microplates. Incubation (5% CO_2, 95% humidity, 37 °C) of cells following addition of cisplatin or the test compounds **2** and **3a-c** (dilution series of 10 mM stock solutions in DMSO or DMF, respectively, ranging from 25 nM to 100 µM in H_2O) was continued for 72 h. Solvent controls were treated identically. A 0.05 % solution of MTT (50 µL/well) in phosphate buffered saline (PBS) was added to the cells after centrifugation (300 g, 5 min, 4 °C) and removal of the medium. After another 2 h of incubation the microplates were centrifuged and the supernatant MTT solution was discarded. The precipitated formazan crystals at the bottom of the wells were dissolved in a 10% solution of sodium dodecyl sulfate (SDS) in DMSO containing 0.6% acetic acid (25 µL/well). The microplates were incubated overnight, to ensure a complete dissolution of the violet formazan. The absorbance at 570 and 630 nm was measured using an automatic TECAN plate reader (TECAN Infinite® F200). For

each substance the experiment was carried out in quadruplicate. The test compound concentrations at which viable cells were reduced to 50% (IC_{50} values) are presented as means±S.D. (solvent controls set to 100% viable cells). To assess whether the test compounds exhibit a selectivity for cancer cells with respect to non-malignant cells, we used CCD-18Co human colon fibroblasts in MTT assays at a higher density of 10,000 cells per well due to their slower cell growth rate. Culture plates with CHF were subjected to the MTT assay under identical conditions.

Cellular platinum accumulation

Human colon carcinoma cells HCT-116 were seeded in 100 mm culture dishes at the density $3 \cdot 10^6$ cells/dish (50 000 cells/cm^2). After overnight incubation, the cells were treated with the compounds (10 µM) for 12 h. The attached cells were washed twice with PBS (4 °C). Cell pellets were digested by a high pressure microwave digestion system (MARS5, CEM) with HCl (11 M) to give a fully homogenized solution, and final platinum content was determined by FAAS. Experiments were performed in triplicate and the values are the means ± SD.

Measurement of the partition coefficient

To determine the hydrophilicity/lipophilicity of compounds the shake flask method was used. Octanol-saturated water (OSW) and water-saturated octanol (WSO) were prepared using analytical grade octanol and 0.2 M NaCl MillyQ solution (to suppress hydrolysis of chlorido ligands). Compounds were dissolved in WSO and mixed in equal volume of OSW for 1 h at 25 °C. Both phases were separated with centrifugation (3000 g, 5 min). Samples were carefully separated from octanol and water layer and analyzed for platinum content using FAAS. Partition coefficients of tested compounds were calculated using the equation log P = log ([Pt]WSO/[Pt]OSW). The experiments were done in triplicate.

Table S2. Cellular platinum accumulation in human colon carcinoma cells HCT-116[a] and log P (octanol/water) values[b] obtained by shake flask method

	ng Pt / 10^6 cells [a,b]	**logP** [b]
3a	5.3 ± 0.5	0.71 ± 0.05
3b	51 ± 4	3.3 ± 0.2
3c	448 ± 11	3.9 ± 0.2
cisplatin	13 ± 1	-2.5 ± 0.2

[a] The table shows the uptake of tested compounds (10 µM) into HCT-116 cells after 12 h of exposure (without recovery time). [b] Results are expressed as the mean ± SD for three independent experiments.

Interaction of complex 3c with circular pBR322 DNA

The interaction of *bis*-PPh_3 Pt(II) complex **3c** with circular pBR322 plasmid DNA was analyzed by an electrophoretic mobility shift assay (EMSA). Figure S1 shows the complete EMSA gel. Besides the band shift from the ccc-form of the plasmid to the oc-form, which is characteristic for DNA interaction, treatment of the plasmid DNA with complex **3c** also resulted in additional DNA bands with even less electrophoretic mobility than the plasmid's oc form starting at a concentration of 10 µM of the test compound. When 25 µM or 50 µM of **3c** were applied large amounts of plasmid DNA even remained in the wells of the gel, indicating bigger DNA aggregates that are not able to penetrate the small pores of the agarose gel.

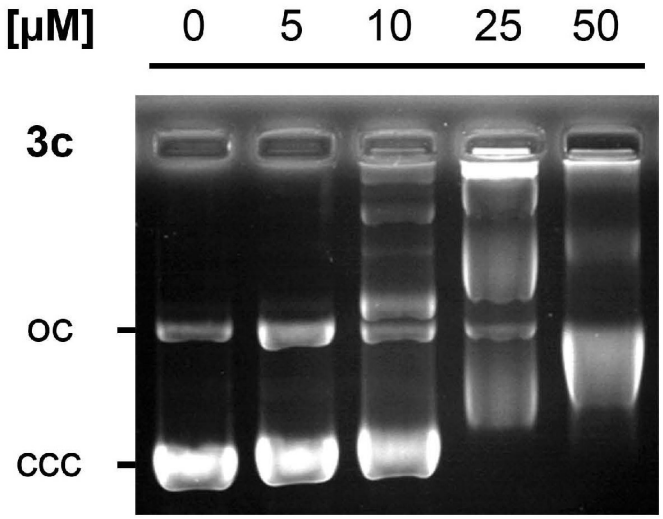

Figure S1: Interaction of Pt(II) NHC complex **3c** with circular pBR322 plasmid DNA as observed by electrophoretic mobility shift assays (EMSA) after 24 h of incubation. The picture is representative of two independent experiments.

Effect on bacterial morphology and on the induction of lysogenic bacteria

Escherichia coli (CCM 7929) was obtained from the Czech Collection of Microorganisms (CCM), Masaryk University, Faculty of Science, Brno, Czech Republic as a freeze-dried pellet. The cells were rehydrated and propagated on LB agar plates according to the supplier protocol. *E. coli* GY 5027 envA uvrB (lambda), which is infected with bacteriophage λ, was obtained from Dr. Vojtiskova, Institute of Biophysics, v.v.i, Czech Republic as a culture on solid agar. The effect of the platinum complexes on bacterial morphology and on the induction of lysogenic bacteria was studied as already described.[37,38] Briefly, for the bacterial

morphology studies, a colony of *E. coli* (CCM 7929) was picked and grown to saturation in LB following overnight incubation at 37 °C. A 100 μL aliquot of this suspension was added to 6 mL of LB which was incubated at 37 °C until the OD_{600} of the solution reached 0.5. Aliquots of this suspension, 50 μL each, were added to 3 mL of LB containing either 30 μM of **3a-c,** cisplatin or no platinum. The mixtures were incubated at 37 °C, after 5 h, a 5 μL drop of each cell suspension was mounted on a separate microscope slide and imaged using confocal microscope Leica TSC SP-5 X, equipped with the objective HCX PL APO lambda blue 63.0x1.20 water UV. Samples were illuminated in the bright field mode with alignment-free, mercury metal halide bulb source Leica EL6000 and visualized with micro max CCD camera HCX 365 FX.

For the lytic transformation studies, a 6 mL volume of LB was inoculated with *E. coli* GY 5027 envA uvrB (lambda) and grown to saturation following overnight incubation at 37 °C. A 100 μL aliquot of this suspension was added to 6 mL of LB, which was then incubated at 37°C until the OD_{600} of the solution reached 0.5. Aliquots of this suspension, 50 μL each, were added to 6 mL of LB containing 30 μM of one of platinum compounds tested (**3a-c** or cisplatin) or no platinum. The cultures were incubated at 37 °C for 5 h. After this time, a 10 μL aliquot of each of the cell suspensions that had been treated with platinum was diluted 1000-fold and 10 μL of each dilution were dabbed onto an LB agar plate with top 0.5% agar containing a lawn of *E. coli* (CCM 7929). As controls, the lawn was also spotted with 30 nM solutions of each platinum complex as well as with a 1000-fold dilution of suspension of *E. coli* GY 5027 envA uvrB (lambda) cells that had not been treated with platinum. After spotting, the plate was incubated at 37 °C overnight to observe the formation of plaques.

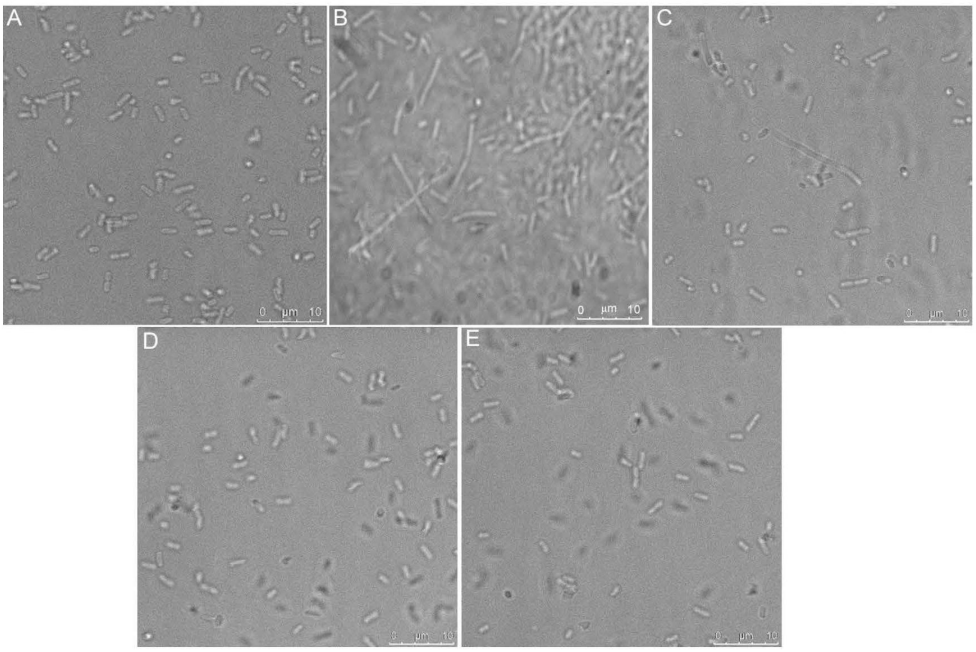

Figure S2. Effect of cisplatin (B) and complexes **3a-c** (panels C-E) on the morphology of *E.coli* K12 cells. Untreated control bacteria are shown in panel A. Scale bars represent 10 µm.

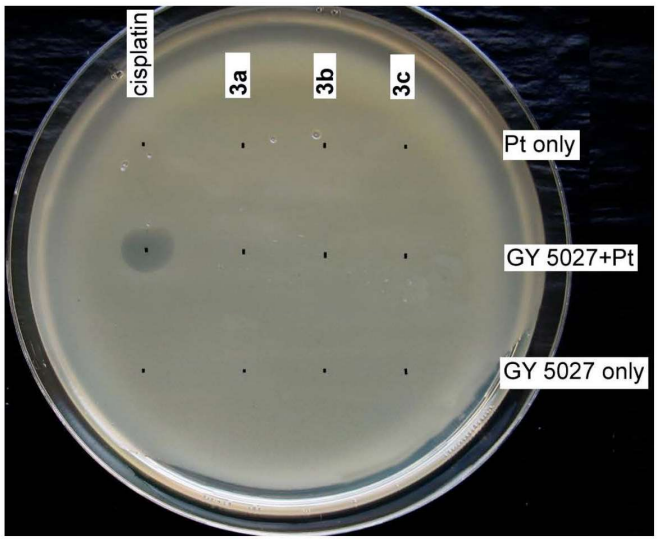

Figure S3. The development of plaques in *E.coli* K12 as the result of an application of a suspension of *E.coli* GY5027 (lambda) cells that had been treated with 30 µM concentrations of cisplatin (cisPt) and **3a-c** (center row). Control rows were dabbed with a solution containing only the corresponding platinum complex or a suspension of *E.coli* GY5027 (lambda) not treated with platinum compounds.

Histomorphology of PCKS treated with bisphosphane complex 3c

The toxic effect of complex **3c** on PCKS was assessed by histomorphology studies. Representative pictures for the treatment with 1 μM of **3c** are shown in Figure S4. They confirm the results of the ATP viability assay. The kidney slices were distinctly affected by the compound already at this low concentration and they showed pronounced necrosis (significant loss of nuclei) in comparison to controls.

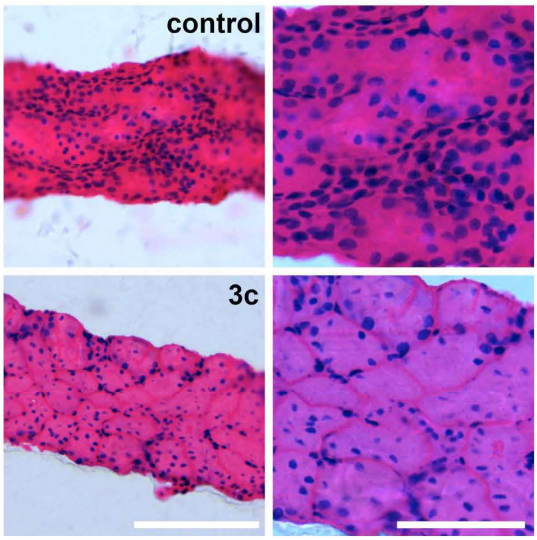

Figure S4. Histomorphology of untreated PCKS (control, top row) and kidney slices treated with 1 μM of complex **3c** (bottom row) after 24 h of incubation at two different magnifications. Scale bars - left: 50 μm, right: 100 μm.

Supplementary References

[S1] Selzer, E.; Pimentel, E.; Wacheck, V.; Schlegel, W.; Pehamberger, H.; Jansen, B.; Kodym, R. Effects of betulinic acid alone and in combination with irradiation in human melanoma cells. *J. Invest. Dermatol.* **2000**, *114*, 935-940.

[S2] Versteeg, R.; Noordermeer, I. A.; Kruse-Wolters, M.; Ruiter, D. J.; Schrier, P. I. c-myc down-regulates class I HLA expression in human melanomas. *EMBO J.* **1988**, *7*, 1023-1029.

[S3] Jansen, B.; Schlagbauer-Wadl, H.; Eichler, H.-G.; Wolff, K.; van Elsas, A.; Schrier, P. I.; Pehamberger, H. Activated N-ras contributes to the chemoresistance of human melanoma in severe combined immunodeficiency (SCID) mice by blocking apoptosis. *Cancer Res.* **1997**, *57*, 362-365.

4.3 PUBLIKATION II

„N,N-Dialkylbenzimidazol-2-ylidene platinum complexes – effects of alkyl residues and ancillary cis-ligands on anticancer activity“

Dalton Transactions **2018**, *47*, 17367

Tobias Rehm,[‡a] Matthias Rothemund,[‡a] Alexander Bär,[a] Thomas Dietel,[b] Rhett Kempe,[b] Hana Kostrhunova,[c] Viktor Brabec,[c] Jana Kasparkova[*c] and Rainer Schobert[*a]

[a]Department of Chemistry, University Bayreuth, Universitaetsstrasse 30, 95440 Bayreuth, Germany. E-mail: Rainer.Schobert@uni-bayreuth.de

[b]Lehrstuhl fuer Anorganische Chemie II, University Bayreuth, Universitaetsstrasse 30, 95440 Bayreuth, Germany

[c]Institute of Biophysics, Academy of Sciences of the Czech Republic, CZ-61265 Brno, Czech Republic. E-mail: jana@ibp.cz

‡These authors contributed equally to this work.

Dalton Transactions

PAPER

Cite this: *Dalton Trans.*, 2018, **47**, 17367

N,N-Dialkylbenzimidazol-2-ylidene platinum complexes – effects of alkyl residues and ancillary *cis*-ligands on anticancer activity†

Tobias Rehm,‡[a] Matthias Rothemund,‡[a] Alexander Bär,[a] Thomas Dietel,[b] Rhett Kempe,[b] Hana Kostrhunova,[c] Viktor Brabec,[c] Jana Kasparkova*[c] and Rainer Schobert*[a]

Received 16th August 2018,
Accepted 13th November 2018

DOI: 10.1039/c8dt03360a

rsc.li/dalton

Eleven complexes of [(1,3-dialkylbenzimidazol-2-ylidene)L_nCl_{3-n}]$Pt^{(n-1)+}$, with L_n = DMSO (**8**), Ph_3P (**9**), $(Ph_3P)_2$ (**10**), and alkyl = Me (**a**), Et (**b**), Bu (**c**), octyl (**d**), were synthesised and tested for cellular accumulation, cytotoxicity, interference with the tumour cell cycle, and interaction with DNA. The delocalised lipophilic cationic bisphosphane complexes **10** were on average found to be more cytotoxic in MTT assays against a panel of seven cancer cell lines than the neutral DMSO and monophosphane complexes **8** and **9**. The uptake of complexes **10**, at least into HCT116 colon carcinoma cells, was also significantly greater than that of analogues **8** and **9**. Their cytotoxicities did not differ significantly with the *N*-alkyl side chain length. The complexes that were most active, with sub-micromolar IC_{50} (72 h) values against $HCT116^{wt}$ cells, that is **8b**, **9b**, **10a–c**, worked by a mode of action that was dependent on the functional p53, yet were still far more active than cisplatin in both of the $HCT116^{wt}$ and $HCT116^{-/-}$ variants. In detailed binding analyses **8c**, **9c** and **10a–c** showed a lower affinity to DNA and different binding modes when compared to cisplatin, preferably forming mono-adducts with DNA and distorting it to a lower extent. Also, unlike cisplatin, they arrested the HCT116 cells of both variants predominantly in the G1 phase.

Introduction

Since its approval in 1979, cisplatin (**1**, CDDP) has established itself as the leading anti-cancer drug for several cancer entities. In nearly 40 years only six more approved platinum drugs have arisen from intensive scientific research. Although these drugs offer quite a few advantages over cisplatin, such as increased tumour specificity and reduced unwanted side effects, they are still hampered by their high toxicity and adverse effects in patients, as well as a tendency to elicit tumoral drug resistance.[1]

A common strategy to overcome these negative effects is the variation of the spectator and the leaving ligands, for example, in the case of cisplatin, the substitution of the ammine residues by mono- or bidentate amines and/or the exchange of the chlorido ligands by chelating carboxylic acids. Since the turn of the millennium, ever more diverse ligands with targeting functions or bioactivity of their own have been attached to Pt^{II} complexes and Pt^{IV} prodrugs.[2]

With the advent of the stable N-heterocyclic carbenes (NHCs), first being made accessible by Arduengo *et al.*,[3] a genuinely new ligand motif became available that allowed the stereoelectronic fine-tuning of catalysts[4] and the pharmacological optimisation of metallodrugs. Owing to their ease of synthesis, their structural variability and their chemical stability, N-heterocyclic carbene (NHC) complexes of metals[5] as diverse as silver,[6] gold,[7] copper,[8] ruthenium[9] and platinum[10] have become an ever-growing branch of medicinal chemistry.

N-Heterocyclic carbenes are often teamed up in square planar Pt^{II} complexes with other ligands such as amines,[10a,b] pyridines[10c] or pnictogen ligands[10d,e] (PPh_3, $AsPh_3$, $SbPh_3$). In the past, we have concentrated on Pt^{II} complexes carrying DMSO or phosphane ligands *cis* to benzylated imidazol-2-ylidene ligands, for example **2–4**.[10d] We have also developed a protocol to introduce a second, optionally different, NHC ligand in the *cis*-position to the first one as show in complex **5** (Fig. 1).[11] We have now found that complexes with *N*-alkylated

[a]*Department of Chemistry, University Bayreuth, Universitaetsstrasse 30, 95440 Bayreuth, Germany. E-mail: Rainer.Schobert@uni-bayreuth.de*
[b]*Lehrstuhl fuer Anorganische Chemie II, University Bayreuth, Universitaetsstrasse 30, 95440 Bayreuth, Germany*
[c]*Institute of Biophysics, Academy of Sciences of the Czech Republic, CZ-61265 Brno, Czech Republic. E-mail: jana@ibp.cz*

†Electronic supplementary information (ESI) available: Ligand synthesis; NMR spectra; X-ray structural data, values for cellular accumulation, cell cycle analysis in HCT116 cells. CCDC 1857511–1857513. For ESI and crystallographic data in CIF or other electronic format see DOI: 10.1039/c8dt03360a

‡These authors contributed equally to this work.

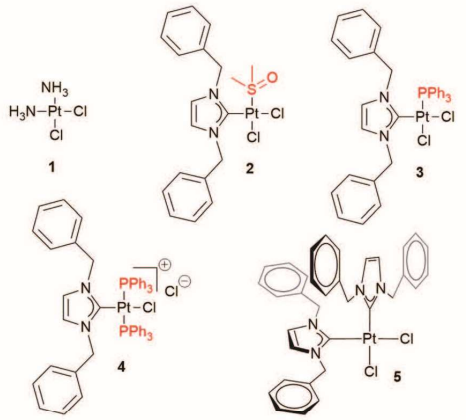

Fig. 1 Structures of cisplatin (1) and the NHC complexes 2–5.

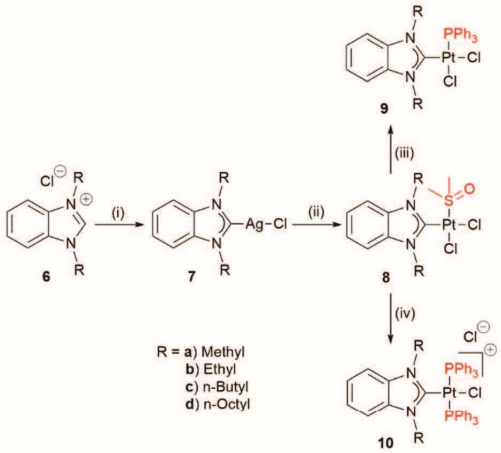

Scheme 1 Synthesis of complexes **8a–d**, **9a–d** and **10a–c**. (i) Ag_2O, CH_2Cl_2, rt; (ii) K_2PtCl_4, DMSO, 60 °C; (iii) PPh_3, CH_2Cl_2; (iv) PPh_3, CH_2Cl_2, rt; **10c**: CH_3CN, 60 °C; **10d**: unstable, decomposed upon attempted isolation.

benzimidazoles rather than imidazole ligands show some advantages, including a better solubility combined with chemical stability and the tendency to form easy to purify, and easy to weigh out, crystalline complexes. The aim of this study was to evaluate the influence of structural changes, for example the alkyl chain length, overall size, lipophilicity, and steric encumbrance of the benzimidazol-2-ylidene complexes of Pt^{II}, on the effects of the complexes on cancer cells. To this end, we synthesised the ligand precursors **6a–d** and their downstream complexes of types **8–10** (Scheme 1). By extending the length of the *N*-alkyl chain from the methyl to the ethyl, butyl and up to the octyl we gradually increased the size and lipophilicity of the NHC ligands and their respective platinum complexes. A comparison of the complex patterns *cis*-$[Cl_2(NHC)(DMSO)]Pt^{II}$, *cis*-$[Cl_2(NHC)(PPh_3)]Pt^{II}$ and *trans*-$[Cl(NHC)(PPh_3)_2]Pt^{+}Cl^{-}$, analogous to **2–4**, should allow a prediction of the influence of the lipophilicity, steric encumbrance, and charge on the biological properties of similar NHC-Pt^{II} anticancer drugs. Eleven such NHC-platinum(II) complexes with benzimidazol-2-ylidene ligands of varying size and lipophilicity were prepared and studied. Complex **10d** was inaccessible as it decomposed upon attempted isolation.

Results and discussion

Synthesis and characterisation

Benzimidazolium salts with methyl, ethyl, butyl, and octyl residues were obtained by treating benzimidazole with K_2CO_3 and either iodomethane, iodoethane, 1-bromobutane, or 1-bromooctane, respectively. They were converted to their chlorides **6a–d** to prevent anion exchange during the following steps. Treating them with Ag_2O in CH_2Cl_2 for at least 24 h afforded the NHC silver(I) complexes **7a–d** after filtration and crystallisation. As complex **7a** was poorly soluble it could not be separated from the silver residues and was therefore converted to the platinum complex **8a** without purification. The formation of the silver carbene complex **7d** took several days, probably owing to the bulkiness of its NHC ligand.

Transmetalation to the respective *cis*-$[(NHC)(DMSO)Pt^{II}Cl_2]$ complexes **8** was achieved by adding the silver complexes **7** to K_2PtCl_4 in DMSO to give *cis*-$Pt(DMSO)_2Cl_2$ as a reactive intermediate. The crude silver complex **7a** of uncertain purity was treated only with 0.9 equivalents of K_2PtCl_4 to prevent contamination of the product complex **8a** by leftover *cis*–$Pt(DMSO)_2Cl_2$. After extraction and crystallisation all of the complexes of **8** were obtained in good yield and a purity sufficient for biochemical assessment.

For the synthesis of the phosphane complexes of types **9** and **10** we intended to apply the same protocols as for the preparation of the imidazol-2-ylidene analogues **3** and **4**. Complex **3** had been obtained by substitution of the labile DMSO ligand of complex **2** with 1.1 equivalents of PPh_3 in CH_2Cl_2 at room temperature within 90 min. The conversion of complex **2** to the cationic bisphosphane complex **4** required stirring with five equivalents of PPh_3 for 30 min. However, the benzimidazol-2-ylidene complexes **9** and **10** were not accessible in this way. When treated with 1.1 equivalents of PPh_3 only 50% of the DMSO complex **8a**, bearing a 1,3-dimethylbenzimidazol-2-ylidene ligand, reacted to afford the exclusively bisphosphane complex **10a**, but none of the monophosphane complex **9a**, which is obviously more reactive than **8a**. To prepare complex **9a** in an acceptable yield, a solution of PPh_3 was added slowly to a highly diluted solution of **8a**. The product was then separated and purified using column chromatography and crystallisation. When the sterically more hindered *N*,*N*-diethyl substituted analogue **8b** was reacted overnight with five equivalents of PPh_3, the monophosphane complex **9b** was isolated in good yield besides only trace amounts of the cationic bisphosphane complex **10b**. To gain

the latter in a moderate yield **8b** was stirred with 10 equivalents of PPh_3 for a full five days, followed by careful crystallisation. Unsurprisingly, the sterically even more hindered DMSO complex **8c**, bearing a 1,3-dibutylbenzimidazol-2-ylidene ligand, when reacted with 10 equivalents of PPh_3 for several days afforded the monophosphane complex **9c** exclusively. The cationic bisphosphane complex **10c** could be prepared in acceptable yield only by heating the DMSO complex **8c** with 20equivalents of PPh_3 in acetonitrile at 80 °C for four days. Similarly, the DMSO complex **8d**, bearing a 1,3-dioctylbenzimidazol-2-ylidene ligand, reacted with five equivalents of PPh_3 in CH_2Cl_2 at room temperature for 16 h to give monophosphane complex **9d**. A second PPh_3 was incorporated only upon heating with a large excess of PPh_3 in acetonitrile at 80 °C. Attempts to isolate the bisphosphane complex **10d** always gave mixtures of **10d**, **9d** and PPh_3. ^{31}P NMR spectra revealed that in solution, with an excess of phosphane, the signals for **9d** and PPh_3 at 9.1 ppm and −5.5 ppm, respectively, would disappear over time to generate more **10d** at 18.9 ppm, as shown in Fig. 2. Repeated attempts to isolate the cationic product from such solutions, with only traces of **9d** and PPh_3 left, led to equilibrated mixtures again, or even pure **9d** in significant amounts. This indicates that **10d** is stable in solution only in the presence of an excess of PPh_3 and decomposes upon isolation. It was therefore not possible to purify this compound for biological studies.

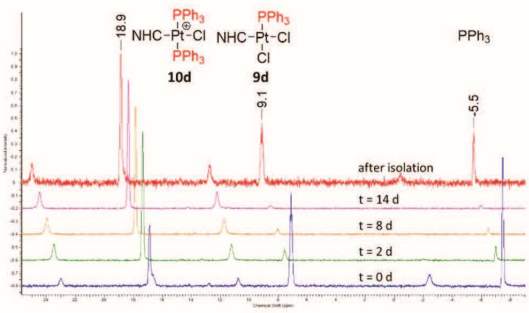

Fig. 2 ^{31}P NMR spectra of reactions over time between PPh_3 and **9d** to give **10d**, and for the decomposition products obtained upon attempts to isolate it from the "*t* = 14 d" sample.

The new Pt^{II} complexes **8**, **9** and **10** were characterised using ^{1}H, ^{13}C, ^{195}Pt and ^{31}P nuclear magnetic resonance (NMR) spectroscopy, as well as mass spectrometry and elemental analysis. Single crystal X-ray structure analyses were performed for complexes **8b**, **9c** and **10a** (Fig. 3).

The completion of the formation of the DMSO complexes **8** can be seen from the equivalent benzimidazole and DMSO signals in the ^{1}H NMR spectra. For **8b–d** the N–CH_2 protons of the side chains were inequivalent and gave rise to two sets of signals. As seen before with the benzylated imidazole ligands,[10d] this confirms the *cis* configuration of the NHC and DMSO ligands as well as a perpendicular orientation of the benzimidazole relative to the plane spanned by the $PtCl_2$(DMSO) fragment. This effect recurs for **9b–d**, while the spectra of the symmetric complexes **10** show no inequivalent protons.

To monitor the formation of complexes **9** and **10** and to also verify their conformation, ^{31}P NMR spectroscopy is a convenient technique. The neutral complexes **9** exhibit a signal between 8.83 and 9.19 ppm with coupling constants ranging from 3861 to 3901 Hz. The cationic complexes **10** with two equivalent PPh_3 moieties show a signal between 17.7 and 18.9 ppm, coupling with a J_{P-Pt} = 2478 Hz to 2486 Hz typical of the *trans*-configured phosphanes.[10d,e]

The same Pt–P couplings are present in the ^{195}Pt NMR spectra. Complexes **8a–d** give a singlet around −3554 to −3566 ppm, complexes **9** show the expected doublets at −4017 to −4018 ppm and **10** shows triplets at −4378 to −4383 ppm. With J_{Pt-P} = 3871–3895 Hz for **9** and 2486–2490 Hz for **10** the

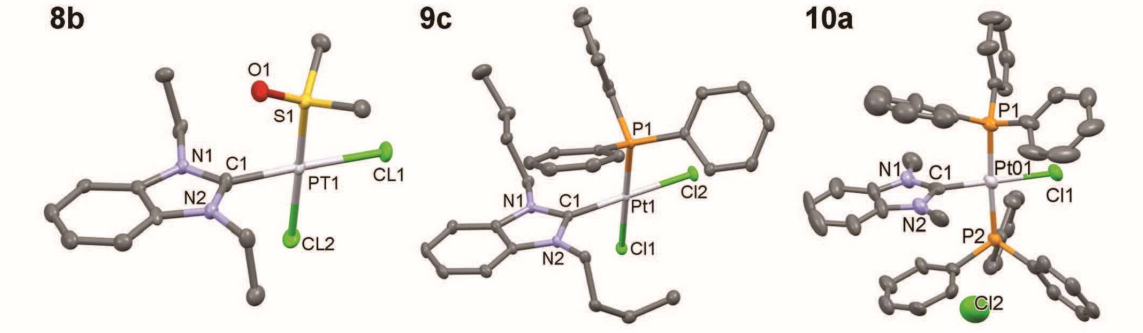

Fig. 3 Molecular structures of complexes **8b**, **9c** and **10a** as thermal ellipsoid representations at the 50% probability level (H atoms omitted). Selected bond lengths [Å] and angles [°]: **8b**: Pt1–Cl1 2.3447(19), Pt1–Cl2 2.332(2), Pt1–C1 1.983(7), Pt1–S1 2.202(2), Cl1–Pt1–Cl2 90.71(7), Cl1–Pt1–S1 90.35(7), Cl1–Pt1–C1 177.6(2), Cl2–Pt1–C1 86.9(2), Cl2–Pt1–S1 178.84(7), C1–Pt1–S1 92.1(2), N1–C1–N2 107.7(6); **9c**: Pt1–C1 1.980(2), Pt1–P1 2.2345(8), Pt1–Cl1 2.3603(8), Pt1–Cl2 2.3480(8), C1–Pt1–P1 95.34(7), C1–Pt1–Cl1 86.76(7), C1–Pt1–Cl2 175.80(6), P1–Pt1–Cl1 175.686(19), P1–Pt1–Cl2 88.09(4), Cl1–Pt1–Cl2 89.65(3), N1–C1–N2 106.70(19); **10a**: Pt1–Cl1 2.349(3), Pt1–C1 1.959(10), Pt1–P1 2.309(3), Pt1–P2 2.311(3), C1–Pt1–Cl1 179.4(4), C1–Pt1–P1 92.2(3), C1–Pt1–P2 90.7(3), P1–Pt1–P2 176.87(10), P1–Pt1–Cl1 87.77(10), P2–Pt1–Cl1 89.33(9), N1–C1–N2 105.3(9).

coupling constants agree with those obtained from the ^{31}P NMR spectra and with the literature values of similar complexes.[10d,e] In the ^{13}C NMR spectra the carbene signals are of special interest. They were found at around 154 ppm for complexes **8**, between 160.6 ppm and 162.0 ppm for **9**, and between 158.0 and 159.9 ppm for the cationic complexes **10**.

Crystallography

Crystals suitable for X-ray diffraction analyses were grown by slow infusion of hexane or diethyl ether into saturated solutions of **8b**, **9c** or **10a** in CH_2Cl_2 kept at 4 °C. Fig. 3 shows their molecular structures. The distances between the platinum and the carbene carbon atoms were in the range of 1.959 to 1.983 Å. The Pt–Cl distances lay between 2.347 to 2.349 Å for those *trans* to the NHC ligand, while the *cis* coordinated varied from 2.332 Å in the DMSO-complex **8b** to 2.360 Å in **9c** *trans* to a phosphine. In cationic **10a**, Pt–P distances were both around 2.31 Å, while in neutral **9c**, this was 2.234 Å and the Pt–S bond in **8b** was even shorter at 2.202 Å. The bond angles between the carbene and the *cis*-phosphine or DMSO ligand were slightly above 90° with a maximum of 95.3° for **9c**.

Cytotoxicity

The new benzimidazol-2-ylidene Pt^{II} complexes **8a–d**, **9a–d**, **10a–c**, and CDDP as a reference, were evaluated using a MTT-assays for their *in vitro* cytotoxicity against a panel of seven cancer cell lines of various entities, including a p53 knock-out mutant ($HCT116^{-/-}$) and the two multi-drug resistant (*mdr*) cell lines $Kb\text{–}V1^{Vbl}$ and $MCF\text{-}7^{Topo}$. The complexes showed a structure-dependent cytotoxicity, with IC_{50} values ranging from inactive (IC_{50} > 100 μM) to low nanomolar (Table 1). A trend emerged with respect to the three complex types **8**, **9**, and **10**, reminiscent of that previously observed for the imidazol-2-ylidene complexes **2–4**.[10d] Substitution of the DMSO ligand in complexes **8** by a PPh_3 ligand led to a slight increase of the overall cytotoxicity of the resulting complexes **9** in some cell lines, while the addition of a second PPh_3 ligand, as seen in the cationic complexes **10**, gave rise to low nanomolar IC_{50} values against most cell lines. The efficacy of complexes **10** was superior to that of CDDP in all cell lines except for the resistant $Kb\text{-}V1^{Vbl}$ cervix carcinoma cell line.

There was no clear trend for the effect of the *N*-alkyl side chain length on the cytotoxicity of the individual complex types **8**, **9**, and **10** over all of the tested cell lines. The neutral *N*-methyl derivatives **8a** and **9a** were inactive (IC_{50} > 100 μM) in all tested cell lines, while the lipophilic delocalised cation **10a** was highly active with low nanomolar IC_{50} values in all but the cervix carcinoma cell line. The *N*-ethyl substituted complex **8b** was the most active DMSO complex in all of the cell lines bar the 518A2 melanoma in which it was virtually inactive. Its high cytotoxicity in the slow-growing colon carcinoma cell lines DLD-1 and $HCT116^{wt}$, as well as in the re-sensitised cervix carcinoma cell line $Kb\text{-}V1^{Vbl+Vpm}$, is worthy of note. Elongation of the side chain as in **8c** and **8d** had no distinct effect.

Amongst the generally bigger and more lipophilic monophosphine complexes the *N*-ethyl substituted **9b** was roughly as active as its *N*-butyl analogue **9c** while complex **9d**, the biggest and most lipophilic, was distinctly less active. The delocalised lipophilic cations **10** were less affected by changes at their NHC ligands and showed similar IC50 values in the nanomolar range, or the low micromolar range in the case of complex **10c**.

Judging by their IC_{50} values, the complexes **8b–d**, **9b–d** and **10a–c** were as active against the *mdr* breast cancer cell line $MCF\text{–}7^{Topo}$ as against all other cell lines, suggesting that they are not recognised as substrates by the breast cancer resistance protein (BCRP) which is overexpressed in this cell line.[13a] In contrast, all of these complexes were conspicuously less effective against the *mdr* cervix carcinoma cell line $Kb\text{–}V1^{Vbl}$ which overexpresses P-glycoprotein 1 (P-gp1), presumably because they are substrates of this efflux transporter.[13b,c] To corroborate this assumption, the IC_{50} values were determined

Table 1 Mean ± SD of IC_{50} (72 h) values [μM] of complexes **8**, **9**, **10a–c** and CDDP in MTT assays against human cancer cell lines[a] as calculated from four independent measurements

	IC_{50} (72 h) [μM]								
Compounds	518A2[a]	HT-29[a]	DLD-1[a]	$HCT116^{wt\,a}$	$HCT116^{-/-\,a}$	$MCF\text{-}7^{Topo\,a}$	$Kb\text{-}V1^{Vbl\,a}$	$Kb\text{-}V1^{Vbl+Vpm\,a}$	$r^{p53\,b}$
8a	>100	>100	>100	>100	n.d.	n.d.	n.d.	n.d.	—
8b	>50	8.6 ± 1.7	0.24 ± 0.03	0.12 ± 0.01	5.9 ± 0.5	6.5 ± 1.6	25.2 ± 0.6	0.28 ± 0.06	−0.979
8c	7.6 ± 0.2	29.4 ± 0.9	12.7 ± 0.9	8.1 ± 0.7	6.0 ± 0.2	10.1 ± 0.3	21.2 ± 0.5	0.25 ± 0.09	0.356
8d	3.1 ± 0.1	11.6 ± 0.5	11.0 ± 1.0	3.9 ± 0.3	9.9 ± 0.7	8.1 ± 0.4	28.3 ± 6.8	4.5 ± 0.9	−0.627
9a	>100	>100	>100	>100	n.d.	n.d.	n.d.	n.d.	—
9b	1.8 ± 0.2	1.9 ± 0.4	1.5 ± 0.1	0.91 ± 0.09	3.7 ± 0.3	3.9 ± 0.3	20.4 ± 1.2	5.6 ± 0.3	−0.755
9c	2.5 ± 0.1	1.3 ± 0.0	0.61 ± 0,06	2.6 ± 0.8	2.4 ± 0.4	1.5 ± 0.1	11.5 ± 0.3	1.6 ± 0.3	0.058
9d	11.0 ± 0.3	11.0 ± 0.5	9.4 ± 0.7	12.3 ± 1.2	12.3 ± 0.5	14.5 ± 3.1	14.1 ± 2.8	4.5 ± 0.9	−0.002
10a	0.21 ± 0.03	0.17 ± 0.01	0.30 ± 0.06	0.15 ± 0.01	0.28 ± 0.03	0.10 ± 0.01	18.5 ± 0.9	1.10 ± 0.2	−0.464
10b	0.29 ± 0.04	0.16 ± 0.04	0.45 ± 0.14	0.20 ± 0.03	0.50 ± 0.04	0.29 ± 0.05	4.6 ± 0.2	0.12 ± 0.02	−0.599
10c	0.24 ± 0.03	0.08 ± 0.01	2.6 ± 0.1	0.15 ± 0.01	2.1 ± 0.2	1.1 ± 0.1	2.6 ± 0.2	0.13 ± 0.03	−0.928
CDDP	2.6 ± 0.7	8.3 ± 0.5	5.5 ± 0.2	5.7 ± 0.3	9.2 ± 0.5	13.5 ± 1.7	0.13 ± 0.01	0.23 ± 0.08	−0.380

[a] 518A2 – melanoma, HT-29 – colon adenocarcinoma, DLD-1 – Dukes type C colorectal adenocarcinoma, $HCT116^{wt}$ – colon carcinoma (wildtype); $HCT116^{-/-}$ – colon carcinoma (p53 knock-out mutant); $MCF\text{-}7^{Topo}$ – mamma carcinoma, $Kb\text{-}V1^{Vbl}$ – cervix carcinoma. [b] p53 dependency of IC_{50} values in HCT116 cells, indicated by $r^{p53} = (IC_{50}{}^{wt}/IC_{50}{}^{-/-}) - 1$.

once more in the presence of the competitive P-gp1 inhibitor verapamil and found to be significantly lower when compared to those obtained without added verapamil (Table 1, second column from the right).

p53 dependency

To investigate the dependency of the cytotoxic activity on p53, which represents one activator of the apoptotic cascade after DNA damage and prolonged cell cycle arrest, and which is normally activated upon treatment with CDDP,[14,15] the IC_{50} values of **8b–d**, **9b–d**, **10a–c** and CDDP were determined in the $HCT116^{-/-}$ p53 knock-out mutant cell line and the p53 dependency factor r^{p53}(= ($IC_{50}^{wt}/IC_{50}^{-/-}$) − 1) was calculated (Table 1). In Fig. 4 the r^{p53} values are depicted as bars to illustrate the differences in the IC_{50} values in the wildtype (wt) and the p53 knock-out mutant (−/−). The longer the bar the greater the effect that the deletion of p53 has on the cytotoxic activity of each complex. Bars in the negative range indicate a lower cytotoxicity in the $p53^{-/-}$ mutant in comparison to the wildtype cells, bars in the positive range indicate a higher cytotoxicity. Owing to the inactivity of **8a** and **9a** against the wildtype cell line these complexes were not tested in the p53 negative cell line. Except for **9d**, all tested compounds seemed to be dependent on p53 to various degrees. The cationic complexes **10a–c** showed a correlation between the length of the *N*-alkyl residues and the difference between the toxicity in the wildtype cells and the $p53^{-/-}$ cells.

Cellular uptake

In order to check whether the observed differences in the cytotoxicities of the new complexes are a consequence of different uptake rates and intracellular concentrations, the latter were measured *via* inductively coupled plasma mass spectrometry (ICP-MS) in $HCT116^{wt}$ cells treated with **8a–c**, **9a–d**, **10a–c** and CDDP. These complexes cover the whole spectrum of chain length, variation of the secondary ligands (DMSO, PPh_3, $(PPh_3)_2$), and a potential positive charge. Fig. 5 shows the amount of Pt (pmol per 10^6 cells) taken up by the cells after 5 h of incubation with the compounds (*cf.* ESI† for values ± SD).

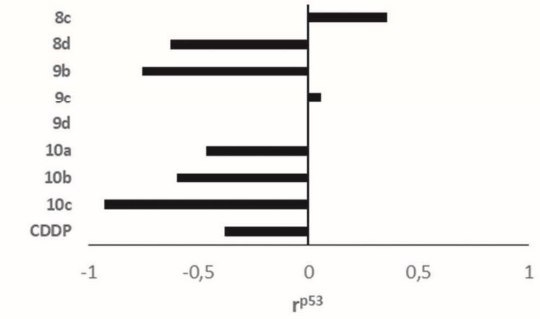

Fig. 4 Comparison of the IC_{50} values (72 h) of **8c–d**, **9b–d**, **10a–c**, and CDDP against the HCT116 colon carcinoma cells with wildtype p53 (wt) and the p53 knock out mutant (−/−) *via* the dependency factor r^{p53} which is defined as ($IC_{50}^{wt}/IC_{50}^{-/-}$) − 1. The further r^{p53} deviates from zero, the wider apart the two IC_{50} values are set. Negative r^{p53} values indicate a lower cytotoxicity of the compound in the knock out mutant, positive values indicate a higher cytotoxicity.

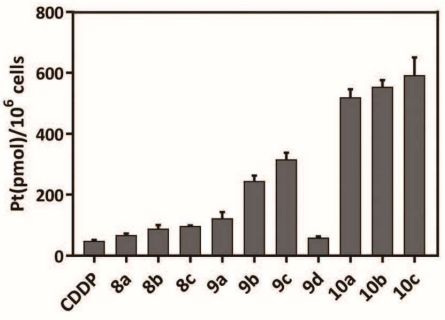

Fig. 5 Intracellular platinum levels in $HCT116^{wt}$ colon carcinoma cells after 5 h of incubation with 8 μM of Pt(II) complexes CDDP, **8a–c**, **9a–d** and **10a–c**, measured *via* ICP-MS. Mean ± SD from three independent experiments. Exact values can be found in ESI Table S2.†

Complexes **8a–c**, carrying DMSO as an ancillary ligand, are not taken up much better than CDDP. The increased toxicity of **8b** for example, over that of CDDP or **8a** is owed to mechanistic reasons rather than the uptake rates. Within the group of complexes **9**, the uptake rises with the growing length of the *N*-alkyl chain from methyl (**9a**) to butyl (**9c**). However, the *N*-octyl substituted complex **9d** is taken up to a far lesser extent, ranging between that of CDDP and **9a**. However, when the cytotoxicities of **9b–d** measured against $HCT116^{wt}$ were adjusted to their uptake rates the resulting relative 'intrinsic' cytotoxicities were found to be quite similar.

A comparison of complexes **8**, **9** and the charged complex **10**, shows that the exchange of the secondary ligands (DMSO or Cl) for one or two phosphanes vastly promotes the cellular uptake of the platinum complexes, independent of the chain length. Almost six times as much of the bisphosphino complex **10c** was taken up as that of **8a–c** and about 12 times as much as the of CDDP. Consequently, the 'intrinsic' cytotoxicities against $HCT116^{wt}$ differed less markedly than the actual measured ones. The upshot is that we found a weak correlation between the uptake and the *N*-alkyl side chain length for complexes **a–d**, yet no decisive influence was found for the side chains ranging from ethyl to octyl on the cytotoxicity.

DNA interaction

EMSA and ethidium bromide assays. One of the main targets of CDDP is the nuclear DNA. By intra- and inter-strand crosslinking, CDDP drastically changes the DNA morphology, and essential cellular processes, such as DNA replication or protein expression are hindered, and ultimately apoptotic mechanisms are activated.[14c] We examined the potential DNA interaction of complexes **8**, **9**, **10** and CDDP using ethidium bromide saturation assays with salmon sperm DNA (Fig. 6 top) and electrophoretic mobility shift assays (EMSA) with circular

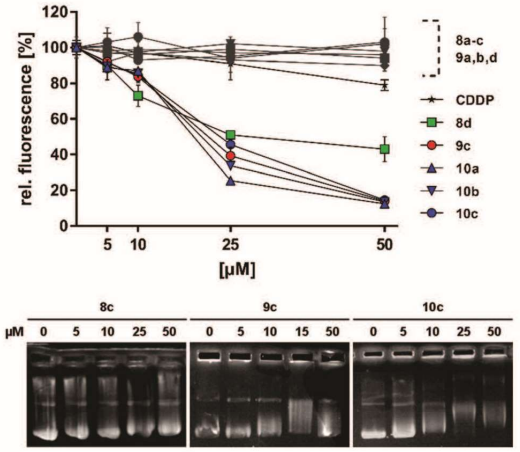

Fig. 6 Top: Ethidium bromide – DNA adduct fluorescence after 2 h of incubation with complexes **8**, **9**, **10** or CDDP, relative to a vehicle control (set to 100%). Mean ± SD calculated from 3 independent measurements. Bottom: EMSA of circular pBR322 plasmid DNA after 24 h of incubation with 0, 5, 25 and 50 μM of **8c**, **9c** or **10c**. Staining of DNA bands was performed using ethidium bromide.

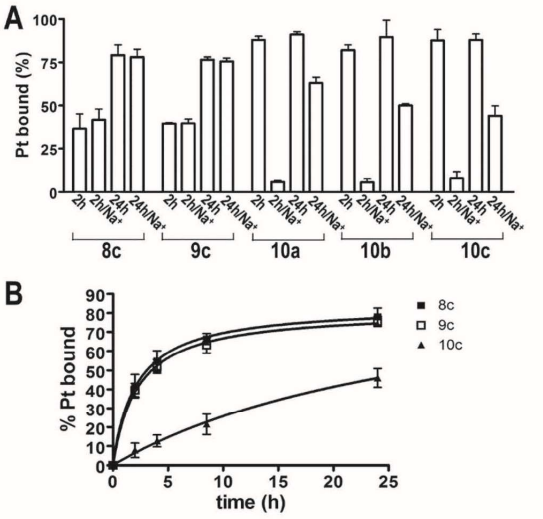

Fig. 7 (A) Quantification of Pt from **8c**, **9c** and **10a–c** bound to DNA in 0.01 M $NaClO_4$ at 37 °C after 2 or 24 h. Samples were dialysed against water (columns 2 h and 24 h) or against 0.1 M NaCl (columns 2 h/Na^+ or 24 h/Na^+). The platinum content associated with the DNA was determined using FAAS. (B) Progress of DNA platination by **8c**, **9c**, and **10c**. Samples, withdrawn after indicated time intervals were exhaustively dialysed against 0.1 M NaCl and analysed using FAAS.

pBR322 plasmid DNA (Fig. 6 bottom). Complexes **8a–c** neither reduced the ethidium bromide (EtBr) fluorescence after incubation with salmon sperm DNA, nor caused any band shifts or aggregations of the plasmid DNA in EMSA. This coincides nicely with the lack of DNA affinity that we found recently for the related complexes **2**.[10d] Although **9a**, **9b** and **9d** showed no impact in the EtBr saturation assay, complex **9c** reduced the EtBr fluorescence to a similar extent as the charged complexes **10**. Despite the negative result from the EtBr saturation assay, **9b** (ethyl) induced, like **9c** (butyl), a band shift in the EMSA at a concentration of 25 μM. However, complex **9d**, carrying the longest *N*-alkyl side chain, showed virtually no effect in the EMSA. The positive charge of complexes **10** likely facilitates their interaction with the negatively charged phosphate backbone of the DNA,[16] resulting in a reduction of the EtBr fluorescence to about 15% of the vehicle control value, and a band shift in the EMSA as well as the formation of DNA aggregates, which are too bulky to leave the pockets of the agarose gel during electrophoresis.

Kinetics and DNA base preferences. As neither the EMSA nor the ethidium bromide saturation assays gave detailed information on the DNA–complex interaction, more sophisticated biophysical methods were applied, with a focus on complexes **8c**, **9c** and **10a–c** which cover the whole spectrum of ancillary ligands (DMSO, PPh_3, $(PPh_3)_2$) while sharing a butyl chain, but also allow us to gauge the influence of the side chain length.

The speed and degree of platination of double-stranded calf thymus (ct) DNA was investigated using its incubation with defined concentrations of the respective complexes, dialysis against water or high salt buffer (0.1 M NaCl), and measurement of the Pt content using flame atomic absorption spectroscopy (FAAS) after 2 and 24 h. As indicated in Fig. 7A, there was a significant difference in the DNA binding between the neutral complexes **8c** and **9c** and the cationic compounds **10a–c**. After a short incubation time, approximately 40% of **8c** and **9c** were bound to the DNA, while *ca.* 80% were associated with it after 24 h. The amount of platinum bound to the DNA did not change after dialysis with a high salt buffer. In contrast, complexes **10a–c** associated much faster with DNA, but when the treated DNA samples were dialysed after 2 h against a buffer of high ionic strength, the amount of Pt that stuck to the DNA was much lower (*ca.* 5%). These results indicate that complexes **10a–c** associate to DNA in a fast, though initially mainly electrostatic, manner. Under the conditions of a high Na^+ concentration, these electrostatic attractions are disrupted by saturation of the negatively charged phosphate backbone of the DNA, and only the Pt coordinatively bound to the DNA remains. The coordinative binding of **10a–c** is much slower than that of **8c** and **9c**, this is probably due to the steric hindrance of the two bulky PPh_3 groups of **10** (Fig. 7B). Next, we investigated the preferences of complexes **8c**, **9c**, and **10a–c** for binding to particular nucleotide sequences by exposing them to various synthetic single-stranded homopolydeoxyribonucleotides. All of the tested complexes bound readily to single-stranded poly(dG) and, to a lesser extent, to poly (dA), but virtually not at all to the single-stranded poly(dT) or poly(dC) (*cf.* ESI† for exact values), in keeping with the base sequence preferences of cisplatin.[17]

DNA stability. The capability of **8c**, **9c**, **10a–c** to distort and destabilise dsDNA was assessed by measuring the absorbance of the platinated ct DNA at 260 nm as a function of the temperature. The Pt/nucleotide ratio was set to r_b = 0.03 and the samples were dialysed against 0.1 M NaCl and, subsequently, against 0.01 M $NaClO_4$ to get rid of any unbound complex molecules. The effect of the resulting DNA platination on its melting temperature (T_m) was measured in samples with low (0.01 M) and high (0.1 M) concentrations of Na^+. In contrast to CDDP, the complexes **8c**, **9c**, and **10a–c** had a slightly increased T_m at low Na^+ concentrations (*cf.* ESI Fig. S41,† left). At high Na^+ concentrations the T_m decreased as with CDDP, but not to the same degree (*cf.* ESI Fig. S41,† right). The observation that the T_m values of DNA modified by **8c**, **9c**, and **10a–c** decreased at a higher salt concentration (0.1 M) is consistent with the presence of conformational alterations induced by these complexes that destabilise the duplex. At higher salt concentrations (0.1 M), the negative DNA phosphate groups are already efficiently neutralised by the cations present in the medium, so that any stabilising electrostatic contribution by the coordinated positively charged platinum fragments is less pronounced than in a medium of a lower salt concentration. However, the destabilisation caused by **8c**, **9c**, and **10a–c** was less prominent then that induced by cisplatin, indicating a lower extent of DNA distortion. In contrast, at low salt concentrations, in which the negative charges of the DNA phosphate groups are not sufficiently neutralised by the Na^+ counterions, the electrostatic stabilising effects of **8c**, **9c**, and **10a–c** override their destabilising effects stemming from conformational distortions. These results suggest that the Pt(II)-benzimidazole complexes induce conformational distortions in dsDNA that differ from those induced by CDDP.

DNA distortion and unwinding. The DNA morphology alterations upon binding of the investigated Pt(II) complexes were further assessed according to their effects on the fluorescence of DNA-terbium ion (Tb^{3+}) adducts and on the unwinding of pSP73 double helical plasmid DNA. Tb^{3+} fluorescence has been used to investigate local perturbations induced in double-helical DNA by various physical or chemical agents including platinum(II) complexes. The fluorescence of Tb^{3+} ions is strongly enhanced when they are bound to unplatinated guanine (G) residues in distorted DNA regions.[18] Ct DNA was treated with the complexes at r_b values of 0.03. Unbound platinum was removed by dialysis as described in the materials and methods. The platinated DNA samples were treated with $TbCl_3$, and subsequently, the fluorescence of the Tb^{3+}-DNA adducts was measured (*cf.* ESI Fig. S42†). The treatment of DNA with complexes **8c**, **9c**, and **10a–c** resulted in a slight enhancement of the terbium fluorescence, which was, however, less pronounced than that induced by CDDP. These results confirm that DNA adducts of these Pt(II)-benzimidazole complexes give rise to local conformational alterations in double-stranded DNA which are less distorting than those of CDDP.

To determine the effect of the DNA adducts of **8c**, **9c**, and **10a–c** on the unwinding of double-helical DNA in more detail than before (*cf.* Fig. 6), the degree of supercoiling of the negatively supercoiled pSP73 plasmid DNA was analysed by agarose gel electrophoresis (*cf.* ESI Fig. S43†).[19] Any unwinding and reduction of the supercoils in a closed circular plasmid affects its electrophoretic mobility. The decrease of the mobility during electrophoresis allows the quantification of the mean unwinding angle θ per adduct. It can be calculated as $\theta = -18\sigma/r_b(c)$, in which σ is the superhelical density and $r_b(c)$ is the value of r_b at which the supercoiled and nicked forms comigrate.[19] Under the conditions used in these experiments, the value for σ of the plasmid DNA was calculated to be −0.029 on the basis of the data for CDDP, for which the $r_b(c)$ was determined in this study and $\theta = 13°$ was calculated.[19] Using this approach, the DNA unwinding angles were determined to be 6.2 ± 0.5°, 6.1 ± 0.3°, 5.6° ± 0.5°, 6 ± 1°, and 6.6 ± 1.0° for **8c**, **9c**, **10a**, **10b**, and **10c**, respectively, which are thus significantly smaller than that found for cisplatin (13°), but very similar to those of the monofunctional complexes $[Pt(NH_3)_3Cl]Cl$ and [*Pt*(*dien*)Cl]Cl, for which unwinding angles of 6° have been measured.[19] Interestingly, none of the complexes tested in this work increased the mobility of the relaxed form (oc) as CDDP does. It has been shown that the bifunctional binding of CDDP and other platinum complexes to DNA shortens and condenses the DNA helix.[20] The observation that the binding of **8c**, **9c**, and **10a–c** does not affect the mobility of oc DNA suggests that these complexes predominantly form DNA monoadducts, even though **8c** and **9c** contain two leaving chloride ligands.

DNA interstrand crosslinking. Apart from the stabilising effect of the coordinated positively charged platinum complex fragments, and the destabilising conformational distortions, crosslinks are a third factor that significantly affect the thermal stability of DNA. It has been shown that interstrand crosslinks (ICLs) in DNA markedly increase its melting temperature by preventing the dissociation of the strands.[21] For complexes **10a–c**, which contain only one leaving chloride ligand, the formation of ICLs in double helical DNA is unlikely, in contrast to complexes **8c** and **9c** which feature two replaceable chlorido ligands. We tested the ability of complexes **8c**, **9c**, and **10a–c**, as well as CDDP, to crosslink pSP73KB DNA which had been linearized and ^{32}P-labeled. The electrophoretic autoradiograms shown in Fig. 8 reveal that CDDP, even at very low concentrations r_b, gave rise to distinct interstrand-crosslinked DNA bands which migrate more slowly through the denaturing agarose gel than single stranded (ss) DNA. In contrast, complexes **8c** and **9c** caused comparably fainter ICL DNA bands, even when applied at r_b values ten times of those for CDDP. Although the frequency of the ICLs caused by CDDP was 6%, it was far less than 1% for complexes **8c** and **9c**. With complex **10c**, as with **10a** and **10b** (not shown), no ICL DNA bands were detected. It should be noted, though, that the absence of DNA crosslinking is not necessarily an indication of a lower biological activity. It has been shown that DNA adducts of monofunctional anticancer Pt(II) complexes, such as pyriplatin, phenanthriplatin, or *cis*-{$Pt(NH_3)_2$[3,5-dichloro-*N*-(3-chloro-4-(quinolin-6-yl-oxy)phenyl)-

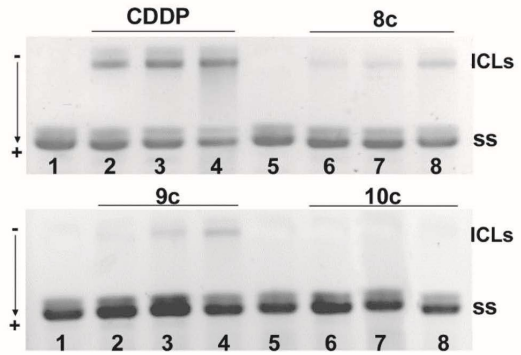

Fig. 8 Autoradiograms of a denaturing agarose gel of linear pSP73 DNA modified by CDDP or complexes **8c**, **9c**, **10c**. Interstrand crosslinked DNA (upper bands, ICLs) migrates more slowly during electrophoresis than single-stranded DNA (bottom bands, ss). Top: CDDP r_b = 0, 0.001, 0.0015, 0.002; **8c** r_b = 0, 0.01, 0.015, 0.02; Bottom: **9c**, **10c** r_b = 0, 0.01, 0.015, 0.02.

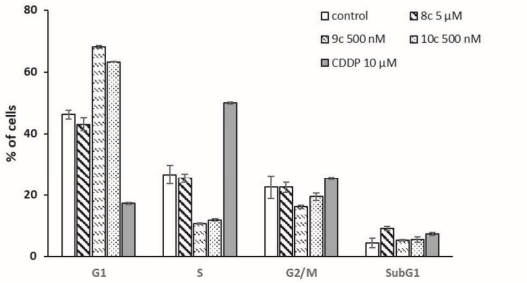

Fig. 9 Effects of **8c** (10 μM), **9c** (500 nM), **10c** (500 nM) and CDDP (10 μM) on the progression of the cell cycle of HCT116^{wt} colon carcinoma cells after 24 h of treatment. The bars represent the percentages of cells in each phase of the cell cycle (G1, S and G2/M) and dead cells (sub-G1). Analysis was performed *via* propidium iodide staining and flow cytometry, values represent mean ± SDs of three experiments.

2-hydroxybenzamide]Cl}NO_3, bearing bulkier aromatic ligands,[22] effectively inhibit the RNA-polymerisation that is considered to be crucial for the biological activity of Pt complexes.[23] Moreover, a less distinct DNA distortion might help to hide the DNA lesions from the repair machinery.[24]

Cell cycle analysis

The binding of small molecules to the DNA and the resulting damages affect various cellular DNA-dependent processes, such as protein expression, DNA replication and mitosis. Changes in the DNA integrity often lead to an arrest of the cell cycle progression of the cells. Key players during the cell cycle arrest and the activation of the apoptotic cascade are the "guardian of the genome" p53 and the CDK1 inhibitor p21, a major target of activated p53.[15] Using propidium iodide staining and flow cytometry, we tested the *N*-butyl substituted complexes **8c**, **9c**, and **10c** for their effect on the cell cycle progression of HCT116^{wt} cells (Fig. 9) and p53 knock-out mutant HCT116$^{-/-}$ cells (*cf.* ESI, Fig. S44†). No distinct changes in the cell cycle progression were observed upon treatment of the wildtype cells with the DMSO complex **8c**, while in the p53 knock-out mutant cells treatment led to a G2/M phase arrest. In contrast, both phosphane complexes **9c** and **10c** at a concentration as low as 500 nM induced a strong G1 phase arrest in the wildtype and the mutant cell lines after 24 h, indicating a mode of action that differs from that of CDDP, which caused an arrest in the S phase.

Upshot: SAR and mode of action

Some structure-uptake and structure–activity relations emerged from our studies. The uptake of the delocalised lipophilic cationic complexes **10** by HCT116 colon carcinoma cells was conspicuously greater than that of the neutral analogues **8** and **9**. The complexes **10** were also—on average—more cytotoxic in the MTT assays against the panel of seven cancer cell lines. With the exception of **9d**, the uptake rates of all three complex types into the HCT116 cells increased with the length of their *N*-alkyl substituents. However, this effect was not mirrored by the course of their cytotoxicities against most of the tested cancer cell lines which were somewhat erratic. Neutral *N*-methyl substituted complexes **8a** and **9a** were virtually inactive against all tested cancer cell lines, while the *N*-ethyl substituted complex **8b** stood out as being specifically efficacious against slow-growing colon carcinoma cell lines, where it reached IC_{50} values like the cationic complexes **10**. The complexes that were most active with sub-micromolar IC_{50} (72 h) values against HCT116^{wt} cells were **8b**, **9b**, **10a–c**, which worked by a mode of action that was dependent on the functional p53, which was evident from their reduced activity against the HCT116$^{-/-}$ cancer cells. They were also far more active than cisplatin in both of the HCT116 variants. In a cell-free context, DNA was a major target for all of the new benzimidazol-2-ylidene complexes, although their molecular interactions differed considerably. Neutral complexes **8** and **9** appear to bind swiftly to DNA at G-residues in a coordinative manner, whereas the cationic complexes **10** quickly pre-associate with DNA by electrostatic attraction, which is only slowly replaced by coordinative binding. The DNA adducts formed eventually in either case are characterised by monofunctional platination, causing lesions which distort dsDNA to a much lesser extent than those caused by cisplatin. This might go hand in hand with reduced side effects in animals or humans. Also, unlike cisplatin, complexes **10** and **9c** arrested the HCT116 cells of both variants in the G1 phase.

Conclusions

The replacement of imidazol-2-ylidene by benzimidazol-2-ylidene ligands in antitumoral platinum(II) complexes with otherwise identical ancillary and leaving ligands changes their chemistry (synthesis, stability, and solubility) more than their biological profile (DNA interaction, cancer cell cycle inter-

ference, dependency of the cytotoxicity on the ancillary ligands and on charge). However, their selectivity and individual efficacies against particular cancer entities may differ significantly. What makes the new *N,N*-dialkylbenzimidazol-2-ylidene platinum complexes interesting as drug candidates is their highly structure-dependent cytotoxicity against cancer cells, in combination with reduced morphology changes to DNA, which bode well for the management of unwanted side effects in patients when compared to cisplatin.

To achieve a rational structure-based optimisation of their drug-like properties, in subsequent studies we need to clarify their uptake pathways and their intracellular distribution, and in particular the potential contribution of antimitochondrial effects by the cationic complexes **10**.

Experimental

Materials and methods

All chemicals and reagents were purchased from Sigma Aldrich, Alfa Aesar, ChemPur or ABCR and were used without further purification. Synthetic double-helical polydeoxyribonucleotides poly (dA), poly (dT), poly (dC), and poly (dG) were purchased from Boehringer-Mannheim. Restriction endonuclease EcoRI and the Klenow fragment of DNA polymerase I were purchased from New England Biolabs. EtBr and agarose were purchased from Merck KgaA. $TbCl_3 \cdot 6H_2O$ was purchased from Fluka Chemie and [α-^{32}P]ATP was obtained from MP Biomedicals. Melting points are uncorrected; NMR spectra were run on a 500 MHz spectrometer; chemical shifts are given in ppm (δ) and referenced relative to the internal solvent signal; ^{195}Pt NMR shifts are quoted relative to $\Xi(^{195}\text{Pt})$ = 21.496784 MHz, K_2PtCl_4 was used as an external standard (δ = −1612.81); mass spectra: direct inlet, EI, 70 eV; elemental analyses: Vario EL III elemental analyser; X-Ray diffractometer: STOE-IPDS II; absorption and fluorescence measurements: Tecan Infinite F200; absorption for DNA melting: Varian Cary 4000 UV-vis spectrophotometer; FAAS measurements: Varian AA240Z Zeeman atomic absorption spectrometer equipped with a GTA 120 graphite tube atomizer; flow cytometry: Beckman Coulter Cytomics FC500. All biotested compounds were >95% pure by elemental analysis. Benzimidazolium salts were synthesised according to the literature procedures as described in the ESI.† [12]

Syntheses and characterisation

Synthesis of NHC silver complexes 7. Solutions of the benzimidazolium chlorides in CH_2Cl_2 were treated with Ag_2O (0.5 eq.) and stirred for 24 h to 3 days in the dark. After filtration, the product complexes 7 were precipitated by addition of Et_2O or hexane.

Chlorido(1,3-diethylbenzimidazol-2-ylidene) silver(I) (7b). **6b** (400 mg, 1.90 mmol), Ag_2O (950 mg, 0.95 mmol, 0.5 eq.), CH_2Cl_2 (40 mL), 24 h; yield: 526 mg (1.66 mmol, 87%); colourless solid; ^{1}H NMR (500 MHz, $CDCl_3$): δ 1.49 (6H, t, J = 7.2 Hz, CH_3), 4.57 (4H, q, J = 7.2 Hz, CH_2), 7.44–7.50 (2H, m, BI), 7.83–7.89 (2H, m, BI).

Chlorido(1,3-di-n-butylbenzimidazol-2-ylidene) silver(I) (7c). **6c** (320 mg, 1.40 mmol), Ag_2O (159 mg, 0.70 mmol, 0.5 eq.), CH_2Cl_2 (35 mL), 24 h; yield: 407 mg (1.09 mmol, 78%); amber solid; ^{1}H NMR (500 MHz, $CDCl_3$): δ 0.97 (6H, t, J = 7.3 Hz, CH_3), 1.48–1.39 (4H, m, CH_3–CH_2), 2.01–1.90 (4H, m, NCH_2–CH_2), 4.54 (4H, t, J = 7.2 Hz, N–CH_2), 7.41 (2H, dd, J = 6.1, 3.0 Hz, BI), 7.53 (2H, dd, J = 6.0, 3.1 Hz, BI).

Chlorido(1,3-dioctylbenzimidazol-2-ylidene) silver(I) (7d). **6d** (240 mg, 633 μmol), Ag_2O (147 mg, 633 μmol, 1 eq.), CH_2Cl_2 (15 mL), 3 d; yield: 238 mg (489 μmol, 77%); beige solid; ^{1}H NMR (500 MHz, $CDCl_3$): δ 0.84 (6H, t, J = 6.9 Hz, CH_3), 1.19–1.29 (12H, m, CH_2), 1.30–1.37 (4H, m, NCCCCH_2), 1.37–1.44 (4H, m, NCCCH_2), 1.98 (4H, quin, J = 7.4 Hz NCCH_2), 4.53 (4H, t, J = 6.5 Hz, NCH_2), 7.43 (2H, dd, J = 6.1, 3.2 Hz, BI), 7.53 (2H, dd, J = 6.1, 3.2 Hz, BI).

Synthesis of *cis*-[Cl_2(DMSO)(1,3-dialkylbenzimidazol-2-ylidene)]Pt^{II} complexes 8. A solution of silver complex 7 in DMSO was treated with K_2PtCl_4 (1 eq.) and heated at 60 °C in the dark for 20 h. After addition of CH_2Cl_2 the precipitating AgCl was filtered off, the filtrate was washed with H_2O and brine, and dried over Na_2SO_4. Residual DMSO was removed *in vacuo* and by crystallising the product from CH_2Cl_2 with Et_2O or hexane.

cis-[Dichlorido(1,3-dimethylbenzimidazol-2-ylidene)(dimethylsulfoxid)]platinum(II) (8a). As the solubility of 7**a** was not sufficient to allow its separation from the by-products, **8a** was synthesised from **6a** directly. Ag_2O (106 mg, 456 μmol, 0.5 eq.) was added to a solution of **6a** (250 mg, 912 μmol) in CH_2Cl_2 (20 mL) and the mixture was stirred in the dark for 19 h. After removal of the solvent, the residue was suspended in DMSO (30 mL) and treated with K_2PtCl_4 (341 mg, 821 μmol, 0.9 eq.). After 24 h at 60 °C in the dark, the reaction was worked up as described above. Yield: 353 mg (720 μmol, 79%); colourless crystals of melting point (mp) 262 °C; elemental analysis (%): calc. for $C_{11}H_{16}N_2SOPtCl_2$ (490.31): C, 26.95; H, 3.29; N, 5.71. Found: C, 27.24; H, 3.99; N, 6.26. ^{1}H NMR (500 MHz, $CDCl_3$): δ 3.57 (6H, s, DMSO), 4.23 (6H, s, NCH_3), 7.37 (2H, dd, J ~ 6.1, 3.1 Hz, BI), 7.44 (2H, dd, J = 6.1, 3.1 Hz, BI); ^{13}C NMR (125 MHz, $CDCl_3$): δ 34.7 (NCH_3), 46.3 (DMSO), 110.9 (BI), 124.3 (BI), 134.2 (BI-C_q), 154.8 (NHC); ^{195}Pt NMR (108 MHz, $CDCl_3$): δ −3565.9; m/z (EI): 491 [M^+], 413, 377, 340, 78.

cis-[Dichlorido-(1,3-diethylbenzimidazol-2-ylidene)(dimethylsulfoxid)]platinum(II) (8b). 7**b** (449 mg, 1.41 mmol), K_2PtCl_4 (587 mg, 1.41 mmol, 1.0 eq.), DMSO (40 mL); yield: 639 mg (1.23 mmol, 87%); colourless crystals of mp 270 °C; elemental analysis (%): calc. for $C_{13}H_{20}N_2SOPtCl_2$ (518.37): C, 30.12; H, 3.89; N, 5.40. Found: C, 30.75; H, 4.203; N, 5.96. ^{1}H NMR (500 MHz, $CDCl_3$): δ 1.63 (6H, t, J = 7.3 Hz, CH_3), 3.57 (6H, s, DMSO), 4.83 (4H, q, J = 7.3 Hz, CH_2), 7.35 (2H, dd, J = 6.1, 3.1 Hz, BI), 7.46 (2H, dd, J = 6.1, 3.1 Hz, BI); ^{13}C NMR (125 MHz, $CDCl_3$): δ 14.5 (CH_3), 43.8 (CH_2), 46.4 (DMSO), 111.4 (BI), 124.0 (BI), 133.4 (BI-C_q), 153.5 (NCN); ^{195}Pt NMR (108 MHz, $CDCl_3$): δ −3561.4; m/z (EI): 518 [M^+], 440, 404, 173, 78. *Crystal data*: $C_{13}H_{20}N_2Cl_2OPtS$, M = 518.36, triclinic, space group $P\bar{1}$,

a = 8.675(5) Å, b = 9.264(5) Å, c = 10.601(5) Å, α = 91.874(5)°, β = 103.182(5)°, γ = 94.722(5)°, V = 825.5(8) Å^3, Z = 2, λ = 0.71069 Å, μ = 8.945 mm^{-1}, T = 133 K; 7449 reflections measured, 3177 unique; $R[F^2 > 2\sigma(F^2)]$ = 0.0329 and R_w = 0.0851, GOF = 1.032. CCDC 1857512.†

*cis-[Dichlorido-(1,3-di-n-butylbenzimidazol-2-ylidene)(dimethylsulfoxid)]platinum(II) (**8c**).* **7c** (143 mg, 382 μmol), K_2PtCl_4 (158 mg, 382 μmol, 1.0 eq.), DMSO (12 mL); yield: 203 mg (353 μmol, 93%); colourless crystals of mp 227 °C; elemental analysis (%): calc. for $C_{17}H_{28}NSOPtCl_2$ (574.47): C, 30.12; H, 3.89; N, 5.40. Found: C, 30.75; H, 4.20; N, 5.96. ^{1}H NMR (500 MHz, $CDCl_3$): δ 1.04 (6H, t, J = 7.4 Hz, CH_3), 1.60–1.51 (4H, m, NCCCH_2), 2.04–1.94 (2H, m, NCCH_2), 2.19–2.09 (2H, m, NCCH_2), 3.56 (6H, s, DMSO), 4.64 (2H, ddd, J = 14.0, 10.2, 6.0 Hz, NCH_2), 4.75 (2H, ddd, J = 14.1, 10.3, 5.6 Hz, NCH_2), 7.33 (2H, dd, J = 6.1, 3.1 Hz, BI), 7.44 (2H, d, J = 9.2 Hz, BI); ^{13}C NMR (125 MHz, $CDCl_3$): δ 14.0 (CH_3), 20.5 (CH_3–CH_2), 31.4 (NCCH_2), 46.3 (DMSO), 48.6 (NCH_2), 111.4 (BI), 123.9 (BI), 133.8 (BI-C_q), 153.7 (NCN); ^{195}Pt NMR ($CDCl_3$): δ −3554.2; m/z (EI): 574 [M$^+$], 538, 501, 421, 229, 78.

*cis-[Dichlorido-(1,3-dioctylbenzimidazol-2-ylidene)(dimethylsulfoxid)]platinum(II) (**8d**).* **7d** (230 mg, 473 μmol), K_2PtCl_4 (196 mg, 473 μmol, 1.0 eq.), DMSO (15 mL); yield: 295 mg (430 μmol, 91%); colourless solid of mp 132 °C; elemental analysis (%): calc. for $C_{25}H_{44}N_2Cl_2SOPt$ (686.68): C, 43.73; H, 6.46; N, 4.08. Found: C, 44.36; H, 6.77; N, 4.36. ^{1}H NMR (500 MHz, $CDCl_3$): δ 0.89 (6H, t, J = 6.87 Hz, CH_3), 1.25–1.36 (12H, m, CH_2), 1.36–1.44 (4H, m, NCCCH_2), 1.48–1.56 (4H, m, NCCCH_2), 1.94–2.07 (2H, m, NCCH_2), 2.09–2.20 (2H, m, NCCH_2), 3.56 (6H, s, DMSO), 4.58–4.68 (2H, m, NCH_2), 4.71–4.81 (2H, m, NCH_2), 7.31–7.38 (2H, m, BI-H), 7.42–7.47 (2H, m, BI-H); ^{13}C NMR (125 MHz, $CDCl_3$): δ 14.1 (CH_3), 22.6 (CH_2), 27.1 (CH_2), 29.2 (CH_2), 29.3 (CH_2), 29.3 (CH_2), 31.6 (NCCH_2), 46.2 (DMSO), 48.72 (NCH_2), 111.3 (BI), 123.8 (BI), 133.6 (C_q), 153.5 (NHC); ^{195}Pt NMR: δ −3556; m/z (EI): 686 [M$^+$], 533, 358, 230, 131, 78.

Synthesis of *cis*-[Cl_2(PPh_3)(1,3-dialkylbenzimidazol-2-ylidene]Pt^{II} complexes 9

*cis-[Dichlorido(1,3-dimethylbenzimidazol-2-ylidene)(triphenylphosphane)]platinum(II) (**9a**).* A solution of triphenylphosphane (29 mg, 112 μmol, 1.1 eq.) in CH_2Cl_2 (15 mL) was added over 15 min to a solution of complex **8a** (50 mg, 102 μmol) in CH_2Cl_2 (30 mL) and the resulting mixture was stirred at room temperature for a further 15 min. The volatiles were removed *in vacuo* and the remaining crude product was purified using column chromatography (silica gel, 2% MeOH in CH_2Cl_2). The product was crystallised from CH_2Cl_2/Et_2O. Yield: 22 mg (32.6 μmol, 32%); colourless crystalline solid of mp 346 °C. Elemental analysis (%): calc. for $C_{27}H_{25}N_2Cl_2PPt$ (674.46): C, 48.08; H, 3.74; N, 4.15. Found: C, 47.71; H, 4.03; N, 4.14. ^{1}H NMR (500 MHz, $CDCl_3$): δ 3.83 (6H, s, CH_3), 7.07–7.15 (2H, m, BI), 7.16–7.26 (8H, m, BI and PPh_3), 7.29–7.37 (3H, m, PPh_3), 7.60 (6H, t, J = 9.5 Hz, PPh_3); ^{13}C NMR (125 MHz, $CDCl_3$): δ 34.1 (CH_3), 109.9 (BI), 123.1 (BI), 128.29 (d, J = 11.8 Hz, o-PPh_3), 129.4 (d, J = 63.5 Hz, *ipso*-PPh_3), 131.1 (d, J = 1.82 Hz, p-PPh_3), 134.0 (d, J = 10.9 Hz, m-PPh_3), 134.1 (BI-C_q), 162.0 (d, J = 7.27 Hz, NCN); ^{31}P NMR ($CDCl_3$): δ 8.83 (J = 3893 Hz); ^{195}Pt NMR ($CDCl_3$): δ −4017 (d, J = 3895 Hz); m/z (EI): 675 [M$^+$], 640, 603, 263, 184, 148, 109.

*cis-[Dichlorido(1,3-diethylbenzimidazol-2-ylidene)(triphenylphosphane)]platinum(II) (**9b**).* Triphenylphosphane (131 mg, 500 μmol, 5 eq.) was added to a solution of complex **8b** (50 mg, 97 μmol) in CH_2Cl_2 (5 mL) and the resulting mixture was stirred at room temperature for 21 h. After precipitation from CH_2Cl_2/hexane the product was purified using column chromatography (silica gel, 1% MeOH in CH_2Cl_2). Yield: 29 mg (41 μmol, 43%); colourless solid of mp 323 °C. Elemental analysis (%): calc. for $C_{29}H_{29}N_2Cl_2PPt$ (702.52): C, 49.58; H, 4.16; N, 3.99. Found: C, 49.19; H, 4.10; N, 3.70. ^{1}H NMR (500 MHz, $CDCl_3$): δ 1.46 (6H, t, J = 7.2 Hz, CH_3), 3.84 (2H, dq, J = 14.5, 7.2 Hz, NCH_2), 4.85 (2H, dq, J = 14.5, 7.2 Hz, NCH_2), 7.12 (2H, dd, J = 6.1, 3.1 Hz, BI), 7.24–7.16 (8H, m, BI, o-PPh_3), 7.31 (3H, t, J = 7.2 Hz, p-PPh_3), 7.64–7.53 (6H, m, m-PPh_3); ^{13}C NMR (125 MHz, $CDCl_3$): δ 14.0 (CH_3), 43.4 (NCH_2), 110.3 (BI), 123.0 (BI), 128.2 (d, J = 10.9 Hz, o-PPh_3), 129.0 (d, J = 64.5 Hz, *ipso*-PPh_3), 131.0 (d, J = 2.72 Hz, p-PPh_3), 133.3 (BI-C_q), 133.9 (d, J = 10.9 Hz, m-PPh_3), 160.6 (d, J = 7.26 Hz, NCN); ^{31}P NMR ($CDCl_3$): δ 8.85 (J = 3861 Hz); ^{195}Pt NMR ($CDCl_3$): δ −4016 (d, J = 3873 Hz); m/z (EI): 702 [M$^+$], 666, 630, 455, 262.

*cis-[Dichlorido(1,3-di-n-butylbenzimidazol-2-ylidene)(triphenylphosphane)]platinum(II) (**9c**).* Triphenylphosphane (114 mg, 434 μmol, 5 eq.) was added to a solution of complex **8c** (50 mg, 86.9 μmol) in CH_2Cl_2 (5 mL) and the resulting mixture was stirred at room temperature for 30 min. The volatiles were removed *in vacuo* and the remaining crude product was purified by crystallisation from CH_2Cl_2/hexane. Yield: 48 mg (63.3 μmol, 73%); colourless crystalline solid of mp 248 °C; elemental analysis (%): calc. for $C_{33}H_{37}N_2Cl_2PPt$ (758.62): C, 52.25; H, 4.92; N, 3.69. Found: C, 52.75; H, 4.69; N, 3.58. ^{1}H NMR (500 MHz, $CDCl_3$): δ 0.94 (6H, t, J = 7.3 Hz, CH_3), 1.35–1.48 (4H, m, NCCCH_2), 1.63–1.73 (2H, m, NCCH_2), 2.00–2.14 (2H, m, NCCH_2), 3.78–3.87 (2H, m, NCH_2), 4.54–4.64 (2H, m, NCH_2), 7.11 (2H, dd, J = 6.0, 3.2 Hz, BI), 7.15–7.24 (8H, m, BI and PPh_3), 7.33 (3H, t, J = 7.3 Hz, PPh_3), 7.48–7.66 (6H, m, PPh_3); ^{13}C NMR (125 MHz, $CDCl_3$): δ 13.7 (CH_3), 20.1 (NCCCH_2), 30.7 (NCCH_2), 48.3 (NCH_2), 110.4 (BI), 123.0 (BI), 128.2 (d, J = 10.9 Hz, o-PPh_3), 129.1 (d, J = 62.7 Hz, *ipso*-PPh_3), 131.1 (d, J = 1.82 Hz, p-PPh_3), 133.7 (BI-Cq), 134.0 (d, J = 10.9 Hz, m-PPh_3), 160.7 (d, J = 7.26 Hz, NCN); ^{31}P NMR ($CDCl_3$): δ 9.19 (J = 3901 Hz); ^{195}Pt NMR: δ −4018 (d, J = 3871 Hz); m/z (EI): 758 [M$^+$], 722, 685, 262, 229, 183, 108. *Crystal data*: $C_{33}H_{37}Cl_2N_2PPt$, M = 758.63, triclinic, space group $P\bar{1}$, a = 9.1067(18) Å, b = 12.792(3) Å, c = 13.803(3) Å, α = 88.02(3)°, β = 87.59(3)°, γ = 71.06(3)°, V = 1519.2(6) Å^3, Z = 2, λ = 0.71073 Å, μ = 4.872 mm^{-1}, T = 133 K; 21 191 reflections measured, 5813 unique; $R[F^2 > 2\sigma(F^2)]$ = 0.0183 and R_w = 0.0447, GOF = 1.030. CCDC 1857511.†

*cis-[Dichlorido(1,3-dioctylbenzimidazol-2-ylidene)(triphenylphosphane)]platinum(II) (**9d**).* Triphenylphosphane (95 mg, 364 μmol, 5 eq.) was added to a solution of complex **8d** (50 mg, 73 μmol) in CH_2Cl_2 (20 mL) and the resulting mixture was stirred at room temperature for 24 h. After crystallisation

from CH_2Cl_2/hexane the crude product was purified using column chromatography (silica gel, 1% MeOH in CH_2Cl_2). Yield: 60 mg (68 μmol, 93%); colourless crystalline solid of mp 168 °C. Elemental analysis (%): calc. for $C_{41}H_{53}N_2Cl_2PPt$ (870.84): C, 56.55; H, 6.13; N, 3.22. Found: C, 57.14; H, 6.03; N, 3.22. ^{1}H NMR (500 MHz, $CDCl_3$): δ 0.91 (6H, t, J = 6.9 Hz, CH_3), 1.26–1.39 (20H, m, CH_2), 1.63–1.72 (2H, m, $NCCH_2$), 2.04–2.13 (2H, m, $NCCH_2$), 3.78–3.88 (2H, m, NCH_2), 4.52–4.78 (2H, m, NCH_2), 7.10 (2H, dd, J = 6.9, 3.05 Hz, BI), 7.16–7.25 (8H, m, BI and PPh_3), 7.33 (3H, t, J = 6.7 Hz, PPh_3), 7.51–7.64 (6H, m, PPh_3); ^{13}C NMR (125 MHz, $CDCl_3$): δ 14.1 (CH_3), 22.6 (CH_2), 27.3 (CH_2), 28.8 (CH_2), 29.1 ($NCCH_2$), 29.3 (CH_2), 31.6 (CH_2), 48.6 (NCH_2), 110.4 (BI), 122.9 (BI), 128.1 (d, J = 11.8 Hz, o-PPh_3), 129.2 (d, J = 62.7 Hz, $ipso$-PPh_3), 131.0 (d, J = 2.7 Hz, p-PPh_3), 134.0 (d, J = 10.9 Hz, m-PPh_3), 160.7 (d, J = 8.17 Hz, NCN); ^{31}P NMR ($CDCl_3$): δ 9.17 (J = 3874 Hz); ^{195}Pt NMR ($CDCl_3$): δ −4018 (d, J = 3879 Hz); m/z (EI): 870 [M^+], 834, 797, 564, 533, 341, 262, 183, 108.

Synthesis of *trans*-[Cl(1,3-dialkylbenzimidazol-2-ylidene)$(PPh_3)_2$] Pt^+ Cl^- complexes 10

*trans-[Chlorido(1,3-dimethylbenzimidazol-2-ylidene)bis(triphenylphosphane)]platinum(II) chloride (**10a**).* Triphenylphosphane (80 mg, 306 μmol, 3 eq.) was added to a solution of complex **8a** (50 mg, 102 μmol) in CH_2Cl_2 (5 mL) and the resulting mixture was stirred at room temperature for 30 min. The volatiles were removed *in vacuo* and the remaining crude product was purified by crystallisation from CH_2Cl_2/hexane. Yield: 80 mg (90 μmol, 83%); colourless crystalline solid of mp 310 °C; elemental analysis (%): calc. for $C_{48}H_{47}N_2P_2PtCl_2$ (979.84): C, 57.70; H, 4.30; N, 2.99. Found: C, 57.98; H, 5.04; N, 3.43. ^{1}H NMR (500 MHz, $CDCl_3$): δ 3.54 (6H, s, CH_3), 7.20 (2H, dd, J = 6.1, 3.1 Hz, BI), 7.29 (12H, t, J = 7.5 Hz, o–PPh_3), 7.32 (2H, dd, J = 6.1, 3.1 Hz, BI), 7.37 (6H, t, J = 7.4 Hz, p–PPh_3), 7.51 (12H, dd, J = 12.4, 6.0 Hz, m-PPh_3); ^{13}C NMR (125 MHz, $CDCl_3$): δ 35.1 (CH_3), 111.1 (BI), 124.3 (BI), 127.5 (t, J = 29.5 Hz, $ipso$-PPh_3), 128.9 (t, J = 5.5 Hz, o-PPh_3), 131.8 (p-PPh_3), 133.7 (t, J = 5.9 Hz, m-PPh_3), 133.9 (BI-C_q), 159.9 (t, J = 10.0 Hz, NCN); ^{31}P NMR ($CDCl_3$): δ 17.7 (J = 2478 Hz); ^{195}Pt NMR: δ −4378 (t, J = 2490 Hz); m/z (EI): 908 [M^+], 673, 653, 602, 262, 183. *Crystal data*: $C_{45}H_{40}ClN_2P_2Pt{\cdot}Cl$, M = 936.72, monoclinic, space group $P2_1/c$, a = 12.578 (5) Å, b = 10.790 (5) Å, c = 32.126 (5) Å, α = 90°, β = 94.531(5)°, γ = 90°, V = 4346 (3) Å^3, Z = 4, λ = 0.71069 Å, μ = 3.46 mm^{-1}, T = 133 K; 32 457 reflections measured, 6540 unique; $R[F^2 > 2\sigma(F^2)]$ = 0.0276 and R_w = 0.0601, GOF = 0.766. CCDC 1857513.†

*trans-[Chlorido(1,3-diethylbenzimidazol-2-ylidene)bis(triphenylphosphane)]platinum(II) chloride (**10b**).* Triphenylphosphane (252 mg, 960 μmol, 10 eq.) was added to a solution of complex **8b** (50 mg, 96 μmol) in CH_2Cl_2 (10 mL) and the resulting mixture was stirred at room temperature for 5 d. The volatiles were removed *in vacuo* and the remaining crude product was purified by crystallisation from CH_2Cl_2/Et_2O. Yield: 22 mg (22.8 μmol, 24%); colourless solid of mp 297 °C; elemental analysis (%): calc. for $C_{50}H_{51}N_2Cl_2P_2Pt$ (1007.89): C, 58.51; H, 4.60; N, 2.90. Found: C, 58.59; H, 4.66; N, 2.89. ^{1}H NMR (500 MHz, $CDCl_3$): δ 0.83 (6H, t, J = 7.3 Hz, CH_3), 3.86 (4H, q, J = 7.2 Hz, CH_2), 7.20–7.42 (24H, m, BI and PPh_3), 7.43–7.54 (10H, m, PPh_3); ^{13}C NMR (125 MHz, $CDCl_3$): δ 13.0 (CH_3), 44.2 (CH_2), 111.5 (BI), 124.6 (BI), 127.1 (t, J = 25.5 Hz, $ipso$-PPh_3), 129.0 (t, J = 5.5 Hz, o-PPh_3), 132.0 (p-PPh_3), 133.5 (BI-C_q), 133.7 (m-PPh_3), 158.0 (t, J = 9.5 Hz, NCN); ^{31}P NMR ($CDCl_3$): δ 18.9 (J = 2485 Hz); ^{195}Pt NMR: δ −4383 (t, J = 2490 Hz); m/z (EI): 702, 667, 630, 456, 297, 262, 183, 108.

*trans-[Chlorido(1,3-di-n-butylbenzimidazol-2-ylidene)bis(triphenylphosphane)]platinum(II) chloride (**10c**).* Triphenylphosphane (456 mg, 1.74 mmol, 20 eq.) was added to a solution of complex **8b** (50 mg, 87 μmol) in CH_2Cl_2 (10 mL) and the resulting mixture was stirred at 80 °C for 4 days. The volatiles were removed *in vacuo* and the remaining crude product was purified by crystallisation from CH_2Cl_2/Et_2O and subsequent column chromatography (silica gel, CH_2Cl_2 with 2–5% MeOH). Yield: 29 mg (28 μmol, 33%); colourless solid of mp 114 °C; elemental analysis (%): calc. for $C_{51}H_{52}N_2Cl_2P_2Pt$ (1020.91): C, 60.00; H, 5.13; N, 2.74. Found: C, 59.26; H, 5.11; N, 3.06. ^{1}H NMR (500 MHz, $CDCl_3$): δ 0.70 (6H, t, J = 7.0 Hz, CH_3), 1.12–1.23 (8H, m, CH_2), 3.62–3.70 (4H, m, NCH_2), 7.15 (2H, dd, J = 6.5, 3.1 Hz, BI), 7.18–7.42 (22H, m, BI and PPh_3), 7.42–7.57 (10H, m, PPh_3); ^{13}C NMR (125 MHz, $CDCl_3$): δ 13.3 (CH_3), 20.4 (CH_2CH_3), 30.2 ($NCCH_2$), 49.1 (CH_2), 111.2 (BI), 124.8 (BI), 127.2 (t, J = 29.1 Hz, $ipso$-PPh_3), 129.0 (t, J = 5.5 Hz, o-PPh_3), 132.1 (p–PPh_3), 133.6 (BI-C_q), 133.9 (m-PPh_3), 158.4 (t, J = 10.0 Hz, NCN); ^{31}P NMR ($CDCl_3$): δ 18.9 (J = 2486 Hz); ^{195}Pt NMR: δ −4379 (t, J = 2486 Hz); m/z (EI): 758, 723, 685, 456, 262, 229, 183, 108.

X-ray data collection and structural determination

Diffractometer used: STOE-STADIVARI; data collection and cell refinement by: STOE-X-AREA. The single crystal samples were measured with Mo-Kα and the reflections collected at 133 K. The structures were solved by direct methods using SIR97 and refined by full matrix least-squares on F^2 for all data using SHELXL2016/6. All hydrogen atoms were added at calculated positions and refined using a riding model. Anisotropic thermal displacement parameters were used for all non-hydrogen atoms. Further details of the data collection and reliability factors are listed together with the analytical data in the ESI (Table S1†). Supplementary crystallographic data were deposited with The Cambridge Crystallographic Data Centre CCDC under no. 1857512 (**8b**), 1857511 (**9c**), 1857513 (**10a**).†

Biological evaluation

Cell culture conditions and stock solutions. Cells of 518A2 melanoma, HT-29, DLD-1, $HCT116^{wt}$ and $HCT116p53^{-/-}$ colon carcinoma, $MCF\text{-}7^{Topo}$ mamma carcinoma, and $Kb\text{-}V1^{Vbl}$ cervix carcinoma were kept in DMEM. All cell lines were cultured at 37 °C, 95% humidity and 5% CO_2. To maintain the *mdr* characteristics of the $MCF\text{-}7^{Topo}$ and $Kb\text{-}V1^{Vbl}$ cell lines, they were regularly treated with either topotecan or vinblastine. Dilutions of platinum(II) complexes **8**, **9** and **10a–c** were made from 10 mM stock solutions (DMSO) in sterile ddH_2O, dilutions of CDDP from a 3.3 mM stock solution in 150 mM saline.[25] Plasmid pSP73 (2464 bp) was isolated

according to standard procedures and banded twice in CsCl equilibrium density gradients.

Growth inhibition assay (MTT-assay). For the investigation of the cytotoxicity an MTT (3-(4,5-dimethylthiazole-2-yl)-2,5-diphenyltetrazoliumbromide) based proliferation assay was performed. Cells were seeded into 96-well plates (0.05×10^6 cells per mL for 518A2, HT-29, HCT116, MCF-7^{Topo} and Kb-V1^{Vbl}, and 0.1×10^6 cells per mL for DLD-1) and incubated for 24 h under cell culture conditions to ensure their adhesion. On the next day the cells were treated with a series of appropriate dilutions (final concentrations ranging from 5 nM, resp. 5 pM, to 100 μM) of **8**, **9**, **10a–c** and CDDP. As a negative control (100% vital cells) the assay was performed analogously with the respective vehicle. The cells were incubated for a further 72 h under cell culture conditions, centrifuged (300*g*, 4 °C) and the media were exchanged for 50 μL of a 0.05% MTT solution in PBS. The cells were incubated for another 2 h at 37 °C before the plates were again centrifuged as before and the MTT solution was discarded. The water insoluble formazan was dissolved by addition of 25 μL of an SDS/DMSO solution (10%; 0.6% AA) to each well. After 1 h of incubation at 37 °C the absorption was measured at 570 nm, and the background absorption at 630 nm. The formazan absorption correlates directly with the number of viable cells. The IC_{50} values were determined with *GraphPad Prism* and means ± SD were calculated from six independent measurements.

Inhibition of P-gp1. The determination of the cytotoxicity of **8b–d**, **9b–d** and **10a–c** in Kb-V1^{Vbl} cervix carcinoma cells in the presence of verapamil, a competitive inhibitor of P-gp1, was conducted analogously to the normal MTT-assay, but with DMEM containing 24 μM of verapamil (10 mM stock solution in 70% EtOH).

Cellular uptake. The uptake of complexes **8a–c**, **9a–d**, **10a–c** and CDDP by HCT116^{wt} cells was measured *via* ICP-MS. The cells were seeded on 100 mm tissue culture dishes (3×10^6 cells per dish in 7 mL of growth medium) and incubated at 37 °C. Confluent cells were treated with the compounds at final equimolar concentrations (8 μM) for 5 h. The attached cells were harvested by trypsinisation and the viability of the cells was tested by a trypan blue exclusion assay. Viabilities of the cells ranged from 76 to 97%, both viable and dead fractions were used for the experiment. The cell pellets were subsequently washed twice with cold PBS and cells were counted by using a TC10 Automated Cell Counter (Bio-Rad). The cells were digested by using a microwave acid (HCl, 11 M) digestion system (MARS5, CEM) to give a fully homogenised solution. The final platinum content in the samples was determined using ICP-MS.

DNA interaction

Ethidium bromide saturation assay. Inside the wells of a black 96-well plate 1 μg salmon sperm DNA in 100 μL of freshly sterile-filtered TE buffer (10 mM Tris/HCl, 1 mM EDTA pH 8.5) was incubated with 5, 10, 25 and 50 μM of **8**, **9**, **10a–c** or CDDP for 2 h at 37 °C (final sample volume 111.1 μL). Control samples were prepared analogously with DMSO to the highest concentration. To determine the background fluorescence, samples were prepared analogously with equal amounts of TE buffer instead of the DNA stock solution. 100 μL of ethidium bromide in TE-buffer (10 μg mL^{-1}) was added to each well and the plate was incubated in the dark for 5 min at room temperature. The ethidium bromide fluorescence was measured at λ_{ex} = 535 nm and λ_{em} = 590 nm. The background signal was subtracted from the respective sample signals and the fluorescence intensities relative to the control (set to 100%) were calculated. Each measurement was run in triplicate. Reduction of the fluorescence indicates an interaction of **8**, **9**, **10a–c** or CDDP with the DNA and thus a hindrance of ethidium bromide intercalation.

Electrophoretic mobility shift assay (EMSA). Circular pBR322 plasmid DNA (1.5 μg) in TE buffer was incubated for 24 h with 0, 5, 10, 25 and 50 μM of complexes **8**, **9** or **10a–c** at 37 °C (final sample volume: 20 μL). On the next day DNA sample buffer (5×, Tris/HCl, pH 8.0; 25% glycerol) was added to each sample and an agarose gel electrophoresis (1% in TBE buffer; 90 mM Tris/HCl, pH 8.3; 90 mM boric acid; 2.5 mM EDTA) was run at 66 V for 4 h. The DNA was stained with ethidium bromide and the plasmid bands were visualised *via* a UV transilluminator.

DNA platination analysis. Calf thymus DNA (1 mM) was incubated with **8c**, **9c** or **10a–c** (100 μM) in 10 mM $NaClO_4$ in the dark at 37 °C. After 2, 4 or 24 h, aliquots were withdrawn and exhaustively dialysed against water or, alternatively, against 0.1 M NaCl and subsequently against water. The amount of platinum associated with the DNA was assessed using FAAS. The percentage of Pt bound to DNA was calculated as the ratio of Pt associated with DNA and the total amount of platinum present in the sample.

DNA melting point analysis. DNA was modified with Pt complexes for 24 h in 10 mM NaClO4 at 37 °C. The DNA was dialysed against 0.1 M NaCl to remove the unbound platinum and subsequently against the medium required for further analysis. An aliquot of the sample was used to determine the level of DNA platination (r_b) using FAAS. The DNA melting curves of unplatinated or platinated DNA were recorded by measuring the absorbance at 260 nm in a medium containing 10 mM or 0.1 M Na^+ with 1 mM Tris-HCl/0.1 mM EDTA, pH 7.4, using a Varian Cary 4000 UV-vis spectrophotometer equipped with a thermoelectrically controlled cell holder and quartz cells with a pathlength of 1 cm. The melting temperature (T_m) was determined as the temperature corresponding to a maximum on the first derivation profile of the melting curves.

Tb^{3+} fluorescence. Ct DNA was modified with Pt complexes in 10 mM $NaClO_4$ at 37 °C. After 24 h of incubation, DNA was dialysed against 0.1 M NaCl and then against 10 mM $NaClO_4$. The level of DNA platination was verified using FAAS. The terbium fluorescence was measured using a previously described method.[18] Briefly, the samples of platinated or unplatinated DNA (2.5×10^{-5} M) were incubated with 5×10^{-5} M $TbCl_3$ for 60 min at 25 °C. Subsequently, the fluorescence intensity was measured in a 1 cm quartz cell using a Varian Cary Eclipse spectrofluorophotometer. Excitation and emission wavelengths

were set to 290 and 546 nm, respectively, the slit widths were 5 nm, and the integration time was set to 5 s.

Unwinding of negatively supercoiled DNA. The unwinding of closed circular supercoiled pSP73 plasmid DNA was assayed using an agarose gel mobility shift assay.[19] Plasmid DNA (pSP73) was incubated with the platinum complex for 24 h, precipitated by ethanol to remove unbound Pt, and redissolved in TAE buffer (0.04 M Tris-acetate, 1 mM EDTA, pH 7.0). An aliquot of the precipitate was subjected to electrophoresis on 1% agarose gels running at 25 °C in the dark with TAE buffer. The gels were stained with EtBr, followed by photography with a transilluminator. Another aliquot was used to determine the r_b values using FAAS. The unwinding angle θ, induced per platinum–DNA adduct, was calculated based upon the r_b value at which the transformation of the supercoiled to a relaxed form of the plasmid was complete.[19]

Interstrand cross-link formation assay. The complexes **8c**, **9c**, **10a–c** and CDDP were incubated at different concentrations (CDDP r_b = 0, 0.001, 0.0015, 0.002; **8c**, **9c**, **10c** r_b = 0, 0.01, 0.015, 0.02) for 24 h with 500 ng of pSP73KB DNA after it had been linearized by EcoRI and 3′-end-labeled by means of a Klenow fragment of DNA polymerase I and [α-32P]dATP. After incubation, the reaction was stopped by addition of NaCl to a final concentration of 0.1 M and samples were precipitated. The sediments were dissolved in 10 mM $NaClO_4$, and the number of interstrand crosslinks was analysed using electrophoresis under denaturing conditions on an alkaline agarose gel (1%). After the electrophoresis had been completed, the gels were dried and visualised using a FUJIFILM BAS 2500 bio-imaging analyser. The intensities of the bands corresponding to single strands of DNA and interstrand cross-linked duplex were quantified using AIDA image analysis software. The frequency of ICLs, was calculated as % ICL/Pt = XL/4910 × r_b (the pSP73KB plasmid contained 4910 nucleotide residues), in which % ICL/Pt is the number of ICLs per adduct and XL is the number of ICLs per molecule of the linearized DNA duplex and was calculated assuming a Poisson distribution of the ICLs as XL = $-\ln A$. In which A is the fraction of molecules running as a band corresponding to the non-crosslinked DNA. The values of r_b were determined using FAAS by measuring the amount of free, unbound platinum in the supernatants after precipitation of the samples; the amount of platinum bound to DNA, r_b, was calculated by subtracting the amount of platinum remaining in the solution from the total amount of platinum present in the reaction.

Cell cycle analysis. The cell cycle analysis of the HCT116 cells was performed *via* flow cytometry of the treated HCT116^{wt} and HCT116$^{-/-}$ cells. They were seeded at 0.1 × 10^6 cells per mL into the wells of a 6-well plate and incubated for 24 h under cell culture conditions. Appropriate dilutions of **8c**, **9c**, **10c** and CDDP in ddH_2O (30.3 μL) were added to each well (final concentrations: **8c** 5 μM, **9c** and **10c** 500 nM, CDDP 10 μM). The cells were incubated for another 24 h under cell culture conditions. On the next day the medium from each well was transferred into a centrifugation tube and the cells were washed with 1 mL PBS. After transferring the PBS to the respective tubes, the cells were trypsinised for *ca.* 2 min at 37 °C. The detached cells were transferred into the tubes and centrifuged (300*g*, 4 °C, 5 min). The supernatant was discarded and the cells were fixed in 1 mL of ice-cold 70% EtOH for 1 h at 4 °C.

For propidium iodide staining, the cells were centrifuged (400*g*, room temperature, 5 min), the supernatant was discarded, and the pellet was layered with 1 mL PBS. After 5 min the cells were again centrifuged and the PBS discarded. The cells were resuspended in 200 μL of a PI staining solution (0.1% sodium citrate, 50 μg mL^{-1} propidium iodide, 50 μg mL^{-1} RNase A) for 30 min at 37 °C. The distribution of the cells in the different phases of the cell cycle was measured *via* flow cytometry.

Conflicts of interest

There are no conflicts to declare.

Acknowledgements

RS thanks the Deutsche Forschungsgemeinschaft for a grant (Scho 402/12), JK, HK and VB thank the Czech Science Foundation and Ministry of Education of the Czech Republic for grant (18-09502S and LTC17003), and MR thanks the Bayreuth University Graduate School for financial support. We also thank the COST Action CM1105 'Functional metal complexes that bind to biomolecules' for financial support.

References

1 (*a*) A.-M. Florea and D. Büsselberg, *Cancers*, 2011, **3**, 1351–1371, DOI: 10.3390/cancers3011351; (*b*) S. Dasari and P. B. Tchounwou, *Eur. J. Pharmacol.*, 2014, **740**, 364–378, DOI: 10.1016/j.ejphar.2014.07.025.

2 (*a*) K. M. Deo, D. L. Ang, B. McGhie, A. Rajamanickam, A. Dhiman, A. Khoury, J. Holland, A. Bjelosevic, B. Pages, C. Gordon and J. R. Aldrich-Wright, *Coord. Chem. Rev.*, 2018, **375**, 148–163, DOI: 10.1016/j.ccr.2017.11.014; (*b*) T. C. Johnstone, K. Suntharalingam and S. J. Lippard, *Chem. Rev.*, 2016, **116**, 3436–3486, DOI: 10.1021/acs.chemrev.5b00597.

3 A. J. Arduengo, R. L. Harlow and M. Kline, *J. Am. Chem. Soc.*, 1991, **113**, 361–363, DOI: 10.1021/ja00001a054.

4 X. Bantreil, J. Broggi and S. P. Nolan, *Annu. Rep. Prog. Chem., Sect. B*, 2009, **105**, 232–263, DOI: 10.1039/b822056p.

5 (*a*) L. Oehninger, R. Rubbiani and I. Ott, *Dalton Trans.*, 2013, **42**, 3269–3284, DOI: 10.1039/c2dt32617e; (*b*) W. Liu and R. Gust, *Coord. Chem. Rev.*, 2016, **329**, 191–213, DOI: 10.1016/j.ccr.2016.09.004.

6 (*a*) S. Patil, A. Deally, B. Gleeson, H. Müller-Bunz, F. Paradisi and M. Tacke, *Metallomics*, 2011, **3**, 74–88, DOI: 10.1039/c0mt00034e; (*b*) R. A. Haque, S. Y. Choo, S. Budagumpi, M. A. Iqbal and A. Al-Ashraf Abdullah,

Eur. J. Med. Chem., 2015, **90**, 82–92, DOI: 10.1016/j.ejmech.2014.11.005.

7 (*a*) R. Rubbiani, S. Can, I. Kitanovic, H. Alborzinia, M. Stefanopoulou, M. Kokoschka, S. Monchgesang, W. S. Sheldrick, S. Wölfl and I. Ott, *J. Med. Chem.*, 2011, **54**, 8646–8657, DOI: 10.1021/jm201220n; (*b*) J. K. Muenzner, B. Biersack, H. Kalie, I. C. Andronache, L. Kaps, D. Schuppan, F. Sasse and R. Schobert, *ChemMedChem*, 2014, **9**, 1195–1204, DOI: 10.1002/cmdc.201400049; (*c*) J. K. Muenzner, B. Biersack, A. Albrecht, T. Rehm, U. Lacher, W. Milius, A. Casini, J. Zhang, I. Ott, V. Brabec, O. Stuchlikova, I. C. Andronache, L. Kaps, D. Schuppan and R. Schobert, *Chem. – Eur. J.*, 2016, **22**, 18953–18962, DOI: 10.1002/chem.201604246.

8 (*a*) W. Streciwilk, F. Hackenberg, H. Müller-Bunz and M. Tacke, *Polyhedron*, 2014, **80**, 3–9, DOI: 10.1016/j.poly.2013.11.039; (*b*) M.-L. Teyssot, A.-S. Jarrousse, A. Chevry, A. De Haze, C. Beaudoin, M. Manin, S. P. Nolan, S. Díez-González, L. Morel and A. Gautier, *Chem. – Eur. J.*, 2009, **15**, 314–318, DOI: 10.1002/chem.200801992.

9 (*a*) G. Lv, L. Guo, L. Qiu, H. Yang, T. Wang, H. Liu and J. Lin, *Dalton Trans.*, 2015, **44**, 7324–7331, DOI: 10.1039/c5dt00169b; (*b*) L. Oehninger, M. Stefanopoulou, H. Alborzinia, J. Schur, S. Ludewig, K. Namikawa, A. Muñoz-Castro, R. W. Köster, K. Baumann, S. Wölfl, W. S. Sheldrick and I. Ott, *Dalton Trans.*, 2013, **42**, 1657–1666, DOI: 10.1039/c2dt32319b.

10 (*a*) M. Skander, P. Retailleau, B. Bourrié, L. Schio, P. Mailliet and A. Marinetti, *J. Med. Chem.*, 2010, **53**, 2146–2154, DOI: 10.1021/jm901693m; (*b*) E. Chardon, G. Dahm, G. Guichard and S. Bellemin-Laponnaz, *Organometallics*, 2012, **31**, 7618–7621, DOI: 10.1021/om300806g; (*c*) R. Wai-Yin Sun, A. Lok-Fung Chow, X.-H. Li, J. J. Yan, S. Sin-Yin Chui and C.-M. Che, *Chem. Sci.*, 2011, **2**, 728–736, DOI: 10.1039/c0sc00593b; (*d*) J. K. Muenzner, T. Rehm, B. Biersack, A. Casini, I. de Graaf, P. Worawutputtapong, A. Noor, R. Kempe, V. Brabec, J. Kasparkova and R. Schobert, *J. Med. Chem.*, 2015, **58**, 6283–6292, DOI: 10.1021/acs.jmedchem.5b00896; (*e*) M. Bouché, G. Dahm, A. Maisse-François, T. Achard and S. Bellemin-Laponnaz, *Eur. J. Inorg. Chem.*, 2016, **17**, 2828–2836, DOI: 10.1002/ejic.201600296.

11 T. Rehm, M. Rothemund, J. K. Muenzner, A. Noor, R. Kempe and R. Schobert, *Dalton Trans.*, 2016, **45**, 15390–15398, DOI: 10.1039/c6dt02350a.

12 (*a*) R. Rubbiani, I. Kitanovic, H. Alborzinia, S. Can, A. Kitanovic, L. A. Onambele, M. Stefanopoulou, Y. Geldmacher, W. S. Sheldrick, G. Wolber, A. Prokop, S. Wölfl and I. Ott, *J. Med. Chem.*, 2010, **53**, 8608–8618, DOI: 10.1021/jm100801e; (*b*) H. Valdés, M. Poyatos, G. Ujaque and E. Peris, *Chem. – Eur. J.*, 2015, **21**, 1578–1588, DOI: 10.1002/chem.201404618; (*c*) H. Lu and R. L. Brutchey, *Chem. Mater.*, 2017, **29**, 1396–1403, DOI: 10.1021/acs.chemmater.6b05293.

13 (*a*) T. Nakanishi and D. D. Ross, *Chin. J. Cancer*, 2012, **31**, 73–99, DOI: 10.5732/cjc.011.10320; (*b*) D. Shen, C. Cararelli, *et al.*, *J. Biol. Chem.*, 1986, **261**, 7762–7770; (*c*) M. M. Cromwell, A. R. Safa, R. L. Felsted, M. M. Gottesman and I. Pastan, *Proc. Natl. Acad. Sci. U. S. A.*, 1986, **83**, 3847–8350, DOI: 10.1073/pnas.83.11.3847.

14 (*a*) P. Bragado, A. Armesilla, A. Silva and A. Porras, *Apoptosis*, 2007, **12**, 1733–1742, DOI: 10.1007/s10495-007-0082-8; (*b*) Q. Kai, L. Ting, W. Jichao, M. Fandi, W. Zhixin, H. Zichao, W. Yong, S. Sidong, L. Sinan, C. Hulin, D. Yafeng and L. Chang, *J. South. Med. Univ.*, 2013, **33**, 1253–1259, DOI: 10.3969/j.ssn.1673-4254.2013.09.01; (*c*) N. S. Pellegata, R. J. Antoniono, J. L. Redpath and E. J. Standbridge, *Proc. Natl. Acad. Sci. U. S. A.*, 1996, **93**, 15209–15214, DOI: 10.1073/pnas.93.26.15209.

15 G. He, Z. H. Siddik, Z. Huang, R. Wang, J. Koomen, R. Kobayashi, A. R. Khokhar and J. Kuang, *Oncogene*, 2005, **24**, 2929–2943, DOI: 10.1038/sj.onc.1208474.

16 (*a*) S. Tabassum, G. Chandra Sharma, F. Arjmad and A. Azam, *Nanotechnology*, 2010, **21**, 195102–114094, DOI: 10.1088/0957-4484/21/19/195102; (*b*) V. Vijayanathan, T. Thomas and T. J. Thomas, *Biochemistry*, 2002, **41**, 14085–14094, DOI: 10.1021/bi0203987.

17 (*a*) N. P. Johnson, *Biochem. Biophys. Res. Commun.*, 1982, **104**, 1394–1400, DOI: 10.1016/0006-291X(82)91404-8; (*b*) A. M. J. Fichtinger-Schepman, J. L. Van der Veer, J. H. J. Den Hartog, P. H. M. Lohman and J. Reedijk, *Biochemistry*, 1985, **24**, 707–713, DOI: 10.1021/bi00324a025; (*c*) A. Eastman, *Pharmacol. Ther.*, 1987, **34**, 155–166, DOI: 10.1016/0163-7258(87)90009-X.

18 Z. Balcarova and V. Brabec, *Biophys. Chem.*, 1989, **33**, 55–61, DOI: 10.1016/0301-4622(89)80007-9.

19 M. V. Keck and S. J. Lippard, *J. Am. Chem. Soc.*, 1992, **114**, 3386–3390, DOI: 10.1021/ja00035a033.

20 (*a*) G. L. Cohen, W. R. Bauer, J. K. Barton and S. J. Lippard, *Science*, 1979, **203**, 1014–1016, DOI: 10.1126/science.370979; (*b*) W. M. Scovell and F. Collart, *Nucleic Acids Res.*, 1985, **13**, 2881–2895.

21 R. Zaludova, V. Kleinwächter and V. Brabec, *Biophys. Chem.*, 1996, **60**, 135–142, DOI: 10.1016/0301-4622(96)00010-5.

22 (*a*) K. S. Lovejoy, M. Serova, I. Bieche, S. Emami, M. D'Incalci, M. Broggini, E. Erba, C. Gespach, E. Cvitkovic, S. Faivre, E. Raymond and S. J. Lippard, *Mol. Cancer Ther.*, 2011, **10**, 1709–1719, DOI: 10.1158/1535-7163.MCT-11-0250; (*b*) G. Y. Park, J. J. Wilson, Y. Song and S. J. Lippard, *Proc. Natl. Acad. Sci. U. S. A.*, 2012, **109**, 11987–11992, DOI: 10.1073/pnas.1207670109; (*c*) B. Wang, Z. Wang, F. Ai, W. K. Tang and G. Zhu, *J. Inorg. Biochem.*, 2015, **142**, 118–125, DOI: 10.1016/j.jinorgbio.2014.10.003; (*d*) G. Y. Zhu, M. Myint, W. H. Ang, L. Song and S. J. Lippard, *Cancer Res.*, 2012, **72**, 790–800, DOI: 10.1158/0008-5472.CAN-11-3151.

23 R. C. Todd and S. J. Lippard, *Metallomics*, 2009, **1**, 280–291, DOI: 10.1039/b907567d.

24 (*a*) S. Teletchéa, S. Komeda, J.-M. Teuben, M. A. Elizondo-Riojas, J. Reedijk and J. Kozelka, *Chem. – Eur. J.*, 2006, **12**, 3741–3753; (*b*) J. Mlcouskova, J. Malina, V. Novohradsky, J. Kasparkova, S. Komeda and V. Brabec, *Biochim. Biophys.*

Acta, 2012, **1820**, 1502–1511, DOI: 10.1016/j.bbagen.2012.05.014; (*c*) J. Mlcouskova, J. Kasparkova, T. Suchankova, S. Komeda and V. Brabec, *J. Inorg. Biochem.*, 2012, **114**, 15–23, DOI: 10.1016/j.jinorgbio.2012.04.015.

25 M. D. Hall, K. A. Telma, K.-E. Chang, T. D. Lee, J. P. Madigan, J. R. Lloyd, I. S. Goldlust, J. D. Hoeschele and M. M. Gottesman, *Cancer Res.*, 2014, **74**, 3913–3922, DOI: 10.1158/0008-5472.CAN-14-0247.

Electronic Supporting Information

N,N-Dialkylbenzimidazol-2-ylidene platinum complexes – effects of alkyl residues and ancillary *cis*-ligands on their anticancer activity

Tobias Rehm,[a] Matthias Rothemund,[a] Thomas Dietel,[b] Rhett Kempe,[b] Jana Kasparkova,[c] Viktor Brabec,[c] and Rainer Schobert[a]

[a]*Organic Chemistry Laboratory, University Bayreuth, Universitaetsstrasse 30, 95440 Bayreuth, Germany.*

E-mail: Rainer.Schobert@uni-bayreuth.de

[b] Lehrstuhl fuer Anorganische Chemie II, University Bayreuth, Universitaetsstrasse 30, 95440 Bayreuth, Germany.

[c] Institute of Biophysics, Academy of Sciences of the Czech Republic, CZ-61265 Brno, Czech Republic.

Table of content:

General information

All the chemicals and reagents were purchased from Sigma Aldrich, Alfa Aesar, ChemPur or ABCR and were used without further purification. Melting points are uncorrected; NMR spectra were run on a 500 MHz spectrometer; chemical shifts are given in ppm (δ) and referenced relative to the internal solvent signal; ^{195}Pt NMR shifts are quoted relative to Ξ(^{195}Pt) = 21.496784 MHz, K_2PtCl_4 was used as external standard (δ = -1612.81); mass spectra: direct inlet, EI, 70 eV; elemental analyses: Vario EL III elemental analyser; X-Ray Diffractometer: STOE-IPDS II. Synthesis of benzimidazolium salts was performed based on literature procedures[1-3] as described herein.

Synthesis and characterization of benzimidazolium chlorides 6

General procedure:

Benzimidazole (1eq) and the respective alkyl iodides or bromides (5 - 10 eq) in acetonitrile (10 mL/mmol) were treated with K_2CO_3 (1.5 eq) and the mixture was heated to 50 - 70 °C for 1-5 days. After filtration the solvent was evaporated in vacuo and the residue was crystalized from CH_2Cl_2 and hexane.

The resulting benzimidazolium iodides/bromides were then stirred with Ag_2CO_3 (1eq) and conc. HNO_3 (kat.) in Ethanol for 3 h and after filtration of the silver halides the solution was treated with conc. HCl to obtain the respective benzimidazolium chlorides. After neutralization with $NaHCO_3$ and further filtration the solvent was evaporated, and the solids were resuspended in CH_2Cl_2 to filter off all inorganic residues. The product was then crystalized by adding hexane.

Synthesis of 1,3-dimethylbenzimidazolium chloride:[1]

Benzimidazole (472 mg, 4.0 mmol), iodomethane (2.48 mL, 40 mmol, 10 eq) and K_2CO_3 (828 mg, 6.0 mmol, 1.5 eq) in acetonitrile (40 mL) for 5 d at 50 °C gave 1.004 g (92 %) of the benzimidazolium iodide which was treated with Ag_2CO_3 (1.0 g, 3.7 mmol), conc. HNO_3 (100 µL) and conc. HCl (800 µL) in EtOH (80 mL). Yield: 632 mg (87 %) white solid; ^{1}H NMR ($CDCl_3$, 500 MHz): δ 4.21 (6 H, s) 7.67 - 7.71 (2 H, m) 7.71 - 7.76 (2 H, m) 10.75 (1 H, s).

Synthesis of 1,3-diethylbenzimidazolium chloride:[1]

Benzimidazole (500 mg, 4.2 mmol), iodoethane (1.26 mL, 21 mmol, 5 eq) and K_2CO_3 (871 mg, 6.3 mmol, 1.5 eq) in acetonitrile (40 mL) for 24 h at 70 °C gave 1.278 g (100 %) of the benzimidazolium iodide which was treated with Ag_2CO_3 (1.16 g, 4.2 mmol), conc. HNO_3 (100 µL) and conc. HCl (800 µL) in EtOH (80 mL). Yield: 880 mg (100 %) white solid; ^{1}H NMR ($CDCl_3$, 500 MHz): δ 1.77 (6 H, t, *J* = 7.3 Hz) 4.70 (4 H, q, *J* = 7.3 Hz) 7.66 - 7.70 (2 H, m) 7.75 - 7.79 (2 H, m) 11.08 (1 H, s).

Synthesis of 1,3-dibutylbenzimidazolium chloride:[2]

Benzimidazole (2.0 g, 17 mmol), 1-bromobutane (7.2 mL, 68 mmol, 4 eq) and K_2CO_3 (3.5 g, 26 mmol, 1.5 eq) in acetonitrile (150 mL) for 5 d at 70 °C gave 3.635 g (69 %) of the benzimidazolium bromide which was treated with Ag_2CO_3 (3.22 g, 12 mmol), conc. HNO_3 (100 µL) and conc. HCl (800 µL) in EtOH (100 mL). Yield: 2.849 mg (63 %) amber solid; ^{1}H NMR ($CDCl_3$, 500 MHz): δ 0.98 (6 H, t, *J* = 7.5 Hz) 1.44 (4 H, sxt, *J* = 7.5 Hz) 2.02 (4 H, quin, *J* = 7.5 Hz) 4.59 (4 H, t, *J* = 7.5 Hz) 7.64 - 7.68 (2 H, m) 7.70 - 7.74 (2 H, m) 11.46 (1 H, s).

Synthesis of 1,3-dioctylbenzimidazolium chloride:[3]

Benzimidazole (236 mg, 2.0 mmol), 1-bromooctane (1.74 mL, 10 mmol, 5 eq) and K_2CO_3 (414 mg, 3.0 mmol, 1.5 eq) in acetonitrile (20 mL) for 3 d at 70 °C gave 461 mg (54 %) of the benzimidazolium bromide which was treated with Ag_2CO_3 (300 mg, 1.1 mmol), conc. HNO_3 (30 µL) and conc. HCl (200 µL) in EtOH (20 mL). Yield: 398 mg (52 %) white solid; ^{1}H NMR ($CDCl_3$, 500 MHz): δ 0.84 - 0.89 (6 H, m) 1.20 - 1.40 (20 H, m) 2.01 (4 H, quin, *J* = 7.5 Hz) 4.54 (4 H, t, *J* = 7.5 Hz) 7.64 - 7.69 (2 H, m) 7.69 - 7.75 (2 H, m) 11.05 (1 H, s).

Table S 1: X-ray structural data of platinum carbene complexes 8b, 9c and 10a.

Crystal data	**8b**	**9c**	**10a**
Chemical formula	$C_{13}H_{20}Cl_2N_2OPtS$	$C_{33}H_{37}Cl_2N_2PPt$	$C_{45}H_{40}ClN_2P_2Pt\cdot Cl$
M_r	518.36	1517.27	936.72
Crystal system, space group	Triclinic, P^{-1}	Triclinic, P^{-1}	Monoclinic, P21/c
Temperature (K)	133	133	133
a, *b*, *c* (Å)	8.675 (5), 9.264 (5), 10.601 (5)	9.1067 (18), 12.792 (3), 13.803 (3)	12.578 (5), 10.790 (5), 32.126 (5)
α, β, γ (°)	91.874 (5), 103.182 (5), 94.722 (5)	88.02 (3), 87.59 (3), 71.06 (3)	90, 94.531 (5), 90
V (Å^3)	825.5 (8)	1519.2 (6)	4346 (3)
Z	2	1	4
F(000)	496	752	1864
D_x (Mg m^{-3})	2085	1.658	1431
Radiation type	Mo *K*α	Mo *K*α	Mo *K*α
No. of reflections for cell measurement	9824	31963	16101
θ range (°) for cell measurement	2.0–28.5	1.5–30.1	1.6–27.7
μ (mm^{-1})	8.95	4.87	3.46
Crystal shape	Needles	Block	Platte
Colour	Colourless	Colourless	Colourless
Crystal size (mm)	0.11 × 0.08 × 0.07	0.36 × 0.19 × 0.15	0.20 × 0.09 × 0.08
Data collection			
Diffractometer	STOE-STADIVARI	STOE-STADIVARI	STOE-STADIVARI
Scan method	ω–scan	ω–scan	ω–scan
Absorption correction	Numerical STOE *X-RED32*	Numerical STOE X-RED32	Numerical SROE X-RED32
T_{min}, T_{max}	0.680, 0.761	0.553, 0.719	0.863, 0.953
No. of measured, independent and observed [$I > 2\sigma(I)$] reflections	7449, 3177, 2704	21191, 5907, 5605	32457, 8450, 5359
R_{int}	0.042	0.022	0.104
θ values (°)	θ_{max} = 26.0, θ_{min} = 2.0	θmax = 26.0, θmin = 1.5	θmax = 26.0, θmin = 1.6
$(\sin\theta/\lambda)_{max}$ (Å^{-1})	0.617	0.617	0.617
Range of *h*, *k*, *l*	*h* = −9 → 10 *k* = −11 → 9 *l* = −13 → 11	h = −5 → 11 k = −15 → 15 l = −16 → 17	h = −15 → 8 k = −13 → 13 l = −39 → 37
Refinement			
Refinement on	F^2	F^2	F^2
$R[F^2 > 2\sigma(F^2)]$, $wR(F^2)$, *S*	0.033, 0.085, 1.03	0.017, 0.040, 1.04	0.072, 0.190, 0.95
No. of reflections	3177	5907	8450
No. of parameters	185	354	471
No. of restraints	0	0	27
H-atom treatment	H-atom parameters constrained	H-atom parameters constrained	H-atom parameters constrained
Weighting scheme	$w = 1/[\sigma^2(F_o^2) + (0.0485P)^2]$ where $P = (F_o^2 + 2F_c^2)/3$	w = 1/[σ2(Fo2) + (0.0275P)2 + 0.1532P] where P = (Fo2 + 2Fc2)/3	w = 1/[σ2(Fo2) + (0.1181P)2] where P = (Fo2 + 2Fc2)/3
$(\Delta/\sigma)_{max}$	< 0.001	0.001	0.001
$\Delta\rho_{max}$, $\Delta\rho_{min}$ (e Å^{-3})	2.52, −2.72	0.45, −1.24	1.99, −2.96

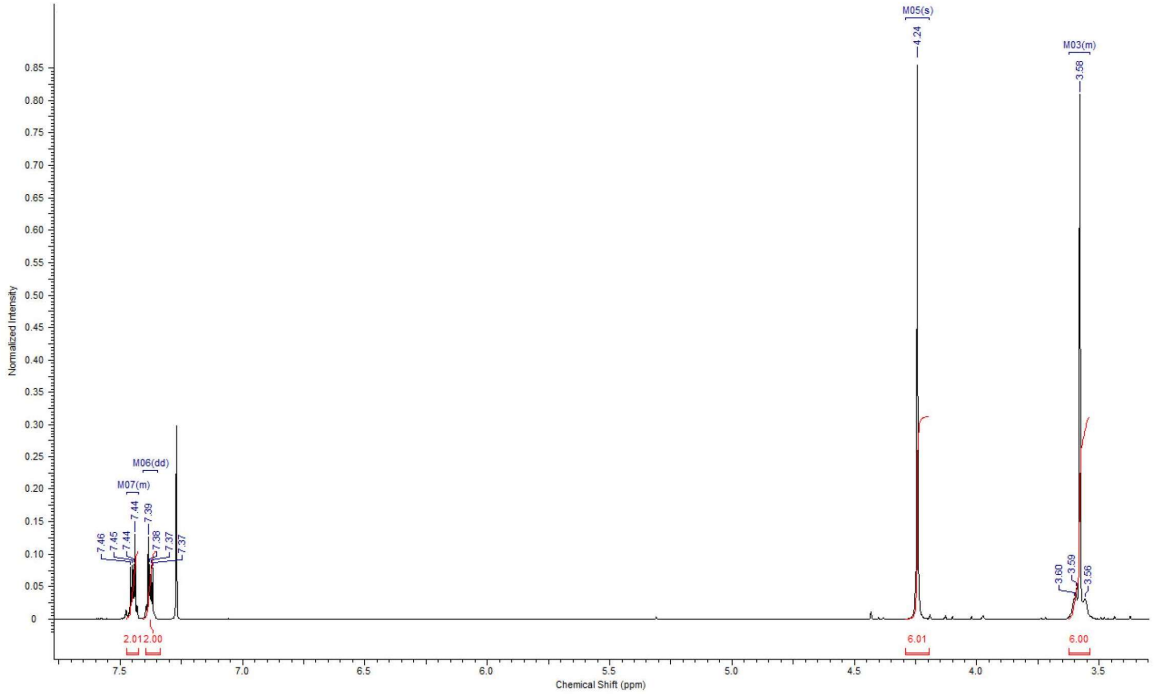

Fig. S1: ^{1}H-NMR spectrum (500 MHz, $CDCl_3$) of complex **8a**.

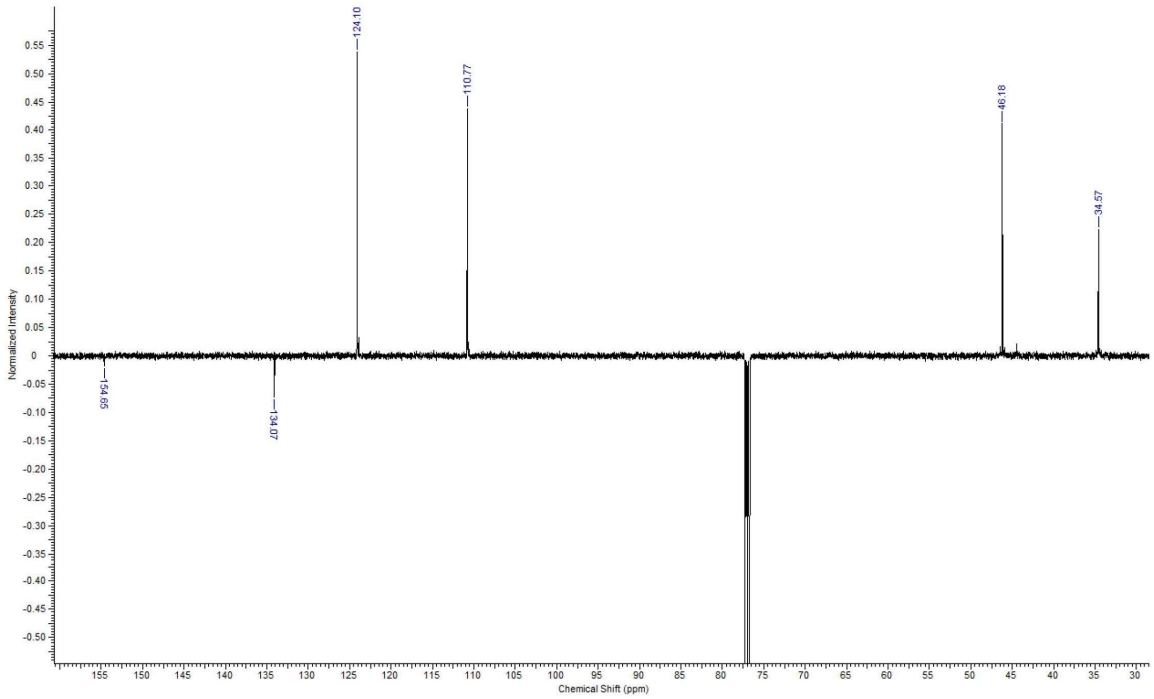

Fig. S 2: ^{13}C-NMR spectrum (126 MHz, $CDCl_3$) of complex **8a**.

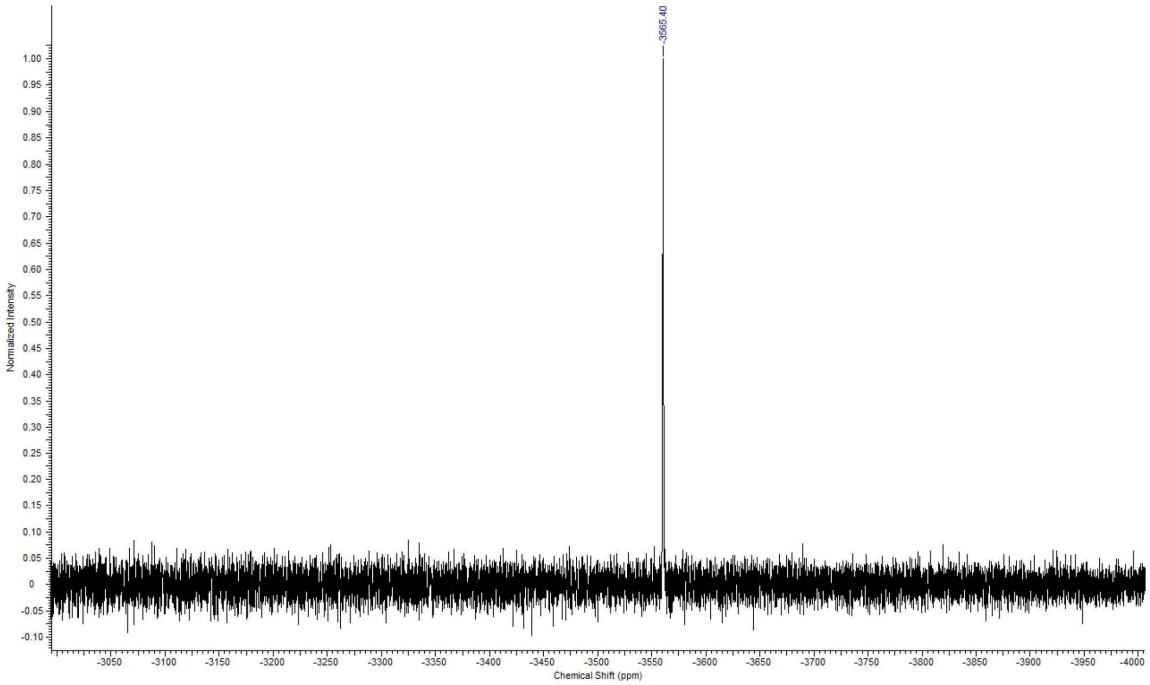

Fig. S 3: ^{195}Pt-NMR spectrum (108 MHz, $CDCl_3$) of complex **8a**.

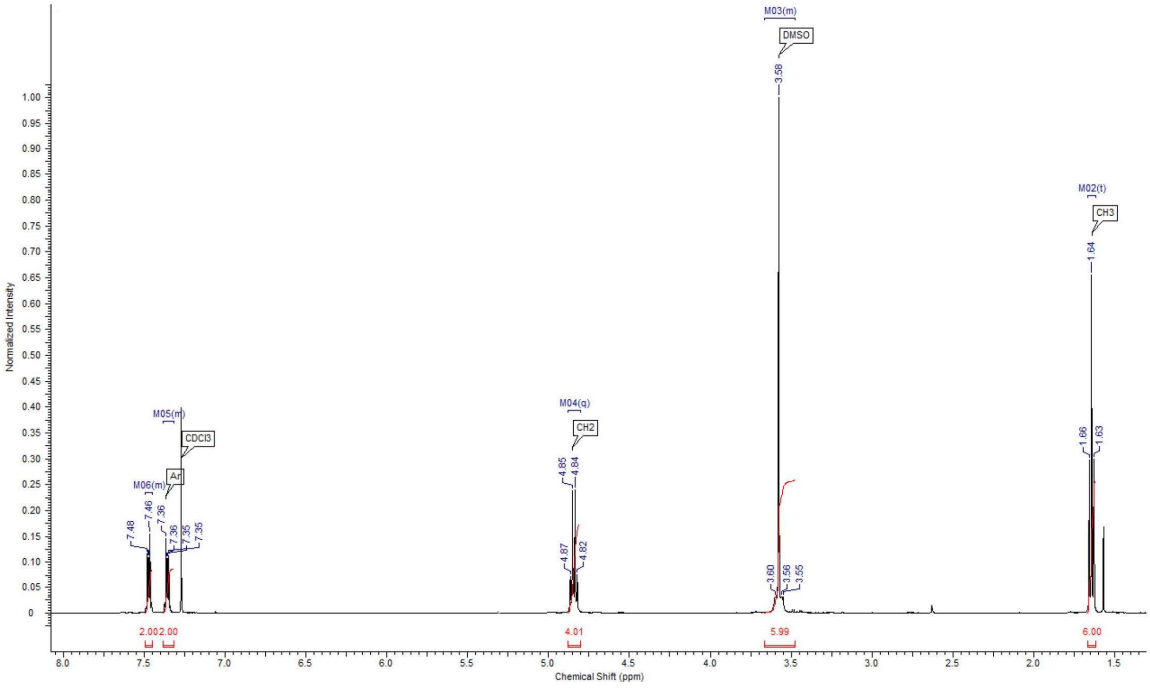

Fig. S 4: ^{1}H-NMR spectrum (500 MHz, $CDCl_3$) of complex **8b**.

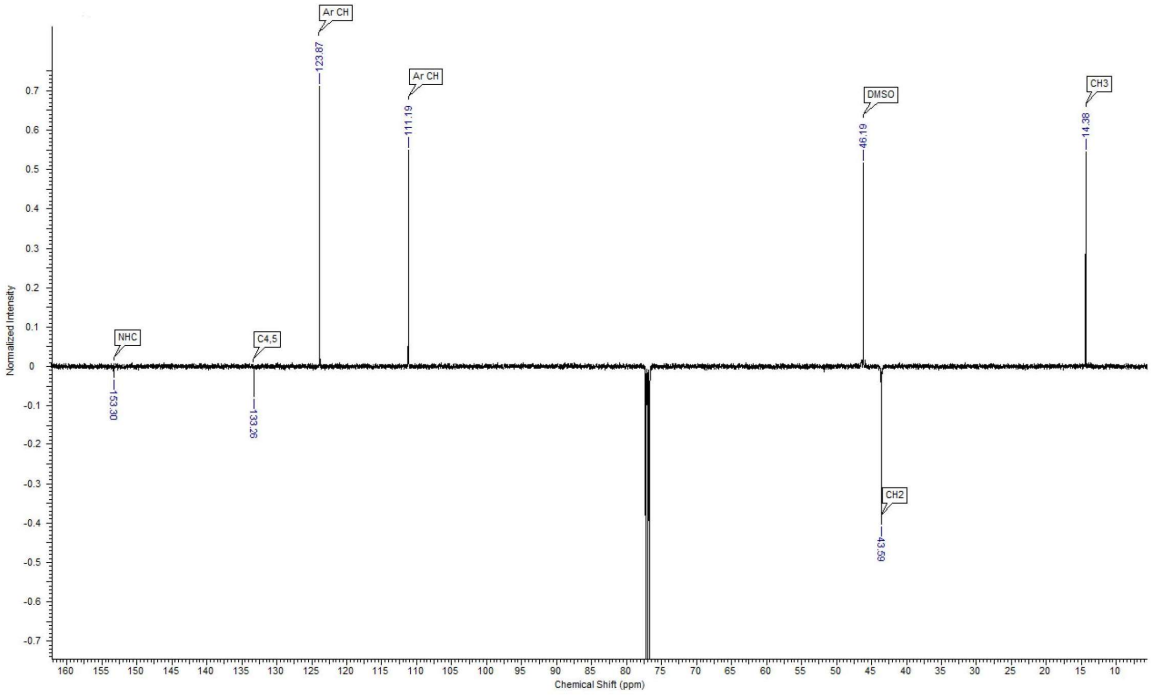

Fig. S 5: ^{13}C-NMR spectrum (126 MHz, $CDCl_3$) of complex **8b**.

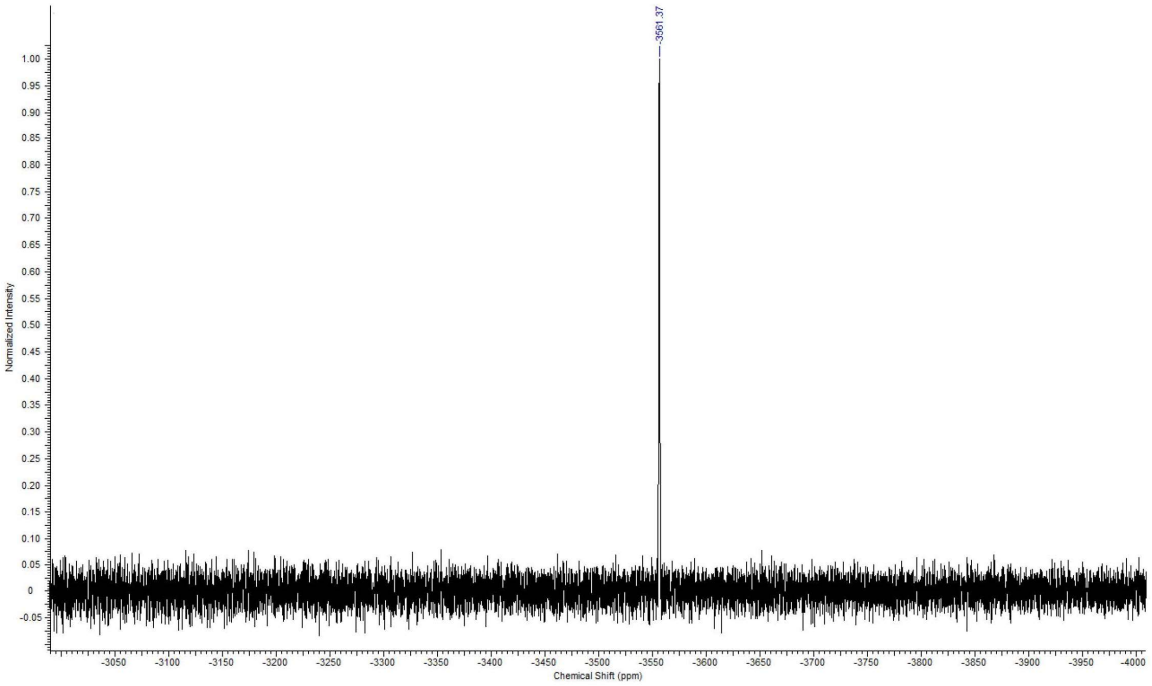

Fig. S 6: ^{195}Pt-NMR spectrum (108 MHz, $CDCl_3$) of complex **8b**.

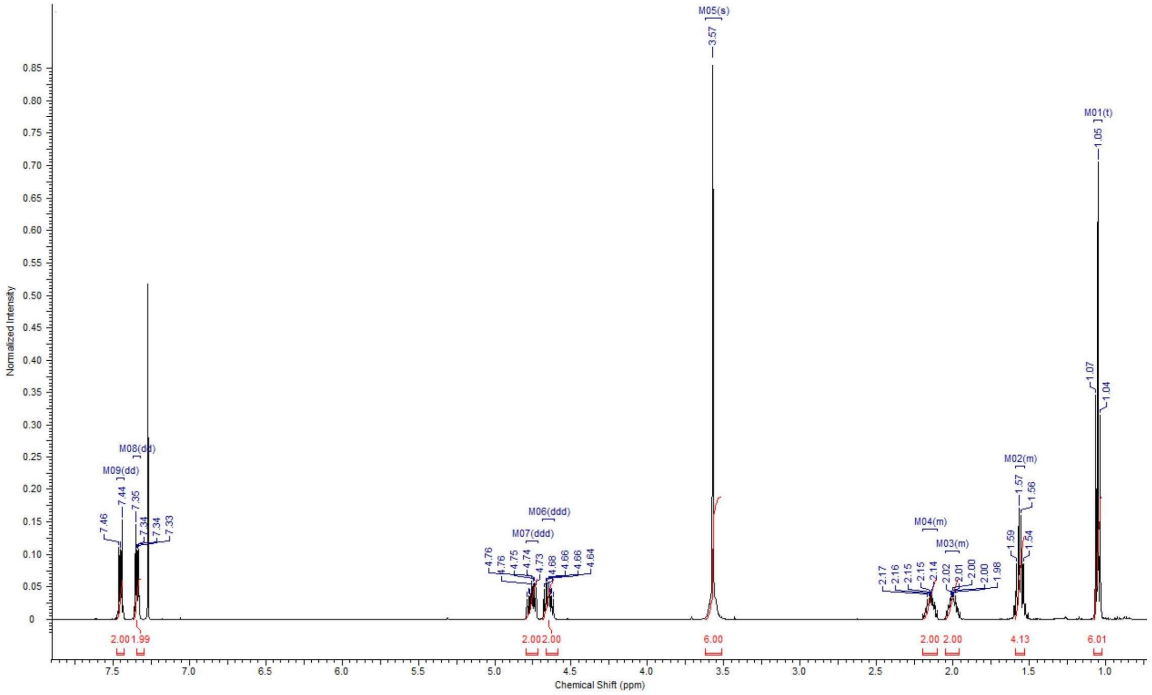

Fig. S 7: ^{1}H-NMR spectrum (500 MHz, $CDCl_3$) of complex **8c**.

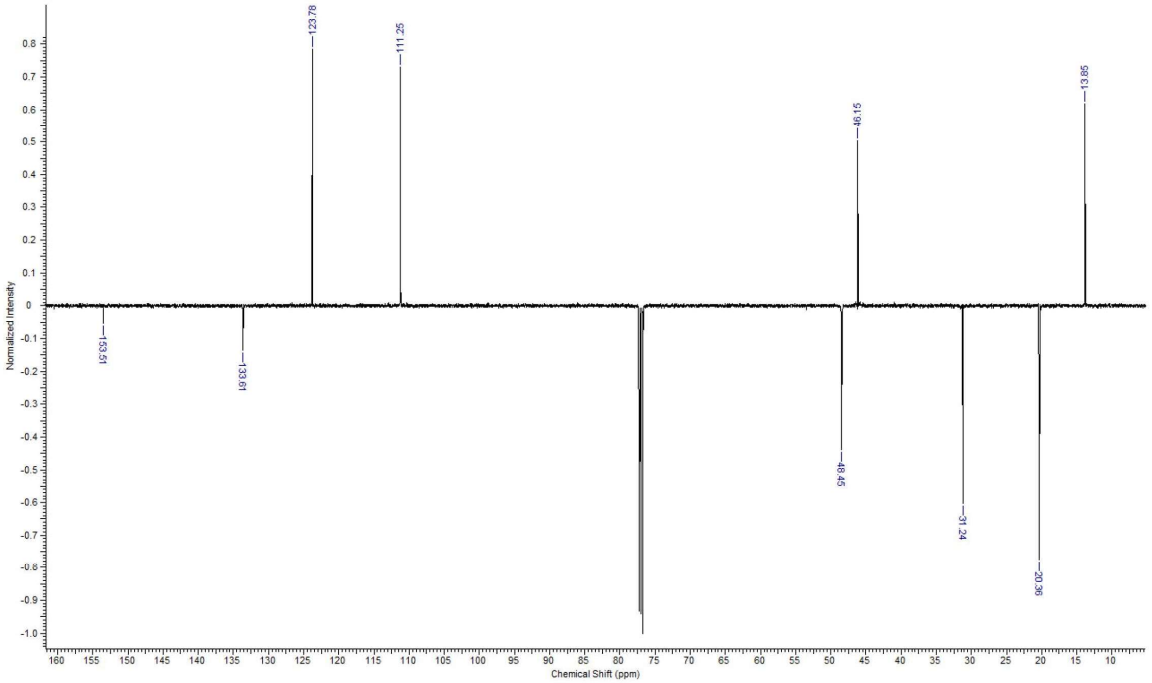

Fig. S 8: ^{13}C-NMR spectrum (126 MHz, $CDCl_3$) of complex **8c**.

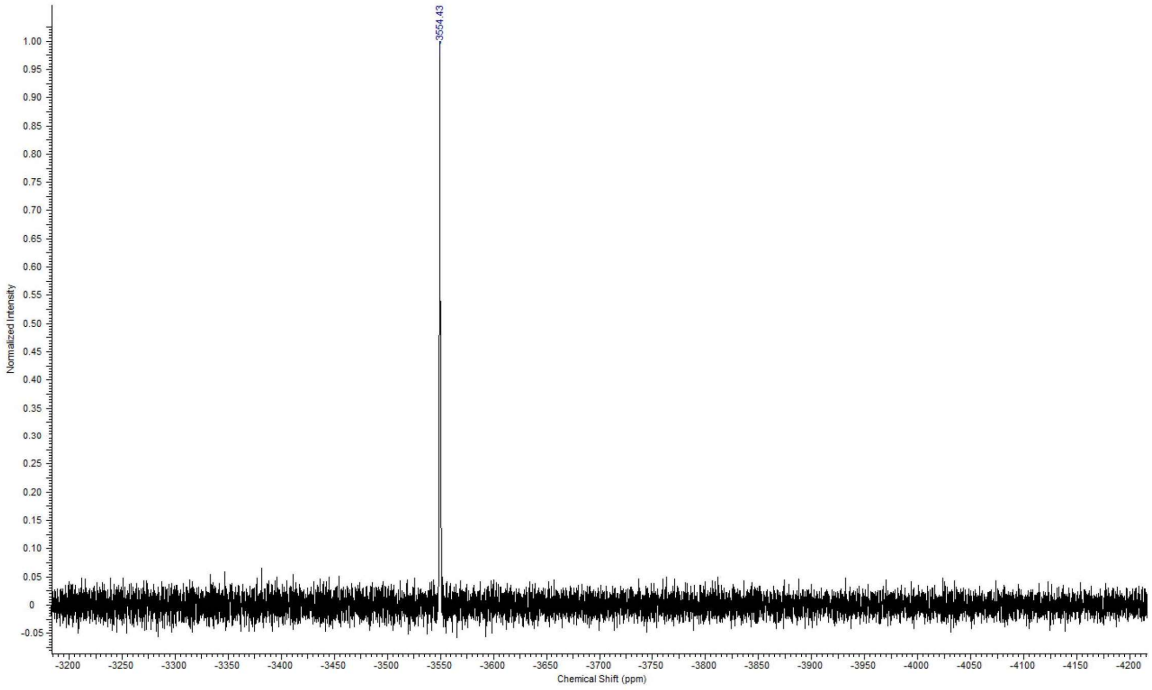

Fig. S 9: ^{195}Pt-NMR spectrum (108 MHz, $CDCl_3$) of complex **8c**.

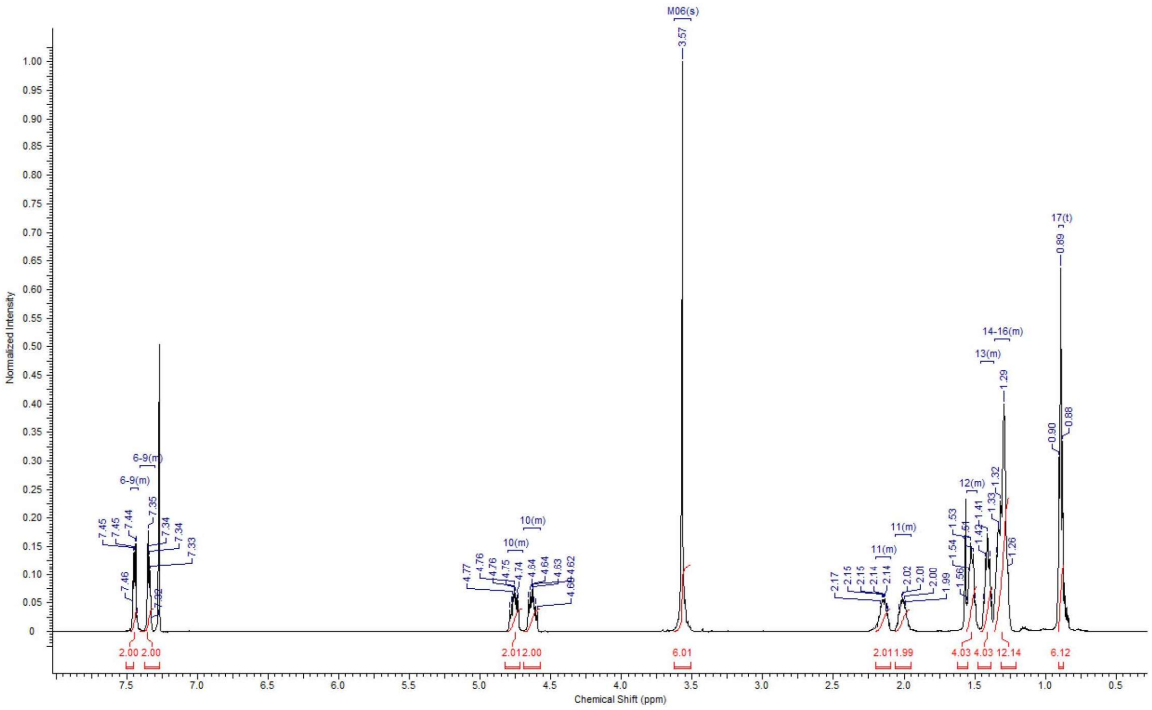

Fig. S 10: ^{1}H-NMR spectrum (500 MHz, $CDCl_3$) of complex **8d**.

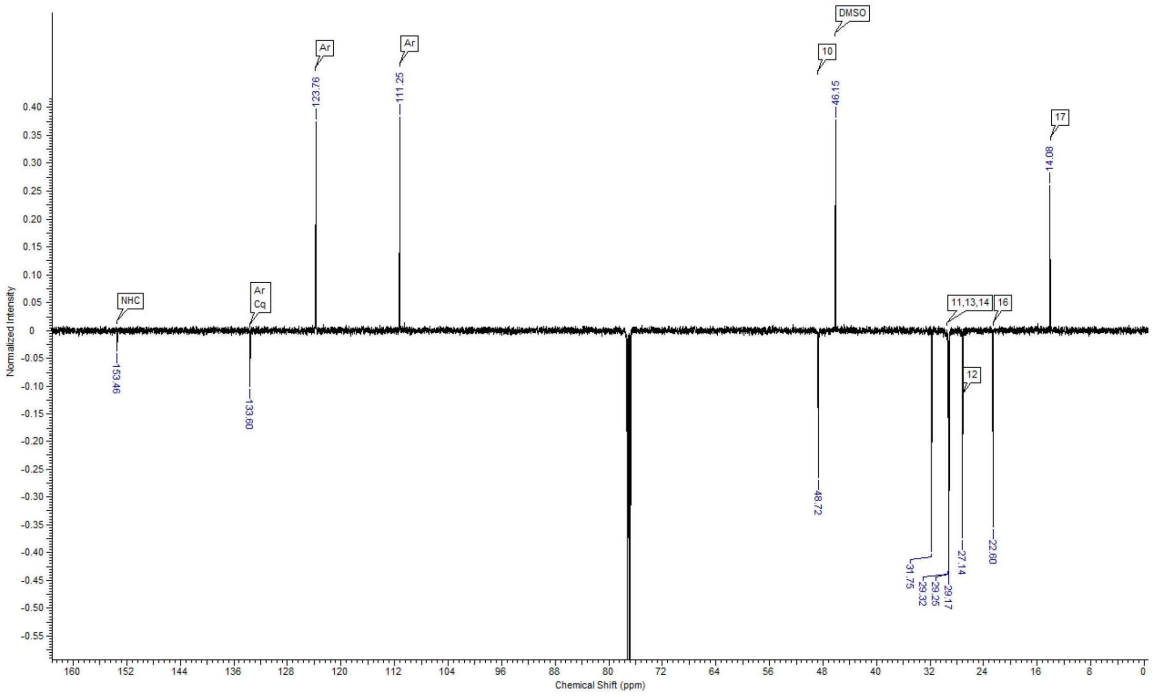

Fig. S 11: ^{13}C-NMR spectrum (126 MHz, $CDCl_3$) of complex **8d**.

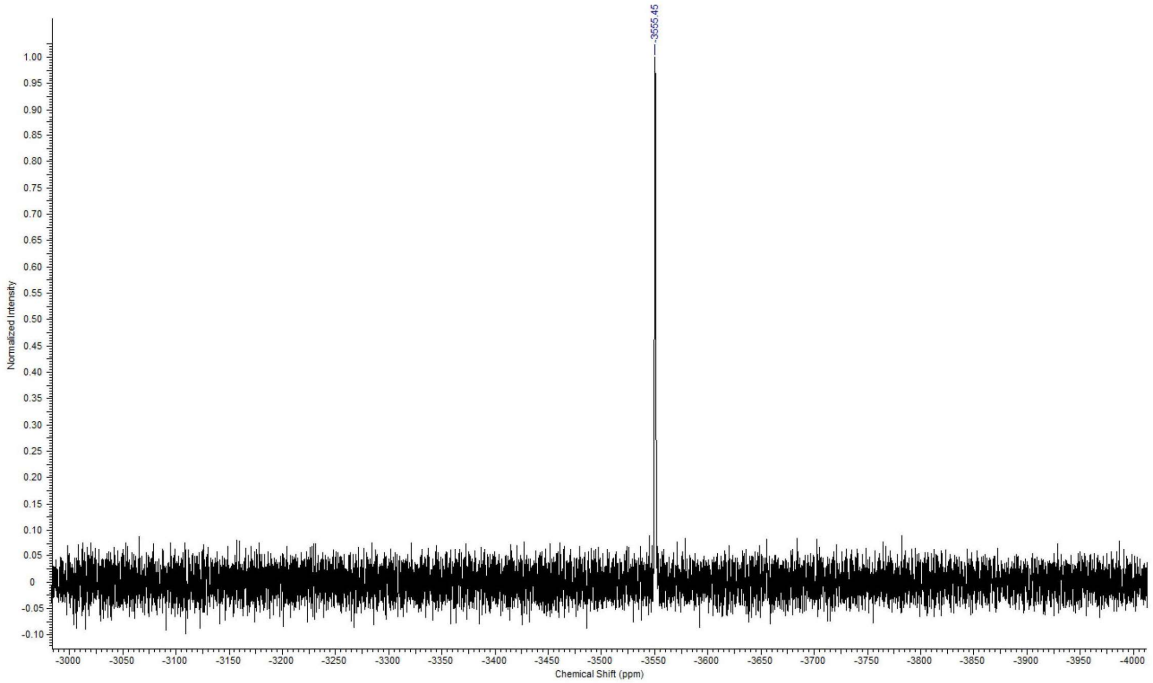

Fig. S 12: ^{195}Pt-NMR spectrum (108 MHz, $CDCl_3$) of complex **8d**.

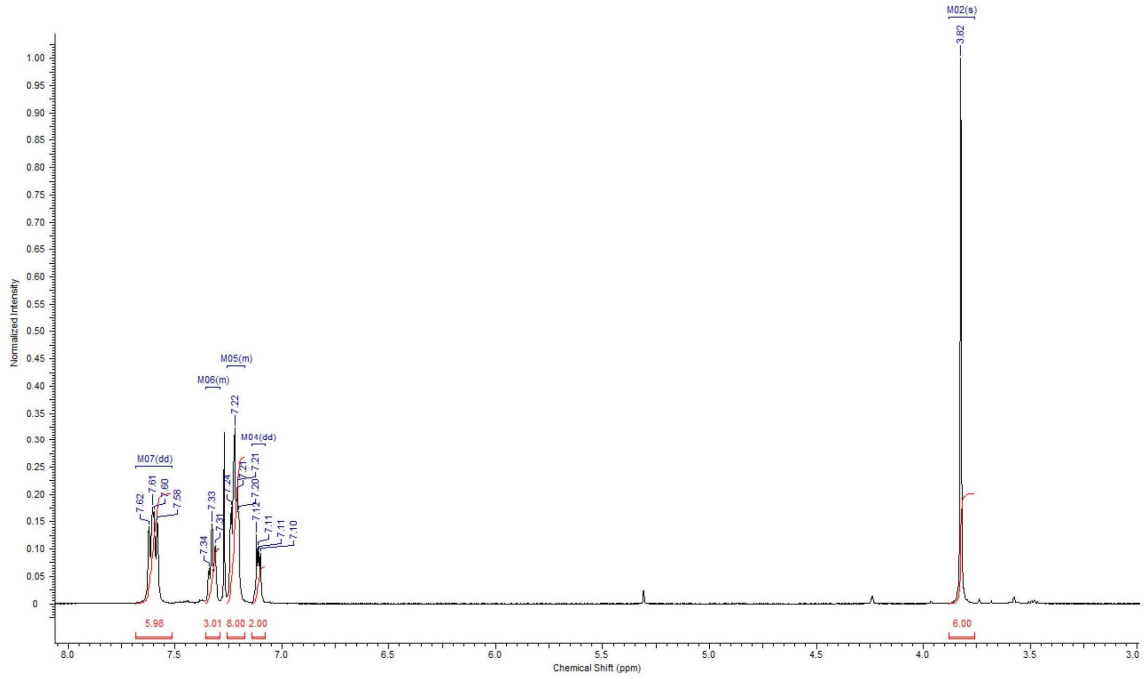

Fig. S 13: ^{1}H-NMR spectrum (500 MHz, $CDCl_3$) of complex **9a**.

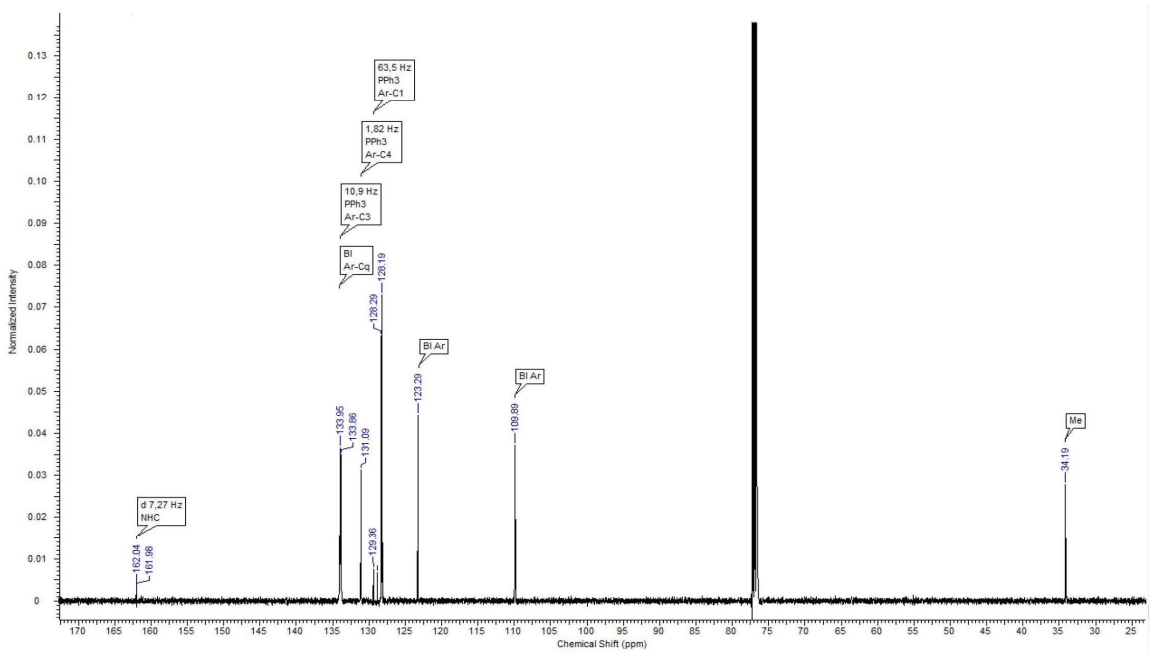

Fig. S 14: ^{13}C-NMR spectrum (126 MHz, $CDCl_3$) of complex **9a**.

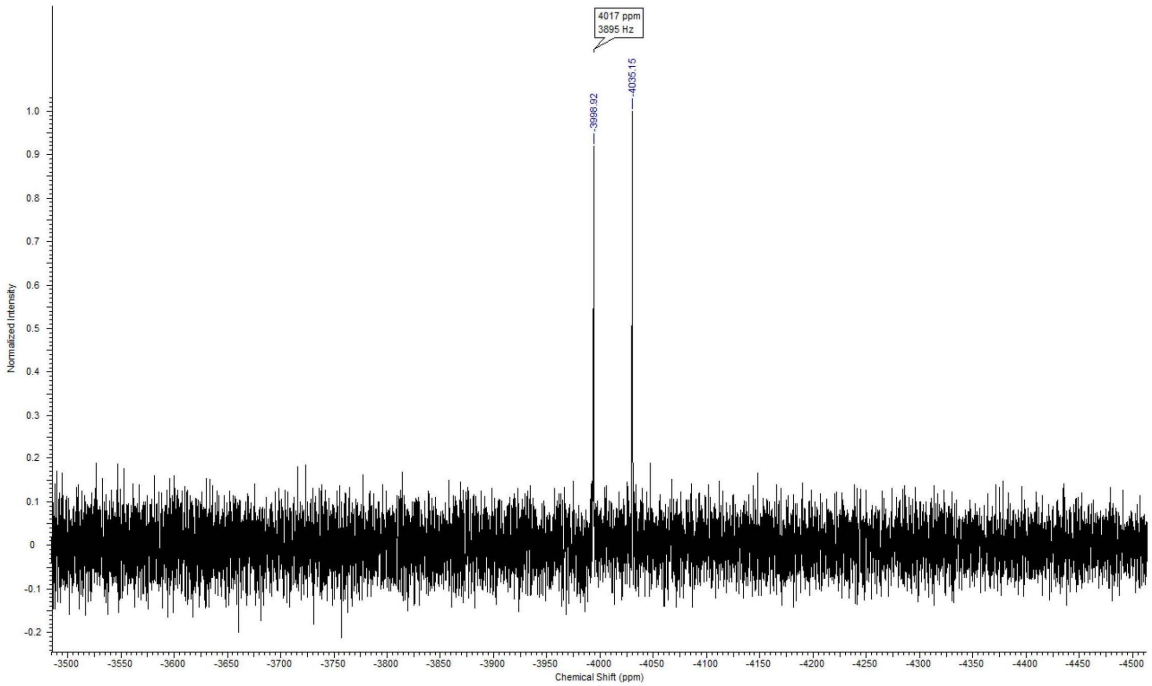

Fig. S 15: ^{195}Pt-NMR spectrum (108 MHz, $CDCl_3$) of complex **9a**.

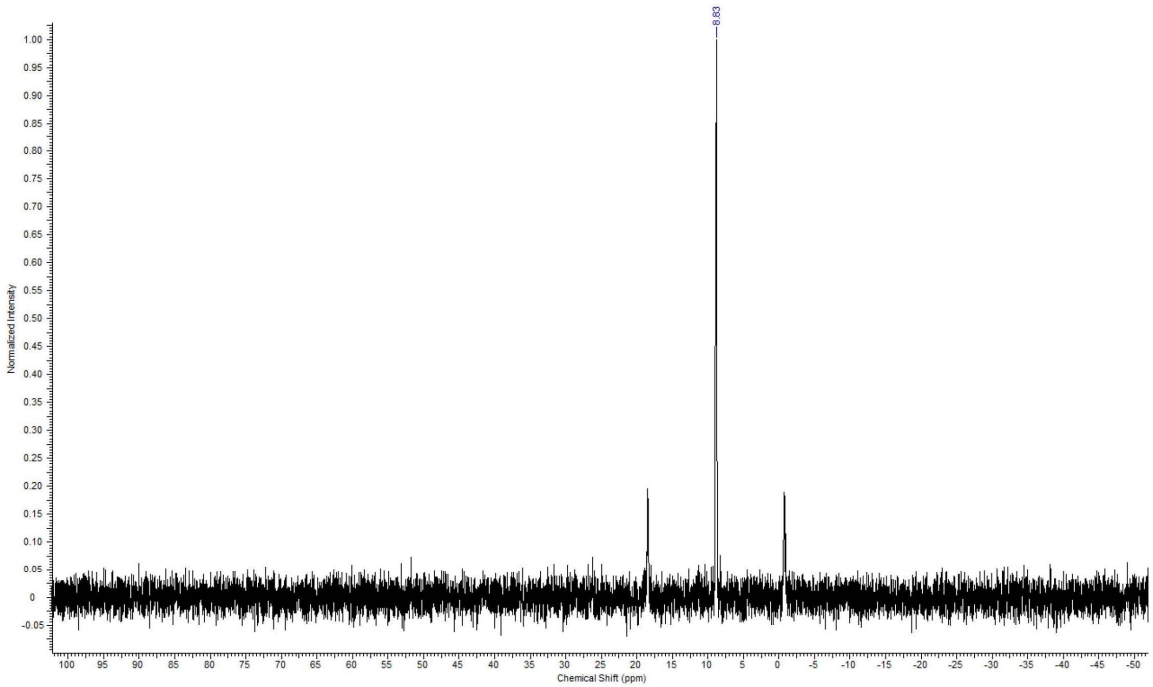

Fig. S 16: ^{31}P-NMR spectrum (202 MHz, $CDCl_3$) of complex **9a**.

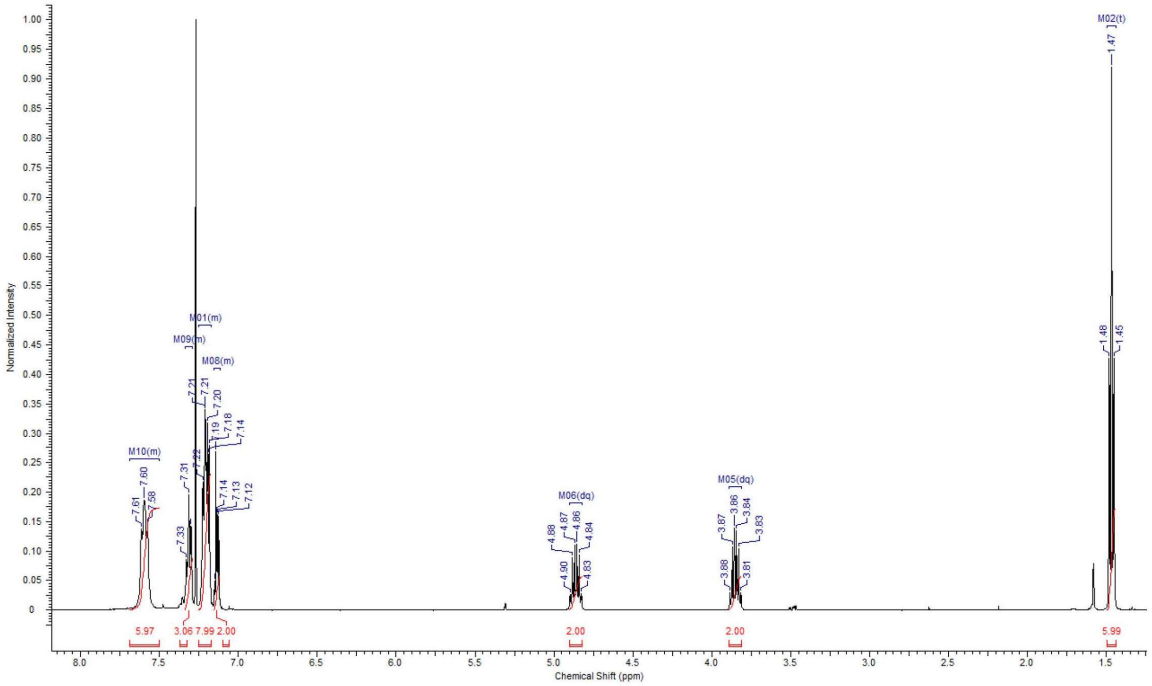

Fig. S 17: ^{1}H-NMR spectrum (500 MHz, $CDCl_3$) of complex **9b**.

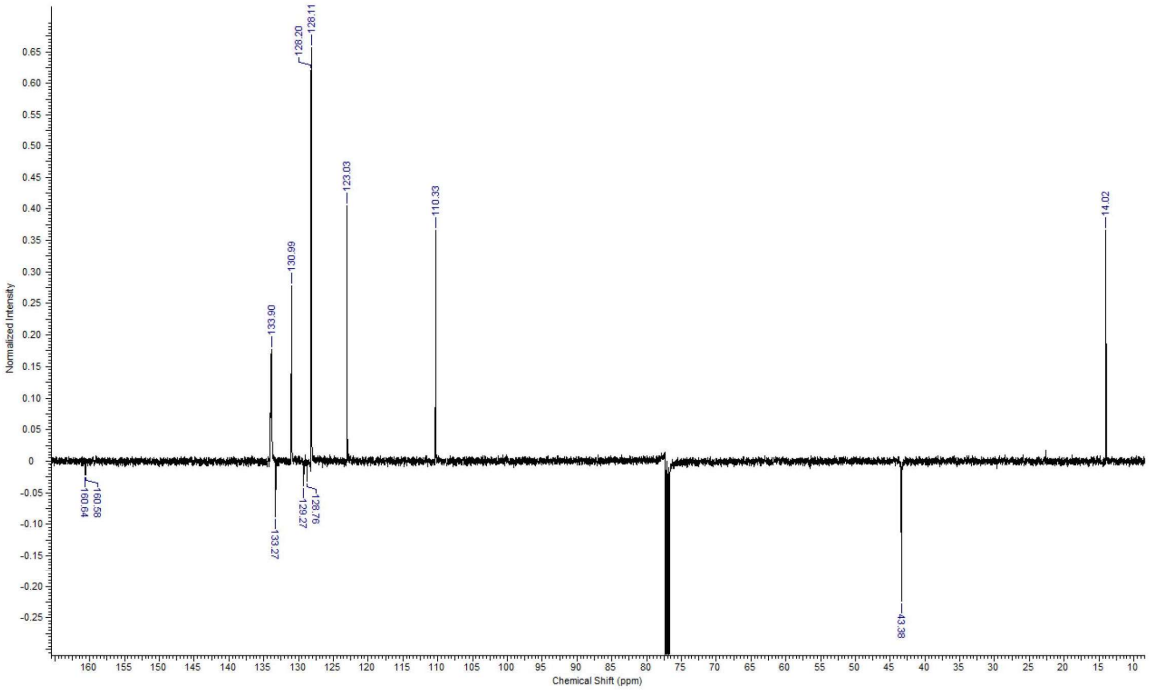

Fig. S 18: ^{13}C-NMR spectrum (126 MHz, $CDCl_3$) of complex **9b**.

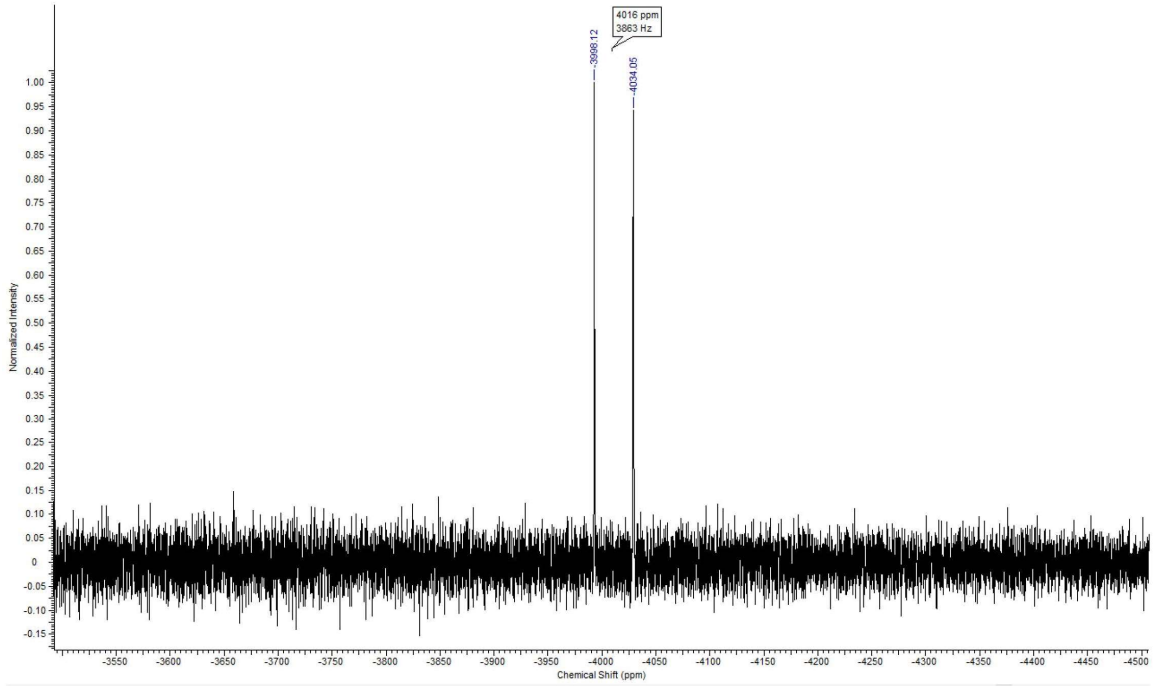

Fig. S 19: ^{195}Pt-NMR spectrum (108 MHz, $CDCl_3$) of complex **9b**.

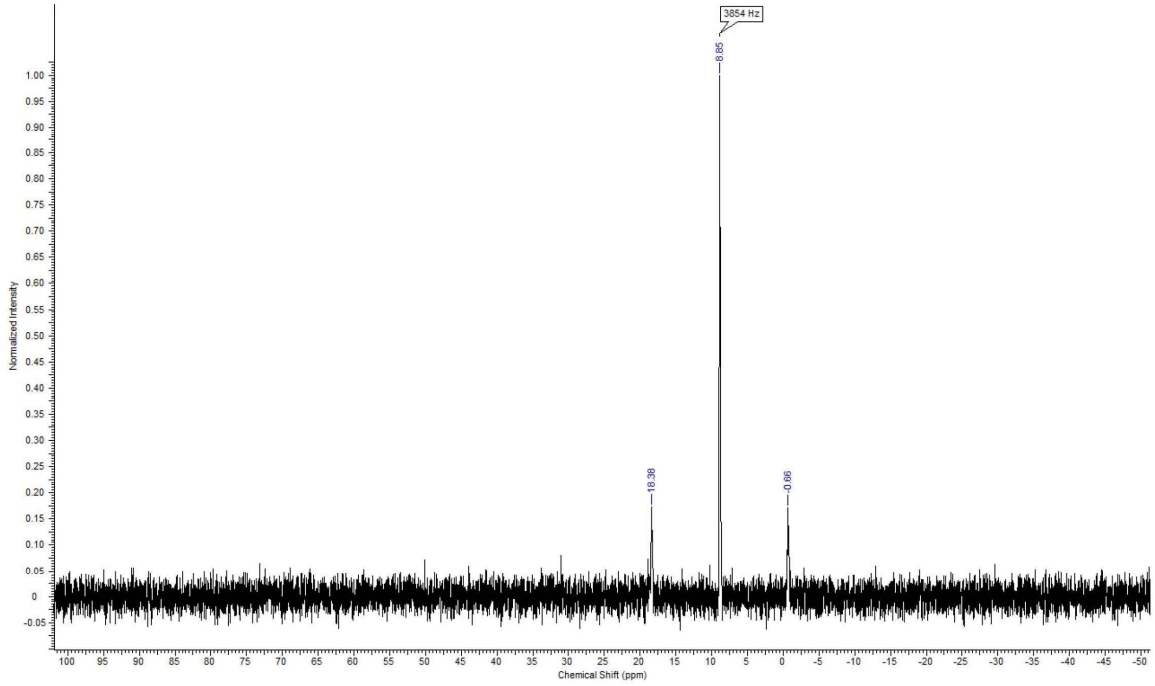

Fig. S 20: ^{31}P-NMR spectrum (202 MHz, $CDCl_3$) of complex **9b**.

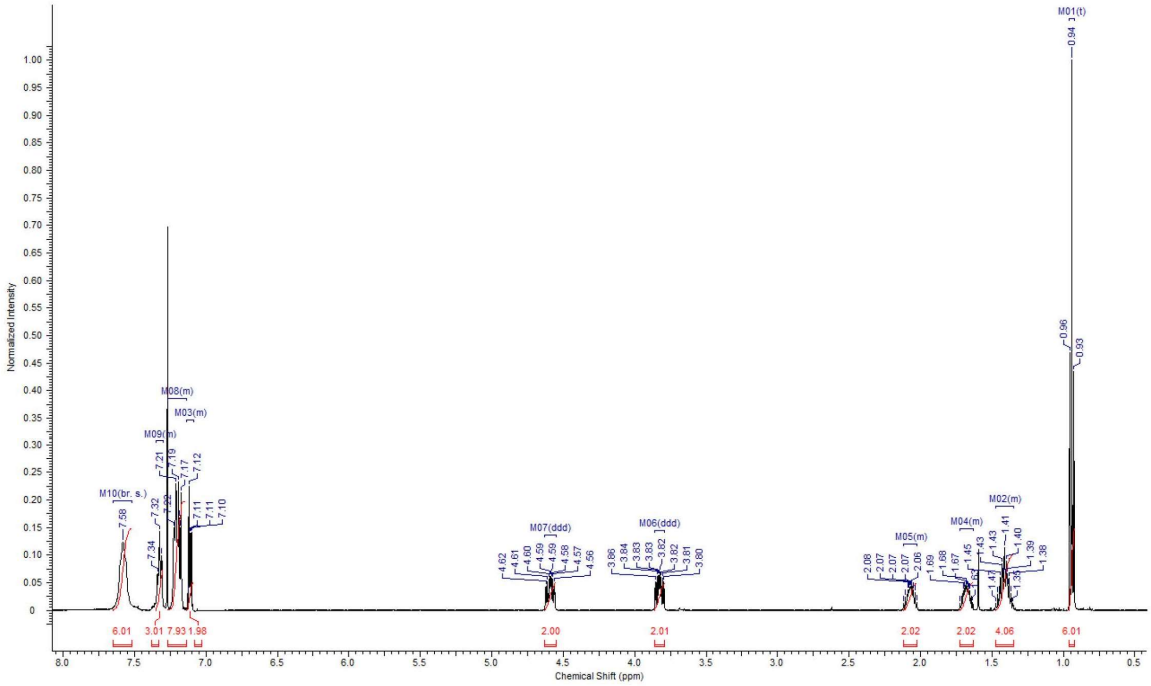

Fig. S 21: ^{1}H-NMR spectrum (500 MHz, $CDCl_3$) of complex **9c**.

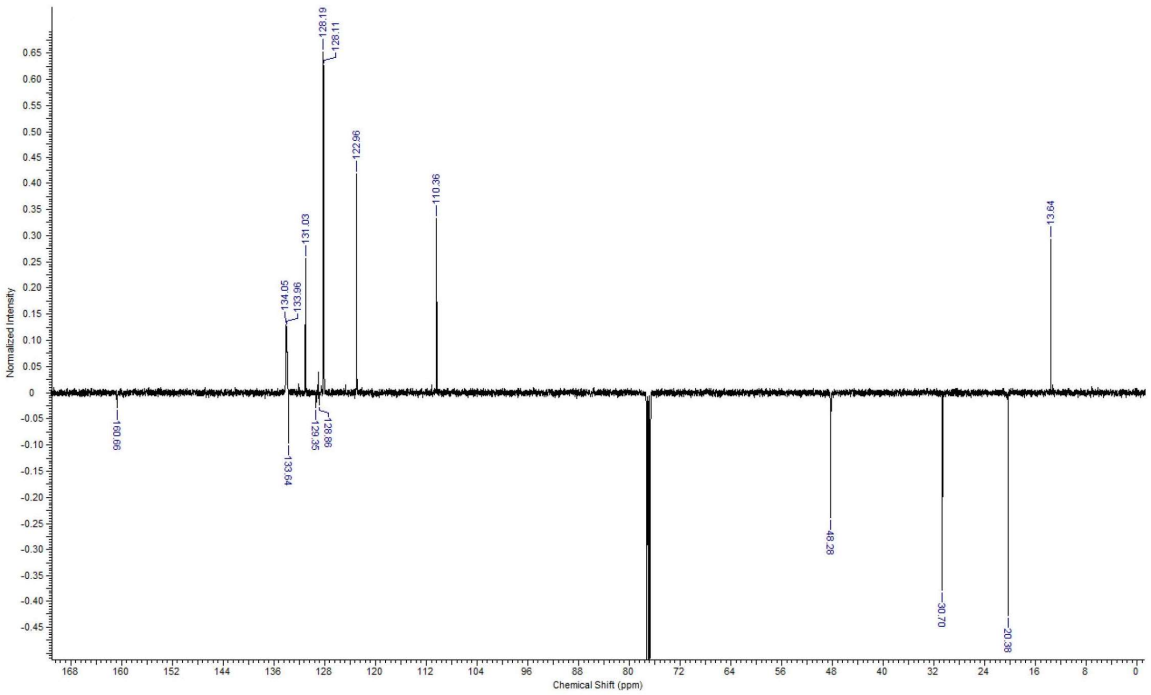

Fig. S 22: ^{13}C-NMR spectrum (126 MHz, $CDCl_3$) of complex **9c**.

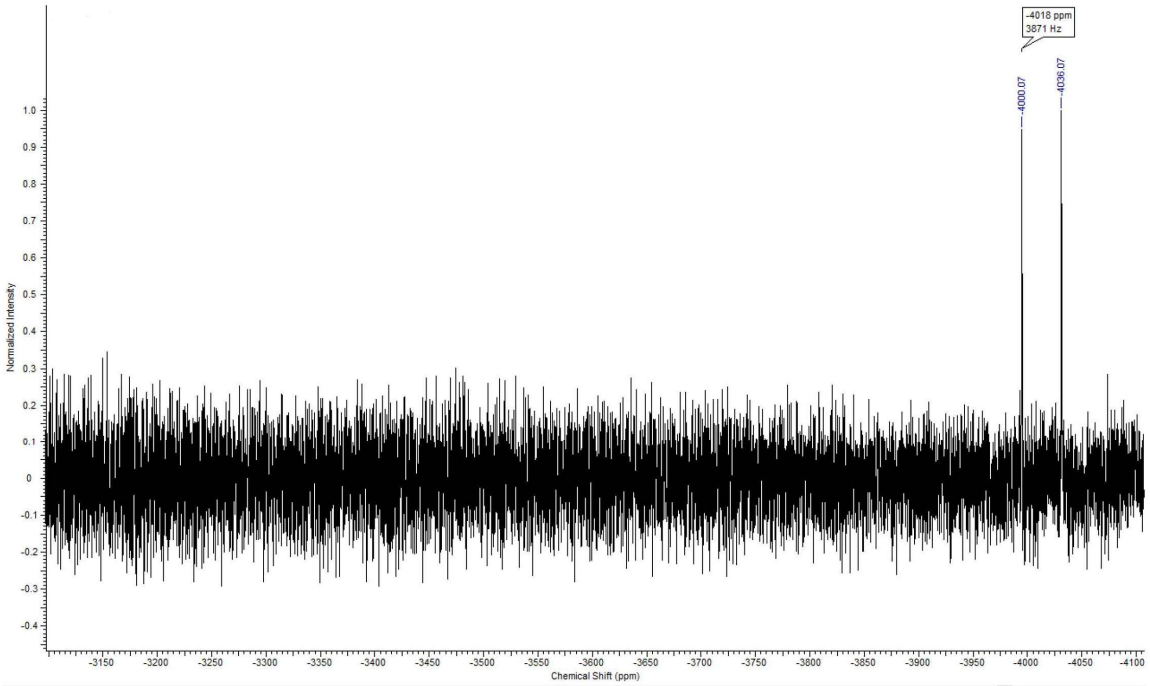

Fig. S 23: ^{195}Pt-NMR spectrum (108 MHz, $CDCl_3$) of complex **9c**.

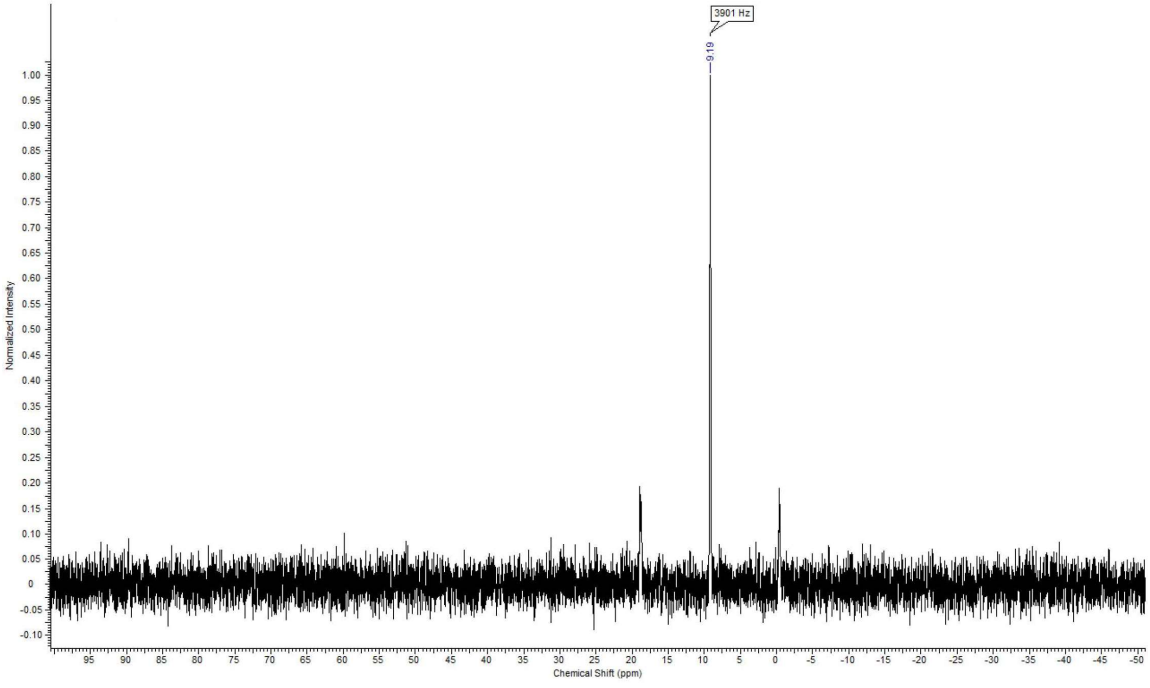

Fig. S 24: ^{31}P-NMR spectrum (202 MHz, $CDCl_3$) of complex **9c**.

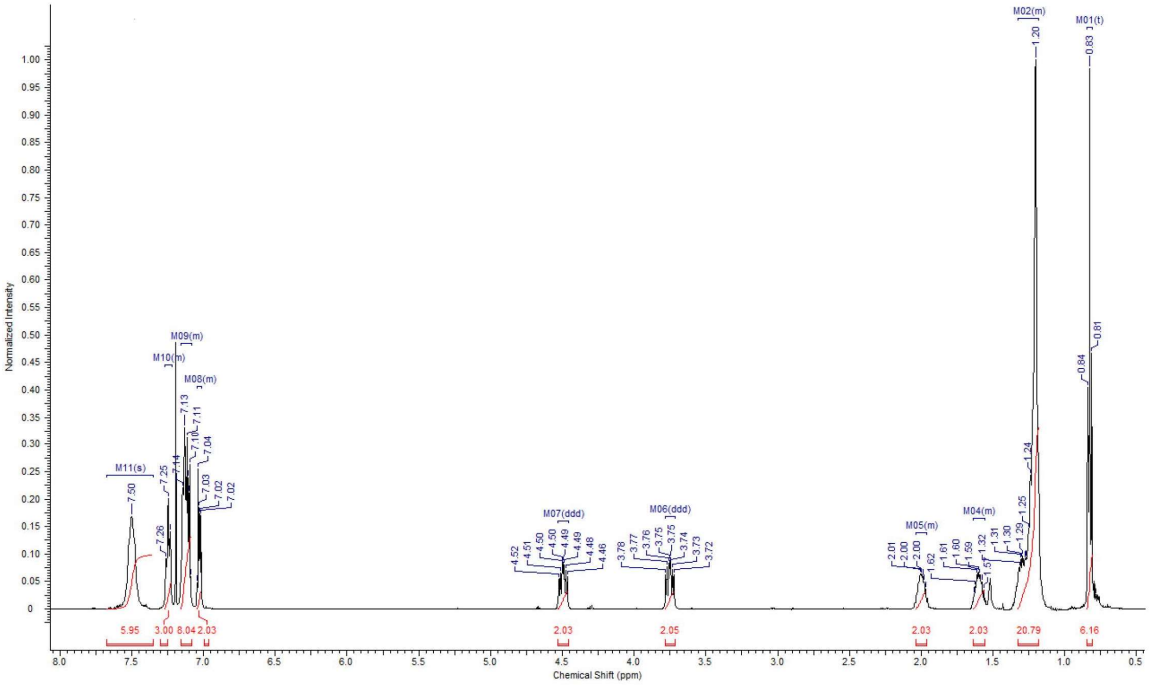

Fig. S 25: ^{1}H-NMR spectrum (500 MHz, $CDCl_3$) of complex **9d**.

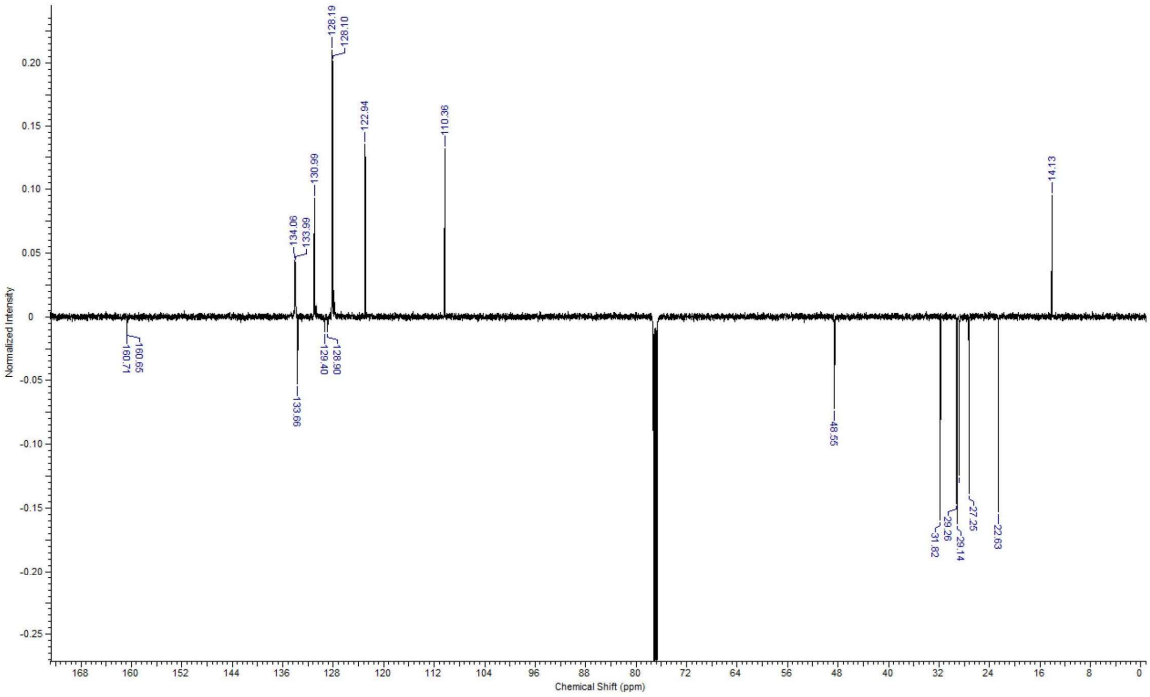

Fig. S 26: ^{13}C-NMR spectrum (126 MHz, $CDCl_3$) of complex **9d**.

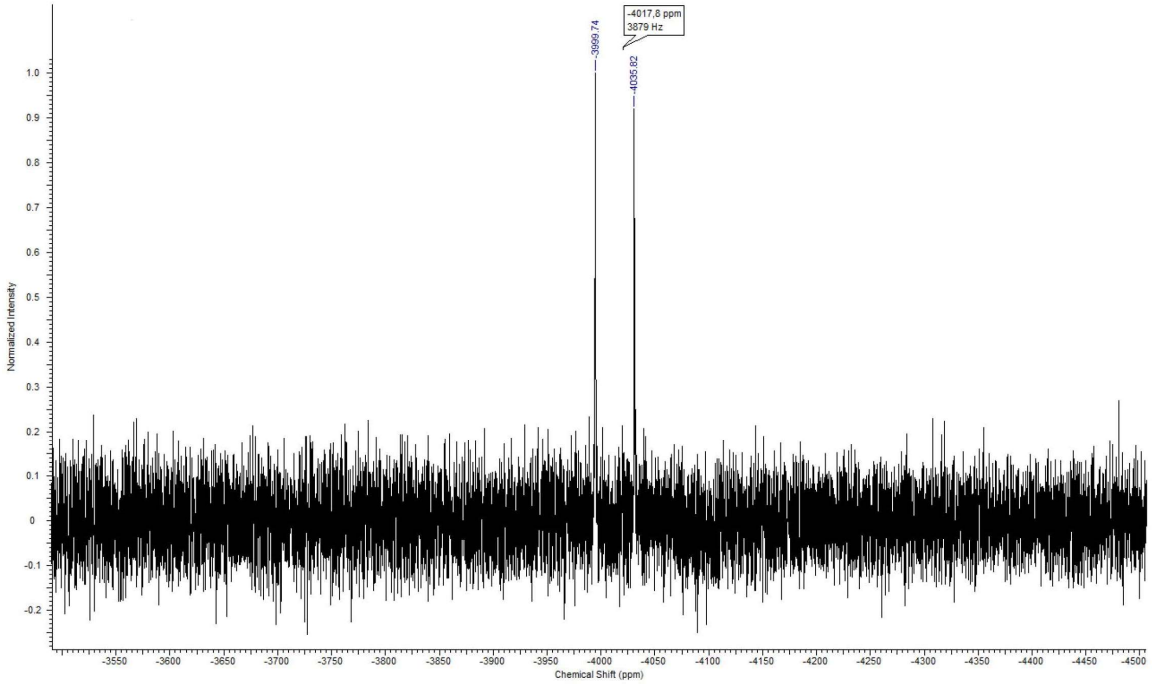

Fig. S 27: ^{195}Pt-NMR spectrum (108 MHz, $CDCl_3$) of complex **9d**.

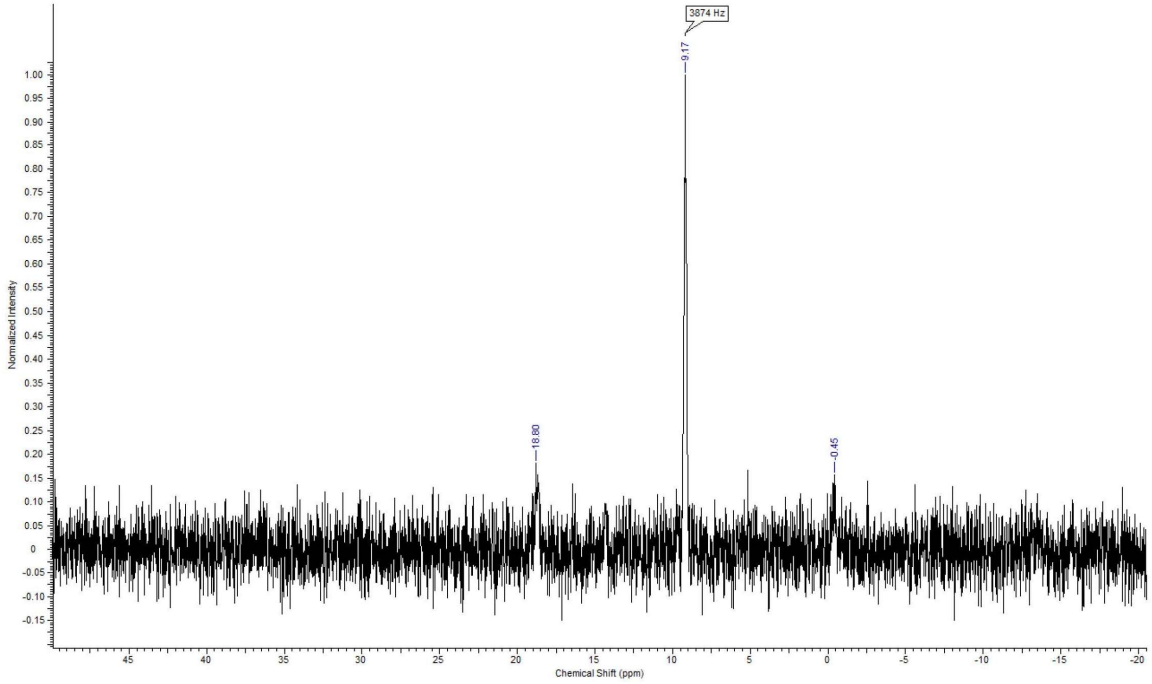

Fig. S 28: ^{31}P-NMR spectrum (202 MHz, $CDCl_3$) of complex **9d**.

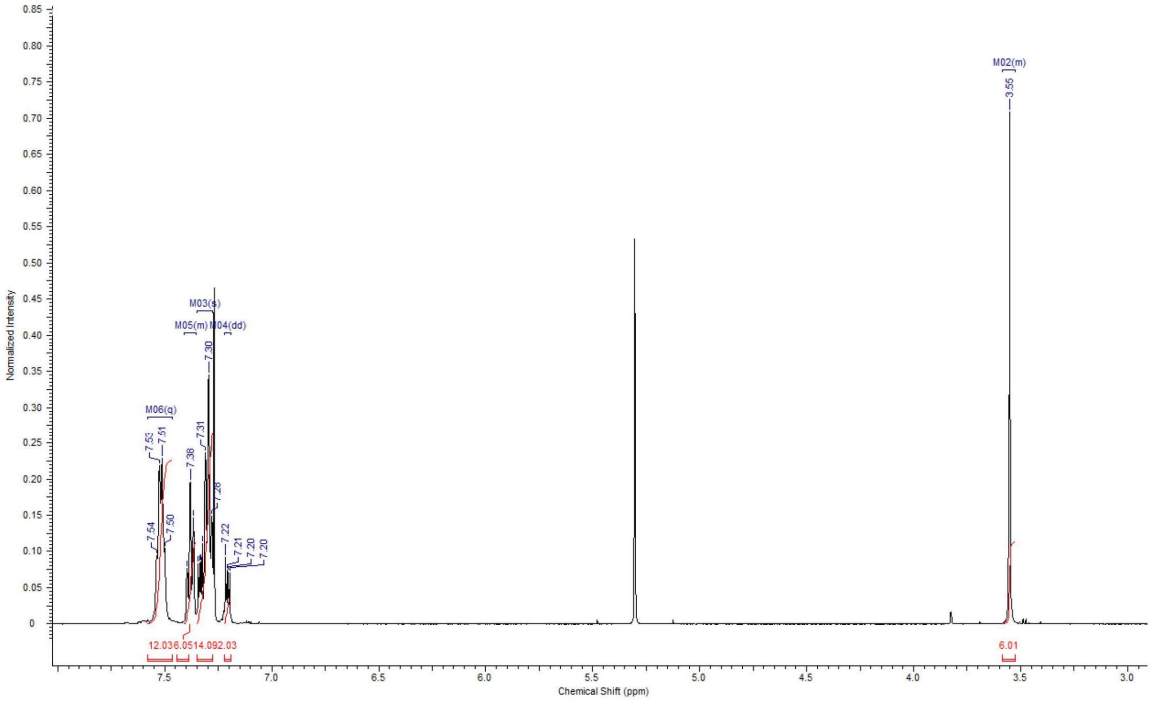

Fig. S 29: ^{1}H-NMR spectrum (500 MHz, $CDCl_3$) of complex **10a**.

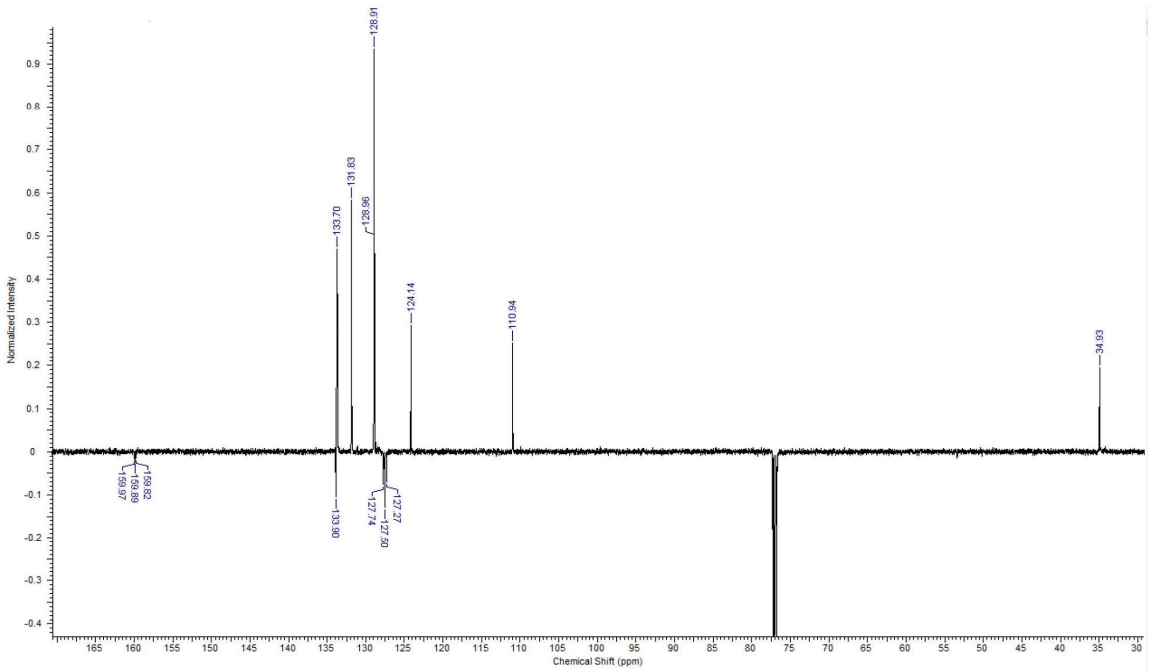

Fig. S 30: ^{13}C-NMR spectrum (126 MHz, $CDCl_3$) of complex **10a**.

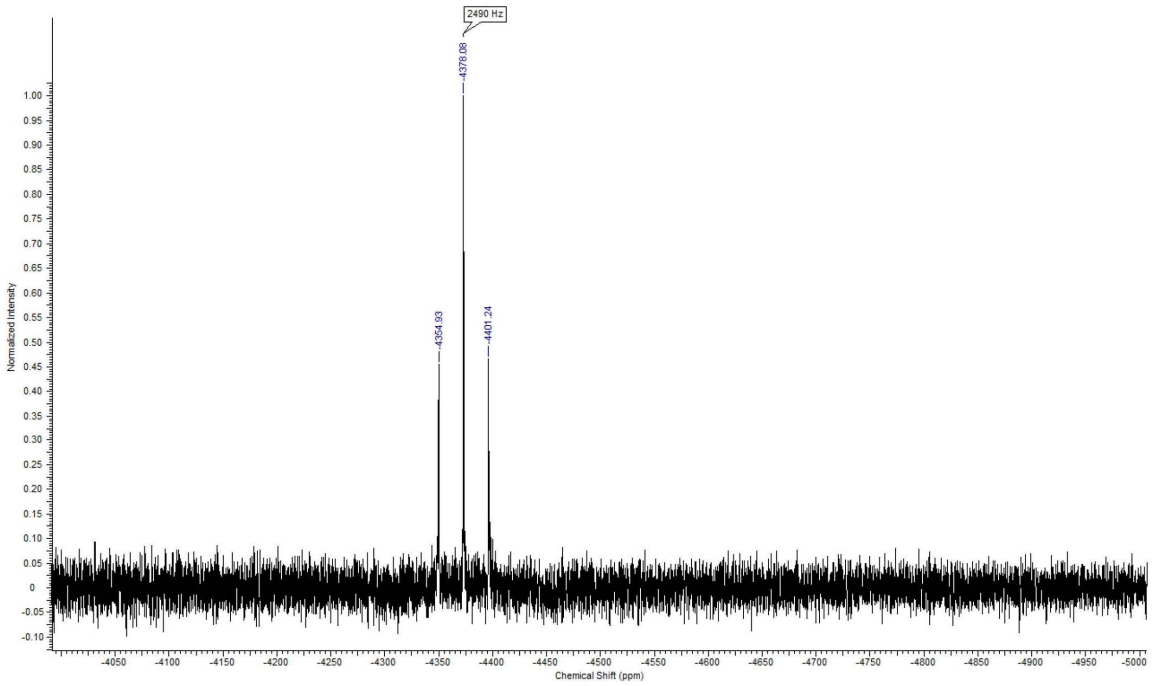

Fig. S 31: ^{195}Pt-NMR spectrum (108 MHz, $CDCl_3$) of complex **10a**.

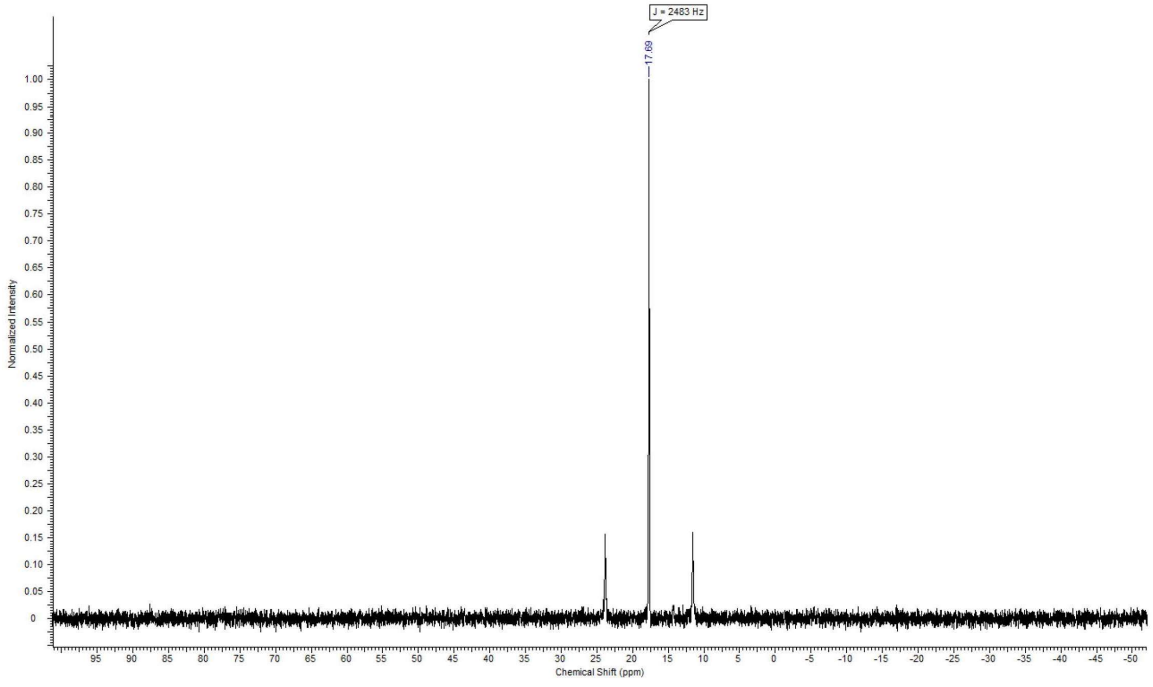

Fig. S 32: ^{31}P-NMR spectrum (202 MHz, $CDCl_3$) of complex **10a**.

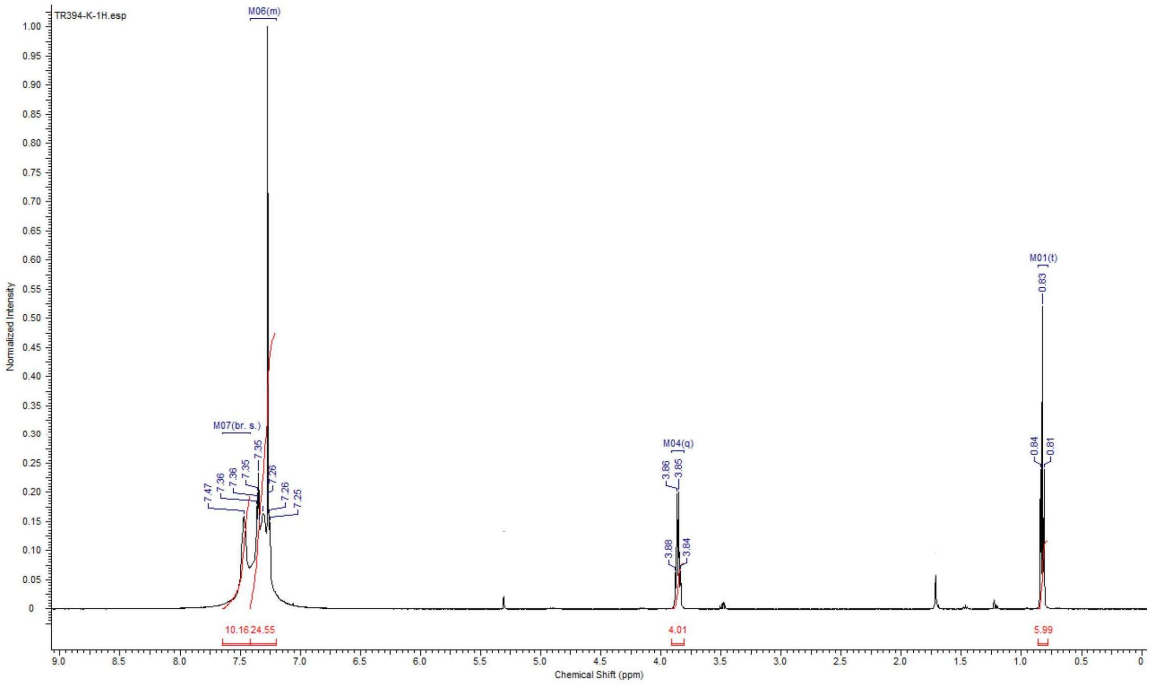

Fig. S 33: ^{1}H-NMR spectrum (500 MHz, $CDCl_3$) of complex **10b**.

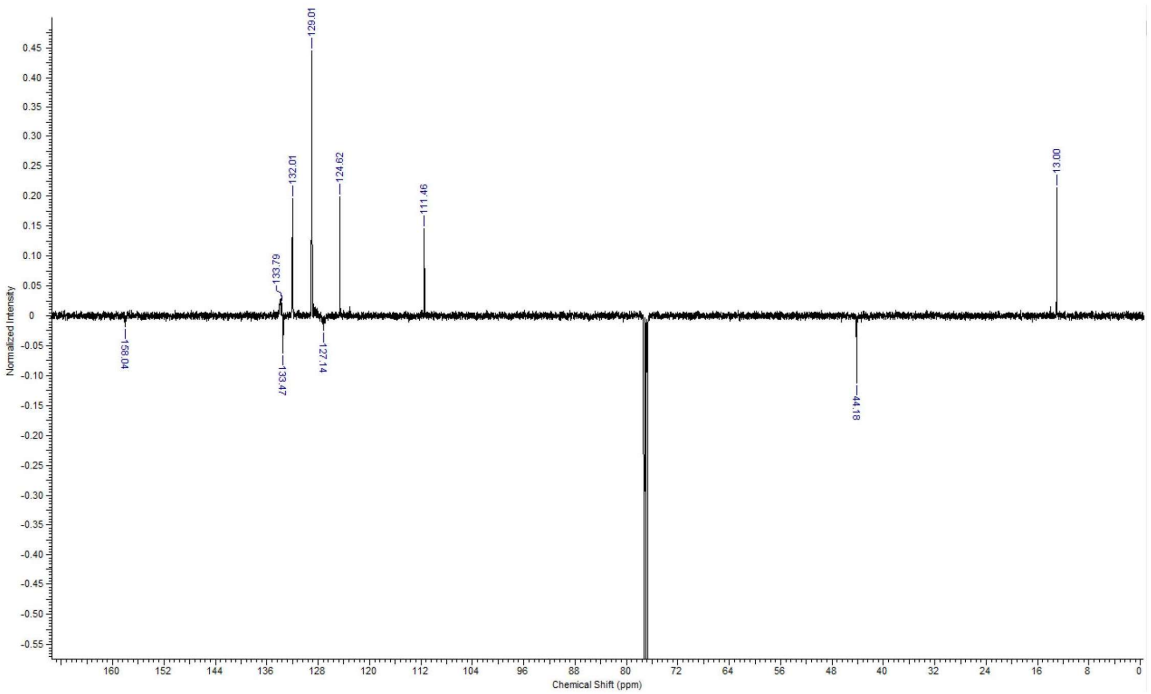

Fig. S 34: ^{13}C-NMR spectrum (126 MHz, $CDCl_3$) of complex **10b**.

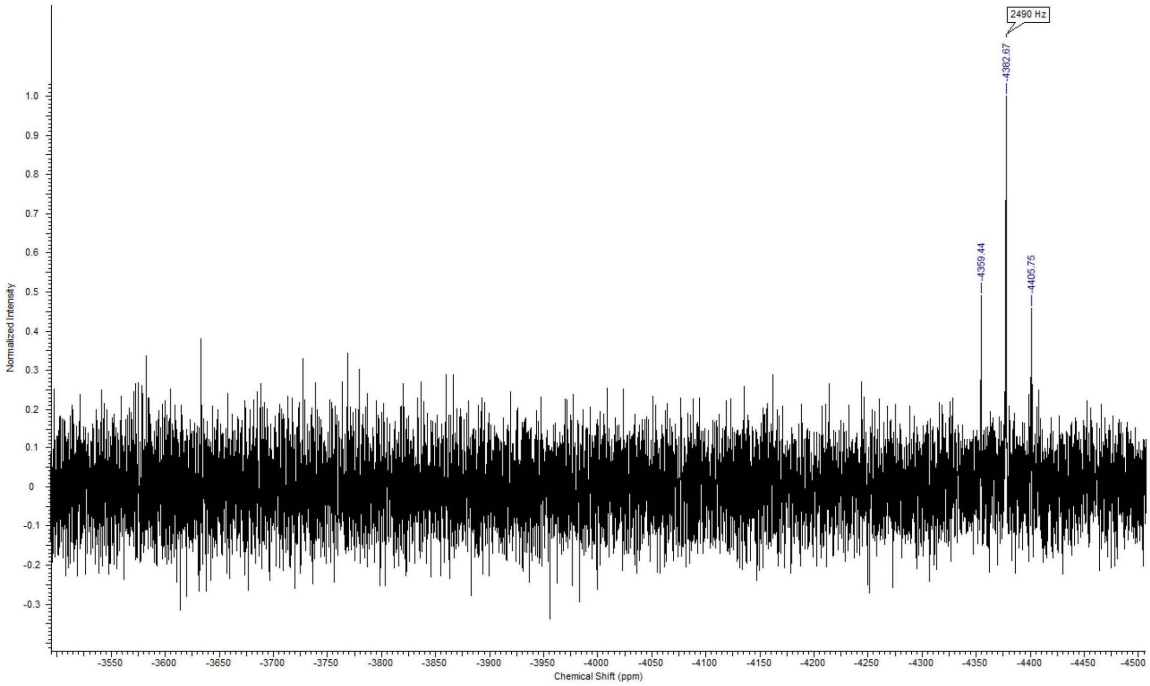

Fig. S 35: ^{195}Pt-NMR spectrum (108 MHz, $CDCl_3$) of complex **10b**.

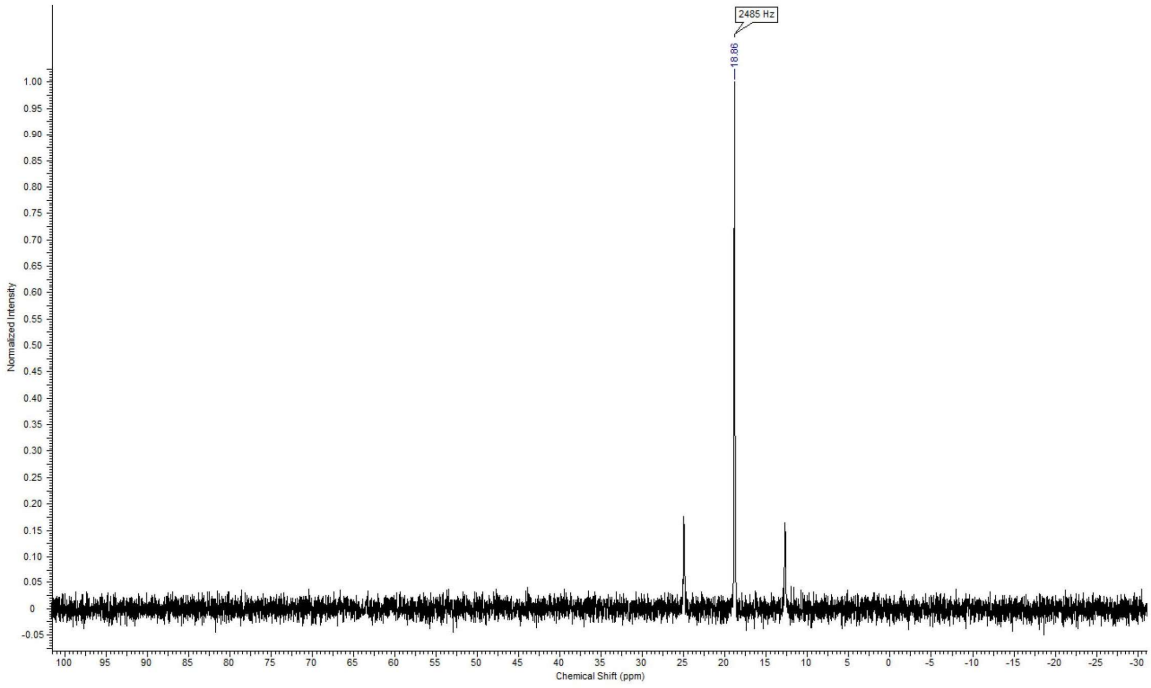

Fig. S 36: ^{31}P-NMR spectrum (202 MHz, $CDCl_3$) of complex **10b**.

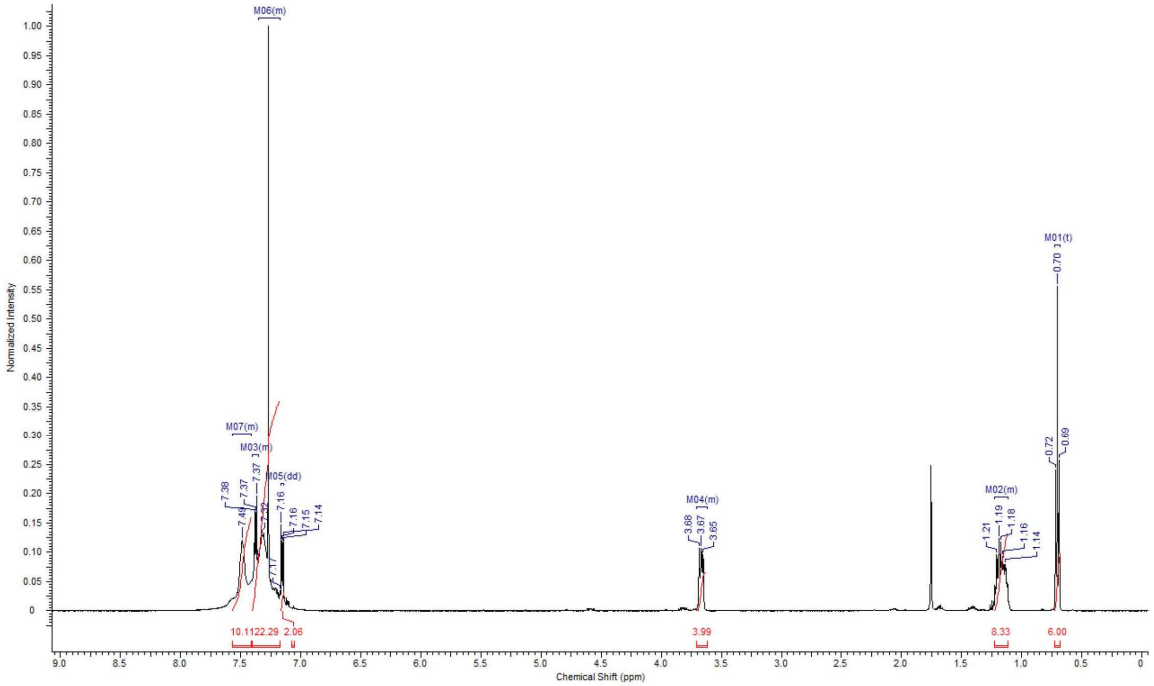

Fig. S 37: ^{1}H-NMR spectrum (500 MHz, $CDCl_3$) of complex **10c**.

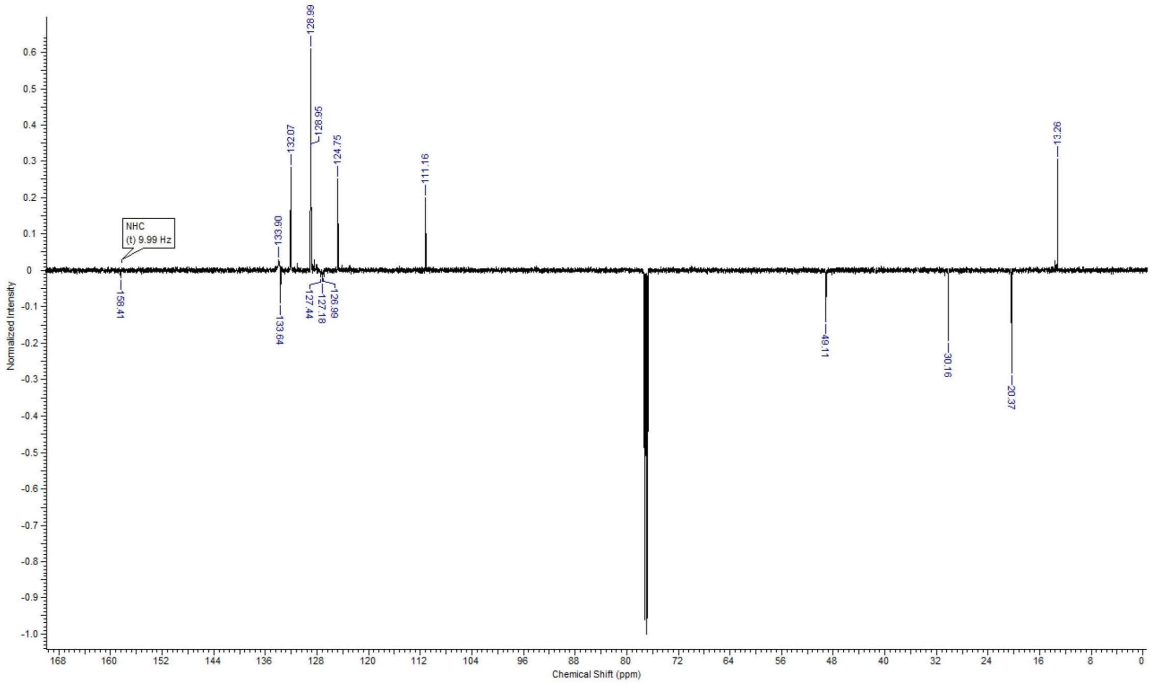

Fig. S 38: ^{13}C-NMR spectrum (126 MHz, $CDCl_3$) of complex **10c**.

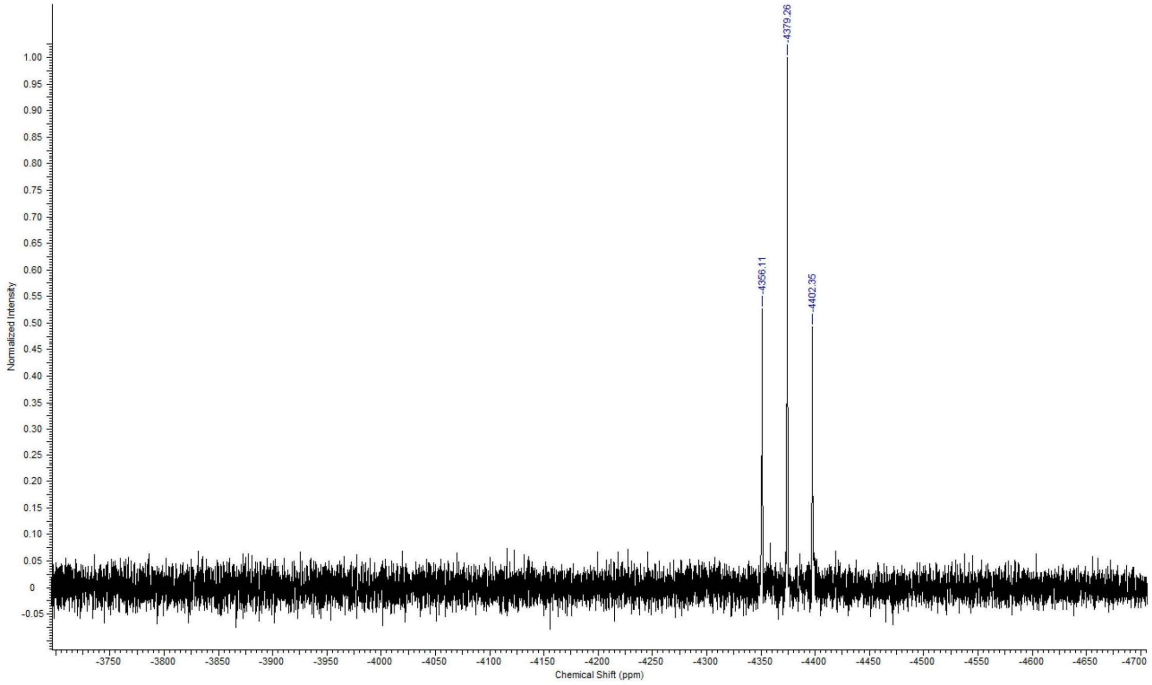

Fig. S 39: ^{195}Pt-NMR spectrum (108 MHz, $CDCl_3$) of complex **10c**.

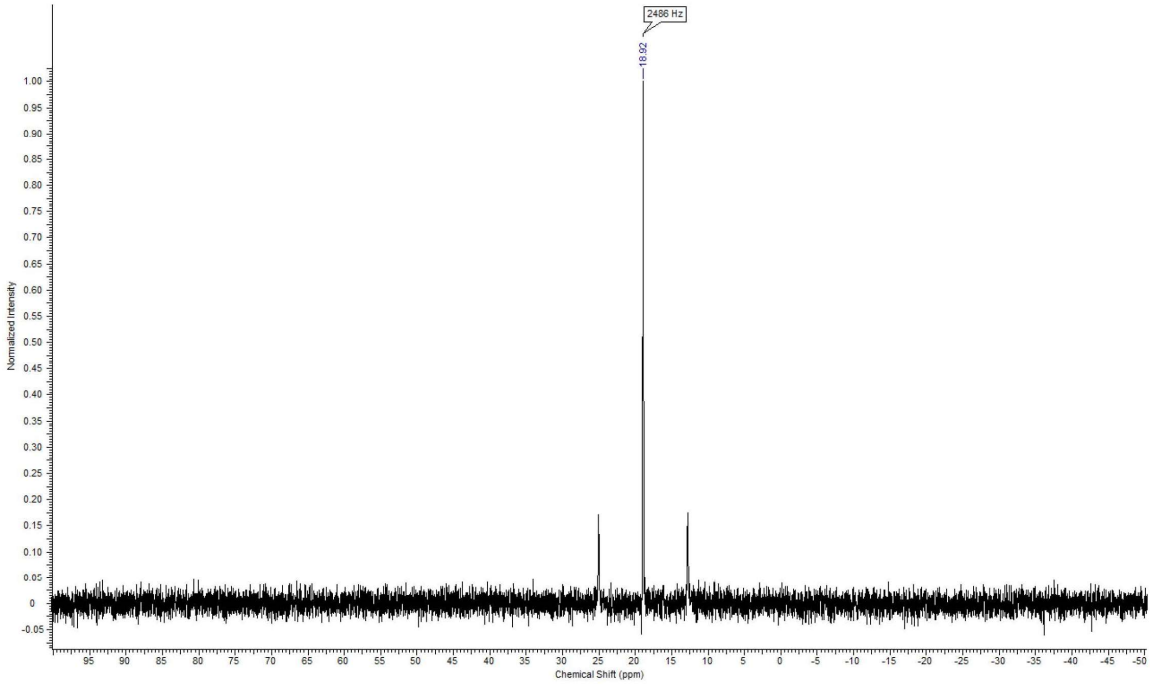

Fig. S 40: ^{31}P-NMR spectrum (202 MHz, $CDCl_3$) of complex **10c**.

Table S 41. Cellular accumulation of cisplatin and tested complexes in HCT116 cells.[a]

Compound	pmolPt/10^6cells
CDDP	49 ± 3
8c	97 ± 2
9a	122 ± 21
9b	245 ± 18
9c	316 ± 22
9d	59 ± 4
10c	592 ± 59

[a]Cellular accumulation of Pt from tested compounds (8 µM in media) in HCT116 cells after 5 h of treatment. Each value in the table is in pmol Pt/10^6 cells. The results are expressed as the mean ± SD of three independent experiments.

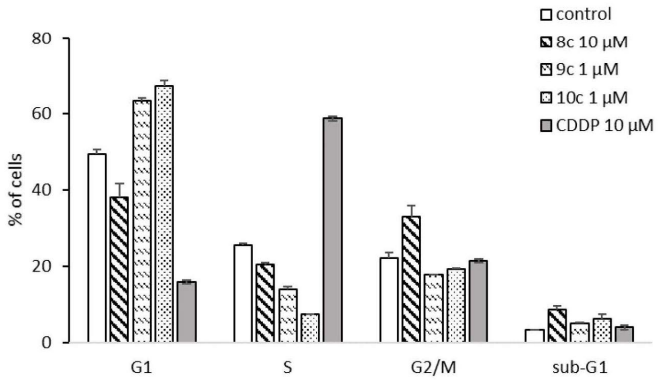

Fig. S 42: Effects of **8c** (10 µM), **9c** (1 µM), **10c** (1 µM), **CDDP** (10 µM) on the progression of the cell cycle of HCT116 $p53^{-/-}$ colon carcinoma cells after 24 h of treatment in comparison to untreated cells (vehicle control). The bars represent the percentages of cells in each phase of the cell cycle (G1, S and G2/M) and dead cells (sub-G1). Analysis was done via propidium iodide staining and flow cytometry, values represent means ± SDs of three experiments.

References

[1] R. Rubbiani, I. Ott *et al.*, *J. Med. Chem.*, 2010, **53**, 8608–8618, DOI: 10.1021/jm100801e.

[2] H. Valdés, M. Poyatos, G. Ujaque, E. Peris, *Chem. Eur. J.*, 2015, **21**, 1578 – 1588, DOI: 10.1002/chem.201404618.

[3] H. Lu and R. L. Brutchey, *Chem. Mater.,* 2017, **29**, 1396−1403, DOI: 10.1021/acs.chemmater.6b05293.

4.4 PUBLIKATION III

„Novel cis-[(NHC)^1(NHC)^2(L)Cl]platinum(II) complexes – synthesis, structures, and anticancer activities“

Dalton Transactions **2016**, *45*, 15390

Tobias Rehm,[a] Matthias Rothemund,[a] Julienne K. Muenzner,[a] Awal Noor,[b] Rhett Kempe[b] and Rainer Schobert*[a]

[a]Organic Chemistry Laboratory, University Bayreuth, Universitaetsstrasse 30, 95440 Bayreuth, Germany. E-mail: Rainer.Schobert@uni-bayreuth.de

[b]Lehrstuhl fuer Anorganische Chemie II (Catalyst Design), University Bayreuth, Universitaetsstrasse 30, 95440 Bayreuth, Germany

Dalton Transactions

PAPER

Cite this: *Dalton Trans.*, 2016, **45**, 15390

Novel *cis*-[(NHC)^1(NHC)^2(L)Cl]platinum(II) complexes – synthesis, structures, and anticancer activities†

Tobias Rehm,[a] Matthias Rothemund,[a] Julienne K. Muenzner,[a] Awal Noor,[b] Rhett Kempe[b] and Rainer Schobert*[a]

Received 13th June 2016,
Accepted 28th August 2016

DOI: 10.1039/c6dt02350a

www.rsc.org/dalton

A general synthesis of novel platinum(II) complexes bearing two different, *cis*-oriented, N-heterocyclic carbene (NHC) ligands is presented. Easily accessible *cis*-[Pt^{II}(NHC)(DMSO)] precursor complexes were converted to either *cis*-[Pt^{II}(NHC)$_2$Cl$_2$] complexes such as **5a** and **5b**, or to novel mixed *cis*-[Pt^{II}(NHC)^1(NHC)^{2}Cl$_2$] complexes such as **5c–h** by successive introduction of the individual carbene ligands. The 'symmetric' complexes **5a** and **5b** were also converted to cationic *cis*-[Pt^{II}(NHC)$_2$(PPh$_3$)-Cl]$^+$Cl$^-$ complexes **8a** and **8b**. The structures of the ten new complexes, comprising benzylated and alkylated imidazol-2-ylidene ligands, were analysed by ^{1}H, ^{13}C and ^{195}Pt NMR spectroscopy and also by X-ray diffraction for **5a**, **5d**, **5h**, and **8a**. The neutral complexes **5** were cytotoxic against a panel of seven human cancer cell lines with IC$_{50}$ values in the low micromolar range, while the cationic complexes **8** reached even nanomolar IC$_{50}$ values. Complex **5h** carrying the substitution pattern of the natural anti-tumoral agent Combretastatin A-4 showed a conspicuous specificity for cancer cell lines sensitive to this drug. In electrophoretic mobility shift assays, the *cis*-biscarbene complexes **5b** and **8b** led to an unwinding or aggregation of plasmid DNA, while the *trans*-biscarbene complex **1b** showed no such effect.

Introduction

Metal complexes of N-heterocyclic carbenes (NHCs) were reported as early as 1968 by Wanzlick *et al.* and others.[1,2] But it was not until the isolation of a crystalline carbene by Arduengo *et al.*[3] in 1991 that NHCs turned from mere curiosities into applicable chemical reagents. Nowadays, they are routinely used as organocatalysts for a wide range of established reactions.[4] NHC metal complexes are among the most efficient catalysts for reactions such as olefin metathesis[5] and Pd-catalysed coupling reactions.[6,7] More recently, their medicinal aspects came to the fore.[8,9] With the successful history of anticancer active platinum compounds[10] in mind, bioactive NHC complexes were devised of metals such as Pd,[11] Ag,[12] Cu,[13] Ru,[14] Au,[15] and Pt.[16] Meanwhile, a general picture of structure–activity correlations for such complexes is unfolding, allowing a prediction of the influence of the central metal, the NHC substituents, the charge, the lipophilicity, and the sterical encumbrance around the metal centre on their biological properties. We recently studied the influence of the latter factor, sterical congestion, in a series of platinum complexes.[17]

Unlike complexes *trans*-[Pt^{II}(NHC)$_2$Cl$_2$] **1**, featuring a poor NHC leaving group, the complexes *cis*-[Pt^{II}(DMSO)(NHC)Cl$_2$] **2** which bear a well accessible chlorido leaving ligand, had bound to DNA as expected. Substitution of DMSO for PPh$_3$ gave complex **3** which still, though to a lesser extent, bound coordinatively to DNA but also initiated some DNA aggregation. The cationic complex *trans*-[Pt^{II}(PPh$_3$)$_2$(NHC)Cl]$^+$Cl$^-$ **4**, featuring a sterically shielded chlorido ligand, exclusively induced DNA aggregation (Fig. 1).

For a more nuanced assessment of such steric effects we now developed an access to platinum(II) complexes with two different, *cis*-positioned NHC ligands (Scheme 1). Complexes *cis*-[Pt^{II}(NHC)$_2$L$_2$] with two identical NHC ligands had been synthesised before by Röschenthaler *et al.*,[18] and Nolan *et al.*[19,20] using *cis*-[Pt(DMSO)$_2$Cl$_2$], [Pt(cod)Cl$_2$], or [Pt(cod)Me$_2$] as precursors. Displacement of the leaving ligands DMSO or cod, respectively, by two equivalents of the free or masked NHC led to the desired *cis*-biscarbene complexes. However, these protocols do not allow the synthesis of mixed *cis*-[Pt^{II}(NHC)^1(NHC)^{2}L$_2$] complexes.

[a]*Organic Chemistry Laboratory, University Bayreuth, Universitaetsstrasse 30, 95440 Bayreuth, Germany. E-mail: Rainer.Schobert@uni-bayreuth.de*
[b]*Lehrstuhl fuer Anorganische Chemie II (Catalyst Design), University Bayreuth, Universitaetsstrasse 30, 95440 Bayreuth, Germany*

†Electronic supplementary information (ESI) available: NMR spectra of **5a–h** and **5a,b**; synthesis of **1b**; ligand synthesis. CCDC 1481378–1481381. For ESI and crystallographic data in CIF or other electronic format see DOI: 10.1039/c6dt02350a

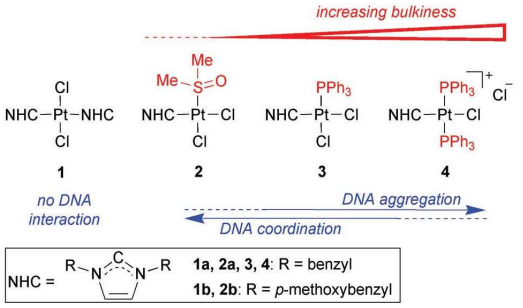

Fig. 1 NHC–platinum(II) complexes with spectator ligands of increasing bulkiness and their modes of DNA interaction.[17]

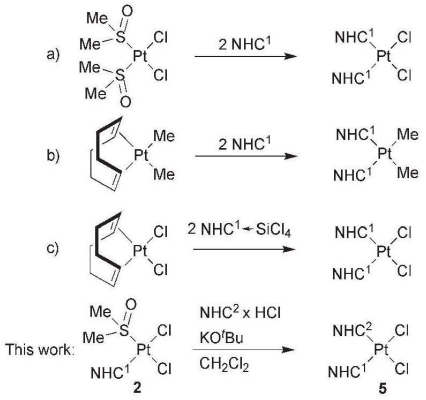

Scheme 1 Syntheses of *cis*-bis(NHC) complexes of platinum(II) by (a) Nolan *et al.*.[19] (b) Nolan *et al.*.[20] (c) Röschenthaler *et al.*.[18] and a new access to complexes *cis*-[Pt^{II}(NHC)^1(NHC)^{2}Cl$_2$] **5**.

Results and discussion

Synthesis and characterisation

The key intermediates for our new synthesis are *cis*-[Pt^{II}(NHC)(DMSO)L$_2$] complexes such as **2**, first synthesised by Rourke *et al.* in 2007.[21] This group found that using DMSO instead of CH_2Cl_2 as the solvent for the carbene transfer from silver NHC complexes to suitable sources of the desired metal, *e.g.* K_2PtCl_4, led to the formation of monocarbene complexes of type **2** rather than to the formation of *trans*-biscarbene complexes of type **1**. The DMSO ligand can then be substituted by a more electron-rich ligand such as a phosphane,[17,21] or, as detailed in this work, a second NHC ligand.

We prepared eight new *cis*-[Pt^{II}(NHC)^1(NHC)^{2}Cl$_2$] complexes **5** with six different NHCs as ligands *via* DMSO precursor complexes **2**. Since the two NHC ligands are introduced one at a time, complexes with two different NHCs can be synthesised starting from two different imidazolium salts **6** (ImH^1) and **7** (ImH^2)[22–26] (Scheme 2). We employed imidazolium chlorides that were 1,3-benzylated, or -alkylated. For the synthesis of *cis*-[Pt^{II}(NHC)^1(NHC)^{2}Cl$_2$] complexes **5** the respective complex *cis*-[Pt^{II}(DMSO)(NHC)^{1}Cl$_2$] **2** was treated with ImH^{2}Cl **7** and KO^{t}Bu to generate (NHC)^2. The resulting mixture was stirred in dry CH_2Cl_2 for 16 hours by which time the DMSO had been completely substituted by (NHC)^2 and the pure product complexes **5** were obtained by precipitation in yields of up to 93%. Replacing the base KO^{t}Bu by K_2CO_3, NaOMe or CaH_2 had little influence on the yields as had the use of acetonitrile as a solvent.

The *cis* configuration of complexes **5** was confirmed by ^{1}H and ^{13}C NMR spectroscopy. In line with a previous study[17] of the complexes **2a** and **3**, the ^{1}H NMR spectra of complexes **5** showed an inequivalency of the two geminal protons of each benzylic CH_2 group (one facing the neighbouring chlorine, the other the second NHC) and their splitting up into two doublets. These corresponding signals are 0.44 to 1.13 ppm apart and couple with $^2J_{AB}$ = 14.34 to 14.95 Hz. This corroborates the *cis* configuration of the NHC ligands as well as the perpendicular orientation of the imidazole ring relative to the plane spanned by the $PtCl_2$ fragment (Fig. 2).

Further evidence is provided by the ^{13}C NMR shifts of the carbene carbon signals ranging from 147.8 to 149.9 ppm, typical of carbon atoms in a *cis*-NHC-L-PtCl$_2$ environment.[17,21,27] While the symmetric complexes **5a** and **5b** showed only one carbene carbon signal, the mixed complexes gave rise to two inequivalent signals for the different NHC ligands.

Complexes **5g** and **5h** showed distinct ^{1}H NMR spectra with coupling constants $^2J_{AB}$ = 15.11 to 15.26 Hz and overall more complex spectra as each CH_2 proton has a different surrounding and thus a distinctive shift. In the ^{13}C NMR spectrum of **5g** the carbene carbon of the *N*-methylated NHC ligand peaks at 146.6 ppm.

We also prepared cationic complexes **8** from the symmetric complexes **5a** and **5b** by substitution of a chlorido for a triphenylphosphane ligand (Scheme 3).

Their ^{1}H NMR spectra showed more complex CH_2 signals due to the additional asymmetry. Their carbene carbon signals in the ^{13}C NMR spectra appeared as doublets with $^2J_{CP}$ = 10 Hz (*cis* to PPh_3) and 151 Hz (*trans* to PPh_3), respectively. The ^{31}P–^{195}Pt coupling of $^1J_{PPt}$ = 2366 Hz (**8a**) and 2361 Hz (**8b**) was visible as were the phosphane signals at 13.09 (**8a**) and 13.34 ppm (**8b**) in the ^{31}P NMR spectra.

X-ray crystallography

Crystals suitable for X-ray diffraction analyses were grown by slow infusion of hexane into saturated solutions of **5a**, **5d**, **5h**, or **8a** in CH_2Cl_2 kept at 4 °C. Fig. 3 shows their molecular structures. The characteristic bond lengths and angles were similar for all four complexes. The distances between the platinum and the carbene carbon atoms were in the range of 1.97–1.99 Å, only in the phosphane complex **8a** the distances were slightly longer with 2.02 Å and 2.07 Å. The Pt–Cl distances lay between 2.35 and 2.36 Å, while the Pt–P bond of **8a** was 2.31 Å long. The C–Pt–C angles ranged from 93.7° (**8a**) to 96.4° (**5d**) for those complexes that bore 1,3-dibenzylimidazol-2-

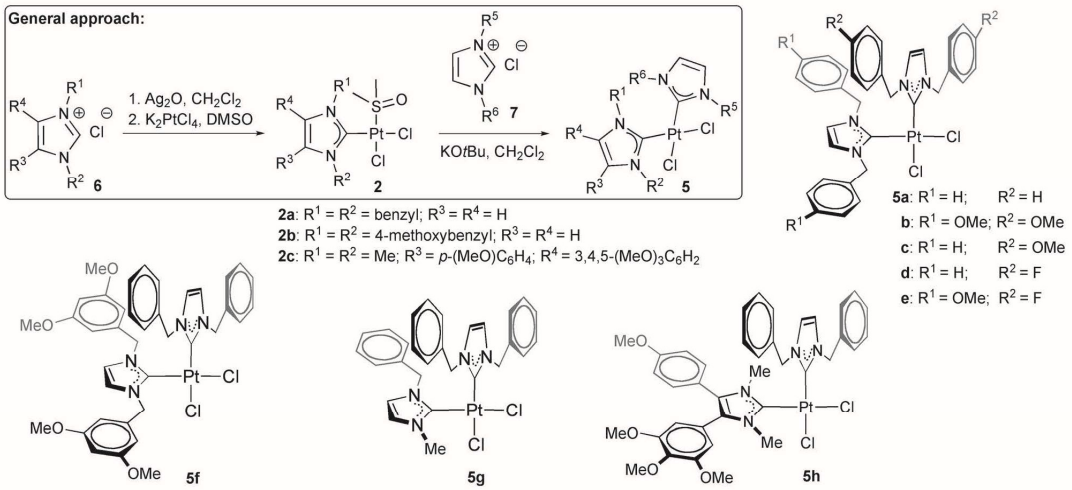

Scheme 2 General synthesis and structures of complexes **5a–h**.

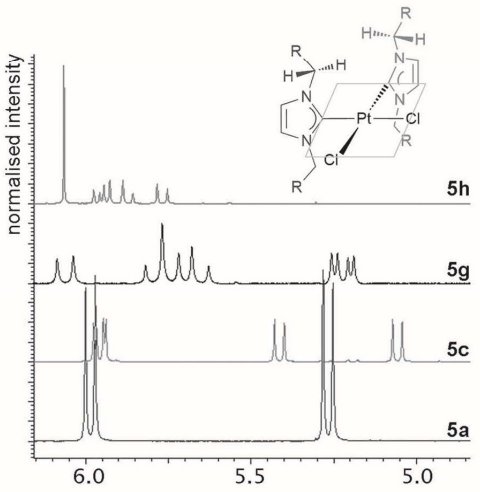

Fig. 2 Relevant ^{1}H NMR signals of inequivalent benzylic CH_2 protons of complexes **5** proving the *cis* configuration.

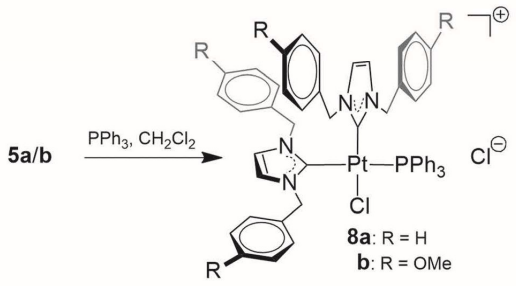

Scheme 3 Synthesis of cationic phosphane complexes **8** from *cis*-$[Pt^{II}(NHC)_2Cl_2]$ complexes **5a** and **5b**.

ylidene ligands. In the case of **5h** the C–Pt–C angle was reduced to 90.4°.

Anticancer activity

Complexes **5** and **8** were investigated for their cytotoxicity against a panel of seven human cancer cell lines of six entities and an endothelial cell line using the MTT-based viability assay.[28,29] Table 1 summarises the resulting IC_{50} (72 h) values. All complexes **5a–h** showed remarkable efficacies with low micromolar IC_{50} values against all cell lines, save for the cisplatin resistant HT-29 colon[30] and the multidrug-resistant (mdr) KB-V1/Vbl cervix[31] carcinoma cell line. The latter, which overexpresses the detoxifying efflux transporter protein p-gp1, was surprisingly unresponsive to all complexes, especially to **5h** that bears the structural motif of the natural anticancer drug combretastatin A-4 (CA-4). Complex **5h** was also less active than most other test compounds against the mdr MCF7/Topo[32] mamma carcinoma cell line which overexpresses the efflux transporter BCRP34 (breast cancer resistance protein). This is an indication for **5h** being a substrate of these drug efflux pumps.

Against CA-4 sensitive cancer cell lines such as DLD-1 colon carcinoma and Panc-1 pancreatic cancer, and also against the hybrid endothelial Ea.Hy926 cells, complex **5h** retained the activity of the natural lead compound CA-4, showing IC_{50} concentrations in the low nanomolar range.

As we have already shown in previous work, exchange of one chlorido for a phosphane ligand can enhance the cytotoxicity significantly, probably due to an increase in lipophilicity, solubility and thus of cellular uptake.[17] This was observed here as well when going from the neutral dichlorido

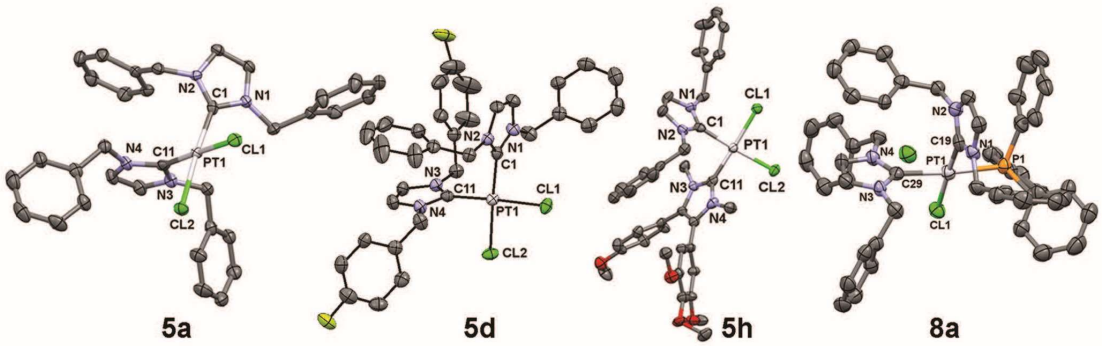

Fig. 3 Molecular structures of complexes **5a**, **5d**, **5h**, and **8a** as thermal ellipsoid representations at 50% probability level (H atoms omitted). Selected bond lengths [Å] and angles [°]: **5a**: Pt1–Cl1 2.362(3), Pt1–Cl2 2.350(2), Pt1–C1 1.969(8), Pt1–C11 1.967(3), Cl1–Pt1–Cl2 90.5(7), Cl1–Pt1–C1 88.5(6), Cl1–Pt1–C11 176.5(1), Cl2–Pt1–C1 175.8(6), Cl2–Pt1–C11 86.2(9), C1–Pt1–C11 94.6(8); **5d**: Pt1–Cl1 2.355(6), Pt1–Cl2 2.355(6), Pt1–C1 1.971(4), Pt1–C11 1.971(4), Cl1–Pt1–Cl2 92.1(7), Cl1–Pt1–C1 85.7(6), Cl1–Pt1–C11 176.9(4), Cl2–Pt1–C1 176.9(4), Cl2–Pt1–C11 85.7(6), C1–Pt1–C11 96.4(0); **5h**: Pt1–Cl1 2.359(2), Pt1–Cl2 2.361(8), Pt1–C1 1.984(4), Pt1–C11 1.991(2), Cl2–Pt1–Cl1 89.5(3), Cl2–Pt1–C11 92.6(2), Cl2–Pt1–C1 176.9(2), Cl1–Pt1–C11 176.2(8), Cl1–Pt1–C1 87.4(0), C1–Pt1–C11 90.4(6); **8a**: Pt1–Cl1 1.348(7), Pt1–P1 2.312(7), Pt1–C29 2.072(7), Pt1–C29 2.016(4), Cl1–Pt1–P1 92.0(5), Cl1–Pt1–C29 87.0(9), Cl1–Pt1–C19 176.2(7), P1–Pt1–C29 172.6(1), P1–Pt1–C19 87.5(7), C19–Pt1–C29 93.7(5).

Table 1 Means ± SD of IC_{50} (72 h) values [μM] of complexes **5**, **8**, and cisplatin (CDDP) in MTT assays against human cancer cell lines and an endothelial hybrid cell line as calculated from four independent measurements

	IC_{50} (72 h) [μM]										
Cell line	**5a**	**5b**	**5c**	**5d**	**5e**	**5f**	**5g**	**5h**	**8a**	**8b**	**CDDP**
518A2	6.2 ± 0.4	7.9 ± 0.4	5.6 ± 0.2	6.1 ± 0.5	5.2 ± 0.3	7.1 ± 0.5	39.0 ± 1.0	6.5 ± 0.2	0.86 ± 0.05	0.60 ± 0.15	5.3 ± 0.4
HT-29	14.6 ± 1.4	11.1 ± 2.0	13.9 ± 1.4	21.6 ± 1.5	4.1 ± 0.4	6.6 ± 0.5	39.7 ± 2.0	11.1 ± 0.7	0.82 ± 0.06	0.45 ± 0.03	>100
DLD-1	4.7 ± 1.4	3.2 ± 0.1	5.1 ± 0.6	4.0 ± 0.2	5.7 ± 1.4	11.1 ± 0.9	30.2 ± 5.2	0.39 ± 0.07	0.77 ± 0.04	0.66 ± 0.02	32.6 ± 2.4
U87	7.2 ± 0.2	7.7 ± 0.5	9.0 ± 1.1	5.0 ± 0.3	4.5 ± 0.4	7.3 ± 0.3	>50	6.1 ± 2.1	0.89 ± 0.19	0.95 ± 0.21	4.0 ± 0.3
Panc-1	3.5 ± 0.7	2.9 ± 0.0	3.0 ± 0.1	4.2 ± 0.4	6.7 ± 1.3	6.0 ± 0.1	38.8 ± 3.7	0.24 ± 0.05	0.36 ± 0.00	0.39 ± 0.03	4.8 ± 0.7
MCF7/Topo	8.6 ± 2.0	4.0 ± 0.2	11.1 ± 5.6	7.6 ± 0.9	3.2 ± 0.5	13.7 ± 0.9	42.1 ± 2.7	37.1 ± 5.6	0.43 ± 0.01	0.52 ± 0.03	10.6 ± 0.7
Kb-V1/Vbl	11.7 ± 0.8	13.9 ± 1.1	16.1 ± 0.8	18.1 ± 2.6	43.5 ± 2.1	21.0 ± 1.0	> 50	35.5 ± 1.3	7.3 ± 1.2	6.0 ± 0.3	>100
Ea.Hy926	6.8 ± 1.6	4.2 ± 0.4	5.6 ± 1.9	7.6 ± 0.2	3.2 ± 0.5	13.4 ± 0.5	45.3 ± 1.2	0.4 ± 0.08	0.48 ± 0.01	0.72 ± 0.03	17.3 ± 1.9

518A2 – human melanoma, HT-29 – human colon adenocarcinoma, DLD-1 – Dukes type C colorectal adenocarcinoma, U87 – human glioblastoma, Panc-1 – human pancreatic carcinoma, MCF7/Topo – human breast cancer, Kb-V1/Vbl – human cervix carcinoma, Ea.Hy926 – endothelial hybrid cells.

complexes **5a–b** to the phosphane complexes **8a–b** which are typical 'delocalised lipophilic cations' (DLCs). They were efficacious with submicromolar IC_{50} values against most of the cell lines. Again, the KbV1/Vbl cells were least responsive requiring single-digit micromolar IC_{50} concentrations (**8a**: 7 μM; **8b**: 6 μM).

In vitro DNA interaction

We investigated the DNA interaction of *trans*-$[Pt^{II}(NHC)_2Cl_2]$ complex **1b**, the isomeric *cis*-complex **5b**, and its cationic analogue *cis*-$[Pt^{II}(NHC)_2(PPh_3)Cl]^+Cl^-$ **8b** by means of an electrophoretic mobility shift assay (EMSA) with circular pBR322 plasmid DNA (Fig. 4). The *trans* configured complex **1b** did not alter the DNA morphology, *i.e.* the ratio of open circular (oc) and covalently closed circular (ccc) forms. In contrast, its *cis* isomer **5b** led to a distinct unwinding of the plasmid DNA in a

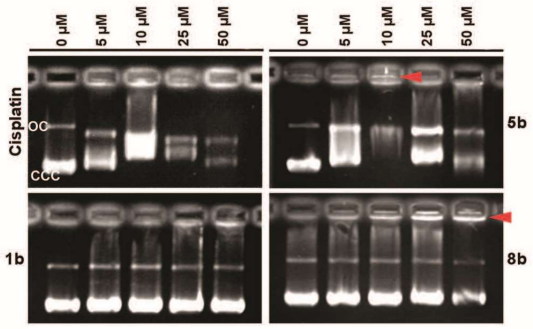

Fig. 4 Modification of gel electrophoretic mobility of pBR322 plasmid DNA when incubated for 24 h with different concentrations of cisplatin, **1b**, **5b**, and **8b** (oc = open circular, ccc = covalently closed circular DNA form; the red arrows mark DNA aggregates).

concentration-dependent manner, as is also typical of cisplatin, apparent from a pronounced band shift with a maximum at a concentration of 10 μM of **5b**. At this concentration the DNA also seems to aggregate to adducts that remain in the gel pocket during electrophoresis, not able to permeate the pores of the gel. The same phenomenon was observed for **8b**, yet to a greater extent. It initiated immediate aggregation of the plasmid DNA without any conversion of its topological oc and ccc isomers. Such effects had previously been observed[17] and corroborated by light scattering experiments and studies of the DNA binding kinetics for complexes **3** and **4**. They suggest that the mode of DNA interaction is mainly governed by the sterical shielding of the chlorido leaving ligand or the metal centre.

Conclusions

We have developed a new synthetic protocol that gives access to *cis*-[Pt^{II}(NHC)^1(NHC)^2L^1L^2] complexes with two different NHC ligands. Ten complexes were prepared, structurally elucidated, and screened for antiproliferative activity against human tumour cells. Their activity was surprisingly high on average, with a considerable degree of structure-dependent cell line specificity. For some complexes we observed a breach of the cisplatin and multidrug resistance of certain cancer cell lines. Mechanistically, DNA seems to be a major target of these new platinum complexes, albeit in a more differentiated way when compared to cisplatin. In EMSA experiments with circular plasmid DNA, the neutral *cis*-biscarbene complex **5b** bound coordinatively to it leading to its unwinding. Apparently, complex **5b** also initiated the aggregation of this form of DNA to some extent. This needs to be confirmed by further experiments. The cationic *cis*-biscarbene complex **8b** seems to have led exclusively to DNA aggregation. The *trans*-biscarbene complex **1b** showed no such effects. Obviously, the mode of DNA interaction is correlated to the replaceability and sterical accessibility of the leaving ligand, and the overall charge of the complex.

Another interesting aspect is the retention of intrinsic ligand bioactivity in the complexes, *e.g.* for the CA-4 derived complex **5h**. This should allow a high degree of liberty in devising new pleiotropic anticancer complexes with various combinations of NHC ligands, spectator ligands, and leaving groups that contribute their inherent activity and so influence the overall pharmacological properties. Likewise, our new access to *cis*-biscarbene complexes, which is very likely not restricted to platinum, will be of interest to catalysis chemists as it offers a way to fine-tune the stereoelectronic properties of NHC complex catalysts more minutely than before.

Experimental

Materials and methods

All chemicals and reagents were purchased from Sigma Aldrich, Alfa Aesar, or ABCR and were used without further purification. Melting points are uncorrected; NMR spectra were run on a 500 MHz spectrometer; chemical shifts are given in ppm (δ) and referenced relative to the internal solvent signal; ^{195}Pt NMR shifts are quoted relative to $\Xi(^{195}Pt)$ = 21.496784 MHz, K_2PtCl_4 was used as external standard (δ = –1612.81); mass spectra: direct inlet, EI, 70 eV; elemental analyses: Vario EL III and HEKAtech EA 3000 elemental analysers; X-ray diffractometers: STOE-IPDS II and STOE-STADIVARI. All biotested compounds were >95% pure by elemental analysis. *N*-Methyl- and *N*-benzylimidazolium salts were prepared according to literature procedures (*cf.* ESI†),[22–25] as were 1,3-dimethyl-4-(3′,4′,5′-trimethoxyphenyl)-5-(4″-methoxyphenyl)imidazolium iodide[26] and complex **2a**.[17] Complex **1b** was prepared analogously to **1a**[17] and is described in the ESI.†

Syntheses and characterisation

***cis*-[Dichlorido-(1,3-di(4-methoxybenzyl)imidazol-2-ylidene)(dimethylsufoxide)]platinum(II) (2b).** A mixture of 1,3-di(4-methoxybenzyl)imidazolium chloride (177 mg, 513 μmol) and CH_2Cl_2 (10 mL) was treated with silver(I) oxide (59 mg, 257 μmol) and stirred for 24 h at room temperature. Solids were filtered off and the silver NHC complex was precipitated by addition of hexane. After decanting and drying *in vacuo* this intermediate complex (200 mg, 443 μmol) was dissolved in DMSO (7.5 mL), treated with K_2PtCl_4 (184 mg, 443 μmol), and the mixture was stirred at 60 °C for 24 h. CH_2Cl_2 was added, the reaction mixture was filtered, and the filtrate was washed with water and dried over Na_2SO_4. The volatiles were removed *in vacuo* and the remainder was recrystallised from CH_2Cl_2/hexane to yield 225 mg (78%) of white crystals of m.p. 206 °C. ^{1}H NMR ($CDCl_3$, 500 MHz): δ 3.26 (s, 6H, CH_3, DMSO), 3.81 (s, 6H, OCH_3), 5.60 (virt. t, J = 15.3 Hz, 4H, CH_2), 6.78 (s, 2H, CH, imidazole), 6.92 (d, J = 8.5 Hz, 4H, Ar), 7.33 (d, J = 8.5 Hz, 4H, Ar); ^{13}C NMR ($CDCl_3$, 126 MHz): δ 45.6 (DMSO), 53.9 (CH_2), 55.3 (OCH_3), 114.3 (Ar), 121.0 (CH, imidazole), 126.9 (Ar), 129.7 (Ar), 143.8 (NCN), 159.7 (Ar); EI-MS: *m*/*z* 502 (5%, $–Cl_2$, –DMSO), 416 (9), 401 (7), 308 (10), 241 (8), 188 (10), 121 (100), 78 (12).

***cis*-[Dichlorido-(1,3-dimethyl-4-(3′,4′,5′-trimethoxyphenyl)-5-(4″-methoxyphenyl)imidazol-2-ylidene)(dimethylsufoxide)]platinum(II) (2c).** Analogously to **2b**, complex **2c** (155 mg, 78%) was obtained from 1,3-dimethyl-4-(3′,4′,5′-trimethoxyphenyl)-5-(4″-methoxyphenyl)imidazolium iodide (143 mg, 287 μmol), silver(I) oxide (33 mg, 144 μmol), K_2PtCl_4 (119 mg, 287 μmol), and DMSO (6 mL) as white crystals of m.p. 143 °C. ^{1}H NMR ($CDCl_3$, 500 MHz): δ 3.59 (s, 6H, CH_3, DMSO), 3.71 (s, 6H, 3′-, 5′-OCH_3), 3.79 (s, 3H, 4″-OCH_3), 3.83 (s, 3H, 4′-OCH_3), 3.90 (s, 3H, NCH_3), 3.94 (s, 3H, NCH_3), 6.33 (s, 2H, Ar), 6.86 (d, J = 8.4 Hz, 2H, Ar), 7.10 (d, J = 8.8 Hz, 2H, Ar); ^{13}C NMR ($CDCl_3$, 126 MHz): δ 36.2 (N–CH_3), 46.3 (DMSO), 55.3 (4″-OCH_3), 56.2 (3′-, 5′-OCH_3), 60.9 (4′-OCH_3), 107.8 (Ar, C-2′, -6′), 114.3 (Ar, C-2″, -6″), 119.5 (Ar, C-1″), 122.7 (Ar, C-1′), 131.5 (C-4, -5, imidazole), 131.8 (Ar, C-3″, -5″), 138.6 (Ar, C-4′), 142.5 (NCN), 153.3 (Ar, C-3′, -5′), 160.2 (Ar, C-4″); EI-MS: *m*/*z* 712 (M^+, 1%),

635 (2, –DMSO), 562 (2, $–Cl_2$, –DMSO), 415 (6), 369 (11), 355 (67), 340 (34), 78 (56), 63 (56), 50 (100), 36 (98).

General procedure for the preparation of *cis*-$[Pt^{II}(NHC)^1(NHC)^2Cl_2]$ complexes 5

Complex 2 (1 equiv.) and the respective imidazolium chloride 7 (1 equiv.) were dissolved in dry CH_2Cl_2 (60 mL $mmol^{-1}$) and treated with KO^{t}Bu (1.2 equiv.) under an atmosphere of dry argon. After stirring at room temperature for 16 h solids were filtered off and the pure product 5 was precipitated by adding diethyl ether at 4 °C.

***cis*-[Dichlorido-bis(1,3-dibenzylimidazol-2-ylidene)] platinum(II) (5a).** Complex **5a** (60 mg, 93%) was obtained from **2a** (50 mg, 84.4 μmol), 1,3-dibenzylimidazolium chloride (24 mg, 84.4 μmol), and KO^{t}Bu (11 mg, 101 μmol) yield 60 mg (93%) as white crystals of m.p. 287 °C. Elemental analysis (%): calc. for $C_{34}H_{32}N_4PtCl_2$ (762.63): C, 53.55; H, 4.23; N, 7.35. Found: C, 53.04; H, 4.48; N, 7.39. ^{1}H NMR ($CDCl_3$, 500 MHz): δ 5.27 (d, J = 14.6 Hz, 4H, CH_2), 5.99 (d, J = 14.6 Hz, 4H, CH_2), 6.52 (s, 4H, imidazole CH), 7.12–7.19 (m, 8H, Ar), 7.27–7.33 (m, 12H, Ar); ^{13}C NMR ($CDCl_3$, 126 MHz): δ 54.1 (CH_2), 120.5 (imidazole CH), 128.2 (Ar), 128.9 (Ar), 134.9 (Ar), 149.0 (NCN); ^{195}Pt NMR ($CDCl_3$): δ –3605.3; EI-MS: m/z 762 (M^+, 7%), 726 (11, –Cl), 689 (24, $–Cl_2$), 441 (18), 247 (51), 157 (29), 91 (100). *Crystal data*: $C_{34}H_{32}N_4PtCl_2$, M = 762.62, monoclinic, space group $P2(1)/c$, a = 7.5380(3), b = 33.6480(12), c = 12.1810(5) Å, $\alpha = \gamma = 90°$, β = 95.951(3)°, V = 3072.9(2) Å^3, Z = 4, λ = 0.71069 Å, μ = 4.77 mm^{-1}, T = 133 K; 12 924 reflections measured, 6540 unique; final refinement to convergence on F^2 gave R = 0.0276 and R_w = 0.0601, GOF = 0.766. CCDC 1481381.

***cis*-[Dichlorido-bis(1,3-di(4-methoxybenzyl)imidazol-2-ylidene)] platinum(II) (5b).** Complex **2b** (88 mg, 135 μmol), 1,3-di(4-methoxybenzyl)imidazolium chloride (47 mg, 135 μmol), and KO^{t}Bu (18 mg, 162 μmol) yielded 74 mg (62%) of **5b** as white crystals of m.p. 211 °C. Elemental analysis (%): calc. for $C_{38}H_{40}O_4N_4PtCl_2$ (882.74): C, 51.70; H, 4.57; N, 6.35. Found: C, 51.75; H, 4.46; N, 6.39. ^{1}H NMR ($CDCl_3$, 500 MHz): δ 3.77 (s, 12H, OCH_3), 5.19 (d, J = 14.3 Hz, 4H, CH_2), 5.93 (d, J = 14.3 Hz, 4H, CH_2), 6.53 (s, 4H, imidazole CH), 6.77–6.83 (d, J = 8.5 Hz, 8H, Ar), 7.08–7.16 (d, J = 8.5 Hz, 8H, Ar); ^{13}C NMR ($CDCl_3$, 126 MHz): δ 53.7 (CH_2), 55.3 (OCH_3), 114.3 (Ar), 120.3 (imidazole CH), 126.9 (Ar), 129.9 (Ar), 148.2 (NCN), 159.6 (Ar); ^{195}Pt NMR ($CDCl_3$): δ –3601.0; EI-MS: m/z 882 (M^+, 2%), 845 (4, –Cl), 809 (18, $–Cl_2$), 502 (16), 379 (9), 307 (11), 187 (11), 121 (100).

***cis*-[Dichlorido-(1,3-dibenzylimidazol-2-ylidene)(1,3-di(4-methoxybenzyl)imidazol-2-ylidene)]platinum(II) (5c).** Complex **2a** (104 mg, 176 μmol), 1,3-di(4-methoxybenzyl)imidazolium chloride (61 mg, 176 μmol), and KO^{t}Bu (24 mg, 211 μmol) gave 78 mg (54%) of **5c** as white crystals of m.p. 243 °C. Elemental analysis (%): calc. for $C_{36}H_{36}O_2N_4PtCl_2$ (822.69): C, 52.56; H, 4.41; N, 6.81. Found: C, 52.18; H, 4.81; N, 6.98; ^{1}H NMR ($CDCl_3$, 500 MHz): δ 3.77 (s, 6H, OCH_3), 5.06 (d, J = 14.3 Hz, 2H, CH_2), 5.41 (d, J = 14.3 Hz, 2H, CH_2), 5.96 (2 × d, J = 14.3 Hz, 4H, CH_2), 6.45 (s, 2H, imidazole CH), 6.59 (s, 2H, imidazole CH), 6.80 (d, J = 8.5 Hz, 4H, Ar), 7.12 (d, J = 8.5 Hz, 4H, Ar), 7.16 (m, 4H, Ar), 7.29 (m, 6H, Ar); ^{13}C NMR ($CDCl_3$, 126 MHz): δ 53.6 (CH_2), 54.1 (CH_2), 55.3 (OCH_3), 114.3 (Ar), 120.2 (imidazole CH), 120.6 (imidazole CH), 126.8 (Ar), 128.2 (Ar), 128.4 (Ar), 128.9 (Ar), 129.9 (Ar), 134.9 (Ar), 147.9 (NCN), 149.3 (NCN), 159.6 (Ar); ^{195}Pt NMR ($CDCl_3$): δ –3603.0; EI-MS: m/z 822 (M^+, 6%), 786 (8, –Cl), 749 (27, $–Cl_2$), 502 (9), 441 (22), 307 (11), 247 (38), 157 (30), 121 (100), 91 (79).

***cis*-[Dichlorido-(1,3-dibenzylimidazol-2-ylidene)(1,3-di(4-fluorobenzyl)imidazol-2-ylidene)]platinum(II) (5d).** Complex **2a** (80 mg, 135 μmol), 1,3-di(4-fluorobenzyl)imidazolium chloride (43 mg, 135 μmol), and KO^{t}Bu (18 mg, 162 μmol) afforded 57 mg (53%) of **5d** as white crystals of m.p. 241 °C. Elemental analysis (%): calc. for $C_{34}H_{30}N_4F_2PtCl_2$ (798.62): C, 51.13; H, 3.79; N, 7.02. Found: C, 50.61; H, 3.66; N, 7.04; ^{1}H NMR ($CDCl_3$, 126 MHz): δ 4.96 (d, J = 14.3 Hz, 2H, CH_2), 5.48 (d, J = 15.0 Hz, 2H, CH_2), 5.92 (d, J = 15.0 Hz, 2H, CH_2), 6.08 (d, J = 14.3 Hz, 2H, CH_2), 6.45 (s, 2H, imidazole CH), 6.63 (s, 2H, imidazole CH), 6.98 (t, J = 8.7 Hz, 4H, Ar), 7.13–7.18 (m, 4H, Ar), 7.21 (dd, J = 8.7, 5.2 Hz, 4H, Ar), 7.28–7.34 (m, 6H, Ar); ^{13}C NMR ($CDCl_3$, 126 MHz): δ 53.4 (CH_2), 54.1 (CH_2), 115.9 (d, $^2J_{CF}$ = 21.8 Hz, Ar), 120.4 (imidazole CH), 120.8 (imidazole CH), 127.9 (Ar), 128.4 (Ar), 129.0 (Ar), 130.3 (d, $^3J_{CF}$ = 8.2 Hz, Ar), 130.6 (Ar), 134.8 (Ar), 149.0 (NCN), 149.1 (NCN), 162.7 (d, $^1J_{CF}$ = 248 Hz, Ar); ^{195}Pt NMR ($CDCl_3$): δ –3605.2; EI-MS: m/z 798 (M^+, 8%), 761 (28, –Cl), 725 (100, $–Cl_2$), 477 (24), 441 (33), 283 (45), 247 (81), 109 (60), 91 (44). *Crystal data*: $C_{34}H_{28}N_4F_2PtCl_2$, M = 796.59, monoclinic, space group $C2/c$, a = 15.6790(6), b = 14.1220(6), c = 15.1390(8) Å, $\alpha = \gamma = 90°$, β = 113.895(5)°, V = 3064.8(3) Å^3, Z = 4, λ = 0.71069 Å, μ = 4.80 mm^{-1}, T = 133 K; 19 249 reflections measured, 3070 unique; final refinement to convergence on F^2 gave R = 0.0267 and R_w = 0.0639, GOF = 0.984. CCDC 1481378.

cis-[Dichlorido-(1,3-di(4-fluorobenzyl)imidazol-2-ylidene)(1,3-di(4-methoxybenzyl)imidazol-2-ylidene)]platinum(II) (5e). Complex **5e** (13 mg, 11%) was obtained from **2b** (88 mg, 135 μmol), 1,3-di(4-fluorobenzyl)imidazolium chloride (43 mg, 135 μmol), and KO^{t}Bu (18 mg, 162 μmol) as white crystals of m.p. 223 °C. Elemental analysis (%): calc. for $C_{36}H_{34}N_4O_2F_2PtCl_2$ (858.67): C, 50.36; H, 3.99; N, 6.52. Found: C, 49.91; H, 4.13; N, 6.32; ^{1}H NMR ($CDCl_3$, 500 MHz): δ 3.77 (s, 6H, OCH_3), 5.13 (d, J = 14.6 Hz, 2H, CH_2), 5.22 (d, J = 14.3 Hz, 2H, CH_2), 5.88 (d, J = 14.3 Hz, 2H, CH_2), 6.04 (d, J = 14.6 Hz, 2H, CH_2), 6.54 (s, 2H, imidazole CH), 6.56 (s, 2H, imidazole CH), 6.80 (d, J = 8.5 Hz, 4H, Ar), 6.97 (t, J = 8.7 Hz, 4H, Ar), 7.12 (d, J = 8.5 Hz, 4H, Ar), 7.21 (dd, J = 8.7, 5.2 Hz, 4H, Ar); ^{13}C NMR ($CDCl_3$, 126 MHz): δ 53.4 (CH_2), 53.6 (CH_2), 55.3 (OCH_3), 114.3 (Ar), 115.9 (d, $^2J_{CF}$ = 21.8 Hz, Ar), 120.5 (imidazole CH), 120.5 (imidazole CH), 126.7 (Ar), 129.7 (Ar), 130.3 (d, $^3J_{CF}$ = 8.2 Hz, Ar), 130.6 (d, $^4J_{CF}$ = 2.7 Hz, Ar), 147.8 (NCN), 149.0 (NCN), 159.7 (Ar), 162.7 (d, $^1J_{CF}$ = 249 Hz, Ar); ^{195}Pt NMR ($CDCl_3$): δ –3601.7; EI-MS: m/z 858 (M^+, 6%), 822 (10, –Cl), 786 (39, $–Cl_2$), 663 (8), 502 (12), 477 (27), 283 (31), 175 (25), 121 (100), 109 (98).

***cis*-[Dichlorido-(1,3-dibenzylimidazol-2-ylidene)(1,3-bis(3,5-dimethoxybenzyl)imidazol-2-ylidene)]platinum(II) (5f).** Complex **5f** (35 mg, 26%) was obtained from **2a** (90 mg,

153 μmol), 1,3-bis(3,5-dimethoxybenzyl)imidazolium chloride (62 mg, 153 μmol), and KO^{t}Bu (21 mg, 184 μmol) as white crystals of m.p. 237 °C. Elemental analysis (%): calc. for $C_{38}H_{40}O_4N_4PtCl_2$ (882.74): C, 51.70; H, 4.57; N, 6.35. Found: C, 51.41; H, 5.18; N, 6.43; ^{1}H NMR ($CDCl_3$, 500 MHz): δ 3.73 (s, 12H, OCH_3), 5.05 (d, J = 14.3 Hz, 2H, CH_2), 5.32 (d, J = 15.0 Hz, 2H, CH_2), 5.97 (dd, J = 14.6, 1.8 Hz, 4H, CH_2), 6.35 (t, J = 2.4 Hz, 2H, Ar), 6.42 (d, J = 2.4 Hz, 4H, Ar), 6.52 (s, 2H, imidazole CH), 6.60 (s, 2H, imidazole CH), 7.17 (m, 4H, Ar), 7.28–7.33 (m, 6H, Ar); ^{13}C NMR ($CDCl_3$, 126 MHz): δ 54.1 (CH_2), 54.1 (CH_2), 55.6 (OCH_3), 100.3 (Ar), 106.3 (Ar), 120.6 (imidazole CH), 120.8 (imidazole CH), 128.2 (Ar), 128.4 (Ar), 129.0 (Ar), 135.0 (Ar), 137.3 (Ar), 148.9 (NCN), 148.9 (NCN), 161.2 (Ar); ^{195}Pt NMR ($CDCl_3$): δ −3604.0; EI-MS: m/z 882 (M^+, 4%), 846 (14, –Cl), 809 (17, –Cl_2), 689 (17), 561 (13), 442 (16), 367 (37), 247 (100), 157 (22), 91 (74).

***cis*-[Dichlorido-(1,3-dibenzylimidazol-2-ylidene)(1-benzyl-3-methylimidazol-2-ylidene)]platinum(II) (5g).** Complex **5g** (29 mg, 50%) was obtained from **2a** (50 mg, 84,4 μmol), 1-benzyl-3-methylimidazolium chloride (18 mg, 84,4 μmol), and KO^{t}Bu (15 mg, 127 μmol) as white crystals of m.p. 243 °C. Elemental analysis (%): calc. for $C_{28}H_{28}N_4PtCl_2$ (686.54): C, 48.98; H, 4.11; N, 8.16. Found: C, 48.55; H, 3.80; N, 7.83; ^{1}H NMR ($CDCl_3$, 500 MHz): δ 3.92 (s, 3H, CH_3), 5.23 (m, 2H, CH_2), 5.61–5.71 (d, J = 15.1 Hz, 1H, CH_2), 5.71–5.83 (2 × d, J = 15.1 Hz, 2H, CH_2), 6.08 (d, J = 14.5 Hz, 1H, CH_2), 6.50 (d, J = 1.4 Hz, 1H, imidazole CH), 6.52 (d, J = 1.4 Hz, 1H, imidazole CH), 6.64 (d, J = 1.4 Hz, 1H, imidazole CH), 6.67 (d, J = 1.4 Hz, 1H, imidazole CH), 7.02–7.09 (m, 2H), 7.11–7.19 (m, 4H), 7.25–7.34 (m, 9H); ^{13}C NMR ($CDCl_3$, 126 MHz): δ 37.9 (CH_3), 53.8 (CH_2), 54.0 (CH_2), 54.1 (CH_2), 120.0 (imidazole CH), 120.4 (imidazole CH), 120.9 (imidazole CH), 122.4 (imidazole CH), 127.7 (Ar), 127.8 (Ar), 128.3 (Ar), 128.9 (Ar), 128.9 (Ar), 129.0 (Ar), 134.8 (Ar), 135.0 (Ar), 148.1 (NCN), 149.0 (NCN); ^{195}Pt NMR ($CDCl_3$): δ −3610.7; EI-MS: m/z 686 (M^+, 3%), 650 (9, –Cl), 613 (21, –Cl_2), 441 (8), 365 (18), 284 (7), 247 (43), 171 (80), 158 (16), 91 (100).

***cis*-[Dichlorido-(1,3-dibenzylimidazol-2-ylidene)(1,3-dimethyl-4-(3′,4′,5′-trimethoxyphenyl)-5-(4″-methoxyphenyl)imidazol-2-ylidene)]platinum(II) (5h).** Complex **5h** (19 mg, 73%) was obtained from **2c** (21 mg, 30 μmol), 1,3-dibenzylimidazolium chloride (9 mg, 30 μmol), and KO^{t}Bu (4 mg, 35 μmol) as white crystals of m.p. 266 °C. Elemental analysis (%): calc. for $C_{38}H_{40}N_4O_4PtCl_2$ (882.74): C, 51.70; H, 4.57; N, 6.35. Found: C, 51.51; H, 4.69; N, 6.26; ^{1}H NMR ($CDCl_3$, 500 MHz): δ 3.66 (s, 6H, OCH_3), 3.73 (s, 3H, NCH_3), 3.79 (s, 3H, OCH_3), 3.81 (s, 3H, NCH_3), 3.82 (s, 3H, OCH_3), 5.77 (d, J = 15.3 Hz, 1H CH_2), 5.87 (d, J = 15.3 Hz, 1H, CH_2), 5.95 (2 × d, J = 15.6 Hz, 2H, CH_2), 6.07 (s, 2H, Ar), 6.71 (d, J = 2.1 Hz, 1H, imidazole CH), 6.73 (d, J = 2.1 Hz, 1H, imidazole CH), 6.82 (m, 4H, Ar), 7.11 (dd, J = 8.0, 1.8 Hz, 2H, Ar), 7.21 (dd, J = 8.0, 1.8 Hz, 2H, Ar), 7.29–7.37 (m, 6H, Ar); ^{13}C NMR ($CDCl_3$, 126 MHz): δ 36.2 (NCH_3), 36.3 (NCH_3), 54.2 (CH_2), 54.3 (CH_2), 55.3 (OCH_3), 56.2 (OCH_3), 60.9 (OCH_3), 107.7 (Ar), 114.1 (Ar), 119.8 (Ar), 120.7 (imidazole CH), 120.9 (imidazole CH), 123.0 (Ar), 127.6 (Ar), 127.9 (Ar), 128.3 (Ar), 129.0 (Ar), 131.1 (Ar), 131.5 (Ar), 135.2 (Ar), 138.5 (Ar), 146.6 (NCN), 149.3 (NCN), 153.1 (Ar), 160.0 (Ar); ^{195}Pt NMR ($CDCl_3$): δ −3616.9; EI-MS: m/z 882 (M^+, 1%), 847 (8, –Cl), 819 (39, –Cl_2), 690 (5), 561 (4), 369 (12), 247 (100), 157 (7), 91 (47). *Crystal data*: $C_{38}H_{40}N_4O_4PtCl_2{\times}CH_2Cl_2$, M = 967.65, monoclinic, space group $P2(1)/c$, a = 11.1330(4), b = 29.7780(14), c = 12.1160(4) Å, $\alpha = \gamma = 90°$, β = 101.539(3)°, V = 3935.5(3) Å^3, Z = 4, λ = 0.71069 Å, μ = 3.88 mm^{-1}, T = 133 K; 23 066 reflections measured, 7701 unique; final refinement to convergence on F^2 gave R = 0.058 and R_w = 0.1494, GOF = 0.934. CCDC 1481379.

General procedure for the preparation of *cis*-[Pt^{II}(NHC)$_2$(PPh$_3$)Cl]$^+$Cl$^-$ complexes 8

A solution of triphenylphosphane (5 equiv.) and complex **5** (1 equiv.) in CH_2Cl_2 (100 mL mmol^{-1}) was stirred at room temperature for 16 h. The solvent was removed *in vacuo*, and the residue was recrystallised from CH_2Cl_2/hexane.

***cis*-[Chlorido-bis(1,3-dibenzylimidazol-2-ylidene)(triphenylphosphane)]platinum(II) chloride (8a).** Complex **8a** (32 mg, 95%) was obtained from **5a** (25 mg, 32.8 μmol) and triphenylphosphane (43 mg, 164 μmol) as colourless crystals of m.p. 173 °C. Elemental analysis (%): calc. for $C_{52}H_{47}N_4PPtCl_2$ (1024.92): C, 60.94; H, 4.62; N, 5.47. Found: C, 60.74; H, 4.58; N, 5.37; ^{1}H NMR ($CDCl_3$, 500 MHz): δ 4.68 (d, J = 14.6 Hz, 2H, CH_2), 4.96 (d, J = 14.0 Hz, 2H, CH_2), 5.69 (d, J = 14.6 Hz, 2H, CH_2), 5.92 (d, J = 14.0 Hz, 2H, CH_2), 6.68 (s, 2H, imidazole CH), 7.02 (d, J = 7.6 Hz, 4H, Ar), 7.12 (t, J = 7.6 Hz, 4H, Ar), 7.19–7.25 (m, 4H, imidazole CH, Ar), 7.25–7.29 (m, 5H, Ar), 7.31–7.42 (m, 17H, Ar, PPh_3), 7.47–7.53 (m, 3H, PPh_3); ^{13}C NMR ($CDCl_3$, 126 MHz): δ 54.0 (CH_2), 54.3 (CH_2), 121.8 (imidazole CH), 123.2 (imidazole CH), 128.1 (Ar), 128.7 (Ar), 128.8 (Ar), 129.0 (d, $^1J_{CP}$ = 55 Hz, PPh_3), 129.0 (d, $^3J_{CP}$ = 11 Hz, PPh_3), 129.1 (Ar), 131.4 (d, $^4J_{CP}$ = 2.7 Hz, PPh_3), 133.7 (Ar), 134.2 (d, $^2J_{CP}$ = 11 Hz, PPh_3), 134.3 (Ar), 144.9 (d, $^2J_{CP\text{-}cis}$ = 10 Hz, NCN), 162.8 (d, $^2J_{CP\text{-}trans}$ = 151 Hz, NCN); ^{31}P NMR ($CDCl_3$, 202 MHz): δ 13.1 ($^1J_{PPt}$ = 2366 Hz); ^{195}Pt NMR ($CDCl_3$): δ −4098.7/−4120.8 (d, J_{PtP} = 2377 Hz); EI-MS: m/z 762 (11%, –PPh_3), 726 (14, –Cl, –PPh_3), 689 (42, –Cl_2, –PPh_3), 597 (9), 441 (33), 350 (11), 262 (99), 247 (100), 183 (52), 157 (34), 91 (95). *Crystal data*: $C_{52}H_{47}N_4PPtCl_2$, CH_2Cl_2, $2H_2O$, M = 1145.84, triclinic, space group $P\bar{1}$, a = 11.4460(4), b = 11.7520(4), c = 19.7120(8) Å, α = 75.959(3)°, β = 74.604(3)°, γ = 73.708(3)°, V = 2412.88(16) Å^3, Z = 2, λ = 0.71069 Å, μ = 3.21 mm^{-1}, T = 133 K; 34 049 reflections measured, 9655 unique; final refinement to convergence on F^2 gave R = 0.0582 and R_w = 0.1538, GOF = 0.994. CCDC 1481380.

***cis*-[Chlorido-bis(1,3-di(4-methoxybenzyl)imidazol-2-ylidene)(triphenylphosphane)]platinum(II) chloride (8b).** Complex **8b** (23 mg, 88%) was obtained from **5b** (20 mg, 22.7 μmol) and triphenylphosphane (30 mg, 114 μmol) as colourless crystals of m.p. 138 °C. Elemental analysis (%): calc. for $C_{56}H_{55}N_4O_4PPtCl_2$ (1145.02): C, 58.74; H, 4.84; N, 4.89. Found: C, 58.39; H, 4.98; N, 4.93; ^{1}H NMR ($CDCl_3$, 500 MHz): δ 3.71 (s, 6H, OCH_3), 3.79 (s, 6H, OCH_3), 4.55 (d, J = 14.3 Hz, 2H, CH_2), 5.00 (d, J = 14.3 Hz, 2H, CH_2), 5.52 (d, J = 14.3 Hz, 2H, CH_2), 5.84 (d, J = 14.3 Hz, 2H, CH_2), 6.56–6.64 (d, J = 8.5 Hz, 4H, Ar),

6.71 (s, 2H, imidazole CH), 6.84–6.90 (d, J = 8.5 Hz, 4H, Ar), 6.90–6.96 (d, J = 8.5 Hz, 4H, Ar), 7.12 (s, 2H, imidazole CH), 7.22–7.26 (d, J = 8.5 Hz, 4H, Ar), 7.29–7.41 (m, 12H, PPh_3), 7.47–7.52 (m, 3H, PPh_3); ^{13}C NMR ($CDCl_3$, 126 MHz): δ 53.6 (CH_2), 53.9 (CH_2), 55.3 (OCH_3), 55.3 (OCH_3), 114.4 (Ar), 114.5 (Ar), 121.6 (imidazole CH), 122.7 (imidazole CH), 125.4 (Ar), 126.3 (Ar), 129.0 (d, $^3J_{CP}$ = 10 Hz, PPh_3), 129.1 (d, $^1J_{CP}$ = 55 Hz, PPh_3), 129.9 (Ar), 130.1 (Ar), 131.3 (d, $^4J_{CP}$ = 2.7 Hz, PPh_3), 134.2 (d, $^2J_{CP}$ = 10 Hz, PPh_3), 144.0 (d, $^2J_{CP\text{-}cis}$ = 10 Hz, NCN), 162.6 (d, $^2J_{CP\text{-}trans}$ = 151 Hz, NCN); ^{31}P NMR ($CDCl_3$, 202 MHz): δ 13.3 ($^1J_{PPt}$ = 2360 Hz); ^{195}Pt NMR ($CDCl_3$): δ −4097.4/−4119.3 (d, J_{PtP} = 2361 Hz); EI-MS: m/z 848 (6%, –Cl, $-PPh_3$), 809 (21, $-Cl_2$, $-PPh_3$), 687 (6), 501 (19), 379 (10), 307 (14), 262 (86), 183 (97), 121 (100).

X-ray data collection and structural determination

Data collection and cell refinement by X-AREA-STOE. The single crystal samples were irradiated with Mo-Kα at 133 K. The structures were solved by direct methods using SIR 97 and refined by full matrix least-squares on F^2 for all data using SHELXL 2014. All hydrogen atoms were added at calculated positions and refined using a riding model. Anisotropic thermal displacement parameters were used for all non-hydrogen atoms. For **5d**, the two fluorine atoms on the phenyl rings were disordered and the corresponding hydrogens could not be located, yet detected in the ^1H NMR spectrum. For further details *cf.* ESI.† The crystallographic data were deposited with The Cambridge Crystallographic Data Centre CCDC under no. 1481381 (**5a**), 1481378 (**5d**), 1481379 (**5h**), 1481380 (**8a**).

Growth inhibition assay (MTT assay)

The antiproliferative effect of the complexes **5a**–**h**, **8a**, and **8b** on cells of 518A2 melanoma, different human colon carcinomas (HT-29, DLD-1), U87 glioblastoma, Panc-1 pancreatic cancer, mdr MCF-7/Topo breast cancer, and KbV1/Vbl cervix carcinoma, and on endothelial hybrid cells Ea.Hy926 was assessed. Cells were seeded in flat-bottom 96-well microtiter plates at a density of 0.05×10^6 mL^{-1} (0.1×10^6 mL^{-1} for U87 and Ea.Hy926) in culture medium and incubated until the cells nearly reached confluency at 37 °C. Test compound solutions were diluted from freshly made 10 mM stock solutions in DMF (5 mM in DMSO for **5g**, 10 mM in DMSO for CDDP) with water, and added to each well of the microtiter plates with working concentrations ranging from 100 μM to 25 nM. DMF or DMSO was used as a negative control. Treatment of the cells with **5a**–**h** and **8a**–**b** lasted for 72 h at 37 °C. The culture medium was replaced with a solution of MTT [3-(4,5-dimethylthiazol-2-yl)-2,5-diphenyltetrazoliumbromide] (0.05% in PBS) and the cells were incubated for another 2 h. The MTT solution was discarded and the water-insoluble formazan crystals, formed by metabolically viable cells, were dissolved in SDS/DMSO. The absorbance of the formazan solution was measured at 630 nm, the background absorbance at 570 nm. Means ± SDs were calculated from four independent values.

Electrophoretic mobility shift assay (EMSA assay)

The complexes **1b**, **5b**, and **8b** were tested for their interaction with circular pBR322 plasmid DNA in electrophoretic mobility shift assays according to a general method by Huq *et al.*[33] Briefly, 1.5 μg pBR322 plasmid DNA in freshly sterile-filtrated TE buffer (10 mM Tris/HCl, 1 mM EDTA, pH 8.0) were incubated with 0 μM (TE buffer with plasmid DNA), 5 μM, 10 μM, 25 μM and 50 μM of the complexes or cisplatin as a positive control for 24 h at 37 °C. Agarose gel electrophoresis (1%) was conducted at 66 V for 4 h. DNA bands were visualised *via* staining with 10 μg mL^{-1} ethidium bromide in 0.5× TBE buffer (900 mM Tris/HCl, 900 mM boric acid, 25 mM EDTA, pH 8.3) for 30 min at room temperature. The stained DNA was documented by UV excitation. EMSA assays were performed at least twice for each of the tested complexes.

Acknowledgements

We thank the Deutsche Forschungsgemeinschaft (grant Scho402/12), the COST Action CM1105 'Functional metal complexes that bind to biomolecules', and the University Bayreuth Graduate School for financial support.

Notes and references

1 H.-W. Wanzlick and H.-J. Schönherr, *Angew. Chem., Int. Ed.*, 1968, 7, 141–142.
2 K. Öfele, *J. Organomet. Chem.*, 1968, **12**, P42–P43.
3 A. Arduengo, R. Harlow and M. Kline, *J. Am. Chem. Soc.*, 1991, **113**, 361–363.
4 (*a*) N. Marion, S. Díez-González and S. Nolan, *Angew. Chem., Int. Ed.*, 2007, **46**, 2988–3000; (*b*) D. M. Flanigan, F. Romanov-Michailidis, N. A. White and T. Rovis, *Chem. Rev.*, 2015, **115**, 9307–9387; (*c*) A. Grossmann and D. Enders, *Angew. Chem., Int. Ed.*, 2012, **51**, 314–325.
5 M. Scholl, S. Ding, C. Lee and R. Grubbs, *Org. Lett.*, 1999, **1**, 953–956.
6 C. Zhang, J. Huang, M. Trudell and S. Nolan, *J. Org. Chem.*, 1999, **64**, 3804–3805.
7 W. Herrmann, M. Elison, J. Fischer, C. Kocher and G. Artus, *Angew. Chem., Int. Ed.*, 1995, **34**, 2371–2374.
8 L. Oehninger, R. Rubbiani and I. Ott, *Dalton Trans.*, 2013, **42**, 3269–3284.
9 A. Gautier and F. Cisnetti, *Metallomics*, 2012, **4**, 23–32.
10 L. Kelland, *Nat. Rev. Cancer*, 2007, **7**, 573–584.
11 S. Ray, R. Mohan, J. K. Singh, M. K. Samantaray, M. Shaikh, D. Panda and P. Ghosh, *J. Am. Chem. Soc.*, 2007, **129**, 15042–15053.
12 L. Eloy, A.-S. Jarrousse, M.-L. Teyssot, A. Gautier, L. Morel, C. Jolivalt, T. Cresteil and S. Roland, *ChemMedChem*, 2012, **7**, 805–814.
13 M.-L. Teyssot, A.-S. Jarrousse, A. Chevry, A. De Haze, C. Beaudoin, M. Manin, S. Nolan, S. Díez-González, L. Morel and A. Gautier, *Chem. – Eur. J.*, 2009, **15**, 314–318.

14 L. Oehninger, M. Stefanopoulou, H. Alborzinia, J. Schur, S. Ludewig, K. Namikawa, A. Muñoz-Castro, R. Köster, K. Baumann, S. Wölfl, W. Sheldrick and I. Ott, *Dalton Trans.*, 2013, **42**, 1657–1666.

15 (*a*) J. Weaver, S. Gaillard, C. Toye, S. Macpherson, S. Nolan and A. Riches, *Chem. – Eur. J.*, 2011, **17**, 6620–6624; (*b*) P. Barnard, M. Baker, S. Berners-Price and D. Day, *J. Inorg. Biochem.*, 2004, **98**, 1642–1647.

16 M. Skander, P. Retailleau, B. Bourrié, L. Schio, P. Maillet and A. Marinetti, *J. Med. Chem.*, 2010, **53**, 2146–2154.

17 J. K. Muenzner, T. Rehm, B. Biersack, A. Casini, I. de Graaf, P. Worawutputtapong, A. Noor, R. Kempe, V. Brabec, J. Kasparkova and R. Schobert, *J. Med. Chem.*, 2015, **58**, 6283–6292.

18 L. C. Lewis-Alleyne, B. S. Bassil, T. Böttcher and G.-V. Röschenthaler, *Dalton Trans.*, 2014, **43**, 15700–15703.

19 S. Fantasia, A. Pasini and S. Nolan, *Dalton Trans.*, 2009, **38**, 8107–8110.

20 G. Fortman, A. Slawin and S. Nolan, *Dalton Trans.*, 2010, **39**, 3923–3930.

21 C. Newman, R. Deeth, G. Clarkson and J. Rourke, *Organometallics*, 2007, **26**, 6225–6233.

22 M. Bouhrara, E. Jeanneau, L. Veyre, C. Copere and C. Thieuleux, *Dalton Trans.*, 2011, **40**, 2995–2999.

23 L. Naya, D. Vazquez-García, A. Fernandez, M. Lopez-Torres, I. Marcos, O. Lenis, M. Pereira, J. Vila and J. Fernandez, *J. Organomet. Chem.*, 2014, **772-773**, 192–201.

24 K. Fujita, K. Inoue, J. Sato, T. Tsuchimoto and H. Yasuda, *Tetrahedron*, 2016, **72**, 1205–1212.

25 H. Shirota, H. Matsuzaki, S. Ramati and J. Wishart, *J. Phys. Chem. B*, 2015, **119**, 9173–9187.

26 L. Kaps, B. Biersack, H. Müller-Bunz, K. Mahal, J. Münzner, M. Tacke, T. Mueller and R. Schobert, *J. Inorg. Biochem.*, 2012, **106**, 52–58.

27 S. Fantasia, J. Petersen, H. Jacobsen, L. Cavallo and S. Nolan, *Organometallics*, 2007, **26**, 5880–5889.

28 T. Mosmann, *J. Immunol. Methods*, 1983, **65**, 55–63.

29 A. Kazuo and M. Norio, *Neurosci. Res.*, 2000, **38**, 325–329.

30 C. Sergent, N. Franco, C. Chapusot, S. Lizard-Nacol, N. Isambert, M. Correia and B. Chauffert, *Cancer Chemother. Pharmacol.*, 2002, **49**, 445–452.

31 D.-W. Shen, C. Cardarelli, J. Hwang, M. Cornwell, N. Richert, S. Ishii, I. Pastan and M. M. Gottesman, *J. Biol. Chem.*, 1986, **261**, 7762–7770.

32 M. Kühnle, M. Egger, C. Müller, A. Mahringer, G. Bernhardt, G. Fricker, B. König and A. Buschauer, *J. Med. Chem.*, 2009, **52**, 1190–1197.

33 M. A. Chowdhury, F. Huq, A. Abdullah, P. Bearle and K. Fisher, *J. Inorg. Biochem.*, 2005, **99**, 1098–1112.

Electronic Supporting Information

Novel *cis*-[(NHC)^1(NHC)^2(L)Cl]platinum(II) complexes – synthesis, structures, and anticancer activities

Tobias Rehm,[a] Matthias Rothemund,[a] Julienne K. Muenzner,[a] Awaal Noor,[b] Rhett Kempe,[b] and Rainer Schobert[a]

[a]*Organic Chemistry Laboratory, University Bayreuth, Universitaetsstrasse 30, 95440 Bayreuth.*

E-mail: Rainer.Schobert@uni-bayreuth.de

[b]*Lehrstuhl fuer Anorganische Chemie II (Catalyst Design), University Bayreuth, Universitaetsstrasse 30, 95440 Bayreuth.*

Table of content:

General information

All chemicals and reagents were purchased from Sigma Aldrich, Alfa Aesar or ABCR and were used without further purification. Melting points are uncorrected; NMR spectra were run on a 500 MHz spectrometer; chemical shifts are given in ppm (δ) and referenced relative to the internal solvent signal; mass spectra: direct inlet, EI, 70 eV; X-Ray diffractometer: STOE-IPDS II. *N*-methyl- and *N*-benzylimidazolium salts were prepared according to literature procedures[1-4] and complex **1b** was prepared analogously to **1a**[5] as described herein.

Synthesis and characterization of imidazolium chlorides and complex 1b

General procedure:

Imidazole (1eq) and the respective benzyl chloride (2.1 eq) in acetonitrile (10 mL/mmol) were treated with K_2CO_3 (1.2 eq) and the resulting mixture was heated to 70 °C for 3-5 days. After filtration the solvent was evaporated in vacuo and the residue was washed several times with Et_2O.

Synthesis of 1,3-dibenzylimidazolium chloride:[1]

Imidazole (100 mg, 1.47 mmol), benzyl chloride (355 µL) and K_2CO_3 (244 mg) in acetonitrile (15 mL) for 72 h gave 333 mg (80%) of a colourless oil. ^{1}H NMR ($CDCl_3$, 500 MHz): δ 5.43 (4 H, s), 7.17 - 7.24 (6 H, m), 7.33 - 7.42 (6 H, m), 10.85 (1 H, s).

Synthesis of 1,3-di(4-methoxybenzyl)imidazolium chloride:

Imidazole (100 mg, 1.47 mmol), 4-methoxybenzyl chloride (417 µL) and K_2CO_3 (244 mg) in acetonitrile (15 mL) for 72 h gave 500 mg (99%) of a pale yellow gum. ^{1}H NMR ($CDCl_3$, 500 MHz): δ 3.74 (6 H, s), 5.43 (4 H, s), 6.84 (4 H, d, J=8.9 Hz), 7.22 (2 H, s), 7.39 (4 H, d, J=8.9 Hz), 10.98 (1 H, s).

Synthesis of 1,3-di(4-fluorobenzyl)imidazolium chloride:[2]

Imidazole (50 mg, 0.735 mmol), 4-fluorobenzyl chloride (182 µL) and K_2CO_3 (122 mg) in acetonitrile (7.5 mL) for 72 h gave 165 mg (70%) of a yellow gum. ^{1}H NMR ($CDCl_3$, 500 MHz): δ 5.51 (4 H, s), 7.00 (2 H, tt, *J*=8.7, 2.6 Hz), 7.34 (2 H, s), 7.49 (1 H, dd, *J*=8.7, 5.0 Hz), 11.02 (1 H, br. s.).

Synthesis of 1,3-di(3,5-dimethoxybenzyl)imidazolium chloride:[3]

Imidazole (50 mg, 0.735 mmol), 3,5-dimethoxybenzyl chloride (288 mg) and K_2CO_3 (122 mg) in acetonitrile (7.5 mL) for 5 d gave 205 mg (69%) of an orange gum. ^{1}H NMR ($CDCl_3$, 500 MHz): δ 3.73 (12 H, s), 5.39 (4 H, s), 6.39 (2 H, t, J=2.3 Hz), 6.56 (4 H, d, J=2.3 Hz), 7.18 (2 H, s), 11.20 (1 H, s).

Synthesis of 1-benzyl-3-methylimidazolium chloride:[4]

Methylimidazole (60 mg, 0.735 mmol) and benzyl chloride (100 µL, 0.882 mmol) in acetonitrile (5 mL) were heated to 70 °C for 72 h. After evaporation of the solvent in vacuo the residue was washed several times with Et_2O to yield 132 mg (86%) of a pale yellow gum. ^{1}H NMR ($CDCl_3$, 500 MHz): δ 3.98 (3 H, s), 5.54 (2 H, s), 7.29 - 7.34 (3 H, m), 7.37 (1 H, t, *J*=1.7 Hz), 7.41 - 7.46 (2 H, m), 7.51 (1 H, t, *J*=1.7 Hz), 10.51 (1 H, s).

Synthesis of *trans*-[dichlorido-bis(1,3-di(4-methoxybenzyl)imidazol-2-ylidene)]platinum(II) (**1b**):[5]

A solution of 1,3-di(4-methoxybenzyl)imidazolium chloride (60 mg, 0.154 mmol) in CH_2Cl_2 was treated with silver(I) oxide (18 mg, 77 µmol), and the resulting mixture was stirred at room temperature for 24 h. Then K_2PtCl_4 (32 mg, 77 µmol) was added and the reaction was allowed to stir for additional 24 h. The suspension was filtered, the filtrate was concentrated in vacuo, and the residue was recrystallized from CH_2Cl_2/hexane. Yield 38 mg (56%) white crystals of m.p. 194 °C (decomp.). ^{1}H NMR ($CDCl_3$, 500 MHz): δ 3.76 (12 H, s), 5.74 (8 H, s), 6.63 (4 H, s), 6.83 (8 H, d, J=8.5 Hz), 7.43 (8 H, d, J=8.5 Hz); ^{13}C NMR ($CDCl_3$, 126 MHz): δ 53.0, 55.2, 114.0, 120.1, 128.6, 129.9, 159.3, 167.2 (NHC). EI-MS: *m/z* 883 (M^+, 5%), 847 (12, -Cl), 810 (35,-2x Cl), 501 (17), 308 (23), 241 (28), 121 (100).

Table S 1: X-ray structural data of platinum carbene complexes **5a**,**d**,**h** and **8a**

	5a (CCDC1481381)	**5d** (CCDC1481378)	**5h** (CCDC1481379)	**8a** (CCDC1481380)
Empirical formula	$C_{34}H_{32}Cl_2N_4Pt$	$C_{34}H_{28}Cl_2F_2N_4Pt$	$C_{39}H_{42}Cl_4N_4O_4Pt$	$C_{53}H_{53}Cl_4N_4O_2PPt$
Formula weight	762.62	796.59	967.65	1145.85
Temperature	133 K	133 K	133 K	133 K
Wavelength	0.71069 Å	0.71069 Å	0.71069 Å	0.71069 Å
Crystal system	monoclinic	monoclinic	monoclinic	triclinic
Space group	$P2_1/c$	C2/c	$P2_1/c$	P-1
Unit cell dimensions	a = 7.5380(3) Å b = 33.6480(12) Å c = 12.1810(5) Å α = γ = 90° β = 95.951(3)°	a = 15.6790(6) Å b = 14.1220(6) Å c = 15.1390(8) Å α = γ = 90° β = 113.895(5)°	a = 11.1330(4) Å b = 29.7780(14) Å c = 12.1160(4) Å α = γ = 90° β = 101.539(3)°	a = 11.4460(4) Å b = 11.7520(4) Å c = 19.7120(8) Å α = 75.959(3)° β = 74.604 (3)° γ = 73.708(3)°
Volume	3072.9(2) $Å^3$	3064.8(3) $Å^3$	3935.5(3) $Å^3$	2412.88(16) $Å^3$
Z	4	4	4	2
Density (calcd)	1.648 Mg/m^3	1.726 Mg/m^3	1.633 Mg/m^3	1.577 Mg/m^3
Absorption coefficient	4.77 mm^{-1}	4.80 mm^{-1}	3.88 mm^{-1}	3.21 mm^{-1}
F(000)	1504	1560	1928	1152
Crystal size / mm	0.16 × 0.11 × 0.08	0.21 × 0.14 × 0.08	0.15 × 0.12 × 0.08	0.25 × 0.18 × 0.11
Theta range (data col.)	3.6–54.5°	4.1–53.1°	4.4–55.3°	3.7–53.2°
Index ranges	–9 ≤ h ≤ 9	–19 ≤ h ≤ 19	–7 ≤ h ≤ 13	–14 ≤ h ≤ 14
Index ranges	–42 ≤ k ≤ 0	–17 ≤ k ≤ 17	–36 ≤ k ≤ 36	–14 ≤ k ≤ 14
Index ranges	–15 ≤ l ≤ 15	–18 ≤ l ≤ 18	–14 ≤ l ≤ 14	–24 ≤ l ≤ 24
Reflections collected	12924	19249	23066	34049
Independent reflexes	6540 [R_{int}=0.040]	3070 [R_{int}=0.073]	7701 [R_{int}=0.069]	9655 [Rint=0.099]
Completeness to qmax	99.4%	99.4%	99.7%	98.9%
Absorption correction	numerical	numerical	numerical	numerical
Max / min transmission	0.740 / 0.454	0.506 / 0.248	0.848 / 0.652	0.712 / 0.424
Refinement method	Full–matrix least–squares on F^2	Full–matrix least–squares on F^2	Full–matrix least–squares on F^2	Full–matrix least–squares on F^2
Data / restraints / param	6540 / 0 / 370	3070 / 18 / 204	7701 / 18 / 475	9655 / 4 / 602
Goodness–of–fit on F^2	0.766	0.984	0.934	0.994
Final R indices	R_1 = 0.0276	R_1 = 0.0267	R_1 = 0.0575	R_1 = 0.0582
[I>2σ(I)]	wR_2 = 0.0601	wR_2 = 0.0639	wR_2 = 0.1494	wR_2 = 0.1538
R indices	R_1 = 0.0471	R_1 = 0.0350	R_1 = 0.0931	R_1 = 0.0794
(all data)	wR_2 = 0.0579	wR_2 = 0.0625	wR_2 = 0.1342	wR_2 = 0.1436
Largest diff. peak / hole	1.40/– 1.21 $eÅ^{-3}$	2.30/– 1.11 $eÅ^{-3}$	1.89/– 2.14 $eÅ^{-3}$	3.43/– 1.47 $eÅ^{-3}$

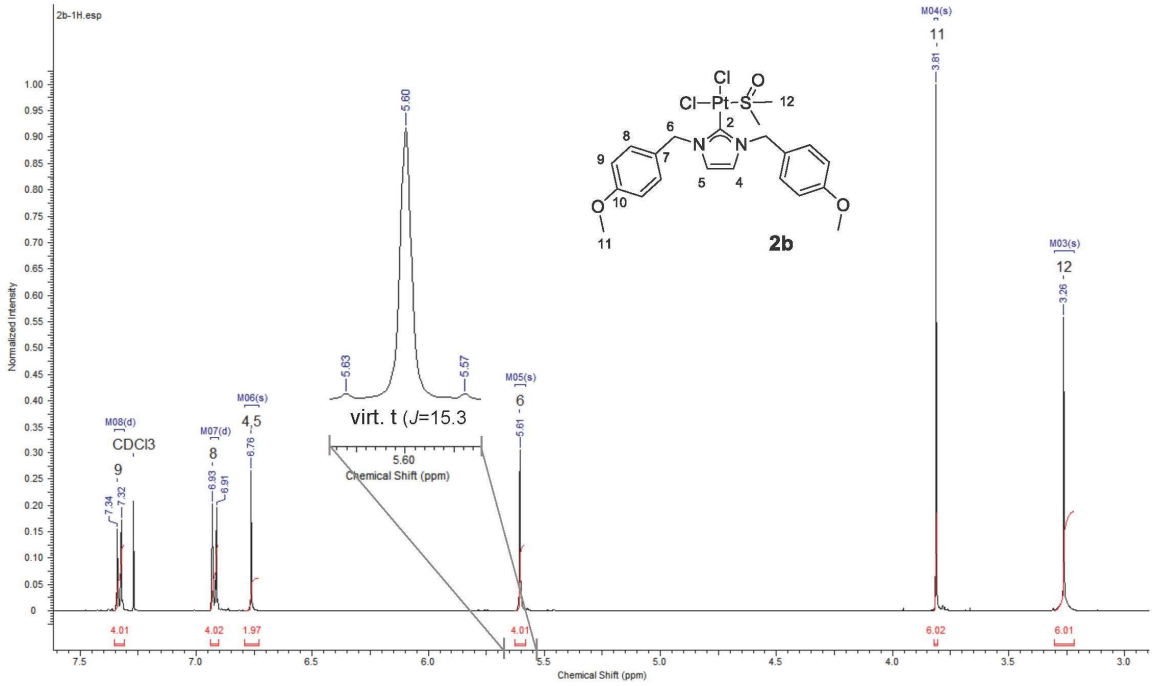

Fig. S 1: ^{1}H-NMR spectrum (500 MHz, $CDCl_3$) of complex **2b**.

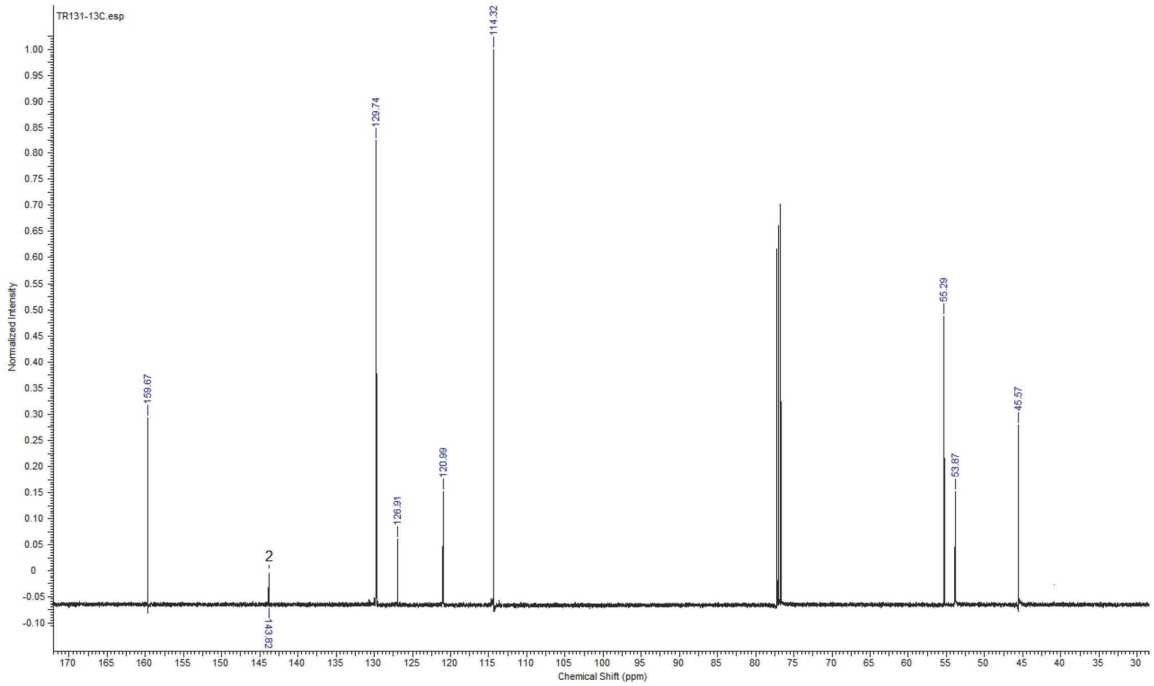

Fig. S 2: ^{13}C-NMR spectrum (126 MHz, $CDCl_3$) of complex **2b**.

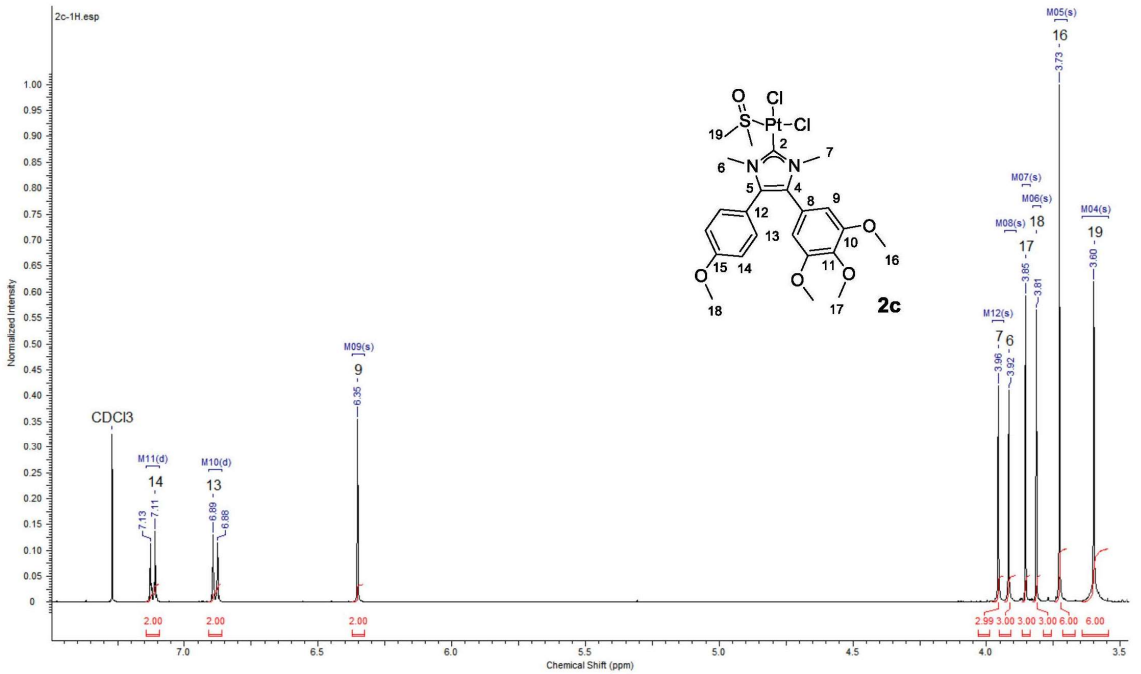

Fig. S 3: ^{1}H-NMR spectrum (500 MHz, $CDCl_3$) of complex **2c**.

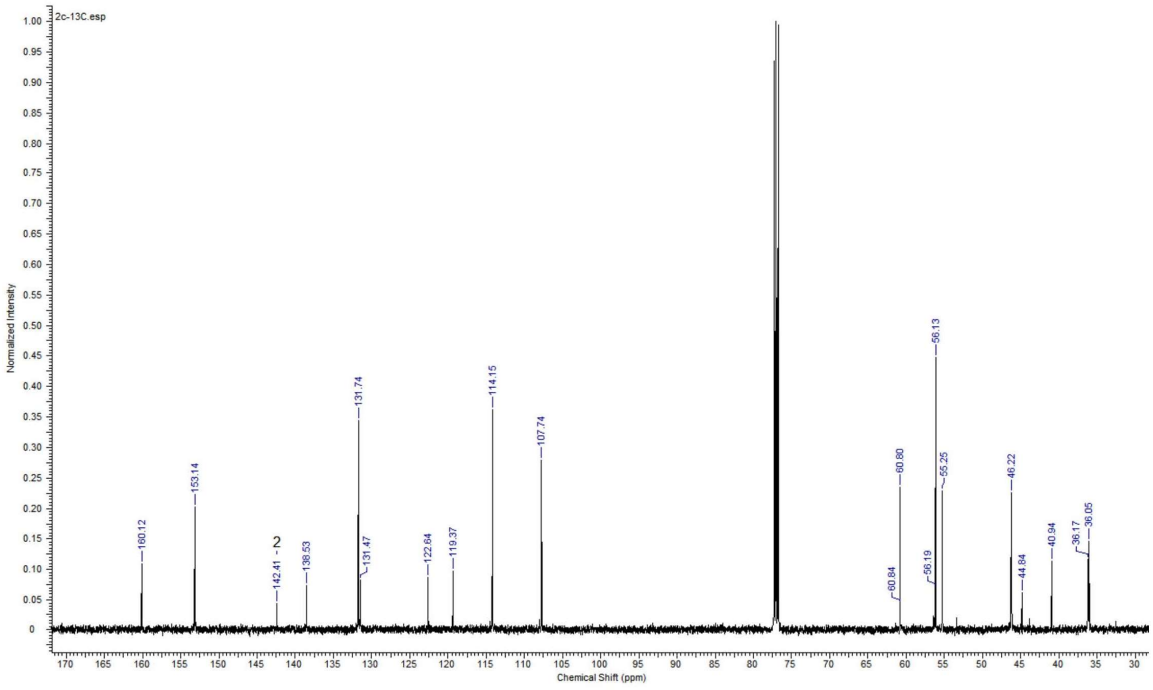

Fig. S 4: ^{13}C-NMR spectrum (126 MHz, $CDCl_3$) of complex **2c**.

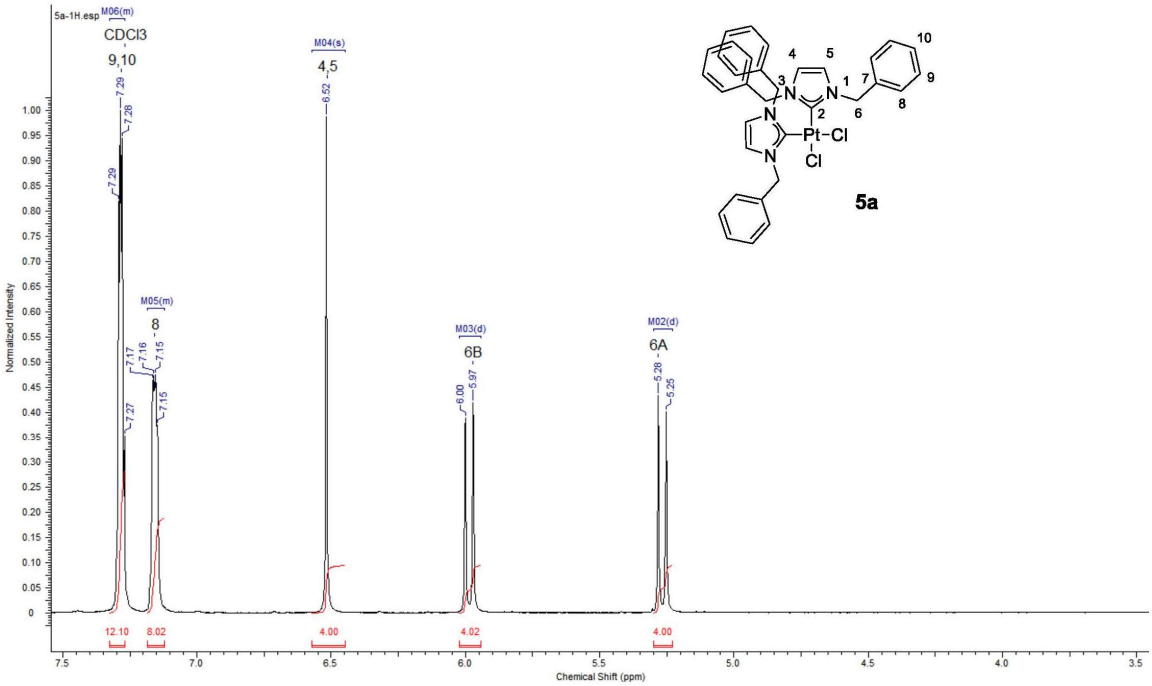

Fig. S5: ^{1}H-NMR spectrum (500 MHz, $CDCl_3$) of complex **5a**.

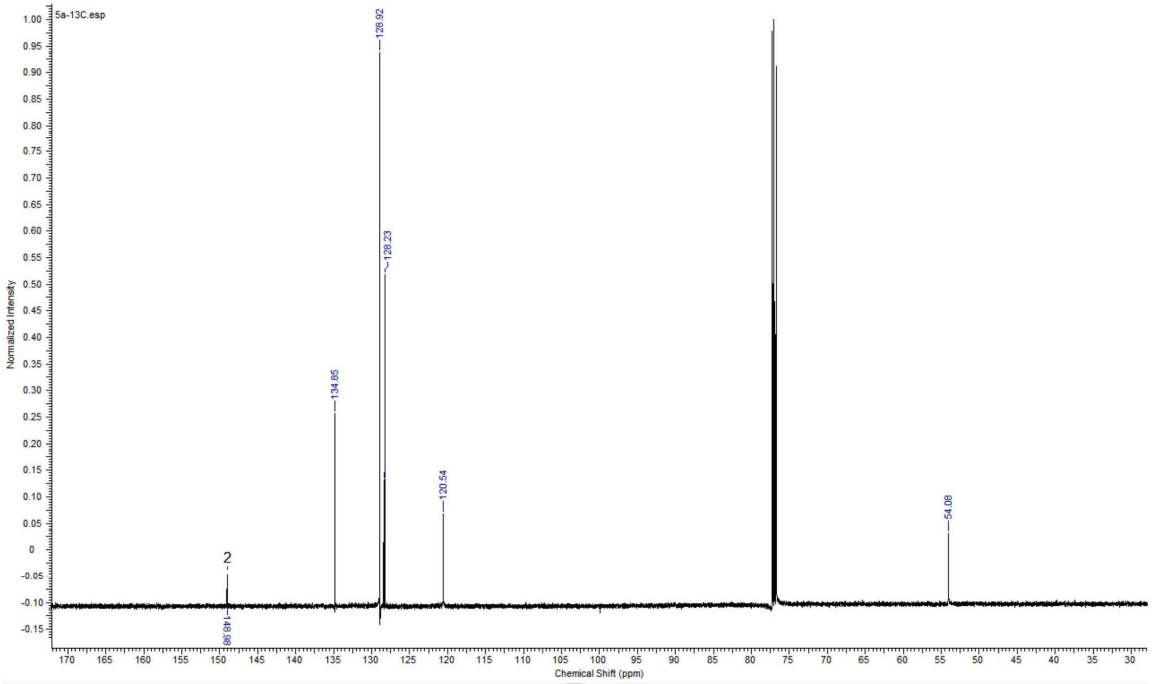

Fig. S 6: ^{13}C-NMR spectrum (126 MHz, $CDCl_3$) of complex **5a**.

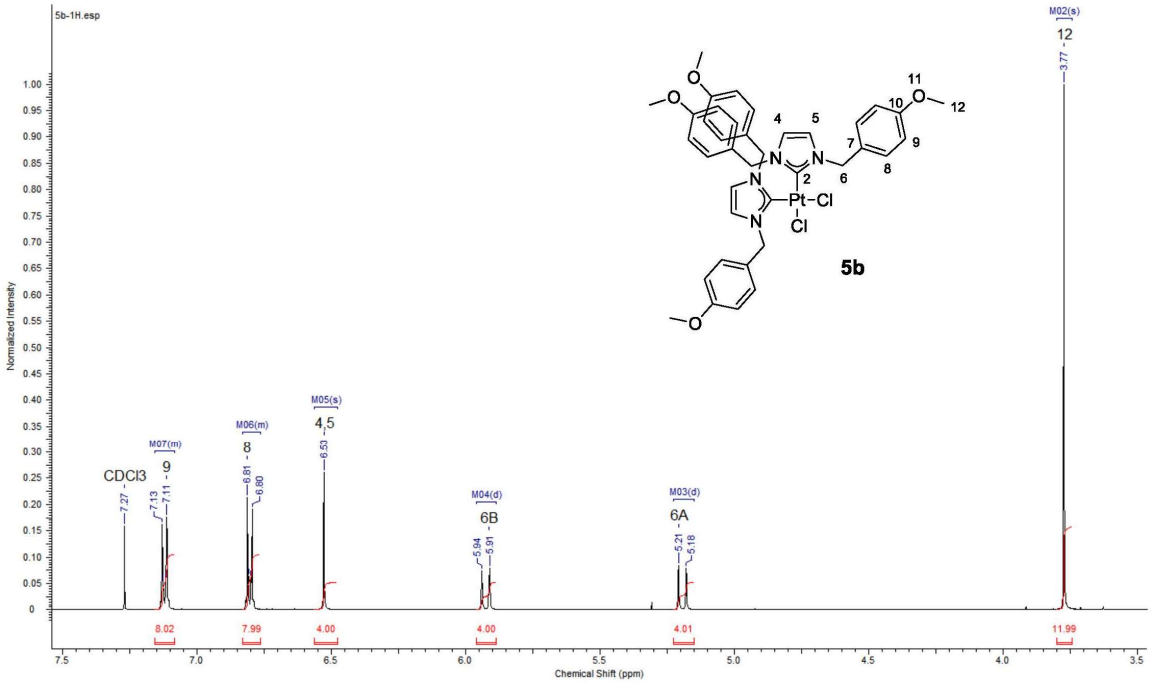

Fig. S7: ^{1}H-NMR spectrum (500 MHz, $CDCl_3$) of complex **5b**.

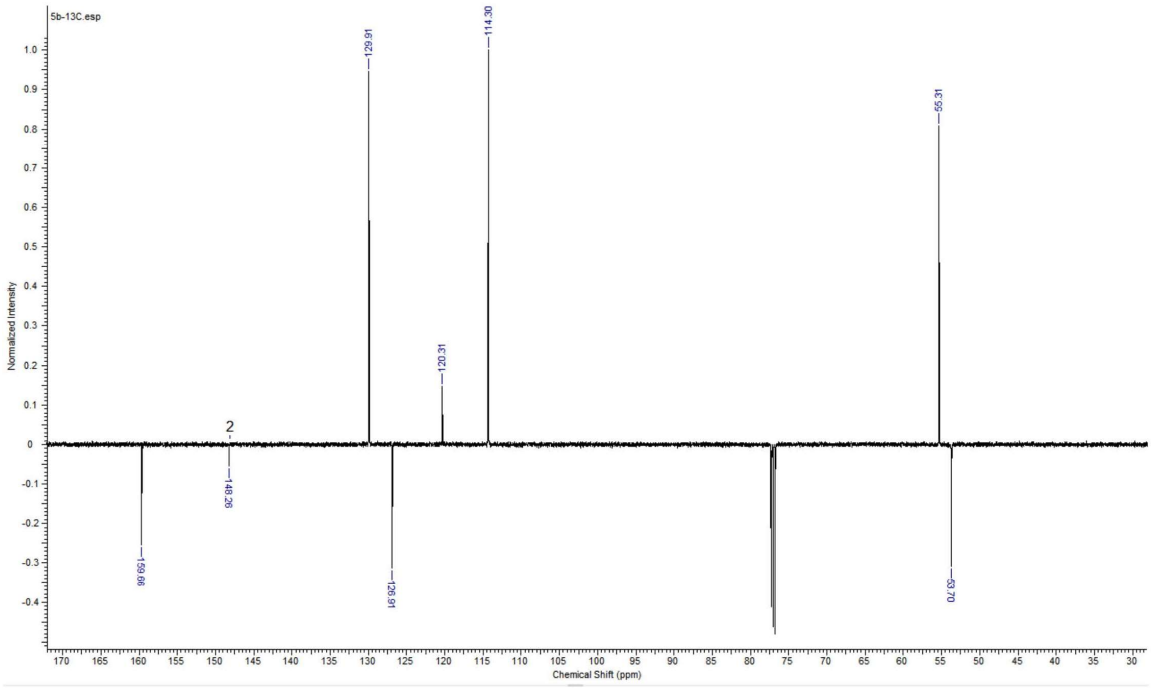

Fig. S 8: ^{13}C-ATP-NMR spectrum (126 MHz, $CDCl_3$) of complex **5b**.

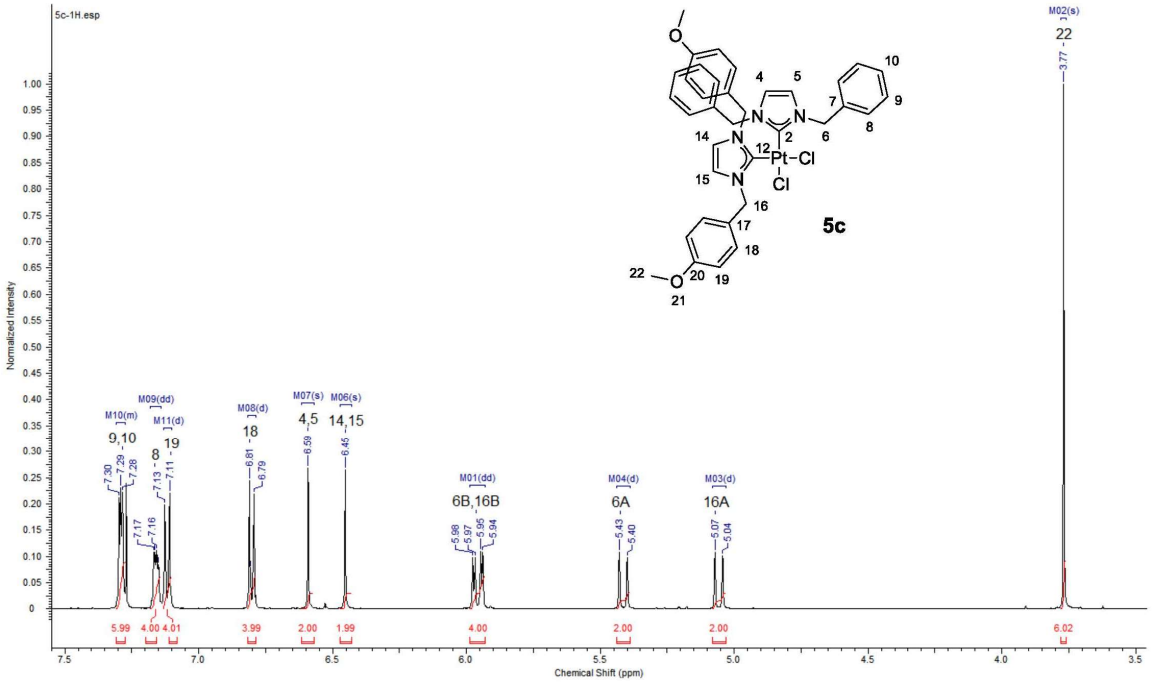

Fig. S9: ^{1}H-NMR spectrum (500 MHz, $CDCl_3$) of complex **5c**.

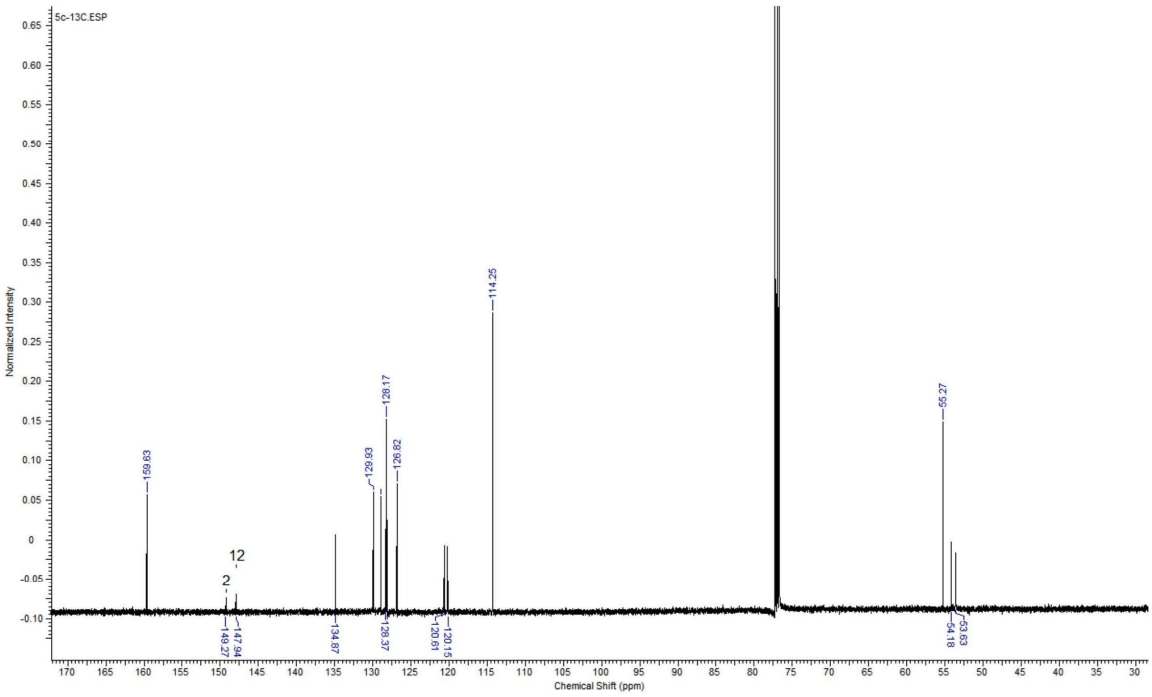

Fig. S 10: ^{13}C-NMR spectrum (126 MHz, $CDCl_3$) of complex **5c**.

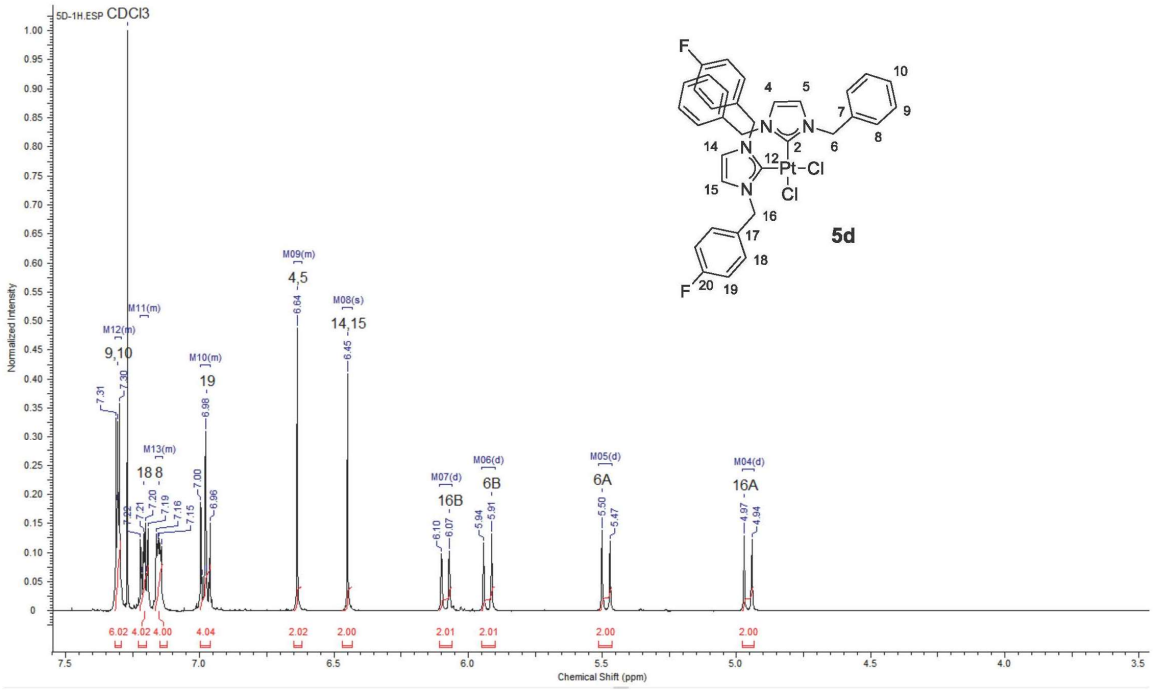

Fig. S11: ^{1}H-NMR spectrum (500 MHz, $CDCl_3$) of complex **5d**.

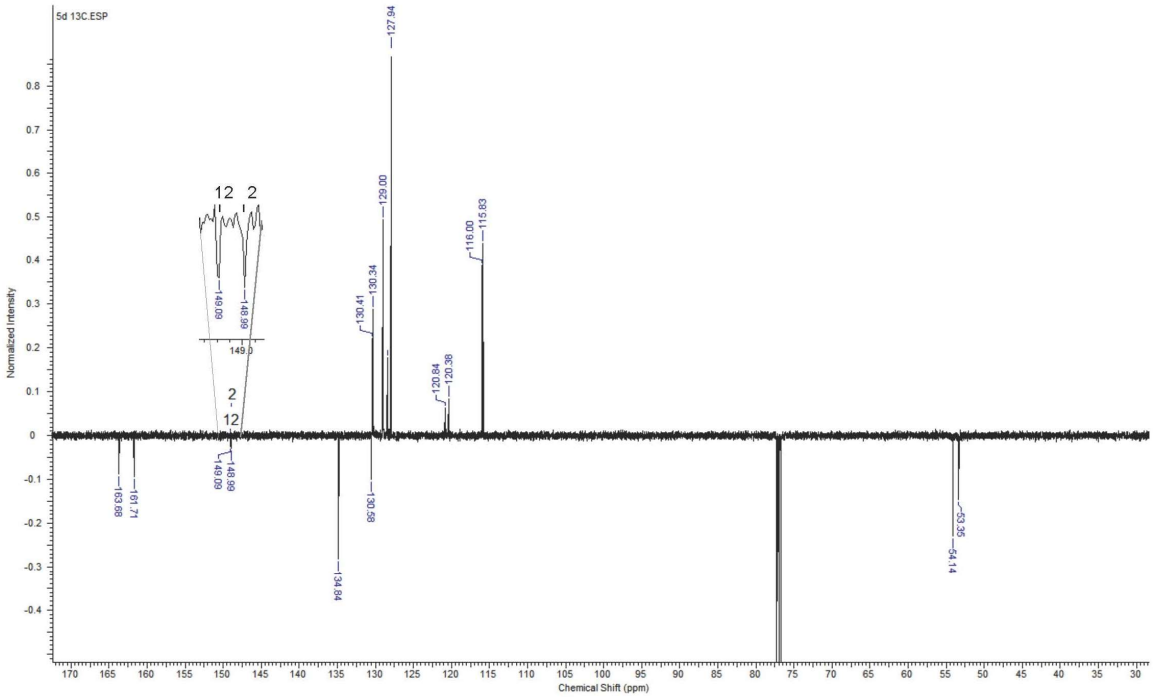

Fig. S 12: ^{13}C-ATP-NMR spectrum (126 MHz, $CDCl_3$) of complex **5d**.

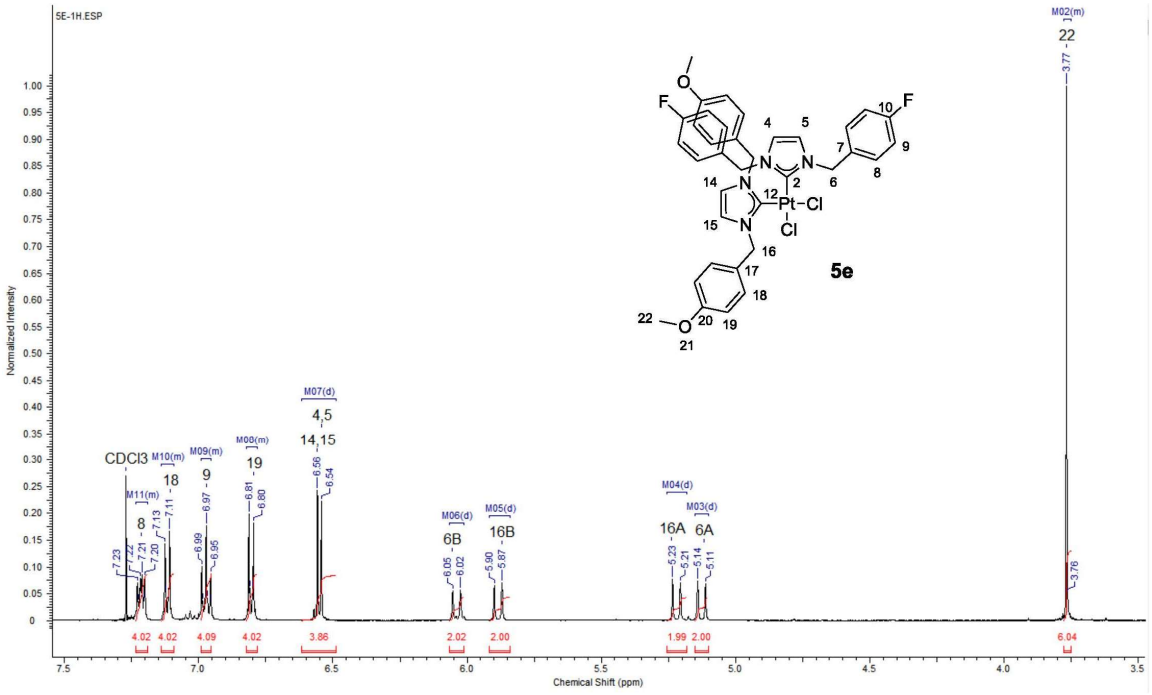

Fig. S13: ^{1}H-NMR spectrum (500 MHz, $CDCl_3$) of complex **5e**.

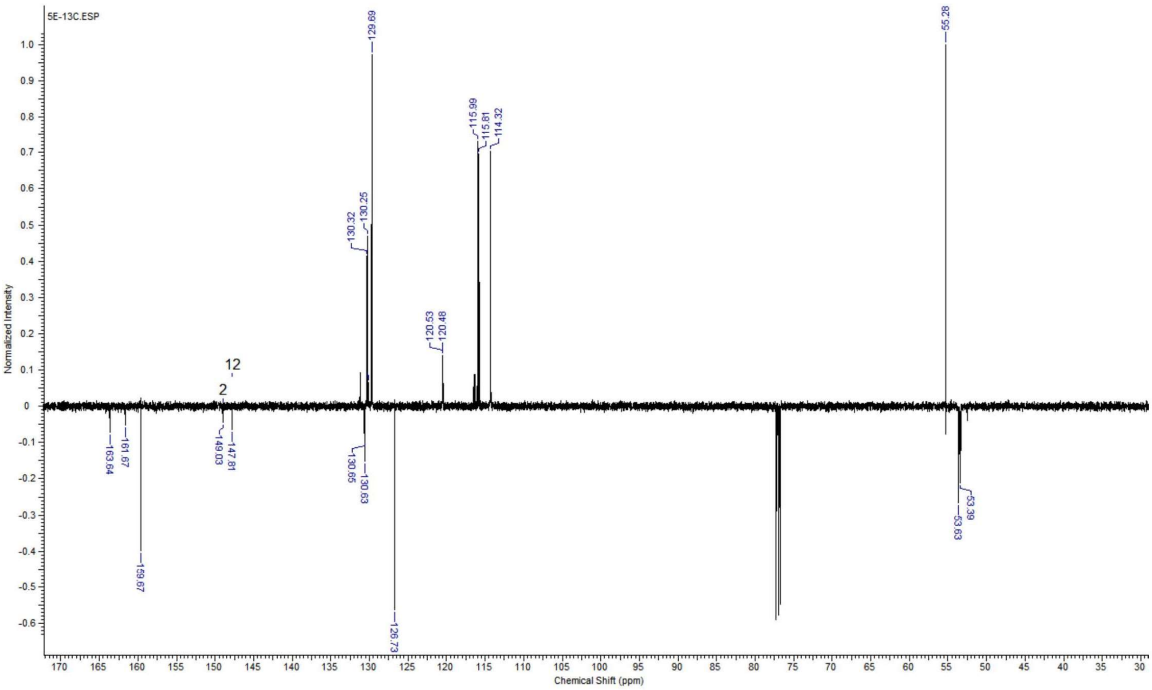

Fig. S 14: ^{13}C-ATP-NMR spectrum (126 MHz, $CDCl_3$) of complex **5e**.

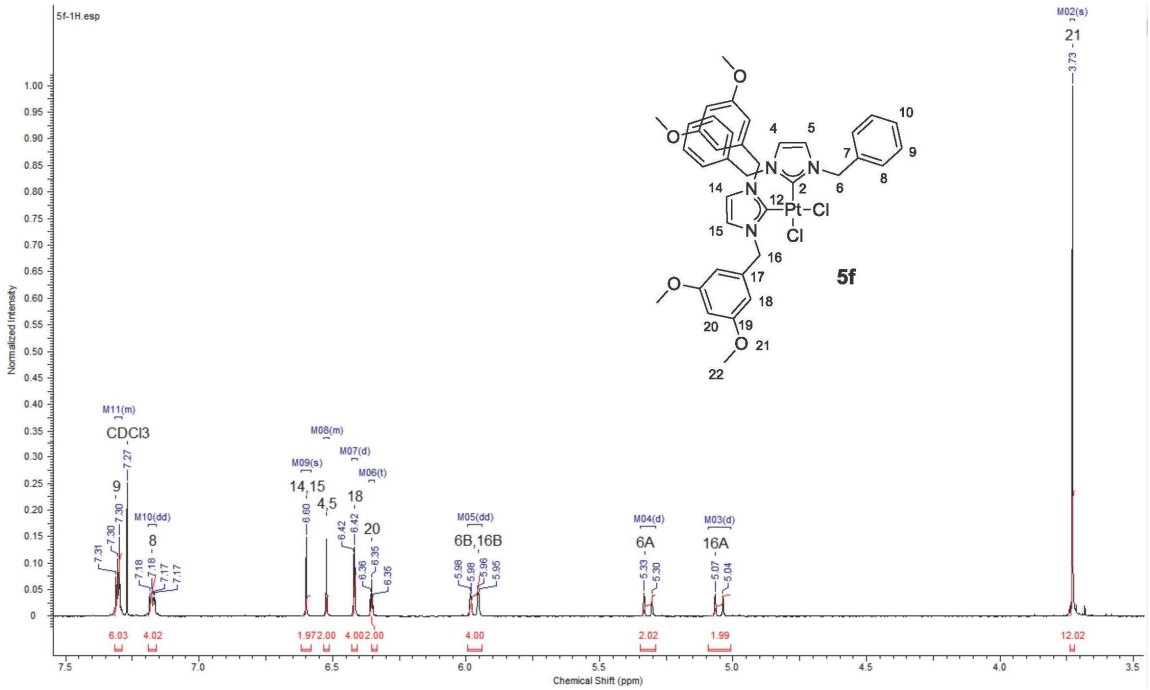

Fig. S15: ^{1}H-NMR spectrum (500 MHz, $CDCl_3$) of complex **5f**.

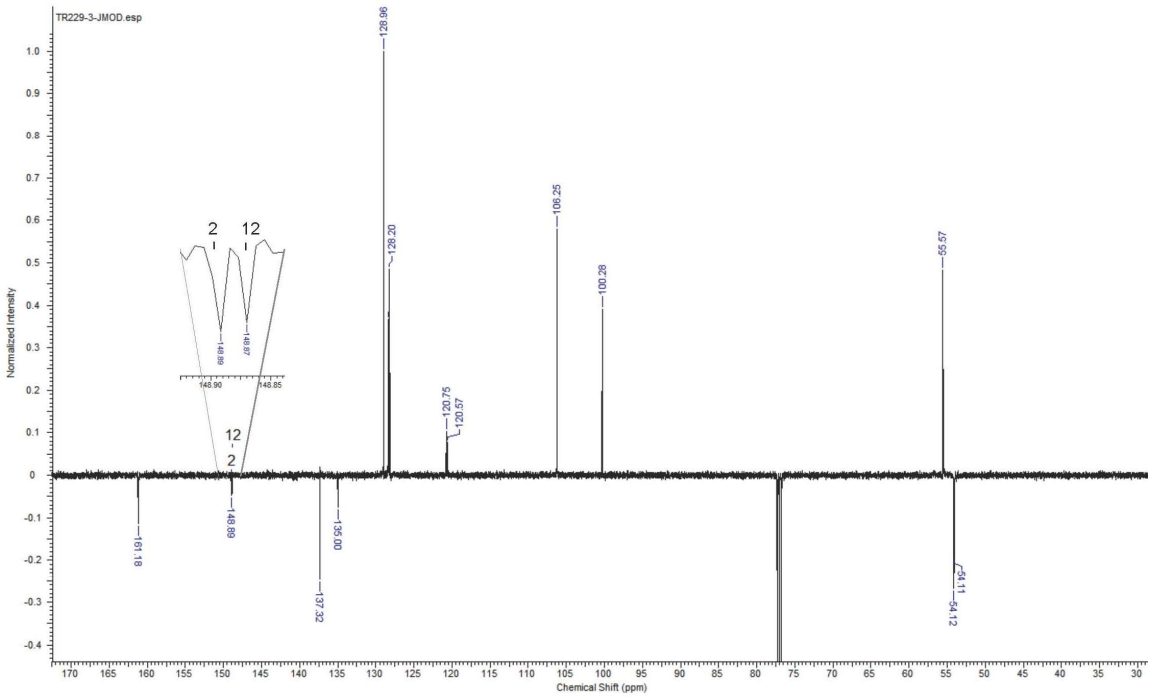

Fig. S 16: ^{13}C-ATP-NMR spectrum (126 MHz, $CDCl_3$) of complex **5f**.

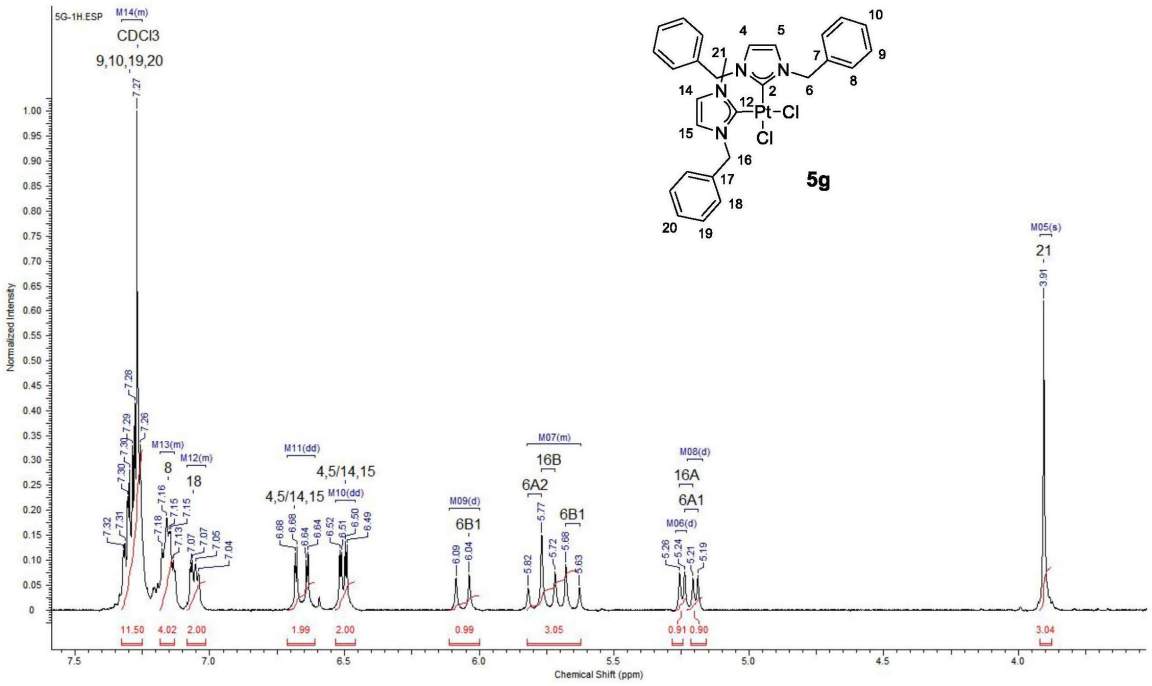

Fig. S17: ^{1}H-NMR spectrum (500 MHz, $CDCl_3$) of complex **5g**.

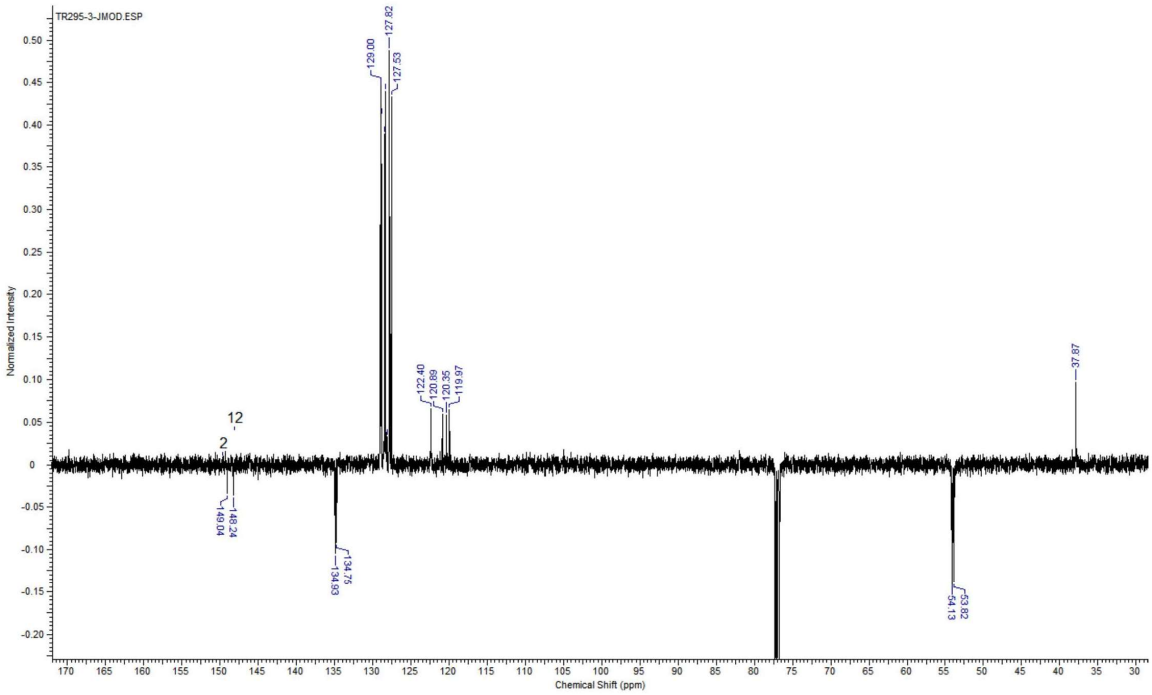

Fig. S 18: ^{13}C-ATP-NMR spectrum (126 MHz, $CDCl_3$) of complex **5g**.

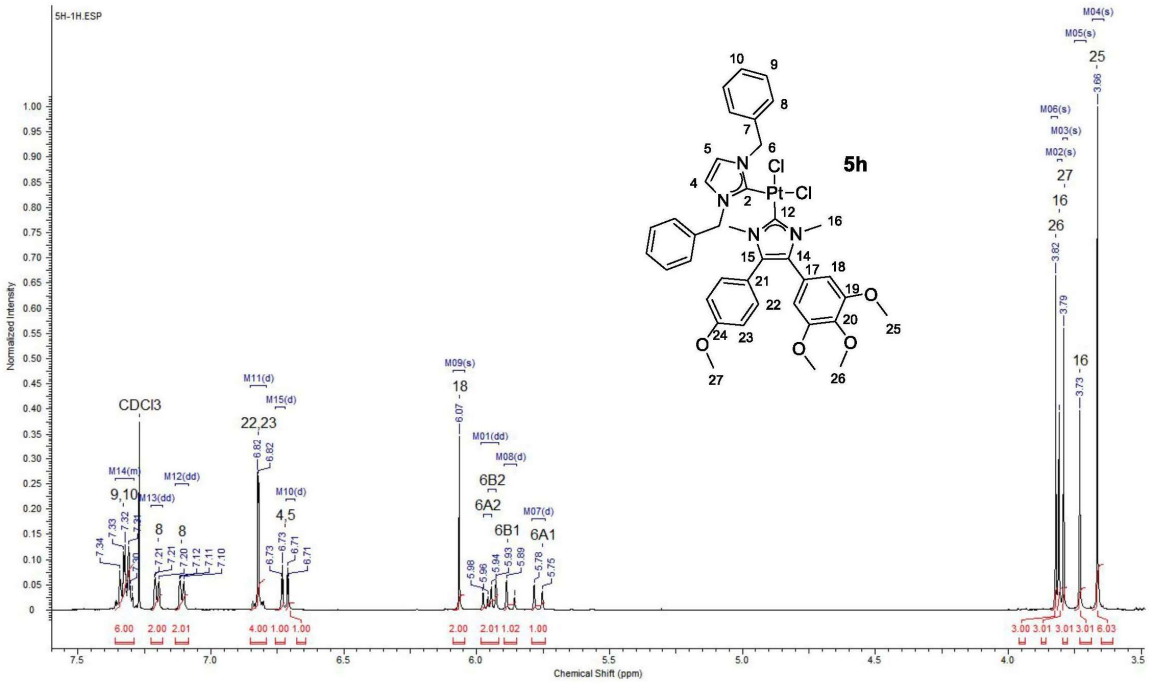

Fig. S19: ^{1}H-NMR spectrum (500 MHz, $CDCl_3$) of complex **5h**.

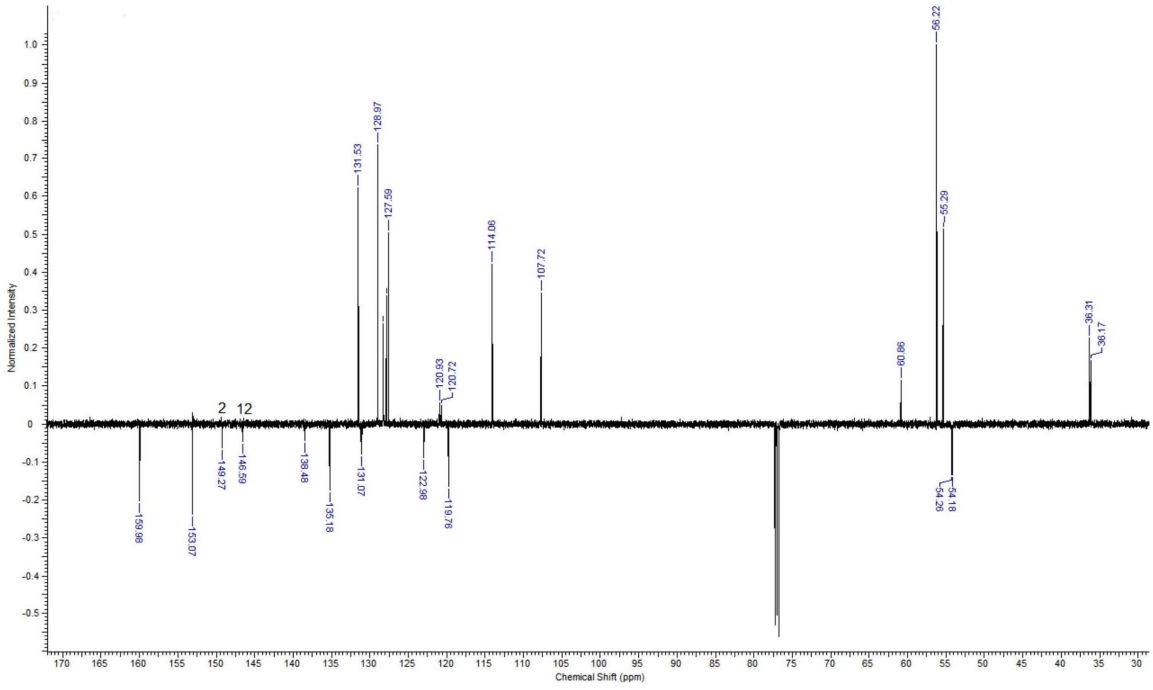

Fig. S 20: ^{13}C-ATP-NMR spectrum (126 MHz, $CDCl_3$) of complex **5g**.

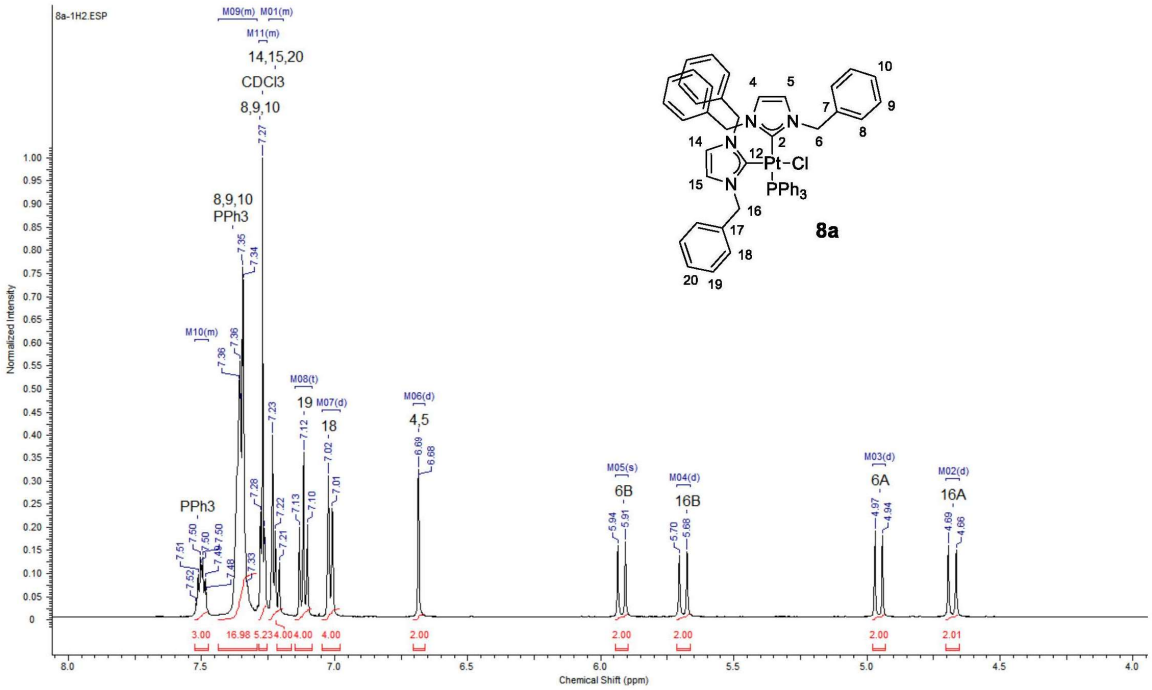

Fig. S 21: ^{1}H-NMR spectrum (500 MHz, $CDCl_3$) of complex **8a**.

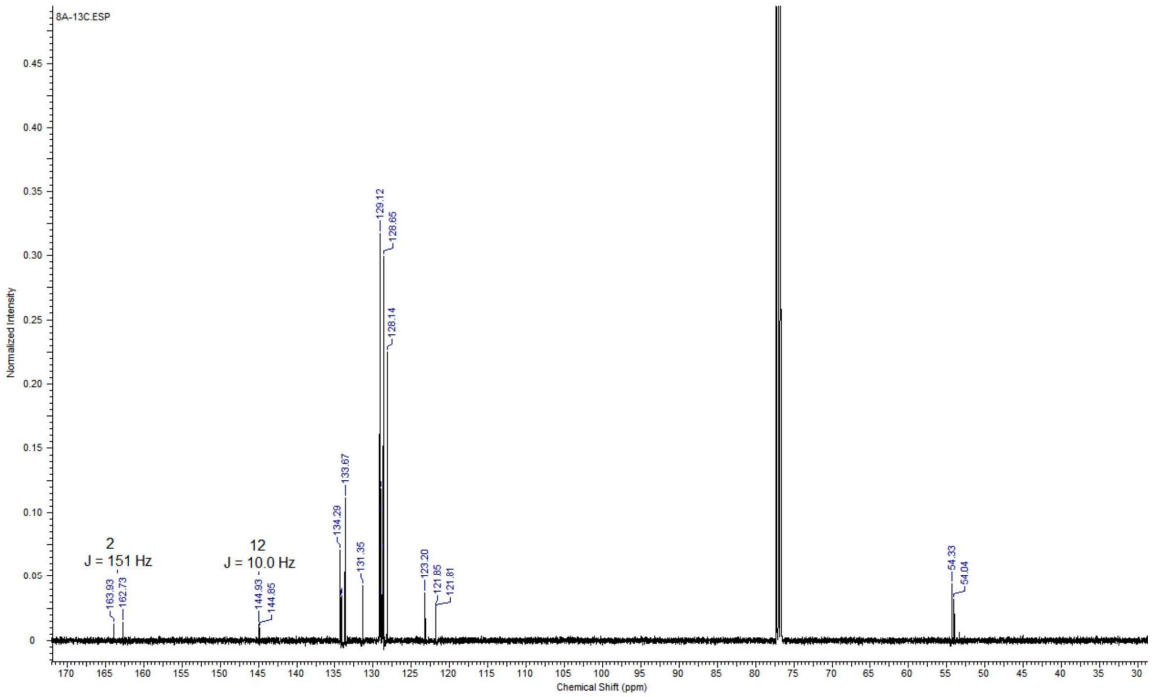

Fig. S 22: ^{13}C-NMR spectrum (126 MHz, $CDCl_3$) of complex **8a**.

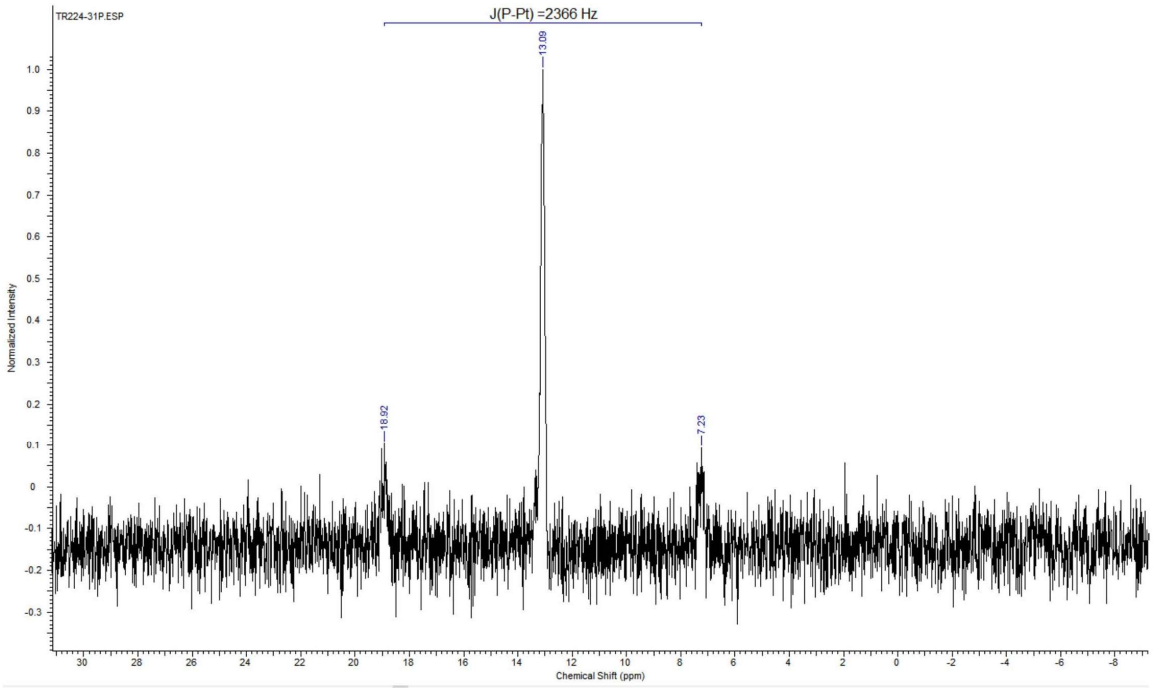

Fig. S 23: ^{31}P-NMR spectrum (202 MHz, $CDCl_3$) of complex **8a**.

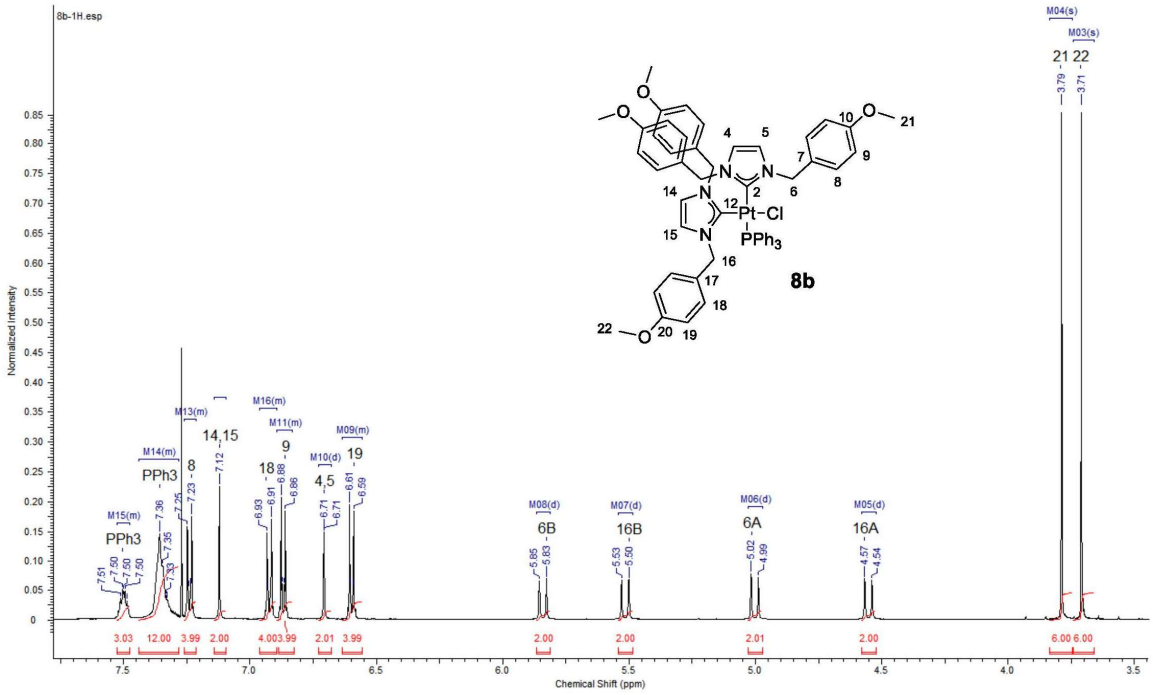

Fig. S 24: ^{1}H-NMR spectrum (500 MHz, $CDCl_3$) of complex **8b**.

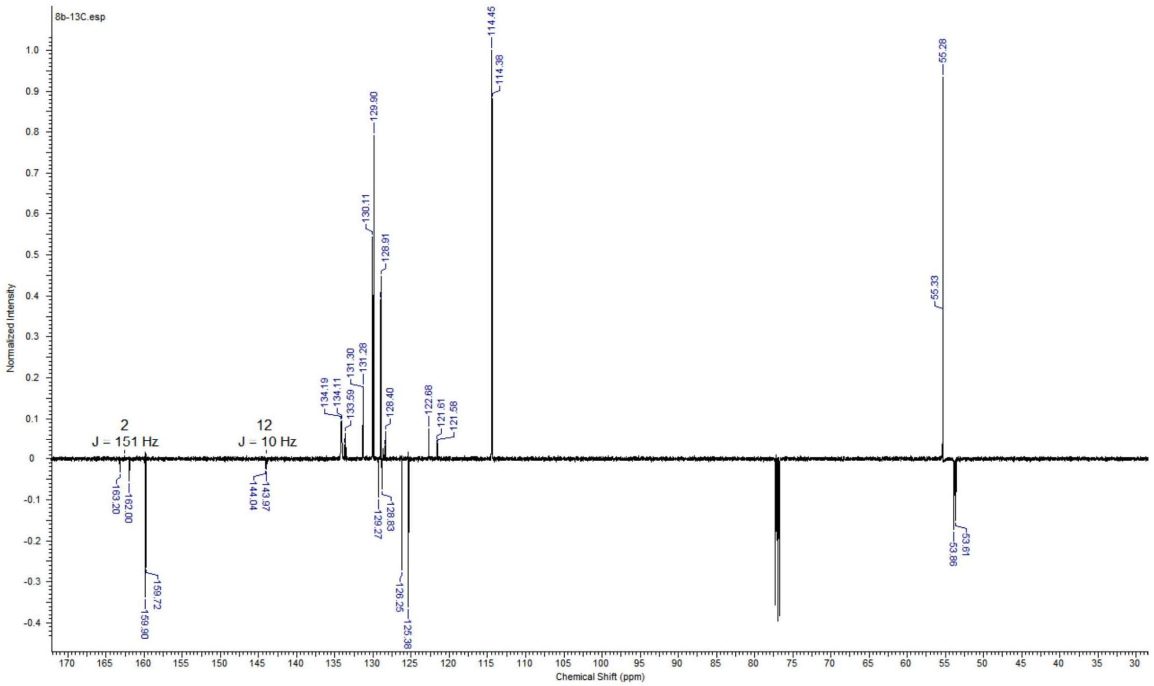

Fig. S 25: ^{13}C-ATP-NMR spectrum (126 MHz, $CDCl_3$) of complex **8b**.

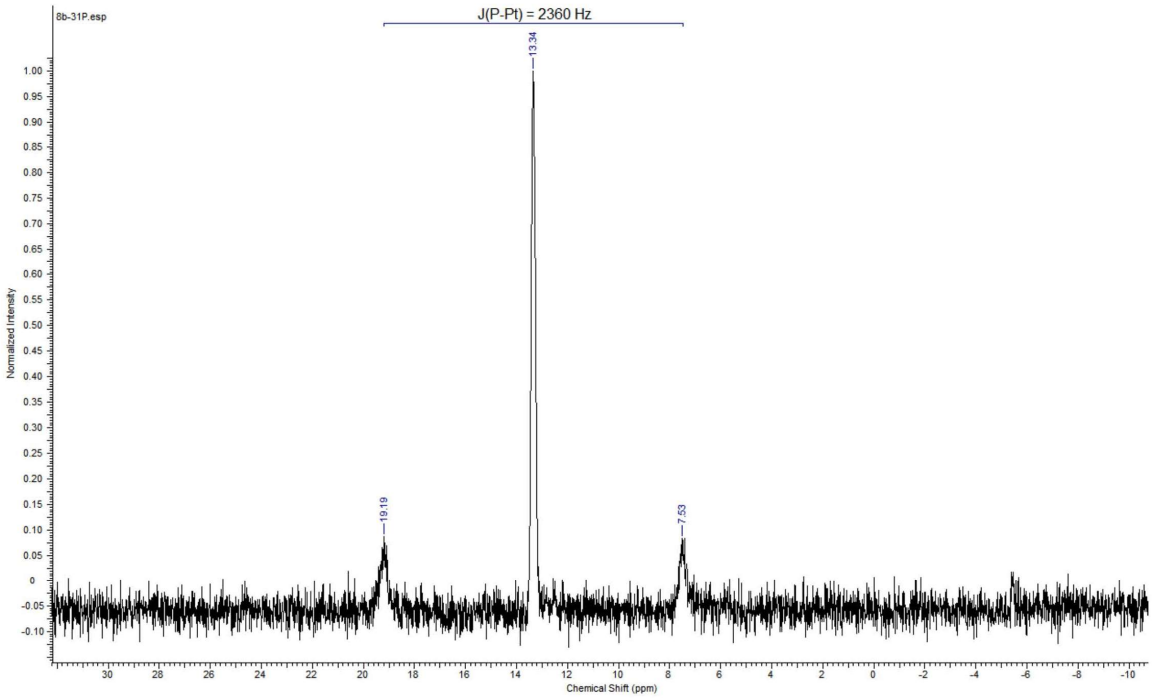

Fig. S 26: ^{31}P-NMR spectrum (202 MHz, $CDCl_3$) of complex **8b**.

References

[1] M. Bouhrara, E. Jeanneau, L. Veyre, C. Coperet, C. Thieuleux, *Dalton Trans.*, 2011, **40**, 2995.

[2] L. Naya, D. Vazquez-García, A. Fernandez, M. Lopez-Torres, I. Marcos, O. Lenis, M. Pereira, J. Vila, J. Fernandez, *J. Organomet. Chem.*, 2014, **772-773**, 192–201.

[3] K. Fujita, K. Inoue, J. Sato, T. Tsuchimoto and H. Yasuda, *Tetrahedron*, 2016, **72**, 1205–1212.

[4] H. Shirota, H. Matsuzaki, S. Ramati and J. Wishart, *J. Phys. Chem. B*, 2015, **119**, 9173–9187.

[5] J. Muenzner, T. Rehm, B. Biersack, A. Casini, I. de Graaf, P. Worawutputtapong, A. Noor, R. Kempe, V. Brabec, J. Kasparkova and R. Schobert, *J. Med. Chem.*, 2015, **58**, 6283–6292.

4.5 PUBLIKATION IV

„Synthesis, structures and cytotoxic effects in vitro of cis- and trans-[$Pt^{IV}Cl_4(NHC)_2$] complexes and their Pt^{II} precursors“

Dalton Transactions **2019**, 48, 16358

Tobias Rehm,[a] Matthias Rothemund,[a] Thomas Dietel,[b] Rhett Kempe[b] and Rainer Schobert*[a]

[a]Organic Chemistry Laboratory, University Bayreuth, Universitaetsstrasse 30, 95440 Bayreuth, Germany. E-mail: Rainer.Schobert@uni-bayreuth.de

[b]Lehrstuhl fuer Anorganische Chemie II (Catalyst Design), University Bayreuth, Universitaetsstrasse 30, 95440 Bayreuth, Germany

Dalton Transactions

PAPER

View Article Online
View Journal

Cite this: DOI: 10.1039/c9dt02438g

Synthesis, structures and cytotoxic effects *in vitro* of *cis*- and *trans*-[$Pt^{IV}Cl_4(NHC)_2$] complexes and their Pt^{II} precursors†

Tobias Rehm,[a] Matthias Rothemund,[a] Thomas Dietel,[b] Rhett Kempe[b] and Rainer Schobert *[a]

Received 8th June 2019,
Accepted 14th October 2019

DOI: 10.1039/c9dt02438g

rsc.li/dalton

Four new bis(*N*,*N*-dialkylbenzimidazol-2-ylidene)dichlorido platinum(II) complexes **2** featuring *N*-alkyl substituents of increasing size (**a**: Me, **b**: Et, **c**: *n*-butyl, **d**: *n*-octyl) were synthesised and oxidised with $PhICl_2$ to give the corresponding [$Pt^{IV}Cl_4$(*N*,*N*-dialkylbenzimidazol-2-ylidene)$_2$] complexes **4** as potential anticancer prodrugs. The known bis(*N*,*N*-dibenzylimidazol-2-ylidene)dichlorido platinum(II) complex **1** was likewise oxidised to [$Pt^{IV}Cl_4$(*N*,*N*-dibenzylimidazol-2-ylidene)$_2$] **3**. In contrast, oxidation of complexes **1** and **2** with H_2O_2 or hypochlorites, or exchange of chlorido for hydroxo ligands in tetrachlorido complexes **4** failed to give isolable complexes of type [$Pt^{IV}Cl_{4-n}(OH)_n$(NHC)$_2$]. In MTT assays the [$Pt^{II}Cl_2$(NHC)$_2$]/[$Pt^{IV}Cl_4$(NHC)$_2$] complex couples **1**/**3**, **2c**/**4c**, and *trans*-**2c**/*trans*-**4c**, bearing either *N*-benzyl or *N*-butyl substituents, each showed similar single-digit micromolar IC_{50} values against at least three out of five human cancer cell lines, presumably due to an intracellular reduction of the Pt^{IV} complexes to their active Pt^{II} congeners. Unlike cisplatin, whose anticancer effect requires functional p53, each of them was active both in wildtype and in p53-negative HCT116 colon carcinoma cells. In ethidium bromide saturation assays with isolated DNA, *cis*-(bis-NHC)Pt^{II} complexes such as **1** caused morphological DNA changes more pronounced than those initiated by cisplatin, while the corresponding *cis*-(bis-NHC)Pt^{IV} complexes such as **3** interacted with DNA in a less structure-modifying way.

Introduction

After the discovery of the biological effects of cisplatin by Barnett Rosenberg in the late 1960s, the FDA eventually approved it as the first platinum chemotherapeutic in 1978.[1] To this day it remains a mainstay drug for the treatment of certain tumour entities, *e.g.* testicular cancer.[2] Its severe side effects and often observed induction of resistance led to an ongoing search for better tolerated and more tumour specific Pt^{II} drugs such as carboplatin and oxaliplatin, that are being clinically applied worldwide (Fig. 1). A more recent line of platinum drug refinement was the development of Pt^{IV} complexes which are thought to act as prodrugs, being themselves less toxic then Pt^{II} complexes, more resistant to substitution, and pharmacologically more adjustable by attaching further axial ligands to the metal centre. Since cancer cells are more hypoxic than nonmalignant cells, Pt^{IV} prodrugs are believed to be reduced and so activated predominantly in cancerous tissues thus minimising unwanted side effects. Upon reduction of the Pt^{IV} prodrug to give the active Pt^{II} drug proper, any axial ligands with additional anticancer effects are released and so enhance the overall impact.[3]

So far only a few Pt^{IV} complexes made it into clinical trials and none of them exhibited significantly greater activity than

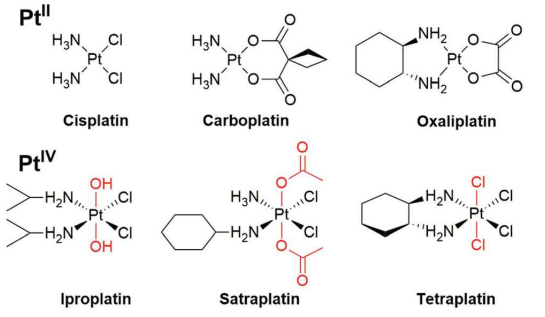

Fig. 1 Structures of approved platinum(II) anticancer drugs and investigational Pt^{IV} prodrugs that entered clinical trials.

[a]Organic Chemistry Laboratory, University Bayreuth, Universitaetsstrasse 30, 95440 Bayreuth, Germany. E-mail: Rainer.Schobert@uni-bayreuth.de
[b]Lehrstuhl fuer Anorganische Chemie II, University Bayreuth, Universitaetsstrasse 30, 95440 Bayreuth, Germany

†Electronic supplementary information (ESI) available: NMR spectra; X-ray structural data. CCDC 1912954 and 1912955. For ESI and crystallographic data in CIF or other electronic format see DOI: 10.1039/c9dt02438g

cisplatin.[4] The first-generation Pt^{IV} prodrugs iproplatin, satraplatin, and tetraplatin consist of cisplatin-analogous square planar *cis*-dichlorido-diamino platinum fragments carrying two biologically innocent axial ligands such as chlorido, hydroxo or acetato, respectively. In recent years more diversified Pt^{IV} complexes have been developed by attaching ancillary drugs or cancer-targeting units as axial ligands to the original Pt^{II} complex fragment.[5–7]

Pt^{IV} complexes with N-heterocyclic carbene (NHC) ligands were investigated for their medicinal potential only recently,[8] despite a rich literature on the synthesis and structures of such complexes with mono-NHC,[9a] *trans*-bis(NHC),[9b] chelating[9a,c,d] and non-chelating[9e] *cis*-bis(NHC), or even tris(NHC)[9a] ligand spheres.

In the past, our group has synthesised bioactive Pt^{II} complexes with (benz)imidazol-2-ylidene ligands in combination with DMSO or phosphine ligands and we also developed a protocol that allows the successive introduction of two different NHC ligands to afford *cis*-$[Pt^{II}Cl_2(NHC)^1(NHC)^2]$ complexes.[10] In continuation of this work, we now report on the synthesis, structures and anticancer effects of four new benzimidazol-2-ylidene complexes *cis*-$[Pt^{II}Cl_2(NHC)_2]$ **2a–d** as well as the *trans*-isomer *trans*-**2c**, and on their oxidation products, including six new complexes $[Pt^{IV}Cl_4(NHC)_2]$ **3**, **4a–d** and *trans*-**2c** (Fig. 2).

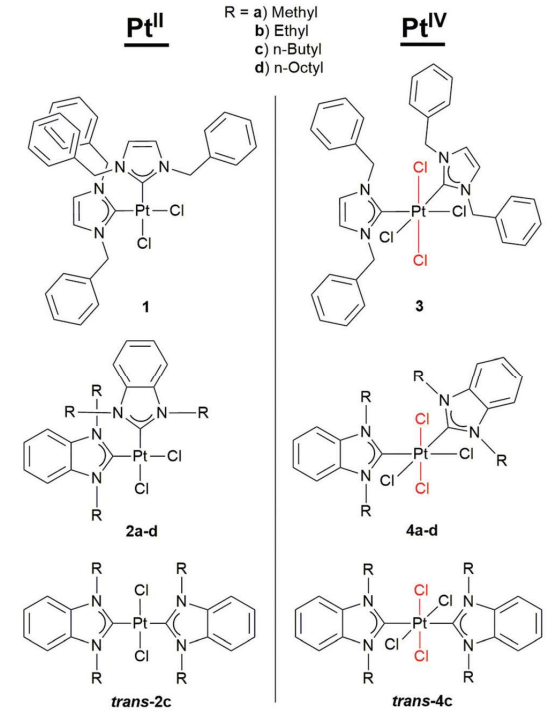

Fig. 2 Structures of 1 and the eleven newly synthesised complexes **2a–d**, *trans*-**2c**, **3**, **4a–d** and *trans*-**4c**.

Results and discussion

Synthesis and characterisation

Following established protocols[10b,c,11] the known benzimidazolium chlorides **5** (**a**: Me, **b**: Et, **c**: *n*-butyl, **d**: *n*-octyl) were treated with silver(I) oxide to afford the corresponding silver carbene complexes **6** which in turn were transmetalated with K_2PtCl_4 in DMSO to leave the *cis*-$[Pt^{II}Cl_2(DMSO)(NHC)]$ complexes **7**.[10c] Substitution of their DMSO by a second NHC ligand, prepared *in situ* from the same benzimidazolium chloride **5** and KOtBu, gave the new biscarbene complexes **2a–d**. The Pt^{II} complex *trans*-**2c** was obtained by treating silver complex **6c** with only half an equivalent of K_2PtCl_4 in dichloromethane.[11] While in DMSO the complex *cis*-$[Pt^{II}Cl_2(DMSO)_2]$ is formed as an intermediate leading to *cis* complexes **7**, in CH_2Cl_2 the *trans* effect of the first NHC at the Pt^{II} centre directs the second NHC into *trans* configuration.

Oxidation of Pt^{II} to Pt^{IV} complexes is customarily performed by means of hydrogen peroxide, bromine or chlorine.[12] Also frequently used and better manageable than chlorine is iodobenzene dichloride ($PhICl_2$), obtained from iodobenzene, NaOCl and HCl.[8,13] By stirring with 10 equivalents of $PhICl_2$ in CH_2Cl_2 for several hours Pt^{II} complexes **1**, **2** and *trans*-**2c** were converted to their respective $[Pt^{IV}Cl_4(NHC)_2]$ complexes **3**, **4** and *trans*-**4c** with retained stereochemistry (Scheme 1).

The new Pt^{II} and Pt^{IV} complexes were characterised by ^1H, ^{13}C and ^{195}Pt NMR spectroscopy, mass spectrometry, and elemental analysis. Crystal structure analyses were carried out for complexes **2c** and **3**. The *N*-methyl substituted Pt^{IV} complex **4a** turned out to be insufficiently soluble in all tested solvents suitable for NMR analysis and was therefore characterised only by elemental analysis and mass spectrometry.

The ^1H NMR spectra of complexes **2b–d** show an inequivalence of the two geminal protons of the CH_2 groups – one proton facing the neighbouring chlorido ligand, the other facing the neighbouring NHC ligand – resulting in two split signals. This effect is strongest for the N–CH_2 groups and peters out along the chain for **2c** and **2d**. While the N–CH_2–CH_3 protons in **2b** show two doublets of quartets (dq), complexes **2c** and **2d** show two ddd's for their N–CH_2 protons corroborating the *cis* configuration of the NHC ligands as well as a perpendicular orientation of the benzimidazole ligands relative to the plane spanned by the $PtCl_2$ fragment. Complex *trans*-**2c**, in contrast, exhibits no split signals since the geminal N–CH_2 protons possess identical environments.[10a]

The ^1H NMR spectra of the Pt^{IV} complexes **3** and **4** show even more complex coupling patterns. In comparison to the Pt^{II} complexes the N–CH_2 protons lead to four dq or td, respectively, instead of just two signals, indicating that the NHC ligands, after addition of the axial chlorido ligands, rotate away from a perpendicular orientation into the space between the axial and equatorial ligands, as confirmed by crystallography (Fig. 3). Thus, one alkyl residue of each NHC faces two chlorido ligands, while the second alkyl residue leans towards one chloride and the neighbouring NHC ligand giving

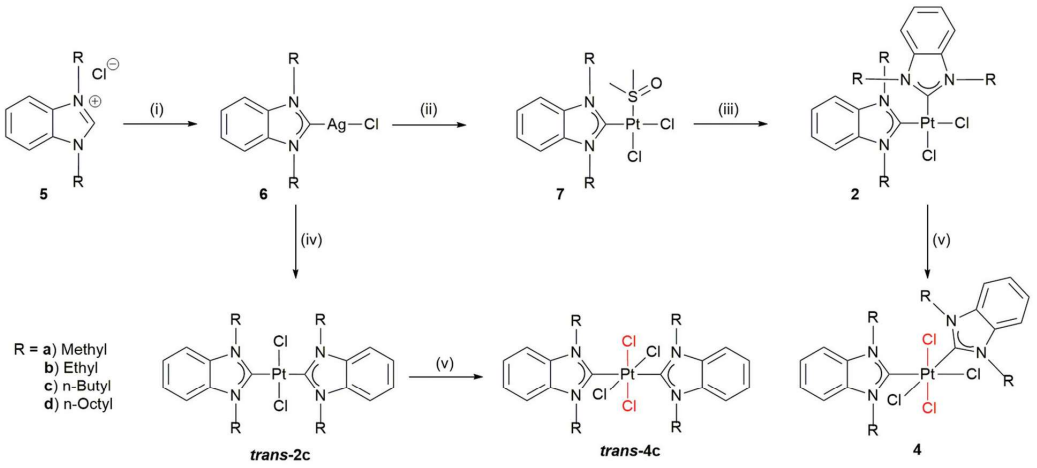

Scheme 1 Synthesis of complexes **2a–d**, *trans*-**2c**, **4a–d** and *trans*-**4c**. Reagents and conditions: (i) Ag_2O, CH_2Cl_2, rt; (ii) K_2PtCl_4, DMSO, 60 °C; (iii) **5**, KO^{t}Bu, dry CH_2Cl_2, Ar atmosphere, rt; (iv) 0.5 eq. K_2PtCl_4, CH_2Cl_2, rt; (v) $PhICl_2$, CH_2Cl_2, rt.

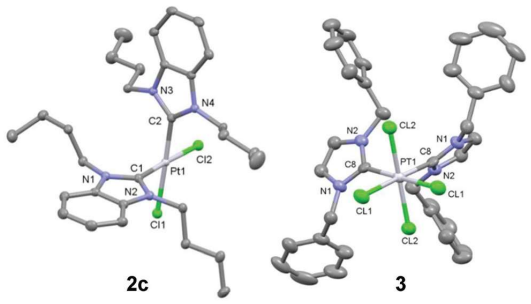

Fig. 3 Molecular structures of complexes **2c** and **3** as thermal ellipsoid representations at the 50% probability level (H atoms omitted). Selected bond lengths [Å], angles [°] and torsion angles [°]: **2c**: Pt1–Cl1 2.3582(10), Pt1–Cl2 2.3571(8), Pt1–C1 1.972(2), Pt1–C2 1.972(2), Cl1–Pt1–Cl2 90.657(17), Cl1–Pt1–C1 86.55(6), Cl2–Pt1–C2 88.50(5), C1–Pt1–C2 94.32(8) N1–C1–N2 106.27(16), N3–C2–N4 106.52(16), Cl1–Pt1–C1–N1 89.3(1), Cl1–Pt1–C1–N2 85.7(8), Cl2–Pt1–C2–N3 85.9(5), Cl2–Pt1–C2–N4 92.9(5); **3**: Pt1–Cl1 2.379(2), Pt1–Cl2 2.330(2), Pt1–C8 2.050(9), Cl1–Pt1–Cl1 85.50(13), Cl1–Pt1–Cl2 85.83(8), Cl1–Pt1–Cl2 90.61(8), Cl2–Pt1–Cl2 175.12(11), Cl1–Pt1–C8 91.7(3), Cl1–Pt1–C8 177.8(2), Cl2–Pt1–C8 87.9(2), Cl2–Pt1–C8 95.5(2), C8–Pt1–C8 90.0(5), N1–C8–N2 106.5(8); Cl2–Pt1–C8–N1 46.8(4), Cl2–Pt1–C8–N2 49.1(6), Cl1–Pt1–C8–N1 43.9(4), C8–Pt1–C8–N2 46.3(6).

a distinct signal splitting (*cf.* Fig. S19, ESI†). Again, the spectra of complex *trans*-**4c** showed no such proton inequivalence.

In the ^{13}C NMR spectra the carbene signals, which are highly diagnostic, agree with these results.[10] The N–*C*–N signals of complexes **2a–d** lay at 158.8–159.5 ppm while, typical of *trans* configured Pt^{II} complexes, *trans*-**2c** showed a downfield signal at 178.0 ppm.[10a,14] When oxidised to $[Pt^{IV}Cl_4(NHC)_2]$ complexes the carbene signals appeared upfield at 136.0–136.8 ppm for the *cis* complexes and at 147.5 ppm for *trans*-**4c**.

With −3622 to −3660 ppm (*cis*) and −3245 ppm (*trans*) the ^{195}Pt NMR signals of all Pt^{II} compounds were in the expected range. Pt^{IV} complexes showed downfield signals at −1427 to −1430 ppm for **4b–d**, at −1250 ppm for complex **3**, and at −1051 ppm in the case of *trans*-**4c**.

For an estimate of the stability of the new Pt^{IV} complexes under biological conditions, a DMSO/water solution of **4b** was monitored over 16 h by ESI-MS. It showed, aside of other minor platinum species, a continuously increasing peak cluster with main peak at m/z = 579 and an isotopic pattern typical of a $[Pt^{II}Cl(NHC)_2]^+$ species. In keeping with that, the UV/vis spectrum of **4b** in DMSO/water showed a steadily decreasing absorption and a change of the band shapes between 230 and 730 nm (*cf.* ESI, Fig. S37–39†).

As Pt^{IV} hydroxo complexes with NHC ligands have not been published yet, we also investigated the oxidation of complexes **1** and **2** with H_2O_2 or hypochlorites[15] as well as an exchange of chlorido for hydroxo ligands in **4** to give $[Pt^{IV}Cl_{4-n}(OH)_n(NHC)_2]$ complexes. However, these were not accessible in this way, although we had some indication of a transient species of this type in the hypochlorite oxidation of complex **2b** (*cf.* ESI†).

Crystallography

Crystals suitable for X-ray diffraction analyses were grown by slow infusion of hexane or diethyl ether into saturated solutions of **2c** in CH_2Cl_2 or **3** in $CHCl_3$ kept at 4 °C. Fig. 3 shows their molecular structures. The Pt–C bond lengths were 1.972 Å for **2c** and 2.050 Å for **3**. The latter is 0.082 Å longer than the corresponding bond in the previously published Pt^{II} complex **1**.[10b] The Pt–Cl^{axial} distances of **3** are 2.330 Å and so slightly shorter than the Pt–Cl^{equat} bonds of **2c** (2.357–2.358 Å) and **1** (2.379 Å). The X-ray diffraction analysis of **3** revealed the NHC ligand rotation away from a perpendicular orientation of its plane relative to the plane spanned by the $PtCl_2^{equat}$ frag-

ment as in Pt^{II} complex **1**.[10b] The torsion angle between these two planes lies between 43.94° and 49.16° for octahedral complex **3** (Fig. 3) and is about 90° for square-planar Pt^{II} complexes **2c** and **1**.

Cytotoxicity

The antiproliferative effect and tumour specificity of the new Pt^{II} and Pt^{IV} complexes were evaluated by means of MTT (3-(4,5-dimethylthiazol-2-yl)-2,5-diphenyltetrazolium bromide) assays on a panel of three human colon carcinoma and a melanoma cell lines, chosen because platinum drugs are part of the most used standard chemotherapy regimens for the treatment of advanced colorectal carcinoma (FOLFOX) and melanoma (TMZ-CDDP), as well as on nonmalignant dermal fibroblasts. For wildtype and p53 knock-out mutant HCT116 colon carcinoma cells we also calculated r^{p53} (= $(IC_{50}{}^{wt}/IC_{50}{}^{-/-}) - 1$) as a measure for the dependency of the complex cytotoxicity on the integrity of the proapoptotic p53-gene which is frequently mutated in cancers. The IC_{50} values of the complexes and their r^{p53} values are listed in Table 1. Of the four *cis*-[(1,3-dialkylbenzimidazol-2-ylidene)$_2$Cl$_2$]Pt^{II} complexes **2a–d** only the *N*-butyl substituted complex **2c** showed a significant cytotoxicity, with low single-digit IC_{50} values against three of the five tested cancer cell lines. This resembles the structure–activity pattern of the *cis*-[(1,3-dialkylbenzimidazol-2-ylidene)(PPh_3)Cl$_2$]Pt^{II} complexes on which we had reported earlier.[10c] Their derivative with *N*-alkyl = methyl was, like **2a**, inactive against the same cell lines, while that bearing an *N*-butyl residue was, like **2c**, distinctly more active than the *N*-octyl derivative. However, unlike the inactive complex **2b**, the *cis*-[(1,3-diethylbenzimidazol-2-ylidene)(PPh_3)Cl$_2$]Pt^{II} complex was highly cytotoxic. The reasons for these structure–activitiy relations are yet unknown, but are unlikely to be correlated to different intracellular complex concentrations as we know from previous uptake studies with the mono-NHC complexes.

Complexes **4a** and **4d** were poorly soluble in aqueous media and so not tested. While Pt^{II} complex **2b** showed no significant cytotoxic activity, its corresponding Pt^{IV} complex **4b** was moderately active with IC_{50} values in the double-digit, or even single-digit micromolar range in the case of DLD-1 colon carcinoma cells. This discrepancy might be due to a higher uptake, to a diminished deactivation/efflux, or to additional modes of action of Pt^{IV} complex **4b**.[15] It showed no antiproliferative effect on the nonmalignant fibroblasts. The butyl substituted complexes **2c** (Pt^{II}) and **4c** (Pt^{IV}) showed a strikingly similar activity pattern with low single-digit micromolar IC_{50} values against 518A2 melanoma, HT-29 and DLD-1 colon carcinoma cells.

To investigate the effect the *cis*-/*trans*-orientation of the NHC ligands has on the cytotoxic activity, complexes *trans*-**2c** and *trans*-**4c** with opposite dibutyl substituted NHC ligands were synthesised and investigated for their cytotoxic activities. Somewhat reminiscent of the butyl-NHC couple **2c**/**4c** both *trans* complexes showed similar and high antiproliferative activities against all cancer cell lines but the 518A2 melanoma. All active complexes **2** and **4** were also more active against the p53 knock out mutant than the wildtype HCT116 cells ($r^{p53} > 0$). For comparison, the IC_{50} values of imidazol-2-ylidene complex **1**, whose biological activity we had reported previously, were added.[10b] Pt^{II} complex **1** and its corresponding Pt^{IV} complex **3** showed a similar antiproliferative effect in most of the cell lines with low single-digit micromolar IC_{50} values, except for the nonmalignant HDfa cells where the Pt^{IV} complex **3** was only a fifth as toxic as the Pt^{II} complex **1**.

DNA interaction

To confirm the general assumption that Pt^{IV} complexes are biologically more inert than Pt^{II} complexes, the DNA interaction of the best soluble Pt^{II} and Pt^{IV} congeners **1** and **3** was investigated by means of ethidium bromide (EtdBr) saturation assays with linear salmon sperm DNA (Fig. 4). The Pt^{II} complex **1** led to a pronounced concentration-dependent attenuation of the EtdBr fluorescence indicating a strong interaction of **1** with the DNA, which exceeded that of cisplatin by far. This is in keeping with the results obtained previously for similar (bis-NHC)Pt^{II} complexes.[10] Unlike complex **1** and cisplatin, the Pt^{IV} complex **3** caused only a slight reduction of the EtdBr fluorescence. Whether this weak effect is due to a real platination of, *i.e.* coordination to, the DNA bases or merely to

Table 1 Means ± SD of IC_{50} (72 h) values [μM] of complexes **1**, **2a–d**, **3**, **4b–c**, *trans*-**2c** and *trans*-**4c** in MTT assays against human cancer cell lines[a] and nonmalignant dermal fibroblasts HDFa as calculated from four independent measurements

	IC_{50} (72 h) [μM]									
Compounds	**1**[10b]	**3**	**2a**	**2b**	**4b**	**2c**	**4c**	**2d**	*trans*-**2c**	*trans*-**4c**
518A2[a]	6.2 ± 0.4	3.7 ± 0.1	>100	>50	18.1 ± 1.7	1.3 ± 0.1	1.7 ± 0.2	>50	9.6 ± 0.9	17.8 ± 0.5
HT29[a]	14.6 ± 1.4	22.0 ± 0.3	>100	n.d.	35.4 ± 1.7	3.4 ± 0.1	5.7 ± 1.2	>50	2.7 ± 0.3	2.9 ± 0.7
DLD-1[a]	4.7 ± 1.4	2.0 ± 0.3	n.d.	>50	7.9 ± 1.9	3.3 ± 0.1	4.2 ± 0.9	>100	2.0 ± 0.5	3.0 ± 0,2
$HCT116^{wt}$ [a]	2.3 ± 0.8	4.6 ± 1.0	>50	>100	32.8 ± 3.3	18.3 ± 1.1	32.8 ± 3.3	>50	3.8 ± 0.5	3.0 ± 0.5
$HCT116^{-/-}$ [a]	2.2 ± 0.6	9.0 ± 0.5	n.d.	>50	17.5 ± 2.3	12.5 ± 0.7	11.4 ± 0.8	>50	1.7 ± 0.1	1.6 ± 0.6
HDfa	3.8 ± 0.1	17.5 ± 0.6	>100	n.d.	>50	20.7 ± 3.3	8.1 ± 0.6	>50	6.0 ± 0.3	13.2 ± 0.5
r^{p53} [b]	0.05	-0.49	—	—	0.87	0.46	4.76	—	1.24	0.88

[a] 518A2 – melanoma, HT-29 – colon adenocarcinoma, DLD-1 – Dukes type C colorectal adenocarcinoma, $HCT116^{wt}$ – colon carcinoma (wildtype); $HCT116^{-/-}$ – colon carcinoma (p53 knock-out mutant). [b] p53 dependency of IC_{50} values in HCT116 colon carcinoma cells, indicated by $r^{p53} = (IC_{50}{}^{wt}/IC_{50}{}^{-/-}) - 1$.

View Article Online
Dalton Transactions Paper

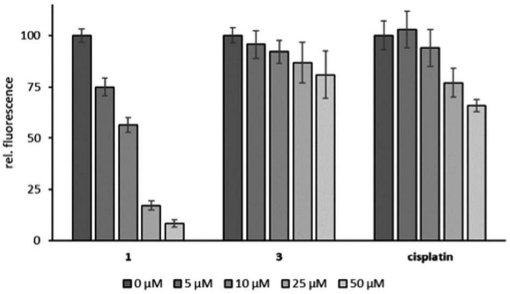

Fig. 4 Relative fluorescence intensities of ethidium bromide after intercalation into salmon sperm DNA treated with 1, 3 or cisplatin for 2 h.

an electrostatic interaction, or to an intercalation of the planar NHC ligands into the DNA helix, remains to be clarified. It seems, however, obvious that bis-NHC complexes of Pt^{II} show a higher affinity for DNA than their Pt^{IV} analogues. Attempts to "switch on" the DNA affinity of complex **3** *in situ* by adding ascorbic acid as a reductant failed (data not shown). This is in line with findings of Gibson *et al.*, who reported that Pt^{IV} complexes are reduced in cells by high molecular weight, membrane-associated molecules (>3000 Da) rather than small ones such as GSH or ascorbic acid.[16] This would also go a long way towards explaining the similar antiproliferative effects of some Pt^{II}/Pt^{IV} complex couples in our MTT cell tests.

Conclusions

The oxidation of complexes **2** and of the known bis(*N*,*N*-dibenzylimidazol-2-ylidene)dichlorido platinum(II) complex **1** with $PhICl_2$ afforded the new stable $[Pt^{IV}Cl_4(NHC)_2]$ complexes **3** and **4** in excellent yields. In contrast, hydroxo complexes of type $[Pt^{IV}Cl_{4-n}(OH)_n(NHC)_2]$ were generally not accessible by oxidation of **1** or **2** with H_2O_2 or hypochlorites, or by exchange of chlorido for hydroxo ligands in tetrachlorido complexes **4**, presumably due to their inherent instability. For future approaches to hydroxo-ligated (bis-NHC)Pt^{IV} complexes, it might be advisable to employ electron-withdrawing residues on the NHC ligands to attenuate their strong donor effect.

The IC_{50} values of the $[Pt^{II}Cl_2(NHC)_2]/[Pt^{IV}Cl_4(NHC)_2]$ complex couples **1**/**3**, **2c**/**4c**, and *trans*-**2c**/*trans*-**4c** against the five selected tumour cell lines were each quite similar and in a clinically meaningful range for most cell lines. This may be rationalised by assuming an intracellular reduction of the Pt^{IV} complexes to their active Pt^{II} congeners. What needs to be done now, is to determine the speed and extent of the cellular uptake of corresponding Pt^{II}/Pt^{IV} complex couples. Under a clinical aspect it is also worthy of note that each of these complexes was of similar activity both in wildtype and in p53-negative HCT116 colon carcinoma cells, in stark contrast to the mentioned [(1,3-dialkylbenzimidazol-2-ylidene)Cl_2L]Pt^{II} complexes and to the mainstay drug cisplatin which rely on functional p53.

Our EtdBr saturation experiments with DNA in a cell-free context suggest that *cis*-(bis-NHC)Pt^{II} complexes such as **1** cause morphological changes to DNA more pronounced than those initiated by cisplatin, while the corresponding *cis*-(bis-NHC)Pt^{IV} complexes such as **3** interact with DNA in a different, less structure-modifying way. This also corroborates the assumption of an intracellular reduction of the latter so as to achieve the antiproliferative effects against cancer cells similar in magnitude to those of the respective Pt^{II} congener. The fact that the *trans* complexes are on average as active as their *cis* analogues hints at a mode of action not involving DNA metalation. Further studies into the uptake, intracellular distribution and details of the modes of action of the new (bis-NHC)Pt^{IV} complexes are now indicated. Their prodrug character and their unique positive features when compared with the established platinum drugs make them interesting candidates for further development.

Experimental

Materials and methods

All chemicals and reagents were purchased from Sigma Aldrich, Alfa Aesar, ChemPur or ABCR and were used without further purification. Melting points are uncorrected; NMR spectra were run on a 500 MHz spectrometer; chemical shifts are given in ppm (δ) and referenced relative to the internal solvent signal; ^{195}Pt NMR shifts are quoted relative to $\Xi(^{195}Pt)$ = 21.496784 MHz, K_2PtCl_4 was used as external standard (δ = −1612.81); mass spectra: direct inlet, EI, 70 eV; elemental analyses: Vario EL III elemental analyser; X-Ray diffractometer: STOE-IPDS II. All biotested compounds were >95% pure by elemental analysis. Synthesis of **1** and precursors **5**, **6c** and **7** was performed as described in the literature.[10b,c] Abbreviations used for NMR signal attribution: Ar = aromatic; BI = Benzimidazole; Cq = quaternary Carbon; Imi = Imidazole.

Syntheses and characterisation

General synthesis of *cis*-$[Pt^{II}Cl_2(NHC)_2]$ complexes 2. The *cis*-$[Pt^{II}Cl_2(DMSO)(NHC)]$ complexes **7** (1 eq.) and the respective benzimidazolium chlorides **5** (1.2 eq.) in dry CH_2Cl_2 were treated with KO^{t}Bu (1.5 eq.) under an argon atmosphere and stirred for 72 h at ambient temperature. After filtration the solvent was reduced *in vacuo* and the product was precipitated by addition of diethyl ether at 4 °C. Lipophilic complex **2d** could not be precipitated and was purified by column chromatography.

***cis*-Dichlorido-bis(1,3-dimethylbenzimidazol-2-ylidene) platinum(II) (2a).** **7a** (200 mg, 408 µmol), **5a** (75 mg, 408 µmol, 1 eq.), KO^{t}Bu (63 mg, 612 µmol, 1.5 eq.), CH_2Cl_2 (25 mL). Yield: 82 mg (146 µmol, 36%); colourless solid of m.p. >400 °C; elemental analysis (%): calc. for $C_{18}H_{20}N_4Cl_2Pt$ (558.37): C, 38.72; H, 3.61; N, 10.03. Found: C, 38.05; H, 4.048; N, 9.921. ^{1}H NMR (500 MHz, DMSO-d_6): δ 4.10 (12 H, s, CH_3), 7.34 (4 H, dd, J = 6.1, 3.1 Hz, BI), 7.63 (4 H, dd, J = 6.1, 3.1 Hz, BI); ^{13}C NMR (125 MHz, DMSO-d_6): δ 34.7 (CH_3), 110.3 (BI),

123.8 (BI), 134.3 (BI-Cq), 159.5 (NHC); ^{195}Pt NMR (108 MHz, DMSO-d_6): δ −3660 ppm; *m*/*z* (EI): 558, 522, 485, 353, 339, 244, 209, 145.

***cis*-Dichlorido-bis(1,3-diethylbenzimidazol-2-ylidene) platinum(II) (2b).** **7b** (500 mg, 837 μmol), **5b** (211 mg, 1.00 mmol, 1.2 eq.), KO^{t}Bu (141 mg, 1.26 mmol, 1.5 eq.), CH_2Cl_2 (100 mL). Yield: 399 mg (649 μmol, 78%); colourless solid of m.p. 353 °C (decomp.); elemental analysis (%): calc. for $C_{22}H_{28}N_4Cl_2Pt$ (614.47): C, 43.00; H, 4.59; N, 9.12. Found: C, 42.04; H, 4.661; N, 8.955. ^{1}H NMR (500 MHz, $CDCl_3$): δ 1.46 (12 H, t, J = 7.0 Hz, CH_3), 4.66 (4 H, dq, J = 14, 7.0 Hz, CH_2), 5.07 (4 H, dq, J = 14, 7.0 Hz, CH_2), 7.25–7.31 (4 H, m, BI), 7.39 (4 H, dd, J = 6.0, 3.2 Hz, BI); ^{13}C NMR (125 MHz, $CDCl_3$): δ 14.3 (CH_3), 43.6 (CH_2), 111.0 (BI), 123.5 (BI), 133.5 (BI-Cq), 158.7 (NHC); ^{195}Pt NMR (108 MHz, $CDCl_3$): δ −3632 ppm; *m*/*z* (EI): 726, 690, 653, 420, 231, 203, 119, 44.

***cis*-Dichlorido-bis(1,3-dibutylbenzimidazol-2-ylidene) platinum(II) (2c).** **7c** (965 mg, 1.68 mmol), **5c** (574 mg, 2.02 mmol, 1.2 eq.), KO^{t}Bu (283 mg, 2.52 mmol, 1.5 eq.), CH_2Cl_2 (105 mL). Yield: 875 mg (1.20 mmol, 72%); colourless solid of m.p. 210 °C; elemental analysis (%): calc. for $C_{30}H_{44}N_4Cl_2Pt$ (726.69): C, 49.58; H, 6.10; N, 7.71. Found: C, 49.01; H, 6.022; N, 7.832. ^{1}H NMR (500 MHz, $CDCl_3$): δ 0.96 (12 H, t, J = 7.3 Hz, CH_3), 1.42–1.51 (4 H, m, CH_2–CH_3), 1.53–1.69 (8 H, m, CH_2–CH_3, NCH_2–CH_2), 2.13–2.26 (4 H, m, NCH_2–CH_2), 4.32 (4 H, ddd, J = 13, 11, 5.0 Hz, N–CH_2), 4.98 (4 H, ddd, J = 13, 11, 5.0 Hz, N–CH_2), 7.25–7.29 (4 H, d, J = 3.2 Hz, BI), 7.32–7.38 (4 H, m, BI); ^{13}C NMR (125 MHz, $CDCl_3$): δ 13.8 (CH_3), 20.4 (CH_2–CH_3), 31.1 (NCH_2–CH_2) 48.7 (N–CH_2), 111.0 (BI), 123.3 (BI), 133.7 (BI-Cq), 158.8 (NHC); ^{195}Pt NMR (108 MHz, $CDCl_3$): δ −3622 ppm; *m*/*z* (EI): 726, 690, 653, 420, 231, 203, 119, 44. Crystal data: $C_{30}H_{44}Cl_2N_4Pt{\cdot}CHCl_3$, M = 846.07, triclinic, space group $P\bar{1}$, a = 8.6162(17) Å, b = 12.200(2) Å, c = 17.892(4) Å, α = 104.49(3)°, β = 95.13(3)°, γ = 104.88(3)°, V = 1736.1(7) Å^3, Z = 2, λ = 0.71073 Å, μ = 4.45 mm^{-1}, T = 133 K; 20 838 reflections measured, 8234 unique; $R[F_2 > 2\sigma(F_2)]$ = 0.0175 and R_w = 0.0382, GOF = 1.040. CCDC 1912955.†

***cis*-Dichlorido-bis(1,3-dioctylbenzimidazol-2-ylidene) platinum(II) (2d).** **7d** (75 mg, 109 μmol), **5d** (50 mg, 164 μmol, 1.5 eq.), KO^{t}Bu (36 mg, 328 μmol, 3 eq.), CH_2Cl_2 (10 mL), SiO_2 hexane : ethyl acetate 6 : 1 → 2 : 1. Yield: 57 mg (60 μmol, 55%); colourless solid of m.p. 146 °C; elemental analysis (%): calc. for $C_{45}H_{76}N_4Cl_2Pt$ (951.11): C, 58.09; H, 8.05; N, 5.89. Found: C, 57.94; H, 7.451; N, 5.305. ^{1}H NMR (500 MHz, $CDCl_3$): δ 0.90 (12 H, t, J = 6.9 Hz, CH_3), 1.25–1.33 (32 H, m, CH_2), 1.38–1.44 (4 H, m, NC_2H_4–CH_2), 1.48–1.55 (4 H, m, NC_2H_4–CH_2), 1.59–1.68 (4 H, m, NCH_2–CH_2), 2.15–2.26 (4 H, m, NCH_2–CH_2), 4.28–4.39 (4 H, ddd, J = 13, 12, 5.0 Hz, N–CH_2), 4.95 (4 H, ddd, J = 13, 12, 5.0 Hz, N–CH_2), 7.26 (4 H, d, J = 3.1 Hz, BI), 7.34 (4 H, dd, J = 6.1, 3.2 Hz, BI); ^{13}C NMR (125 MHz, $CDCl_3$): δ 14.1 (CH_3), 22.6 (CH_2), 27.3 (CH_2), 29.2 (CH_2), 29.3 (CH_2), 29.3 (CH_2), 31.8 (CH_2), 48.9 (N–CH_2), 111.0 (BI), 123.3 (BI), 133.7 (BI-Cq), 158.8 (NHC); ^{195}Pt NMR (108 MHz, $CDCl_3$): δ −3622; *m*/*z* (EI): 950, 914, 877, 843, 532, 341, 285, 119.

General synthesis of *cis*-[Pt^{IV}Cl$_4$(NHC)$_2$] complexes 3 and 4. The *cis*-[Pt^{II}Cl$_2$(NHC)$_2$] complexes **1** and **2** (1 eq.) in CH_2Cl_2 were treated with iodobenzene dichloride ($PhICl_2$, 10 eq.) and stirred at ambient temperature for 4 h to 16 h. The product was precipitated at 4 °C by adding diethyl ether or hexane, respectively, after reducing the solvent *in vacuo*.

***cis*-Tetrachlorido-bis(1,3-dibenzylimidazol-2-ylidene) platinum(IV) (3).** **1** (50 mg, 66 μmol), $PhICl_2$ (180 mg, 655 μmol, 10 eq.), CH_2Cl_2 (20 mL), 4 h. Yield: 49 mg (59 μmol, 90%); pale yellow solid of m.p. 252 °C (decomp.); elemental analysis (%): calc. for $C_{34}H_{32}N_4Cl_4Pt$ (833.54): C, 48.99; H, 3.87; N, 6.72. Found: C, 48.25; H, 3.876; N, 6.574. ^{1}H NMR (500 MHz, DMSO-d_6): δ 4.45 (2 H, d, J = 13.9 Hz, CH_2), 5.34 (2 H, d, J = 13.9 Hz, CH_2), 6.10 (2 H, d, J = 15.0 Hz, CH_2), 6.30 (2 H, d, J = 15.0 Hz, CH_2), 7.08 (2 H, d, J = 2.1 Hz, Imi), 7.18 (2 H, d, J = 2.1 Hz, Imi), 7.23–7.30 (10 H, m, Ar), 7.31–7.39 (6 H, m, Ar), 7.42 (4 H, t, J = 7.4 Hz, Ar); ^{13}C NMR (125 MHz, DMSO-d_6): δ 51.7 (CH_2), 55.3 (CH_2), 122.4 (Imi), 124.9 (Imi), 125.5 (Imi), 127.9 (Ar), 128.1 (Ar), 128.2 (Ar), 128.3 (Ar), 128.6 (Ar), 128.7 (Ar), 135.5 (Ar–C_q), 136.0 (NHC), 137.1 (Ar–C_q); ^{195}Pt NMR (108 MHz, DMSO-d_6): δ −1250 ppm; *m*/*z* (EI): 833, 797, 760, 724, 687, 440, 247, 157, 91. Crystal data: $C_{34}H_{32}Cl_4N_4Pt{\cdot}2(CH_2Cl_2)$, M = 983.87, monoclinic, space group $C2/c$, a = 24.684(5) Å, b = 8.277(5) Å, c = 22.505(5) Å, $\alpha = \beta = \gamma$ = 121.662(5)°, V = 3914(3) Å^3, Z = 4, λ = 0.71069 Å, μ = 3.808 mm^{-1}, T = 133 K; 10 695 reflections measured, 3414 unique; $R[F_2 > 2\sigma(F_2)]$ = 0.0554 and R_w = 0.1630, GOF = 0.987. CCDC 1912954.†

***cis*-Tetrachlorido-bis(1,3-dimethylbenzimidazol-2-ylidene) platinum(IV) (4a).** **2a** (30 mg, 54 μmol), $PhICl_2$ (148 mg, 537 μmol, 10 eq.), CH_2Cl_2 (12 mL), 4 h. Yield: 33 mg (52 μmol, 98%); pale yellow solid of m.p. 330 °C (decomp.); elemental analysis (%): calc. for $C_{18}H_{20}N_4Cl_4Pt$ (629.27): C, 34.36; H, 3.20; N, 8.90. Found: C, 34.88; H, 3.647; N, 9.051; *m*/*z* (EI): 630, 603, 559, 523, 486, 340, 147, 44, 36.

***cis*-Tetrachlorido-bis(1,3-diethylbenzimidazol-2-ylidene) platinum(IV) (4b).** **2b** (100 mg, 163 μmol), $PhICl_2$ (47 mg, 1.63 mmol, 10 eq.), CH_2Cl_2 (50 mL), 4 h. Yield: 111 mg (162 μmol, 100%); yellow solid of m.p. 326 °C (decomp.); elemental analysis (%): calc. for $C_{22}H_{28}N_4Cl_4Pt$ (685.38): C, 38.55; H, 4.12; N, 8.17. Found: C, 38.98; H, 4.846; N, 8.230. ^{1}H NMR (500 MHz, $CDCl_3$): δ 1.36 (6 H, t, J = 6.94 Hz, CH_3), 1.74 (6 H, t, J = 7.02 Hz, CH_3), 3.47 (2 H, dq, J = 14, 7.0 Hz, CH_2), 3.87 (2 H, dq, J = 14, 7.0 Hz, CH_2), 5.36 (2 H, dq, J = 14, 7.1 Hz, CH_2), 5.72 (2 H, dq, J = 14, 7.1 Hz, CH_2), 7.41–7.46 (4 H, m, Ar), 7.51 (2 H, ddd, J = 8.3, 5.4, 2.8 Hz, Ar), 7.72 (2 H, d, J = 8.3 Hz, Ar); ^{13}C NMR (125 MHz, $CDCl_3$): δ 14.9 (CH_3), 15.9 (CH_3), 44.2 (CH_2), 46.3 (CH_2), 112.3 (BI), 113.4 (BI), 125.4 (BI), 125.4 (BI), 133.4 (BI-C_q), 134.4 (BI-C_q), 136.8 (NHC); ^{195}Pt NMR: δ −1430 ppm; *m*/*z* (EI): 684, 648, 615, 576, 542, 368, 339, 176, 36.

***cis*-Tetrachlorido-bis(1,3-dibutylbenzimidazol-2-ylidene) platinum(IV) (4c).** **2c** (100 mg, 138 μmol), $PhICl_2$ (378 mg, 1.38 mmol, 10 eq.), CH_2Cl_2 (50 mL), 4 h. Yield: 96 mg (120 μmol, 88%); yellow solid of m.p. 222 °C; elemental analysis (%): calc. for $C_{30}H_{44}N_4Cl_4Pt$ (797.59): C, 45.18; H, 5.56; N, 7.02. Found: C, 44.69; H, 6.607; N, 7.502. ^{1}H NMR (500 MHz, $CDCl_3$): δ 0.64 (6 H, t, J = 7.3 Hz, CH_3), 0.76–0.87 (2 H, m, CH_3–CH_2), 1.03–1.16 (8 H, m, CH_3–CH_2, CH_3), 1.42–1.52 (2 H,

m, CH_2), 1.59–1.71 (4 H, m, CH_2), 1.98–2.11 (4 H, m, CH_2), 2.18–2.29 (2 H, m, CH_2), 3.33 (2 H, td, J = 13, 4.3 Hz, N–CH_2), 3.75 (2 H, td, J = 13, 4.3 Hz, N–CH_2), 5.30–5.45 (4 H, m, N–CH_2), 7.38 (2 H, d, J = 8.2 Hz, BI), 7.42 (2 H, t, J = 7.6 Hz, BI), 7.49 (2 H, t, J = 7.6 Hz, BI), 7.67 (2 H, d, J = 8.2 Hz, BI); ^{13}C NMR (125 MHz, $CDCl_3$): δ 13.2 (CH_3), 13.9 (CH_3), 19.9 (CH_3–CH_2), 19.9 (CH_3–CH_2), 31.0 (NCH_2–CH_2), 32.4 (NCH_2–CH_2), 49.4 (N–CH_2), 51.1 (N–CH_2), 112.4 (BI), 113.4 (BI), 125.3 (BI), 125.4 (BI), 133.6 (BI-C_q), 134.7 (BI-C_q), 136.4 (NHC); ^{195}Pt NMR: δ −1427 ppm; m/z (EI): 797, 762, 728, 655, 421, 365, 266, 230, 120, 36.

***cis*-Tetrachlorido-bis(1,3-dioctylbenzimidazol-2-ylidene) platinum(IV) (4d).** **2d** (25 mg, 26 μmol), $PhICl_2$ (72 mg, 263 μmol, 10 eq.), CH_2Cl_2 (10 mL), 16 h. Yield: 25 mg (25 μmol, 93%); yellow solid of m.p. 202 °C; elemental analysis (%): calc. for $C_{46}H_{76}N_4Cl_4Pt$ (1022.02): C, 54.06; H, 7.50; N, 5.48. Found: C, 54.29; H, 7.103; N, 5.051. ^{1}H NMR (500 MHz, $CDCl_3$): δ 0.71–0.79 (2 H, m, CH_3–CH_2), 0.83–0.92 (14 H, m, CH_3, CH_2), 1.00–1.14 (10 H, m, CH_2), 1.18–1.24 (4 H, m, CH_2), 1.27–1.38 (14 H, m, CH_2), 1.39–1.48 (6 H, m, CH_2), 1.61 (4 H, dt, J = 14, 7.2 Hz, CH_2), 2.07 (4 H, s, CH_2), 2.23 (2 H, dd, J = 12, 7.3 Hz, CH_2), 3.35 (2 H, td, J = 13, 3.7 Hz, N–CH_2), 3.74 (2 H, td, J = 13, 3.7 Hz), 5.23 (2 H, td, J = 13, 3.7 Hz, N–CH_2), 5.41–5.56 (2 H, td, J = 13, 3.7 Hz, N–CH_2), 7.36 (2 H, d, J = 8.2 Hz, BI), 7.42 (2 H, t, J = 7.6 Hz, BI), 7.48 (2 H, t, J = 7.6 Hz, BI), 7.65 (2 H, d, J = 8.2 Hz, BI); ^{13}C NMR (125 MHz, $CDCl_3$): δ 14.0 (CH_3), 14.1 (CH_3), 22.5 (CH_2), 22.7 (CH_2), 26.6 (CH_2), 26.7 (CH_2), 28.8 (CH_2), 29.0 (CH_2), 29.0 (CH_2), 29.3 (CH_2), 29.3 (CH_2), 30.4 (CH_2), 31.6 (CH_2), 31.7 (CH_2), 49.7 (N–CH_2), 51.3 (N–CH_2), 112.4 (BI), 113.3 (BI), 125.2 (BI), 125.3 (BI), 133.6 (BI-C_q), 134.7 (BI-C_q), 136.3 (NHC); ^{195}Pt NMR: δ −1429 ppm; m/z (EI): 1020, 984, 950, 912, 877, 513, 339, 119, 36.

Synthesis of *trans* complexes *trans*-2c and *trans*-4c

***trans*-Dichlorido-bis(1,3-dibutylbenzimidazol-2-ylidene) platinum(II) (*trans*-2c).** **6c** (100 mg, 267 μmol, 2 eq.) in CH_2Cl_2 (20 mL) was treated with K_2PtCl_4 (55 mg, 133 μmol, 1 eq.) and stirred at ambient temperature for 4 days. After filtration the solution was concentrated *in vacuo* and addition of hexane precipitated the product at 4 °C. Yield: 49 mg (67 μmol, 51%); colourless solid of m.p. 272 °C; elemental analysis (%): calc. for $C_{30}H_{44}N_4Cl_2Pt$ (726.69): C, 49.58; H, 6.10; N, 7.71. Found: C, 49.98; H, 6.295; N, 7.392. ^{1}H NMR (500 MHz, $CDCl_3$): δ 1.06 (12 H, t, J = 7.3 Hz, CH_3), 1.54–1.63 (8 H, m, CH_3–CH_2), 2.21 (8 H, quin, J = 7.8 Hz, NCH_2–CH_2), 4.84–4.95 (8 H, t, J = 7.8 Hz, N–CH_2), 7.26–7.31 (4 H, m, BI), 7.42 (4 H, dd, J = 6.0, 3.1 Hz, BI); ^{13}C NMR (125 MHz, $CDCl_3$): δ 14.0 (CH_3), 20.6 (CH_3–CH_2), 32.0 (NCH_2–CH_2), 47.5 (N–CH_2), 110.5 (BI), 122.7 (BI), 134.3 (BI-C_q), 178.0 (NHC); ^{195}Pt NMR: δ −3245 ppm; m/z (EI): 726, 653, 420, 365, 229, 119.

***trans*-Tetrachlorido-bis(1,3-dibutylbenzimidazol-2-ylidene) platinum(IV) (*trans*-4c).** ***trans*-2c** (41 mg, 56 μmol) and $PhICl_2$ (47 mg, 169 μmol, 10 eq.) in CH_2Cl_2 (5 mL) was stirred at ambient temperature for 3 days. To the concentrated solution was added hexane to precipitate the product at 4 °C. Yield: 40 mg (50 μmol, 89%); yellow solid of m.p. 253 °C; elemental analysis (%): calc. for $C_{30}H_{44}N_4Cl_4Pt$ (797.59): C, 45.18; H, 5.56; N, 7.02. Found: C, 45.04; H, 5.522; N, 7.392. ^{1}H NMR (500 MHz, $CDCl_3$): δ 1.08 (12 H, t, J = 7.4 Hz, CH_3), 1.60 (8 H, sxt, J = 7.4 Hz, CH_3–CH_2), 2.13 (8 H, quin, J = 7.8 Hz, NCH_2–CH_2), 5.05–5.17 (8 H, m, N–CH_2), 7.39 (4 H, dd, J = 6.2, 3.1 Hz, BI), 7.57 (4 H, dd, J = 6.2, 3.1 Hz, BI); ^{13}C NMR (125 MHz, $CDCl_3$): δ 13.9 (CH_3), 20.3 (CH_3–CH_2), 32.0 (NCH_2–CH_2), 49.9 (N–CH_2), 112.5 (BI), 124.0 (BI), 134.5 (BI-C_q), 147.5 (NHC); ^{195}Pt NMR: δ −1051 ppm; m/z (EI): 798, 762, 728, 691, 655, 421, 266, 230, 176, 120.

X-ray data collection and structural determination

Diffractometer used: STOE-IPDS II; data collection by: X-AREA-STOE; cell refinement by: X-AREA-STOE. The single crystal samples were measured with Mo-Kα and reflexes collected at 133 K. The structures were solved by direct methods using SIR97 and refined by full matrix least-squares on F^2 for all data using SHELXL2014. All hydrogen atoms were added at calculated positions and refined using a riding model. Anisotropic thermal displacement parameters were used for all non-hydrogen atoms. Further details about the data collection and reliability factors are listed together with the analytical data and in the ESI.† Supplementary crystallographic data were deposited with The Cambridge Crystallographic Data Centre CCDC under no. 1912955 (**2c**), 1912954 (**3**).†.

MTT based anti-proliferation assay[17]

The cell titer was adjusted to 0.05×10^6 cpm (cells per mL) or 0.1×10^6 cpm (DLD1, Hdfa) and the cells were seeded into the wells (100 μL per well) of 96 well plates. After an incubation period of 24 h at 37 °C, 5% CO_2 and 95% humidity appropriate dilutions of **2**, **3**, **4b**, **4c**, *trans*-**2c** or *trans*-**4c** or DMSO in ddH_2O (final concentrations 100 μM–25 nM) were added into the wells and the plates were incubated for a further 72 h at 37 °C. The plates were centrifuged (5 min, 300 g, 4 °C) and the supernatant was removed. 50 μL of a 0.05% MTT solution (PBS) was added into each well and the plates were further incubated at 37 °C for 2 h. The plates were centrifuged as before and the MTT solution was discarded again. The cells and the formed formazan were dissolved in DMSO (10% SDS, 0.6% AcOH) for 1 h at 37 °C. The absorption of the violet formazan was measured at 570 nm, respectively of the background at 630 nm. Values for the DMSO carrier were set to 100% viability and the percentage of living cells inside the wells treated with the platinum complexes was calculated accordingly. The IC_{50} values were determined using GraphPad Prism. Means ± SDs were calculated from four independent experiments.

Ethidiumbromide saturation assay

All solutions were sterile filtered before use. A 96 black well plate was prepared with wells containing 100 μL of TE-buffer (10 mM Tris/HCl, 1 mM EDTA, pH 8.0) with 10 μg mL^{-1} salmon sperm DNA. 11.1 μL of appropriate dilutions of **1** and **3** in H_2O were added into each well to reach final concentrations of 5, 10, 25 and 50 μM. As negative control wells treated with DMSO analogously to the highest concentration

were prepared. Treatment of the DNA was conducted in triplicates. To remove possible background fluorescence, one well containing 100 μL TE buffer without DNA was prepared for each concentration and compound. After 2 h of incubation at 37 °C 100 μL of a 10 μg mL^{-1} EtdBr solution in TE-buffer was added into each well. After another 5 minutes of incubation in the dark (RT), the fluorescence of the intercalated ethidium-bromide was measured at λ_{ex} = 535 and λ_{em} = 595. The fluorescence values were corrected for their respective background fluorescence and a possible fluorescence decrease was calculated relative to the fluorescence in the control wells which was adjusted to 100%.

Conflicts of interest

There are no conflicts to declare.

Acknowledgements

We thank the Deutsche Forschungsgemeinschaft (grant Scho 402/12-2) and the COST Action CM1105 'Functional metal complexes that bind to biomolecules' for financial support.

We are indebted to Dr Ulrike Lacher (Central Analytical Services) for ESI-MS studies and Sofia Bär for additional MTT-assays.

Notes and references

1 (*a*) B. Rosenberg, L. VanCamp, J. E. Trosko and V. H. Mansour, *Nature*, 1969, **222**, 385–386, DOI: 10.1038/222385a0; (*b*) M. Rozencweig, D. D. Von Hoff, M. Slavik and F. M. Muggia, *Ann. Intern. Med.*, 1977, **86**, 803–812, DOI: 10.7326/0003-4819-86-6-803.

2 P. J. O'Dwyer, J. P. Stevenson and S. W. Johnson, *Clinical Status of Cisplatin, Carboplatin, and Other Platinum-Based Antitumor Drugs, in Cisplatin*, ed. B. Lippert, Verlag Helvetica Chimica Acta, Zürich, Switzerland, 1999.

3 D. Gibson, *Dalton Trans.*, 2016, **45**, 12983–12991, DOI: 10.1039/c6dt01414c.

4 N. J. Wheate, S. Walker, G. E. Craig and R. Oun, *Dalton Trans.*, 2010, **39**, 8113–8127, DOI: 10.1039/c0dt00292e.

5 (*a*) T. C. Johnstone, K. Suntharalingam and S. J. Lippard, *Chem. Rev.*, 2016, **116**, 3436–3486, DOI: 10.1021/acs.chemrev.5b00597; (*b*) H. P. Varbanov, M. A. Jakupec, A. Roller, F. Jensen, M. Galanski and B. K. Keppler, *J. Med. Chem.*, 2013, **56**, 330–344, DOI: 10.1021/jm3016427; (*c*) X. Wang, X. Wang and Z. Guo, *Acc. Chem. Res.*, 2015, **48**, 92622–92631, DOI: 10.1021/acs.accounts.5b00203.

6 (*a*) X. Huang, R. Huang, S. Gou, Z. Wang, Z. Liao and H. Wang, *Bioconjugate Chem.*, 2016, **27**, 2132–2148, DOI: 10.1021/acs.bioconjchem.6b00353; (*b*) E. Petruzzella, R. Sirota, I. Solazzo, V. Gandin and D. Gibson, *Chem. Sci.*, 2018, **9**, 4299–4307, DOI: 10.1039/c8sc00428e; (*c*) L. Gaviglio, A. Gross, N. Metzler-Nolte and M. Ravera, *Metallomics*, 2012, **4**, 260–266, DOI: 10.1039/C2MT00171C.

7 (*a*) V. Brabec, O. Hrabina and J. Kasparkova, *Coord. Chem. Rev.*, 2017, **351**, 2–31, DOI: 10.1016/j.ccr.2017.04.013; (*b*) R. G. Kenny and C. J. Marmion, *Chem. Rev.*, 2019, **119**, 1085–1137, DOI: 10.1021/acs.chemrev.8b00271; (*c*) X. Wang and Z. Guo, *Chem. Soc. Rev.*, 2013, **42**, 202–224, DOI: 10.1039/c2cs35259a.

8 (*a*) M. Bouché, A. Bonnefont, T. Achard and S. Bellemin-Laponnaz, *Dalton Trans.*, 2018, **47**, 11491–11502, DOI: 10.1039/c8dt02113a; (*b*) M. Bouché, G. Dahm, M. Wantz, S. Fournel, T. Achard and S. Bellemin-Laponnaz, *Dalton Trans.*, 2016, **45**, 11362–11368, DOI: 10.1039/c6dt01846g.

9 (*a*) R. Lindner, C. Wagner and D. Steinborn, *J. Am. Chem. Soc.*, 2009, **131**, 8861–8874, DOI: 10.1021/ja901264t; (*b*) V. N. Demidov, Y. N. Kukushkin, L. N. Vedeneeva and A. N. Belyaev, *Zh. Obshch. Khim.*, 1988, **58**, 738; (*c*) V. Khlebnikov, M. Heckenroth, H. Müller-Bunz and M. Albrecht, *Dalton Trans.*, 2013, **42**, 4197–4207, DOI: 10.1039/c2dt32423g; (*d*) D. Meyer, S. Ahrens and T. Strassner, *Organometallics*, 2010, **29**, 3392–3396, DOI: 10.1021/om100488s; (*e*) W. Weigand, U. Nagel and W. Beck, *Z. Naturforsch., B: Chem. Sci.*, 1988, **43**, 328–338.

10 (*a*) J. Muenzner, T. Rehm, B. Biersack, A. Casini, I. de Graaf, P. Worawutputtapong, A. Noor, R. Kempe, V. Brabec, J. Kasparkova and R. Schobert, *J. Med. Chem.*, 2015, **58**, 6283–6292, DOI: 10.1021/acs.jmedchem.5b00896; (*b*) T. Rehm, M. Rothemund, J. K. Muenzner, A. Noor, R. Kempe and R. Schobert, *Dalton Trans.*, 2016, **45**, 15390–15398, DOI: 10.1039/c6dt02350a; (*c*) T. Rehm, M. Rothemund, A. Bär, T. Dietel, R. Kempe, H. Kostrhunova, V. Brabec, J. Kasparkova and R. Schobert, *Dalton Trans.*, 2018, **47**, 17367–17381, DOI: 10.1039/c8dt03360a.

11 C. P. Newman, R. J. Deeth, G. J. Clarkson and J. P. Rourke, *Organometallics*, 2007, **26**, 6225–6233, DOI: 10.1021/om700671y.

12 J. J. Wilson and S. J. Lippard, *Chem. Rev.*, 2014, **114**, 4470–4495, DOI: 10.1021/cr4004314.

13 X.-F. Zhao and C. Zhang, *Synthesis*, 2007, 551–557, DOI: 10.1055/s-2007-965889.

14 A. G. Tennyson, V. M. Lynch and C. W. Bielawski, *J. Am. Chem. Soc.*, 2010, **132**, 9420–9429, DOI: 10.1021/ja102686u.

15 (*a*) L. Ma, R. Ma, Y. Wang, X. Zhu, J. Zhang, H. C. Chan, X. Chen, W. Zhang, S.-K. Chiu and G. Zhu, *Chem. Commun.*, 2015, **51**, 6301–6304, DOI: 10.1039/c4cc10409a; (*b*) R. Haputhanthri, R. Ojha, E. I. Izgorodina, S. X. Guo, G. B. Deacon, D. McNaughton and B. R. Wood, *Vib. Spectrosc.*, 2017, **92**, 82–95, DOI: 10.1016/j.vibspec.2017.02.006; (*c*) E. G. Talman, Y. Kidani, L. Mohrmann and J. Reedijk, *Inorg. Chim. Acta*, 1998, **283**, 251–255.

16 A. Nemirovski, Y. Kasherman, Y. Tzaraf and D. Gibson, *J. Med. Chem.*, 2007, **50**, 5554–5556, DOI: 10.1021/jm070740j.

17 (*a*) T. Mosmann, *J. Immunol. Methods*, 1983, **65**, 55–63, DOI: 10.1016/0022-1759(83)90303-4; (*b*) R. B. Badisa, S. F. Darling-Reed, P. Joseph, J. S. Cooperwood, L. M. Latinwo and C. B. Goodman, *Anticancer Res.*, 2009, **29**, 2993–2996.

Electronic Supporting Information

Synthesis, structures and cytotoxic effects *in vitro* of *cis*- and *trans*-[$Pt^{IV}Cl_4(NHC)_2$] complexes and their Pt^{II} precursors

Tobias Rehm,[a] Matthias Rothemund,[a] Thomas Dietel,[b] Rhett Kempe[b] and Rainer Schobert[a]

[a]*Organic Chemistry Laboratory, University Bayreuth, Universitaetsstrasse 30, 95440 Bayreuth, Germany. E-mail: Rainer.Schobert@uni-bayreuth.de*

[b]*Lehrstuhl fuer Anorganische Chemie II, University Bayreuth, Universitaetsstrasse 30, 95440 Bayreuth, Germany.*

Table of content

Table S 1: Single crystal X-ray diffraction data of platinum carbene complexes **2c** and **3**.

Crystal data	**2c**	**3**
Chemical formula	$C_{30}H_{44}Cl_2N_4Pt \cdot CHCl_3$	$C_{34}H_{32}Cl_4N_4Pt \cdot 2(CH_2Cl_2)$
M_r	846.07	983.87
Crystal system, space group	Triclinic, P	Monoclinic, C2/c
Temperature (K)	133	133
a, *b*, *c* (Å)	8.6162 (17), 12.200 (2), 17.892 (4)	24.684 (5), 8.277 (5), 22.505 (5)
α, β, γ (°)	104.49 (3), 95.13 (3), 104.88 (3)	121.662 (5)
V (Å^3)	1736.1 (7)	3914 (3)
Z	2	4
F(000)	842.5	1945
D_x (Mg m^{-3})	1.618	1.670
Radiation type	Mo Kα	Mo Kα
No. of reflections for cell measurement	1222	8743
θ range (°) for cell measurement	5.7–25.8	1.9–28.3
μ (mm^{-1})	4.45	3.81
Crystal shape	Block	Block
Colour	Clear colourless	Colourless
Crystal size (mm)	0.07 × 0.01 × 0.004	0.21 × 0.12 × 0.09
Data collection		
Diffractometer	STOE-STADIVARI	STOE-STADIVARI
Scan method	ω scans	ω scan
Absorption correction	Numerical	Numerical
		STOE-X-RED32
T_{min}, T_{max}	0.613, 0.733	0.841, 0.912
No. of measured, independent and observed [$I > 2\sigma(I)$] reflections	20838, 8234, 7605	10695, 3414, 2307
R_{int}	0.015	0.077
θ values (°)	θmax = 28.5, θmin = 1.8	θmax = 25.0, θmin = 2.0
$(\sin\theta/\lambda)_{max}$ (Å^{-1})	0.671	0.595
Range of *h*, *k*, *l*	h = −11 → 7	h = −29 → 29
	k = −16 → 16	k = −5 → 9
	l = −23 → 22	l = −26 → 22
Refinement		
Refinement on	F^2	F^2
$R[F^2 > 2\sigma(F^2)]$, $wR(F^2)$, *S*	0.018, 0.038, 1.04	0.055, 0.163, 0.99
No. of reflections	8234	3414
No. of parameters	374	223
No. of restraints	0	18
H-atom treatment	H-atom parameters constrained	H-atom parameters constrained
Weighting scheme	w = 1/[σ2(Fo2) + (0.0198P)2 + 0.8853P]	*w = 1/[σ2(Fo2) + (0.1072P)2]*
	where P = (Fo2 + 2Fc2)/3	where P = (Fo2 + 2Fc2)/3
$(\Delta/\sigma)_{max}$	< 0.001	< 0.001
$\Delta\rho_{max}$, $\Delta\rho_{min}$ (e Å^{-3})	0.62, −0.54	2.14, −2.78

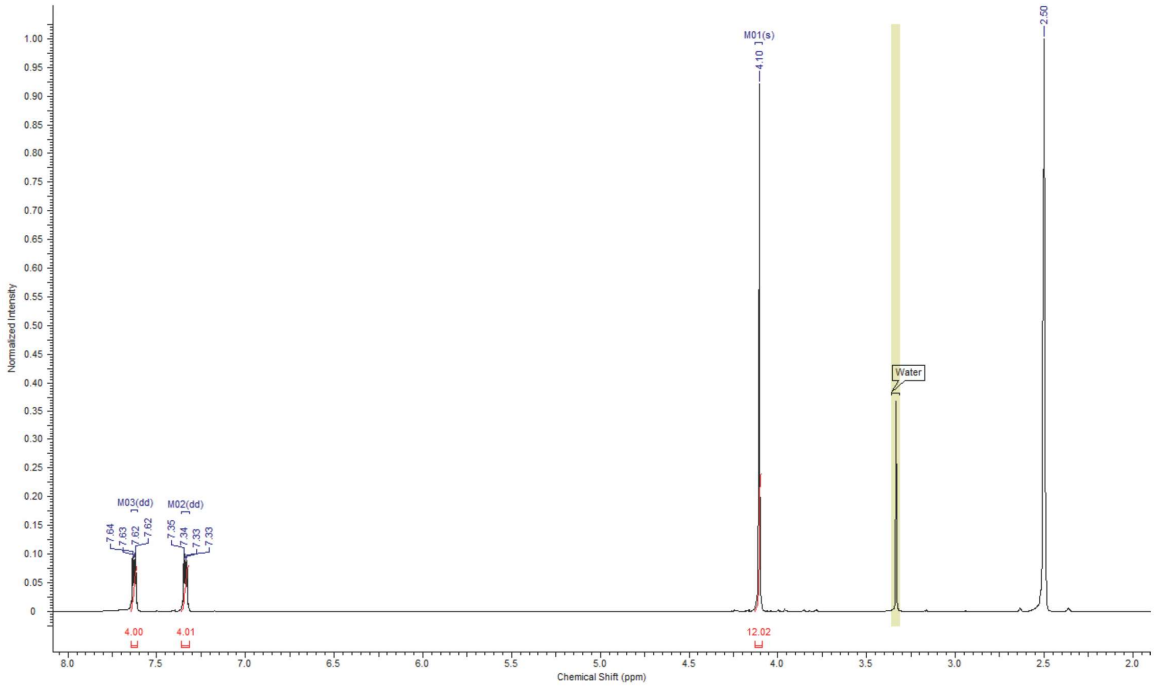

Fig. S 1: ^{1}H-NMR spectrum (500 MHz, DMSO-d_6) of complex **2a**.

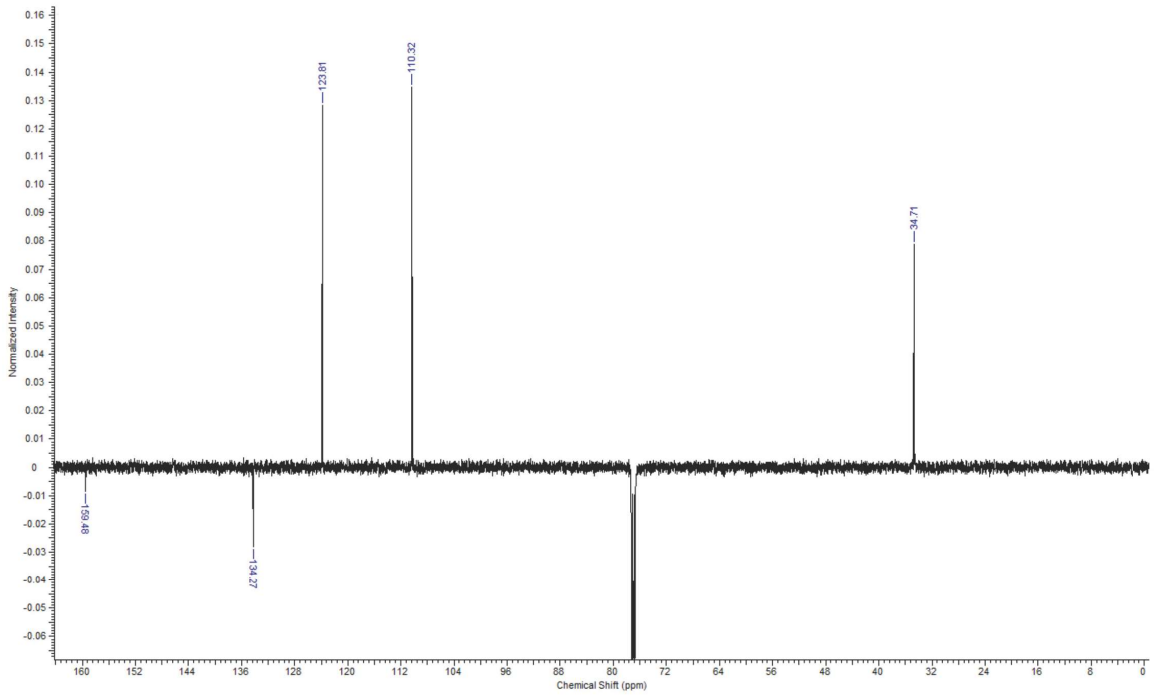

Fig. S 2: ^{13}C-NMR spectrum (126 MHz, $CDCl_3$) of complex **2a**.

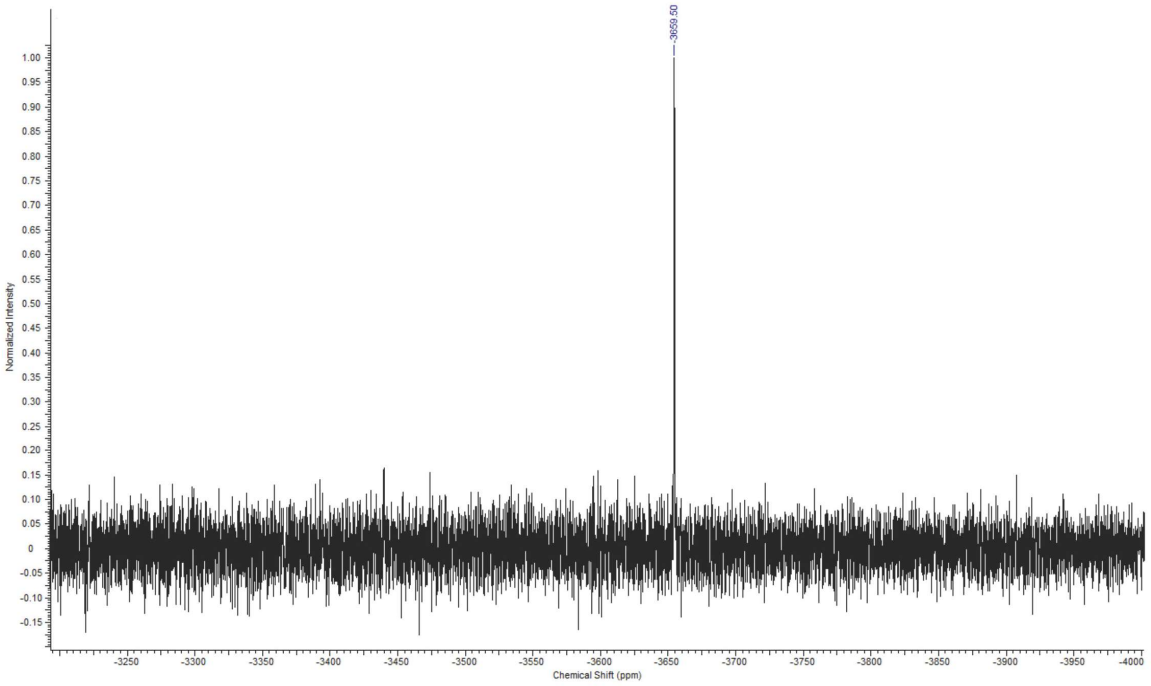

Fig. S 3: ^{195}Pt-NMR spectrum (108 MHz, $CDCl_3$) of complex **2a**.

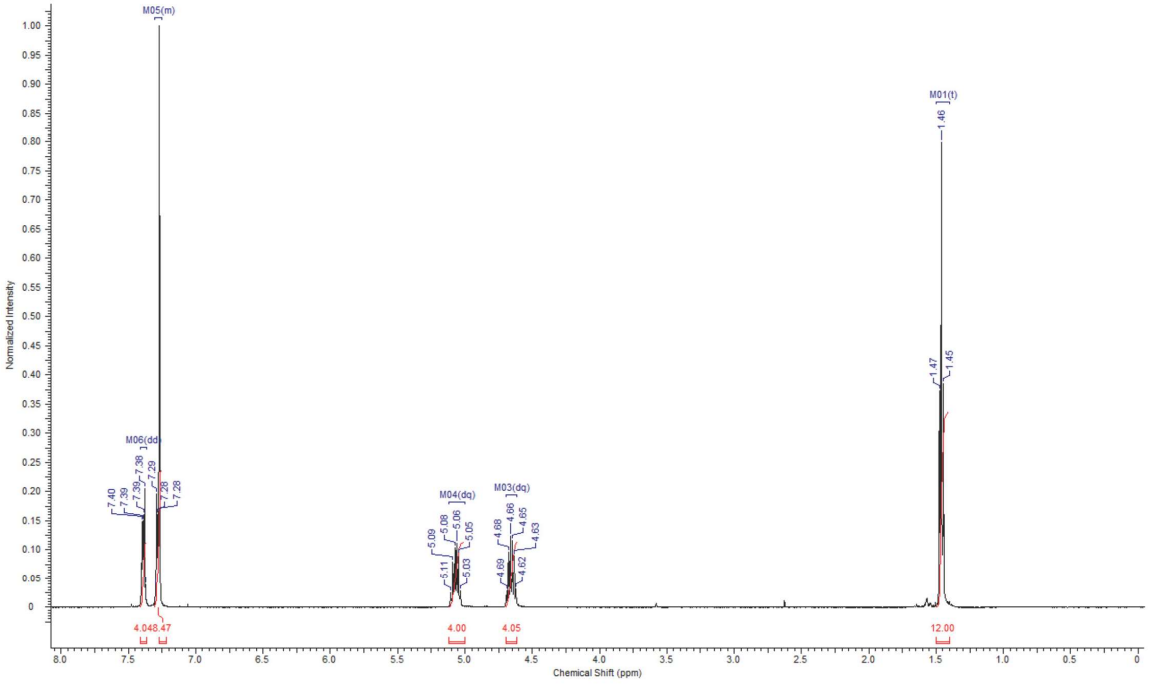

Fig. S 4: ^{1}H-NMR spectrum (500 MHz, $CDCl_3$) of complex **2b**.

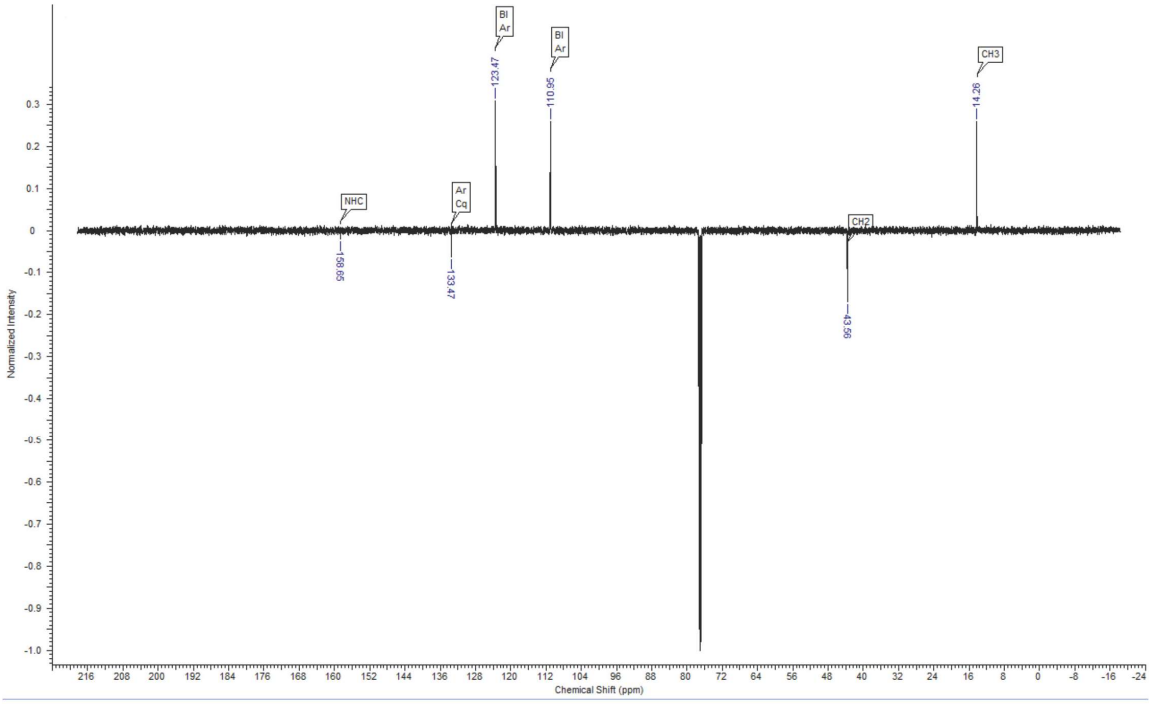

Fig. S 5: ^{13}C-NMR spectrum (126 MHz, $CDCl_3$) of complex **2b**.

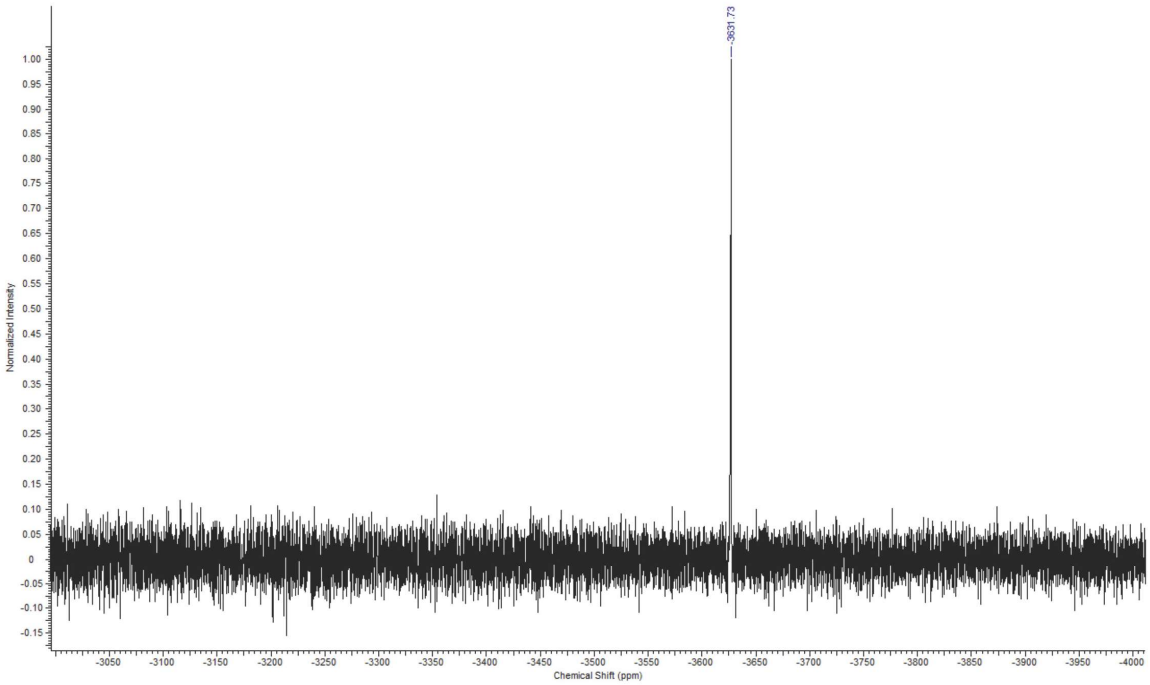

Fig. S 6: ^{195}Pt-NMR spectrum (108 MHz, $CDCl_3$) of complex **2b**.

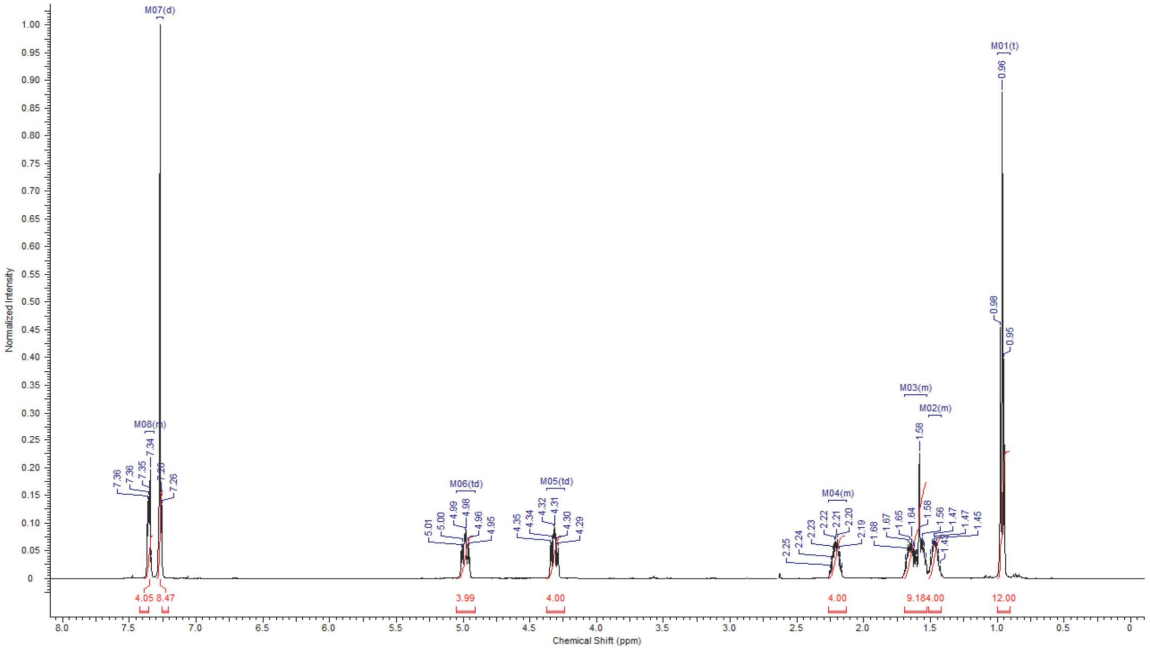

Fig. S 7: ^{1}H-NMR spectrum (500 MHz, $CDCl_3$) of complex **2c**.

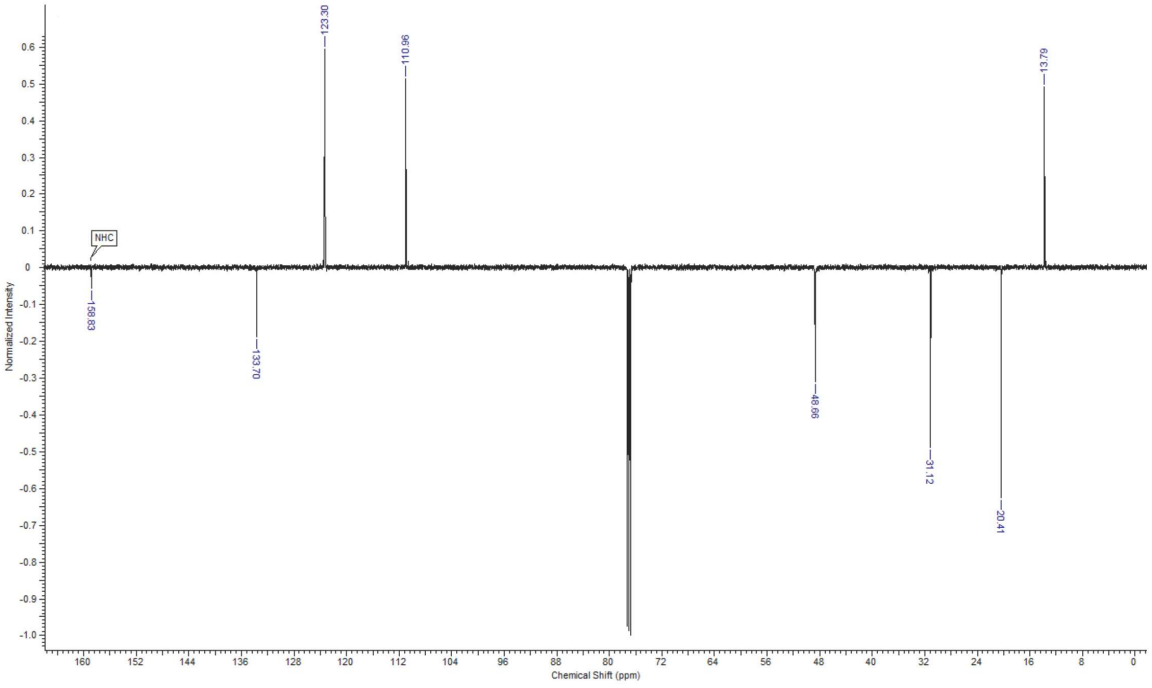

Fig. S 8: ^{13}C-NMR spectrum (126 MHz, $CDCl_3$) of complex **2c**.

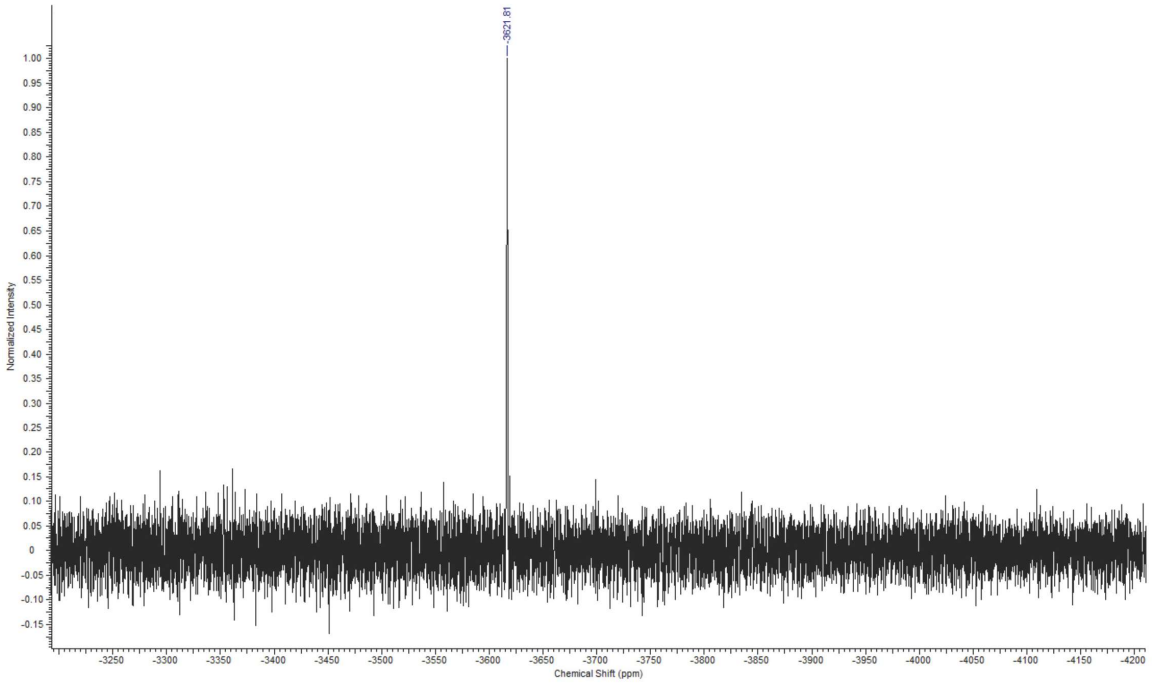

Fig. S 9: ^{195}Pt-NMR spectrum (108 MHz, $CDCl_3$) of complex **2c**.

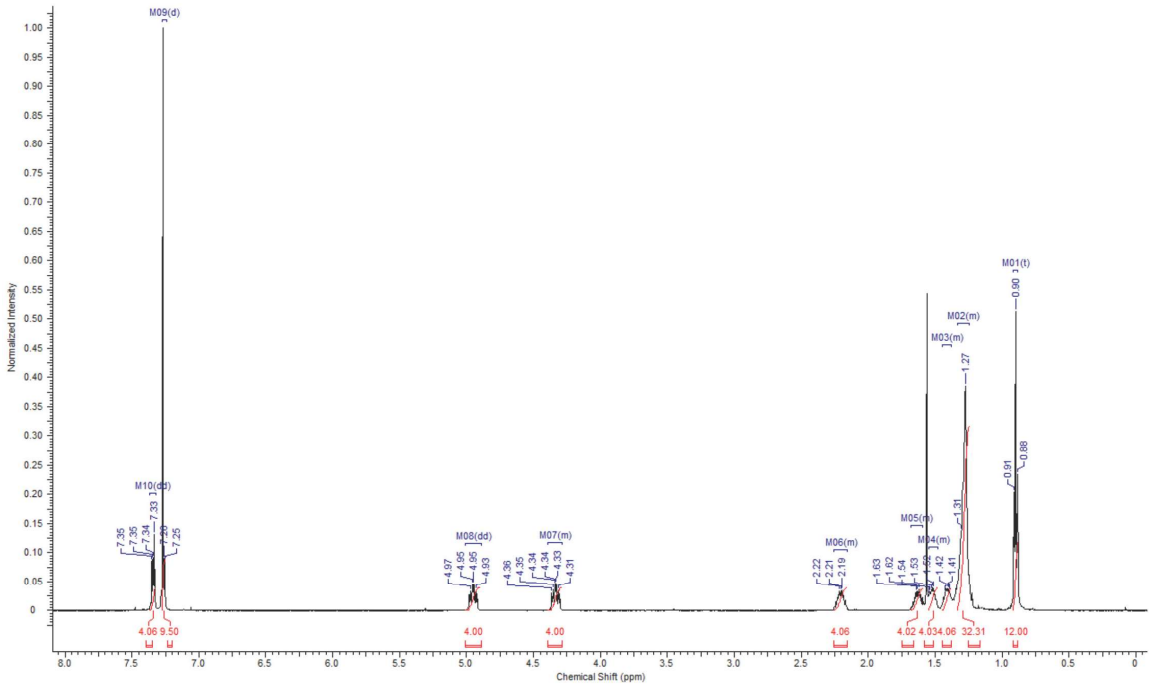

Fig. S 10: ^{1}H-NMR spectrum (500 MHz, $CDCl_3$) of complex **2d**.

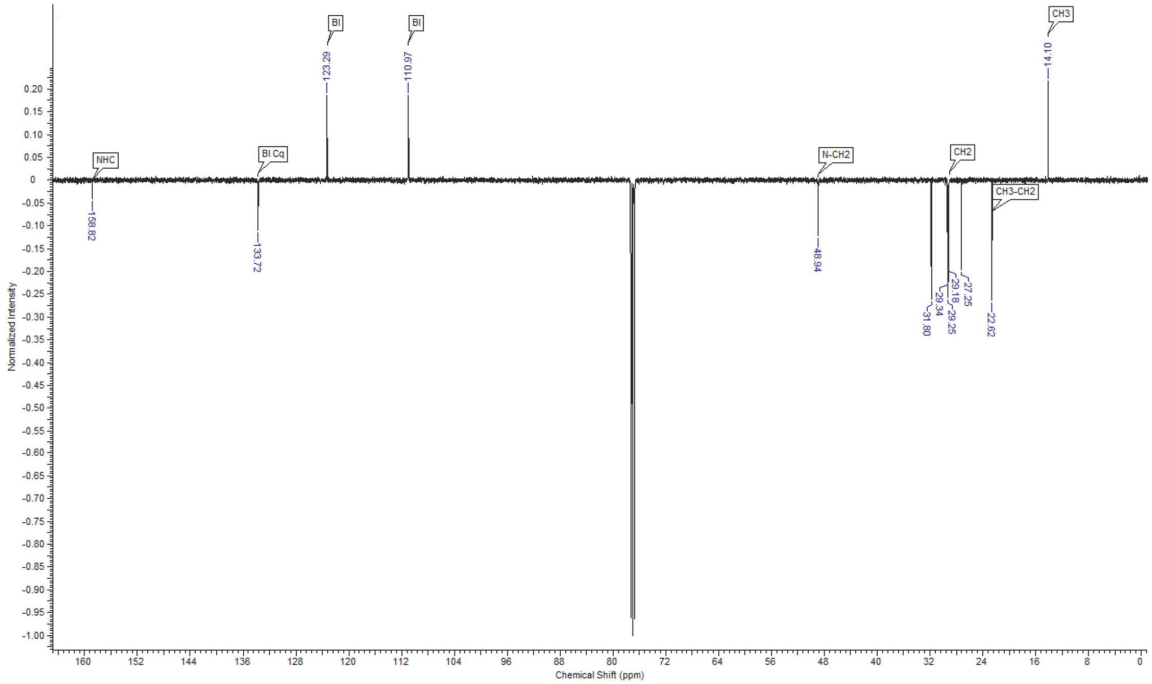

Fig. S 11: ^{13}C-NMR spectrum (126 MHz, $CDCl_3$) of complex **2d**.

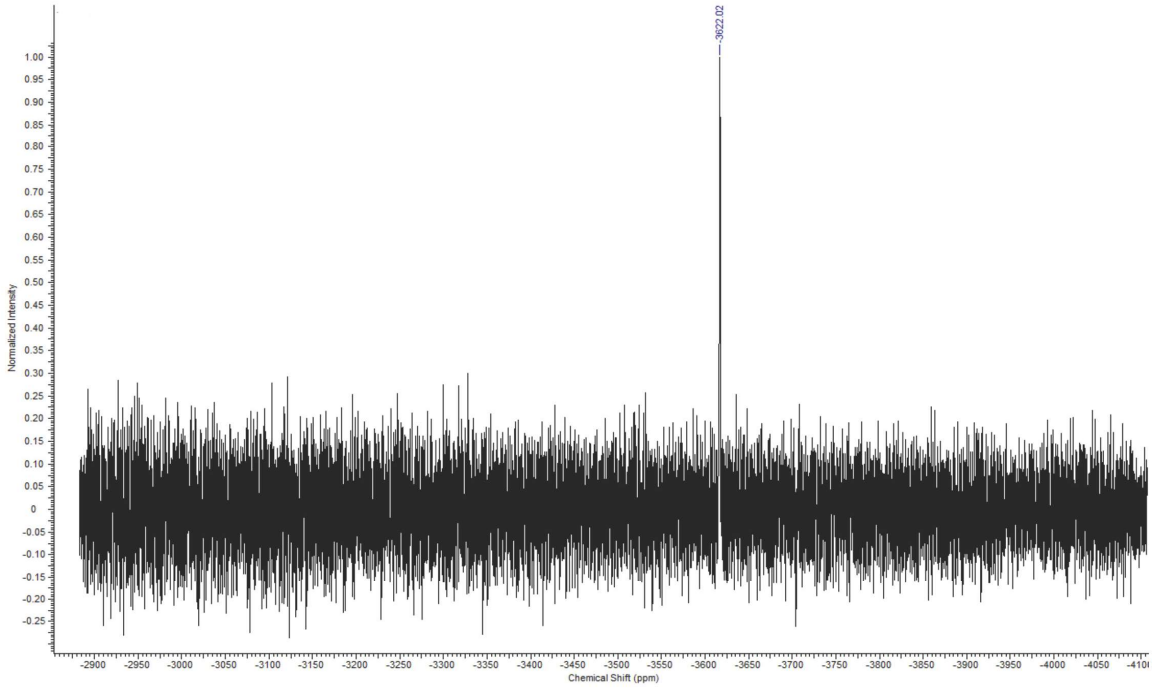

Fig. S 12: ^{195}Pt-NMR spectrum (108 MHz, $CDCl_3$) of complex **2d**.

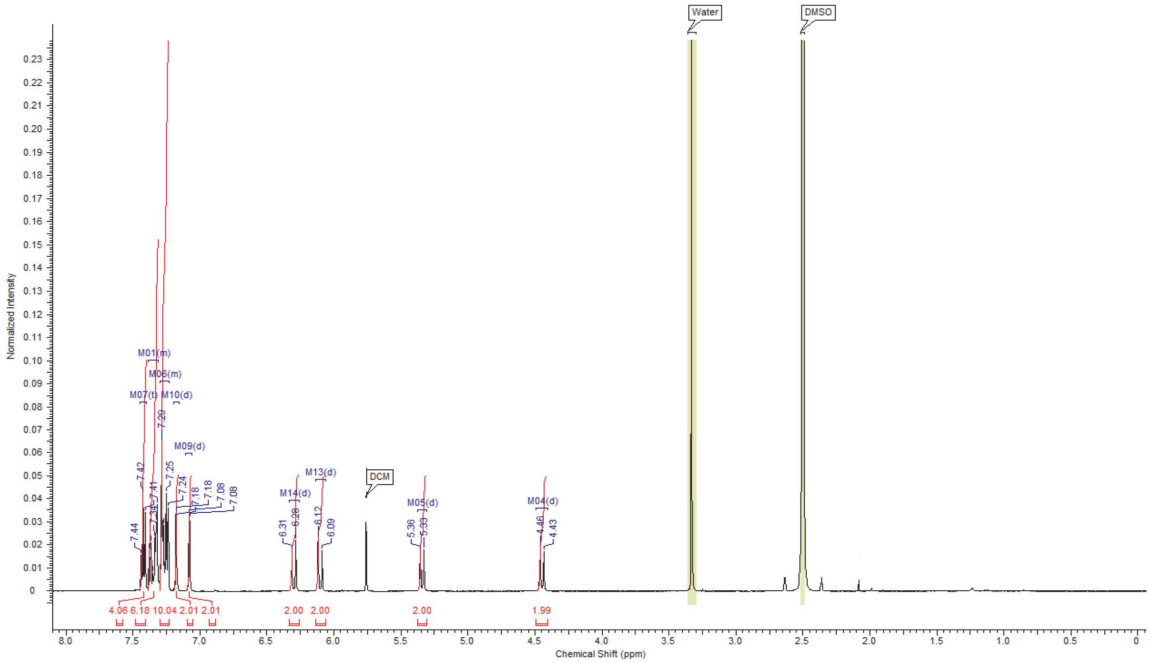

Fig. S 13: ^{1}H-NMR spectrum (500 MHz, DMSO-d_6) of complex **3**.

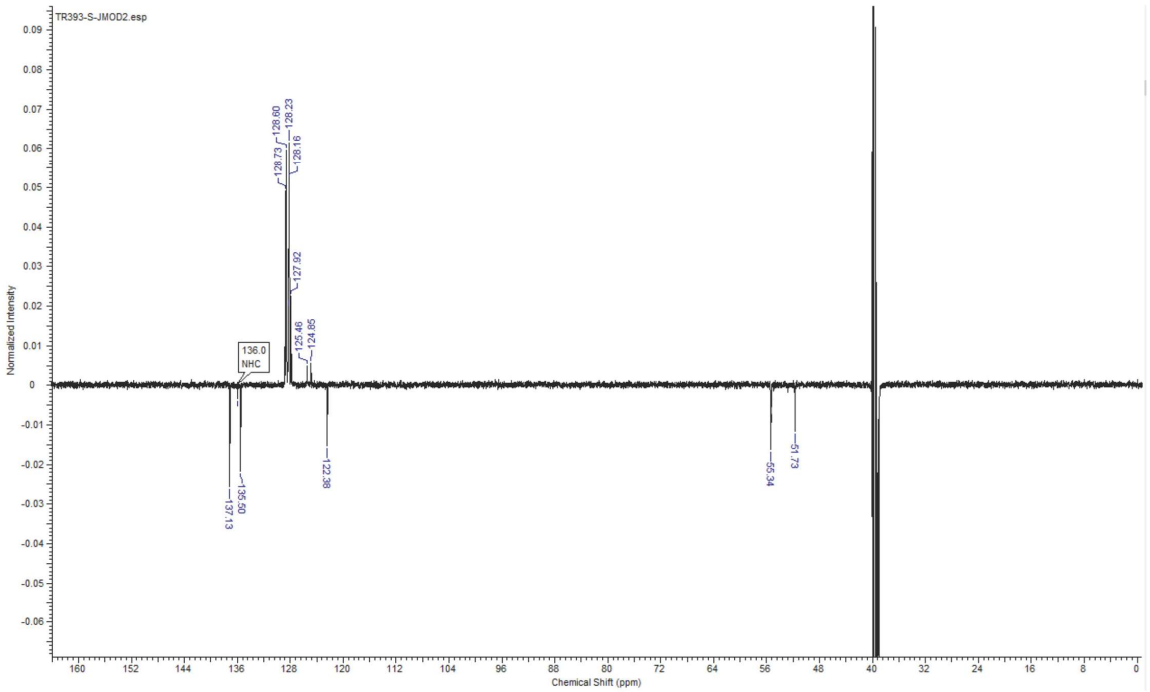

Fig. S 14: ^{13}C-NMR spectrum (126 MHz, DMSO-d_6) of complex **3**.

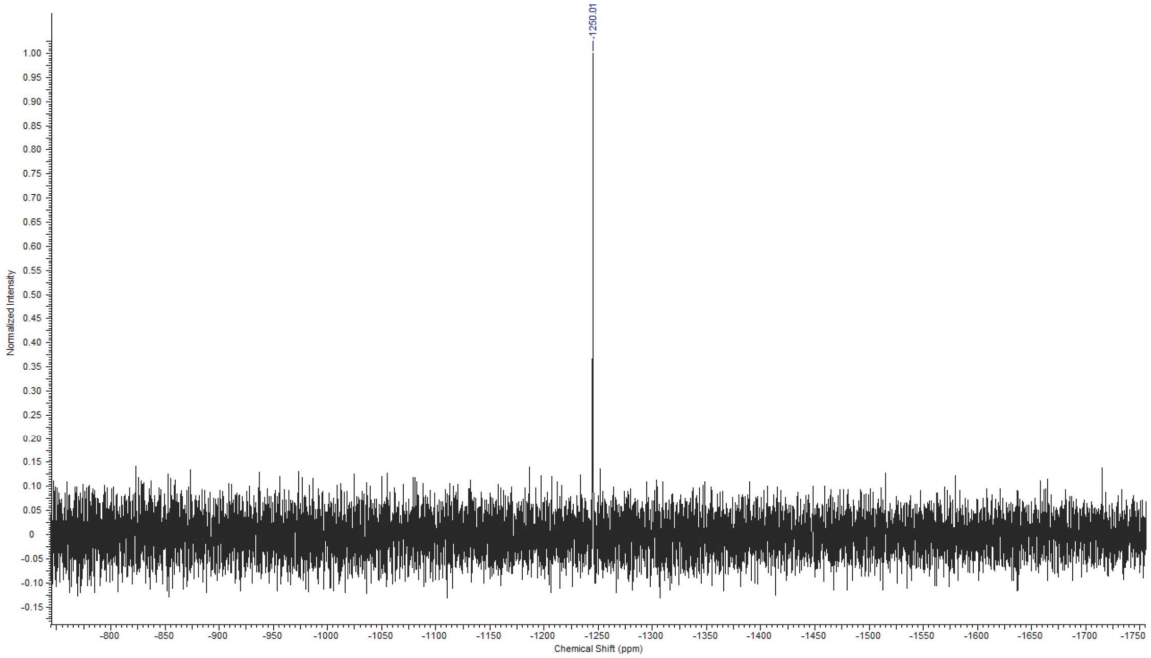

Fig. S 15: ^{195}Pt-NMR spectrum (108 MHz, DMSO-d_6) of complex **3**.

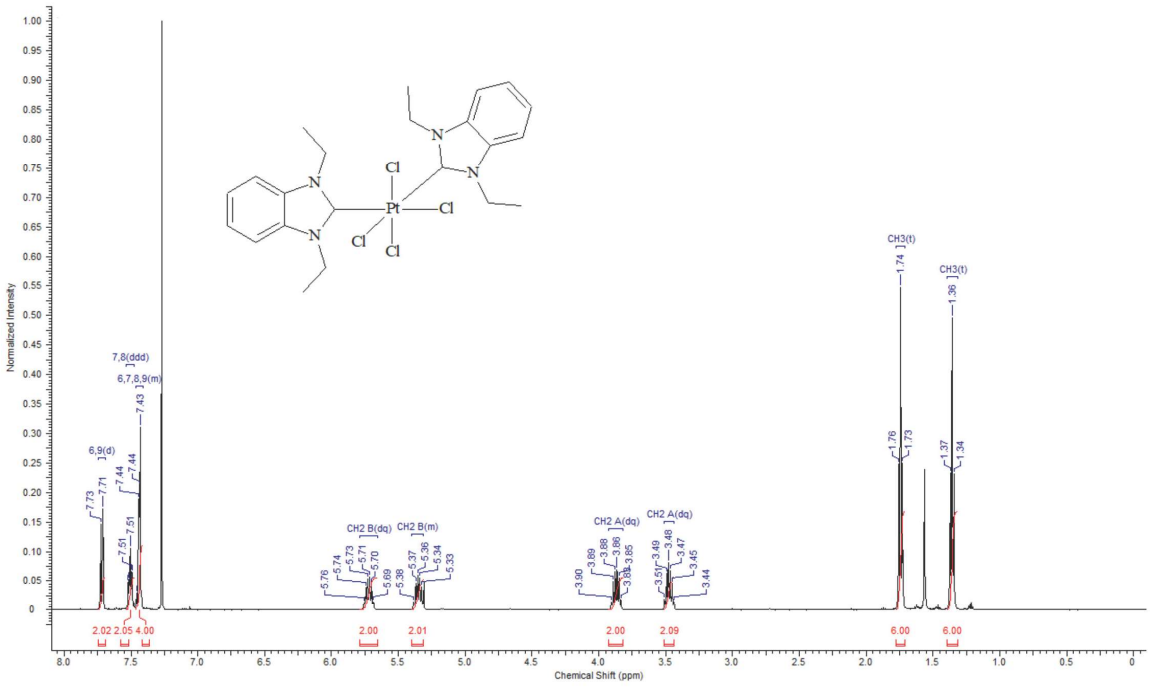

Fig. S 16: ^{1}H-NMR spectrum (500 MHz, $CDCl_3$) of complex **4b**.

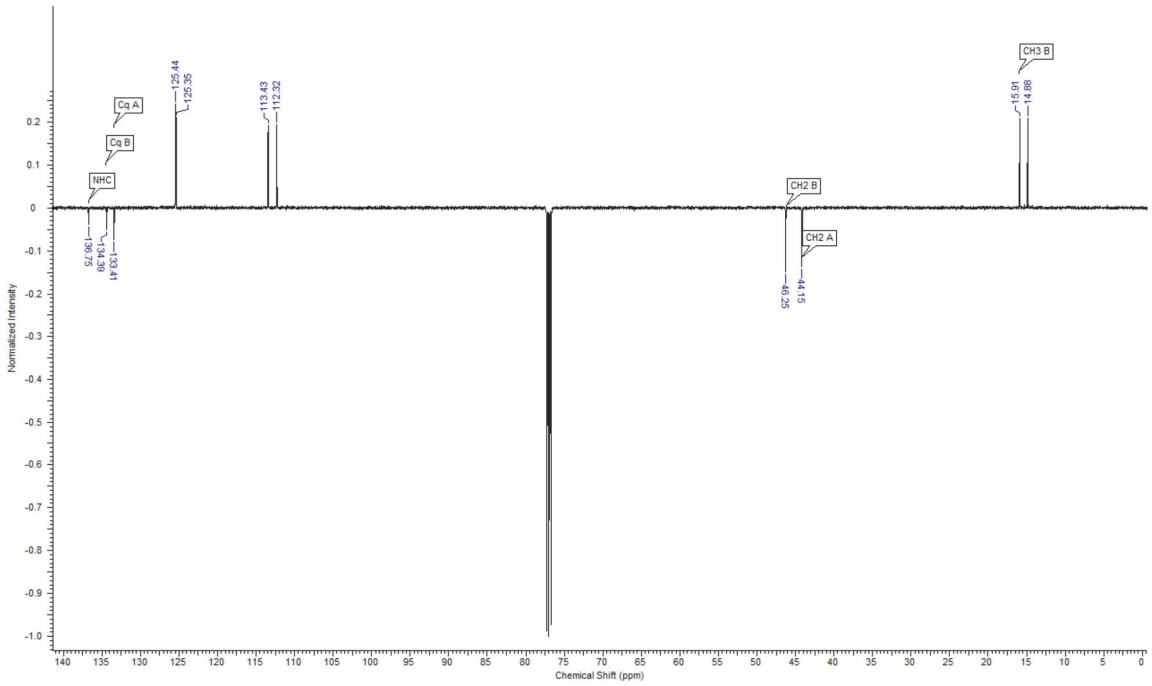

Fig. S 17: ^{13}C-NMR spectrum (126 MHz, $CDCl_3$) of complex **4b**.

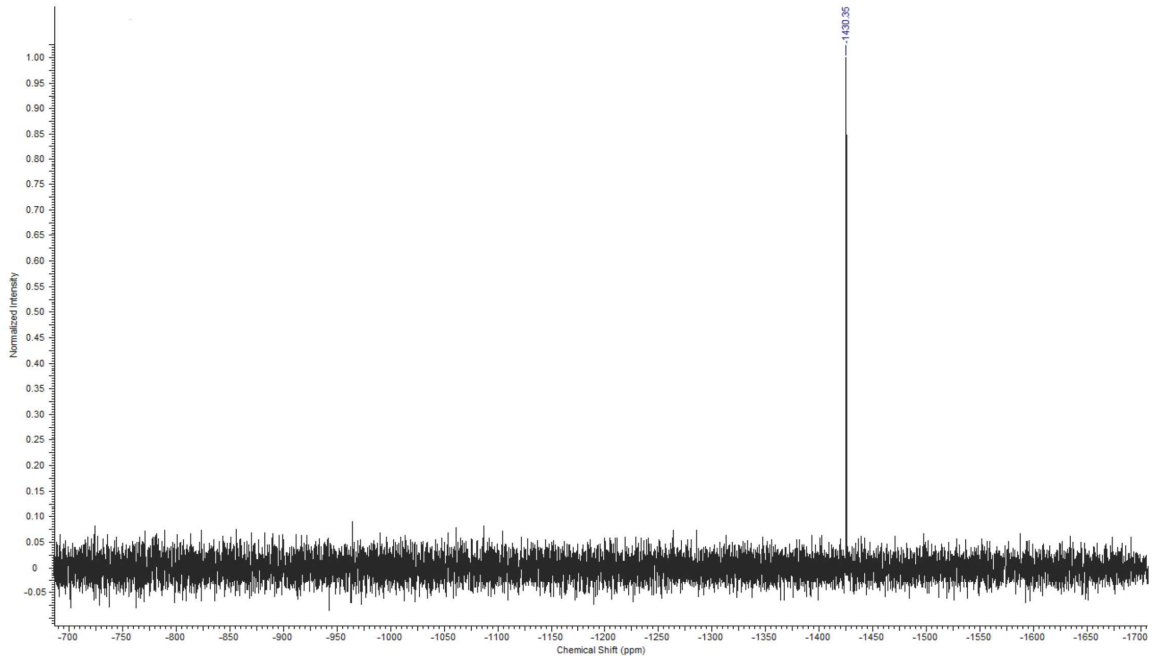

Fig. S 18: ^{195}Pt-NMR spectrum (108 MHz, $CDCl_3$) of complex **4b**.

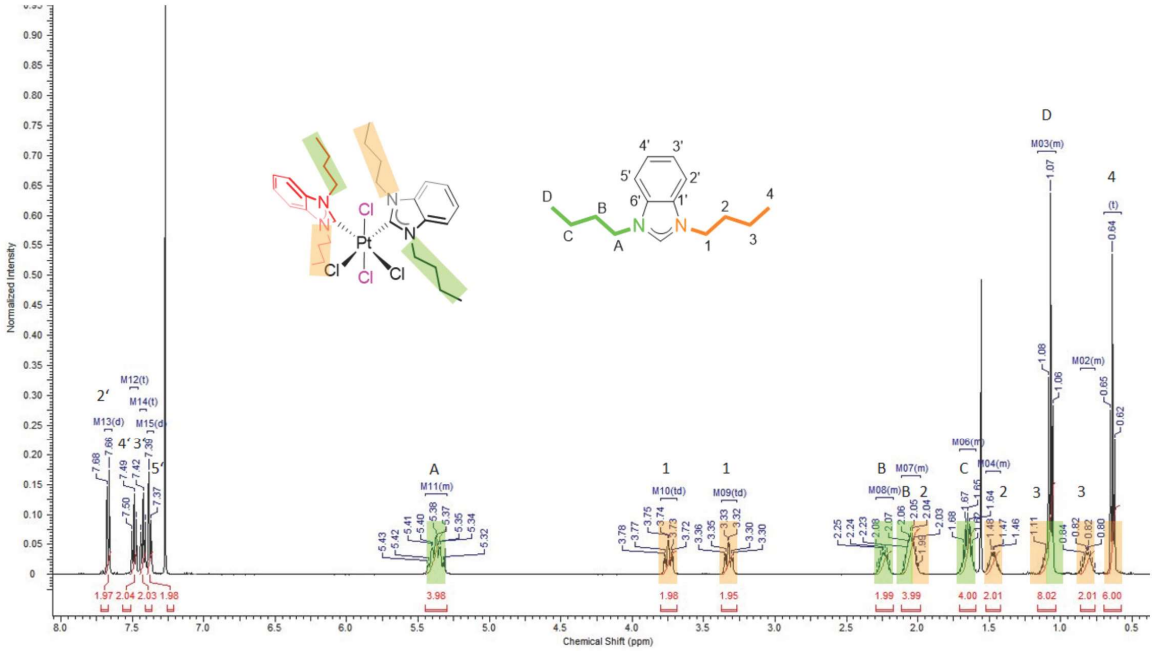

Fig. S 19: ^{1}H-NMR spectrum (500 MHz, $CDCl_3$) of complex **4c**.

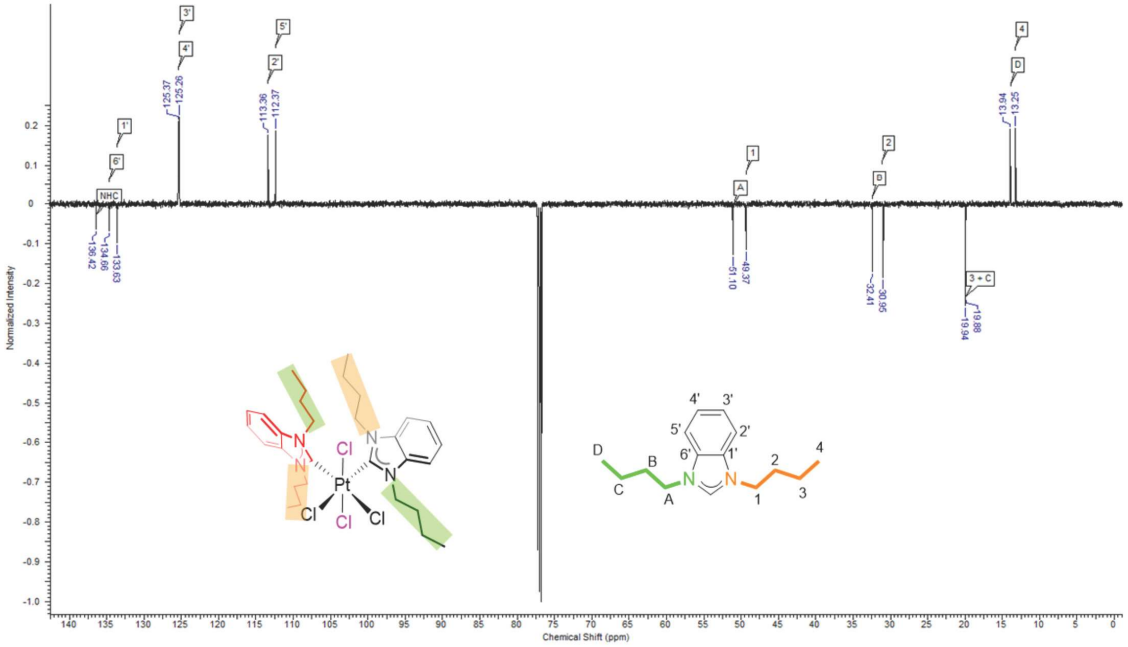

Fig. S 20: ^{13}C-NMR spectrum (126 MHz, $CDCl_3$) of complex **4c**.

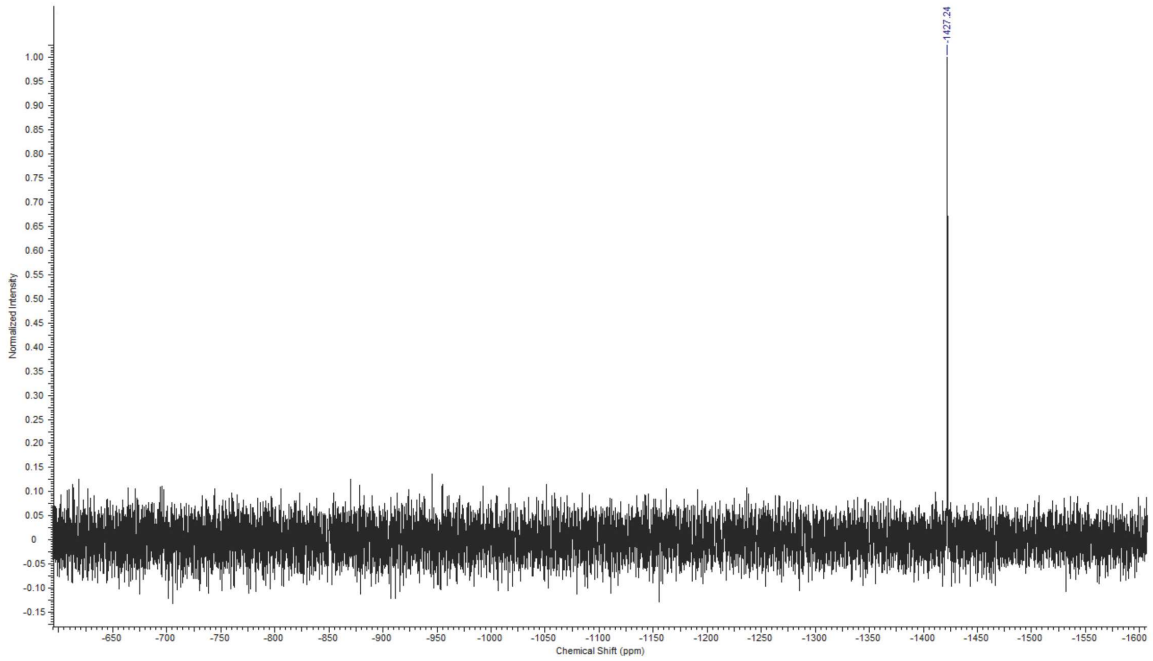

Fig. S 21: ^{195}Pt-NMR spectrum (108 MHz, $CDCl_3$) of complex **4c**.

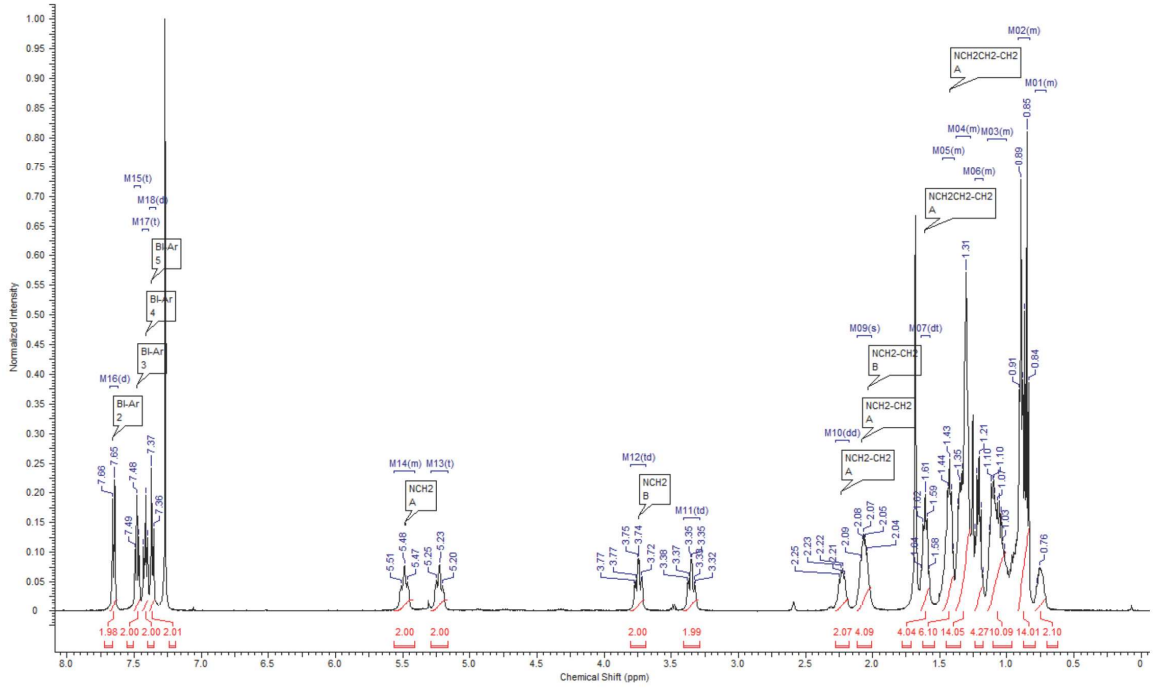

Fig. S 22: ^{1}H-NMR spectrum (500 MHz, $CDCl_3$) of complex **4d**.

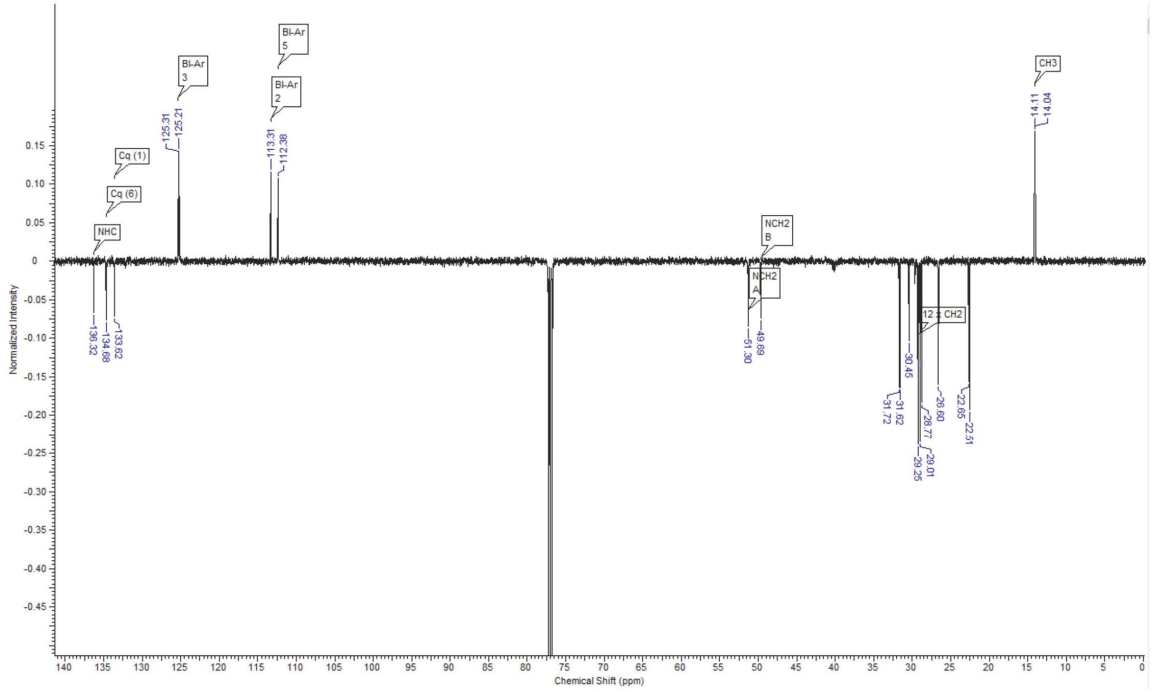

Fig. S 23: ^{13}C-NMR spectrum (126 MHz, $CDCl_3$) of complex **4d**.

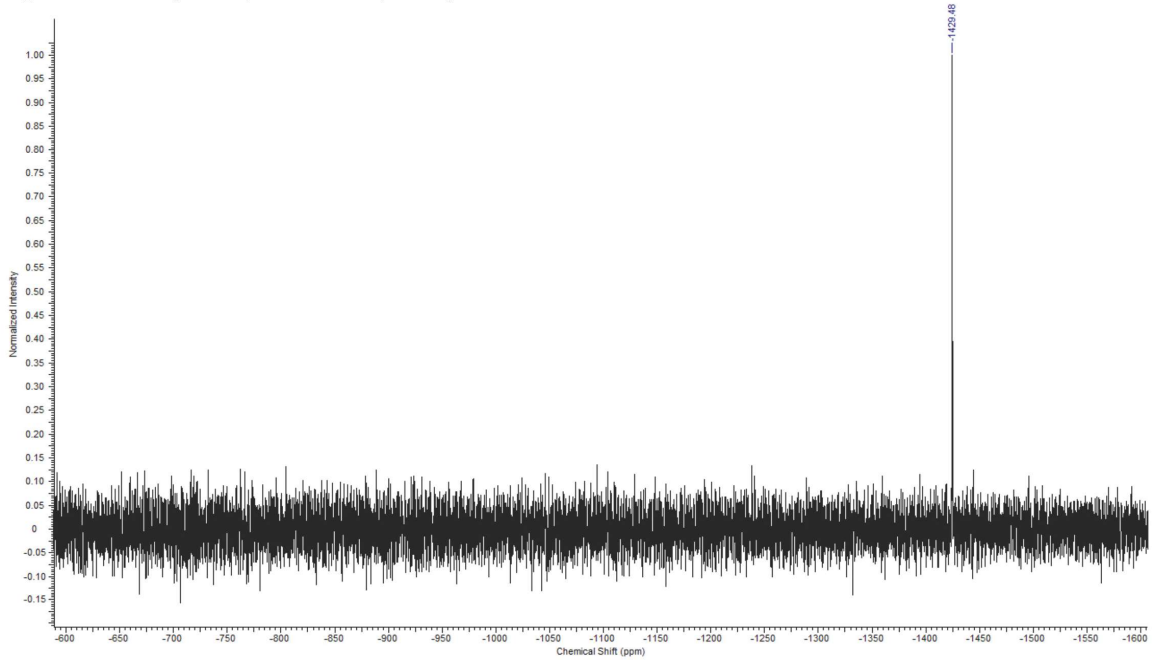

Fig. S 24: ^{195}Pt-NMR spectrum (108 MHz, $CDCl_3$) of complex **4d**.

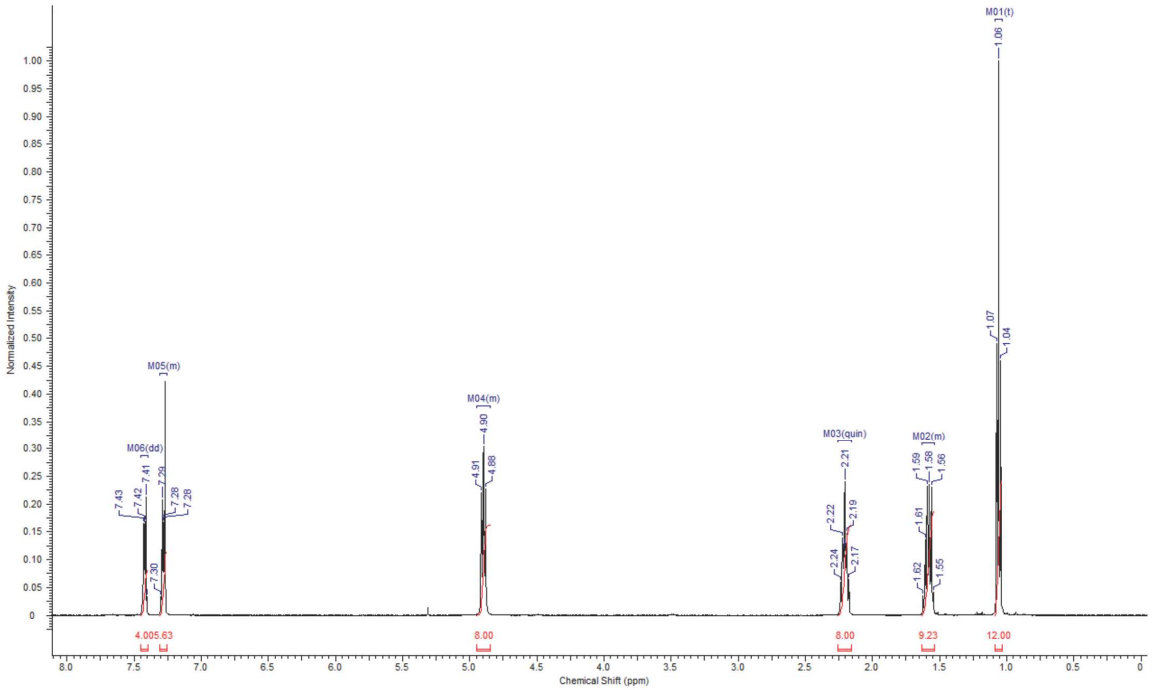

Fig. S 25: ^{1}H-NMR spectrum (500 MHz, $CDCl_3$) of complex ***trans*-2c**.

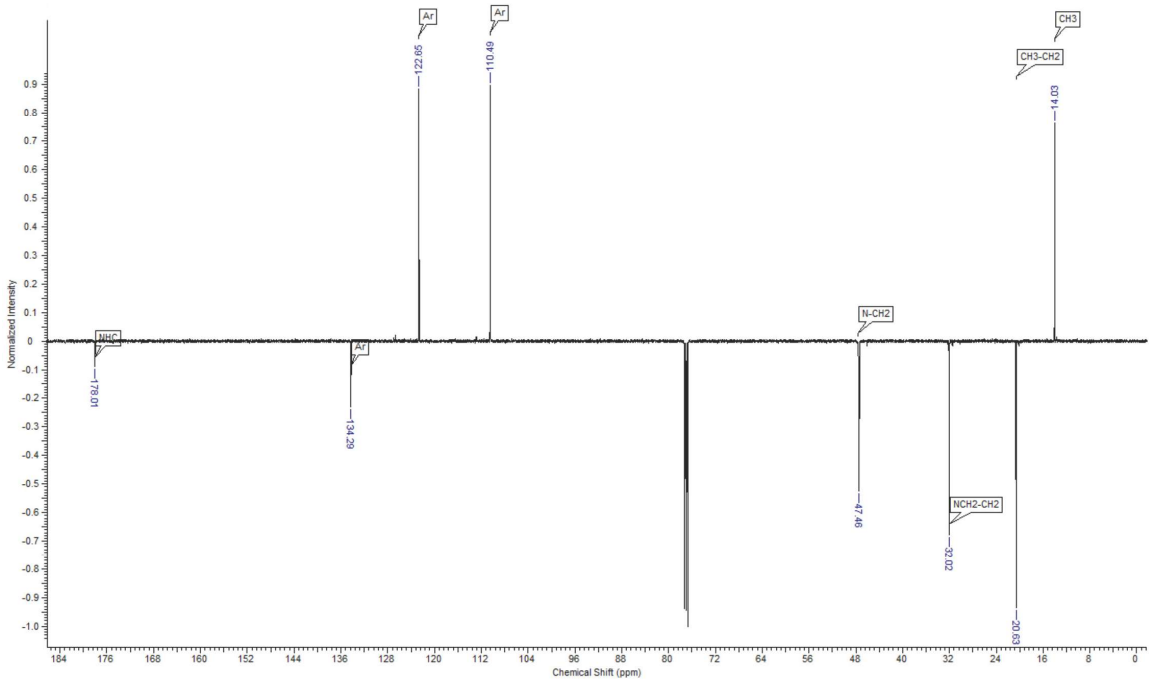

Fig. S 26: ^{13}C-NMR spectrum (126 MHz, $CDCl_3$) of complex ***trans*-2c**.

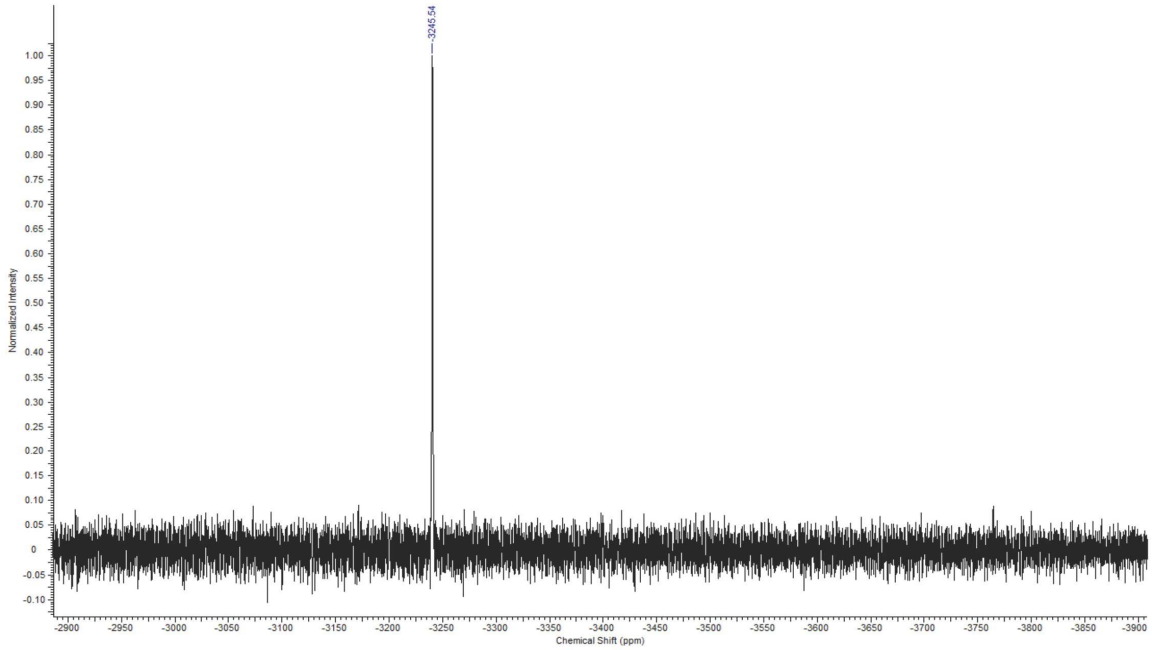

Fig. S 27: ^{195}Pt-NMR spectrum (108 MHz, $CDCl_3$) of complex ***trans*-2c**.

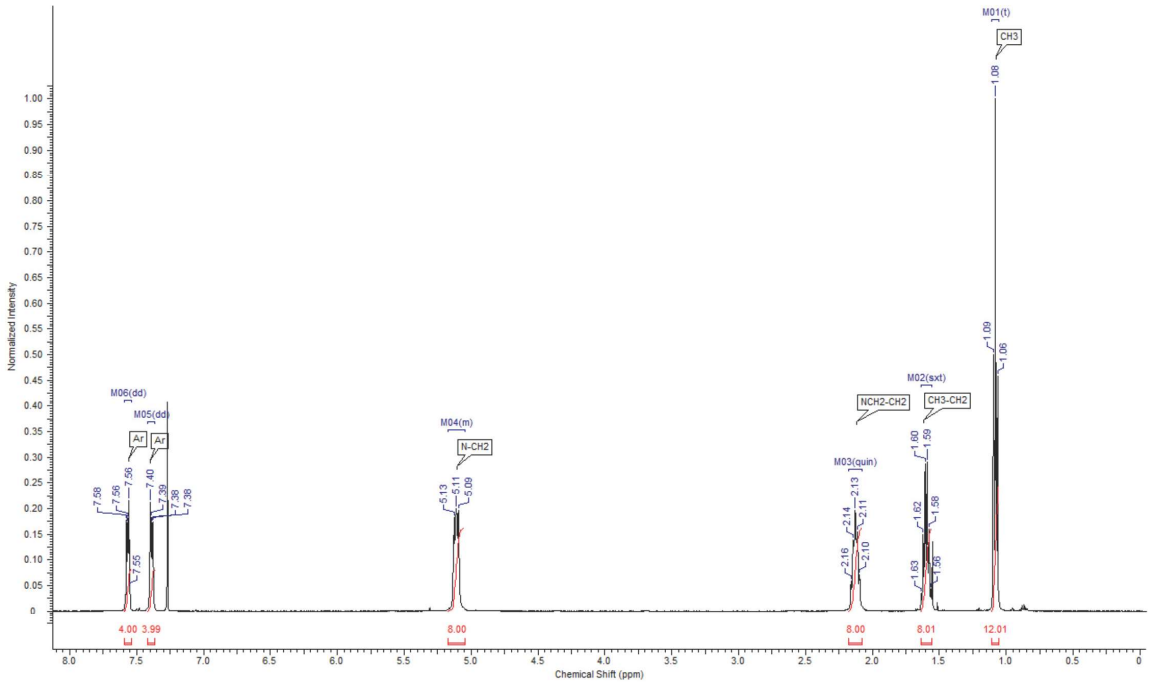

Fig. S 28: ^{1}H-NMR spectrum (500 MHz, $CDCl_3$) of complex ***trans*-4c**.

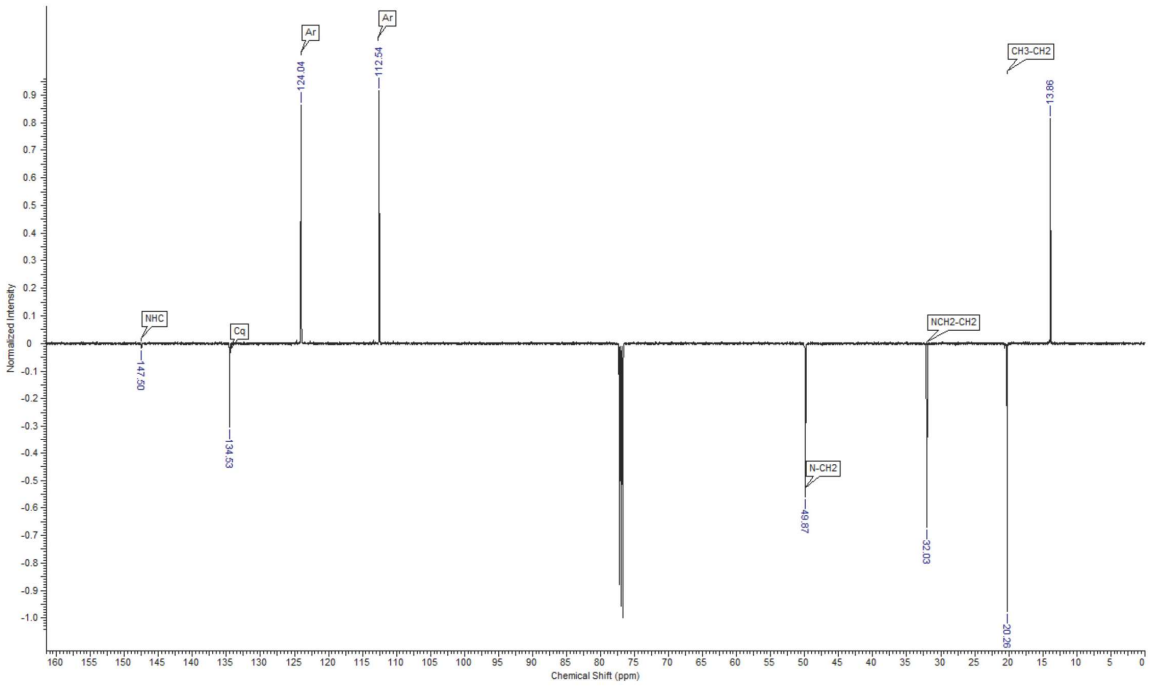

Fig. S 29: ^{13}C-NMR spectrum (126 MHz, $CDCl_3$) of complex ***trans*-4c**.

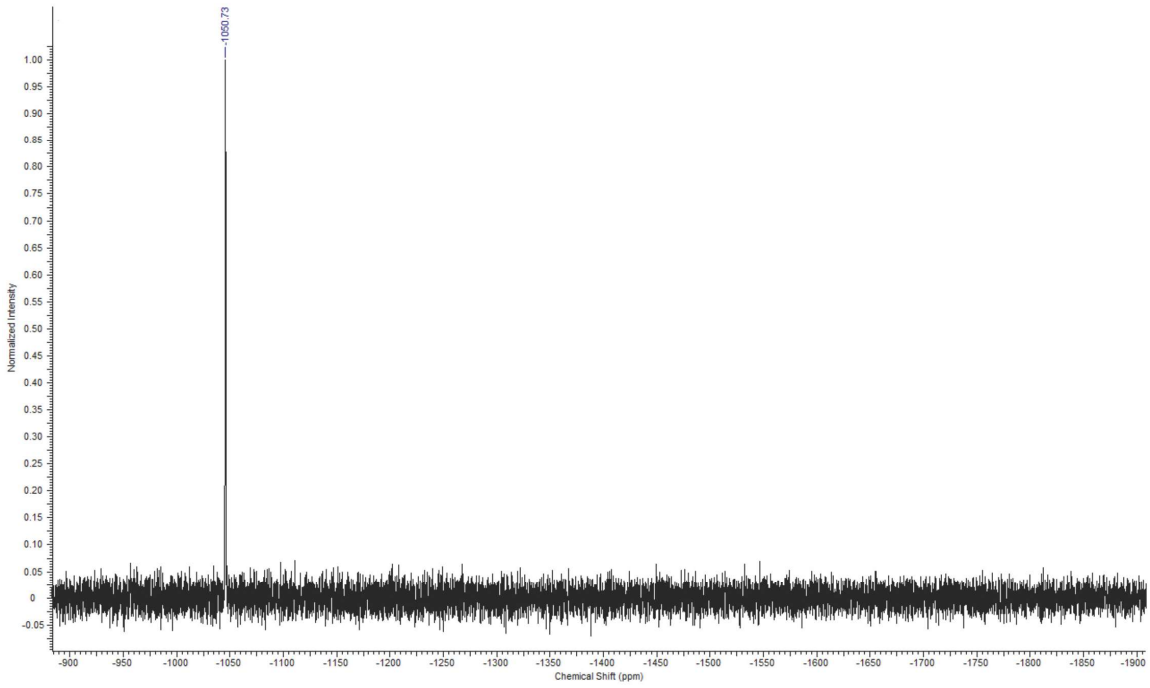

Fig. S 30: ^{195}Pt-NMR spectrum (108 MHz, $CDCl_3$) of complex ***trans*-4c**.

Oxidation of complex 2b with NaOCl

Pt^{IV} hydroxo complexes with NHC ligands have not been published yet.

Upon treating benzylated complex **1** with H_2O_2, a new ^{195}Pt NMR signal around -855 ppm ($CDCl_3$) arose but the reaction was never completed and at the same time accompanied by decomposition due to cleavage of the benzyl group forming benzoic acid.

H_2O_2 oxidation of the *N*-alkylated benzimidazole-2-ylidene complexes **2** afforded only starting material even with a vast excess of peroxide (H_2O_2 or ^{t}BuOOH) at elevated temperatures.

By treating **2b** with NaOCl in water/acetonitrile a new compound with a ^{195}Pt NMR signal at about -905 ppm ($CDCl_3$) appeared, but like before, neither did the reaction go to completion nor was it possible to separate any products from residual starting materials.

In one such run, crystals of a reaction product precipitated from $CDCl_3$ in the NMR tube. NMR spectra of freshly prepared solutions of these crystals in DMSO-d_6 were in agreement with the tentative structure **8** although alternative structures cannot be excluded with certainty. The same sample five days later showed only signals of pure starting Pt^{II} complex **2b**.

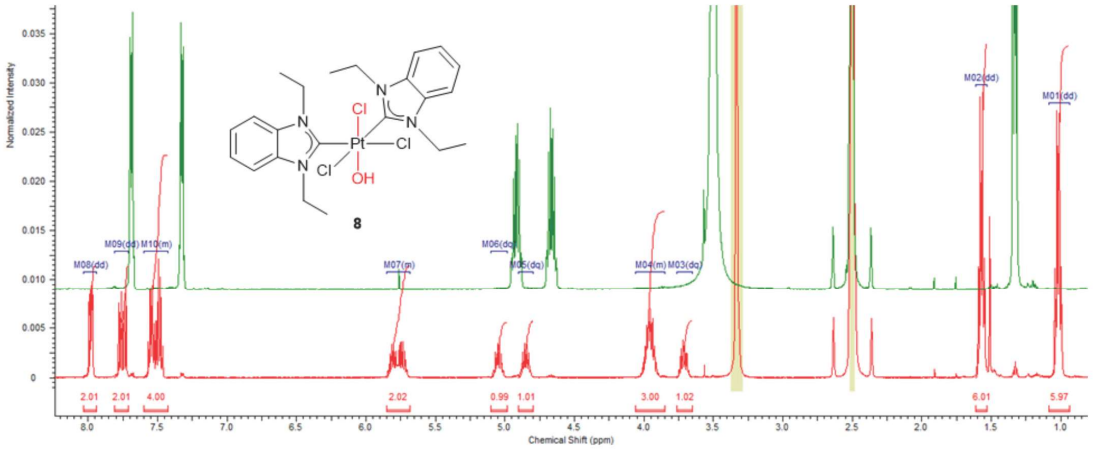

Fig. S 31 red: ^1H NMR (DMSO-d_6) of purported Pt^{IV} hydroxo complex **8** with characteristic signals of individual N-CH_2 protons between 3.5 and 6.0 ppm caused by inequivalent axial ligands;
green: same sample five days later shows spectrum of starting Pt^{II} complex **2b**.

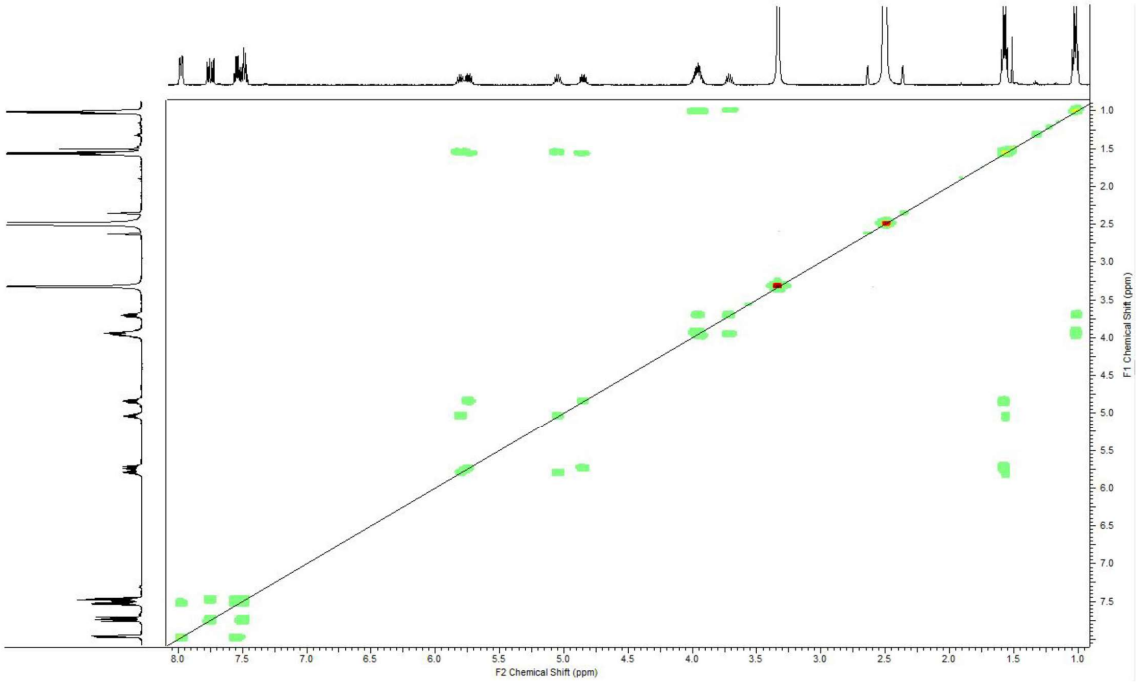

Fig. S 32 COSY-Spectrum of compound **8** in DMSO-d_6

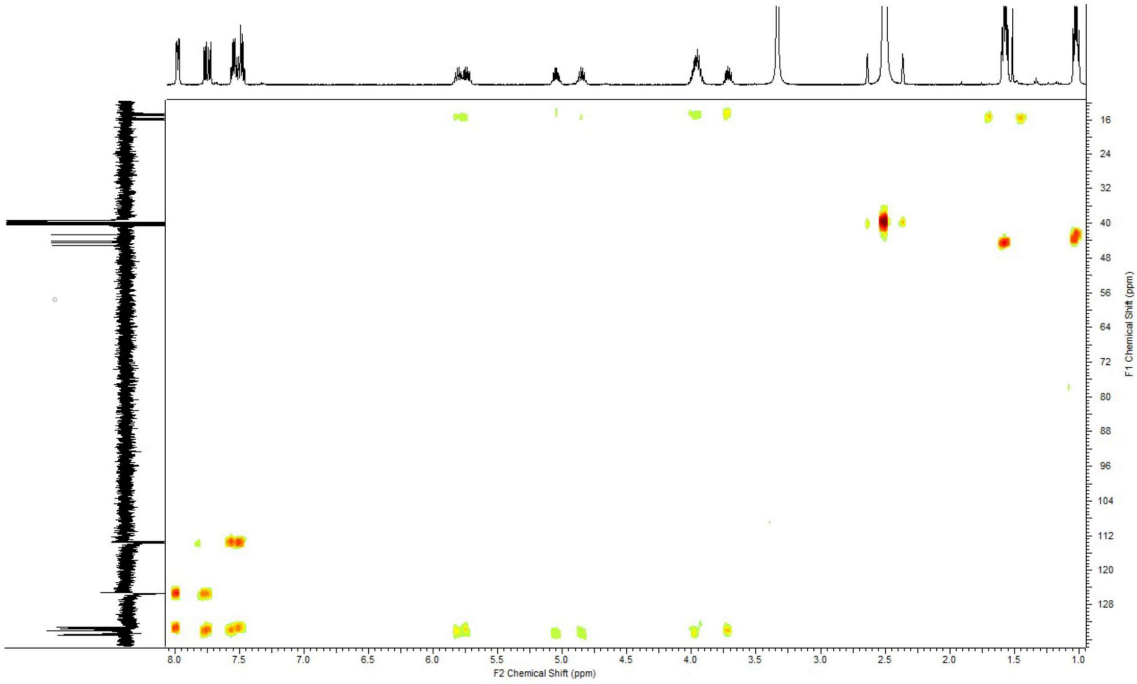

Fig. S 33 HMBC-Spectrum of compound **8** in DMSO-d_6

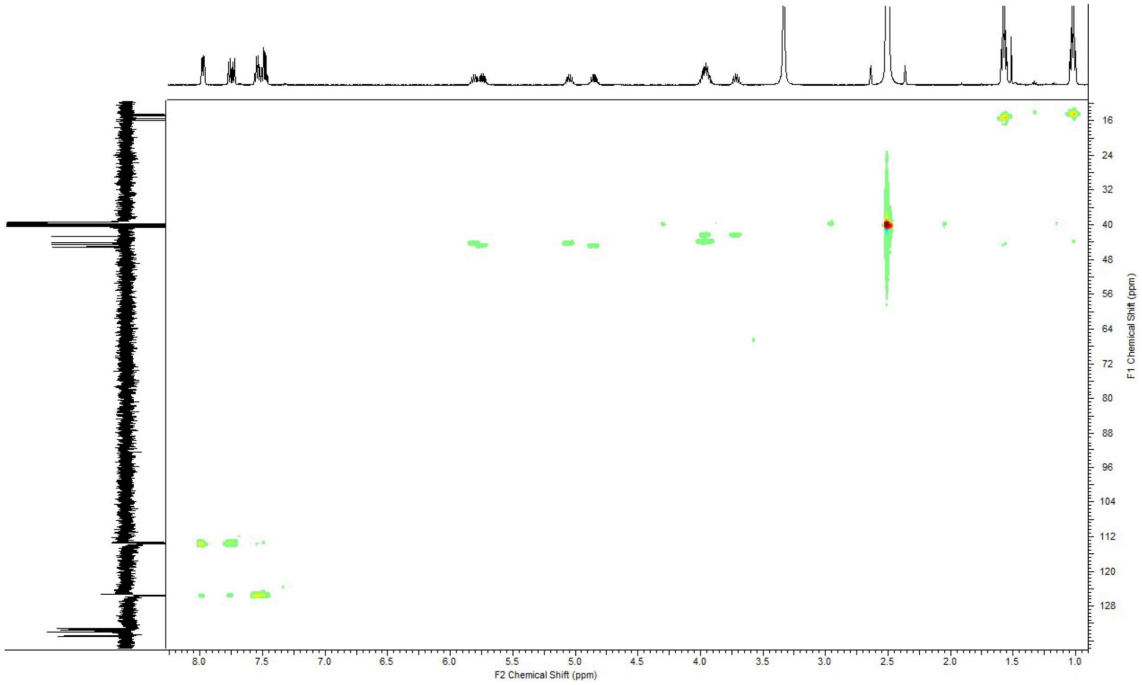

Fig. S 34 HSQC-Spectrum of compound **8** in DMSO-d_6

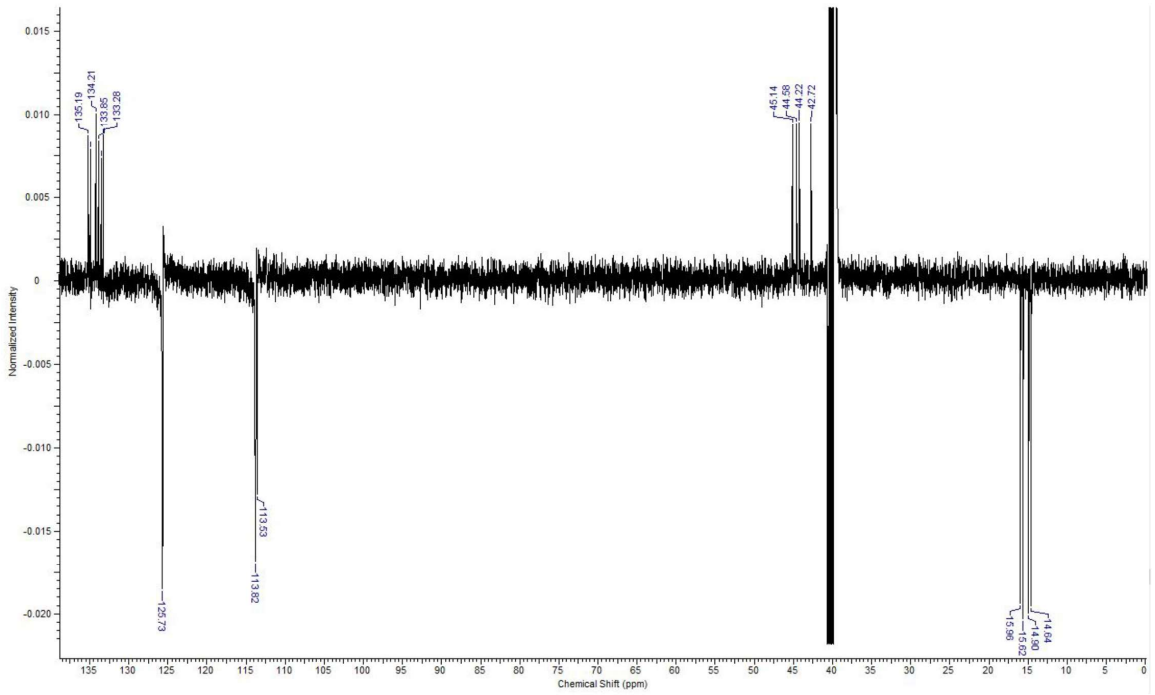

Fig. S 35 JMOD-Spectrum of compound **8** in DMSO-d_6

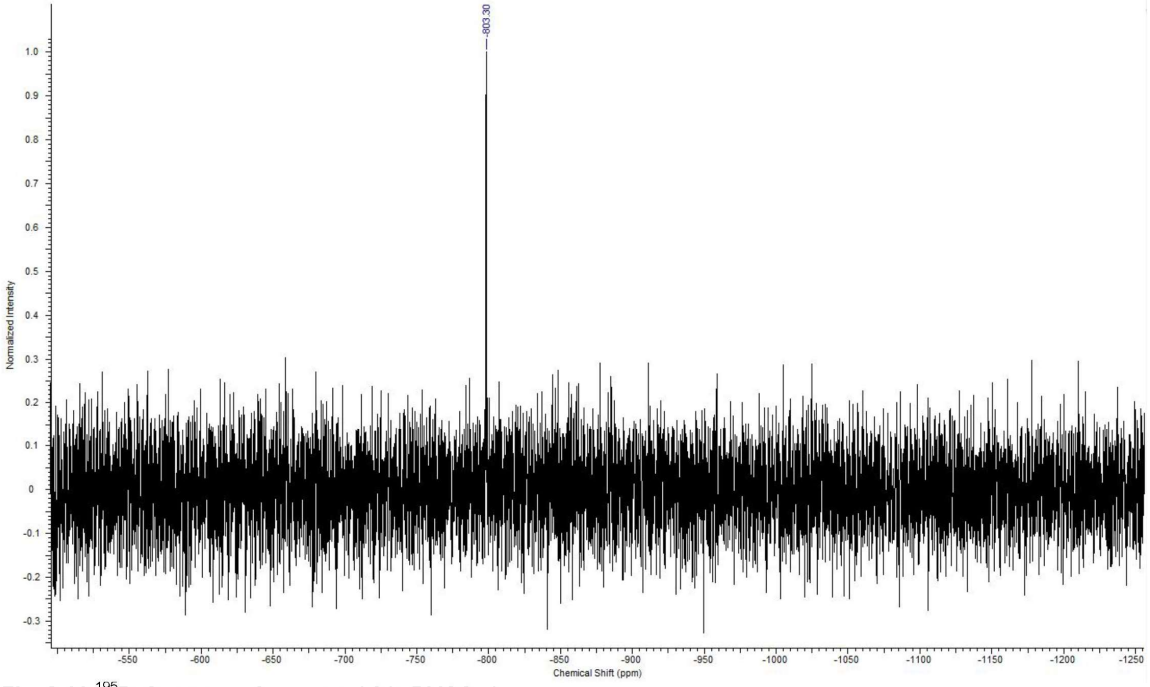

Fig. S 36 ^{195}Pt-Spectrum of compound **8** in DMSO-d_6

S21

Stability of complex 4b in DMSO / water

UV/vis spectra (Fig. S 37): were recorded of 2 mL of a 25 µM solution of complex **4b** (from a 5 mM stock solution in DMSO) in water/DMSO (4:1) over a period of 24 h (every 5 min for the first 3 h) by means of a Cary 60 UV-Vis Spectrometer (Agilent Technologies). Absorptions are relative to a baseline set to 0 at 400 nm.

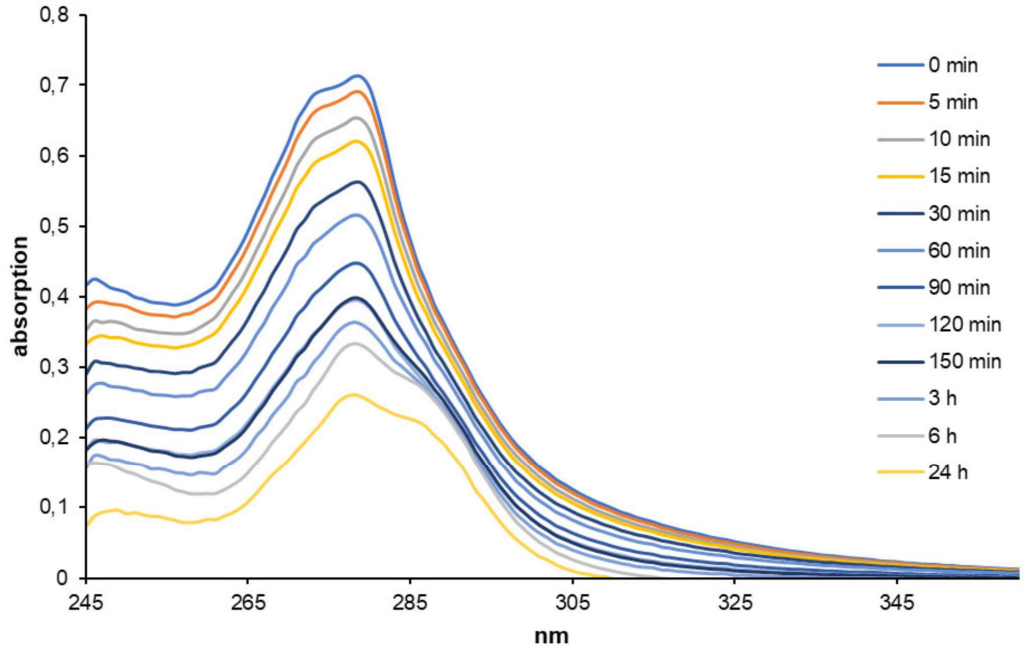

HPLC–ESI mass spectra: were recorded on a Varian 1200 Quadrupole MS/MS spectrometer of diluted NMR solutions of complex **4b** in water / DMSO-d_6 (30:70) after 0 min, 5 min, 10 min, 15 min, 30 min, 1 h, 2 h, and 16 h. The area of the total ion current (TIC) filtered for the main decomposition species with m/z = 579 was calculated for each of these points in time.

Exemplary MS after 10 min:

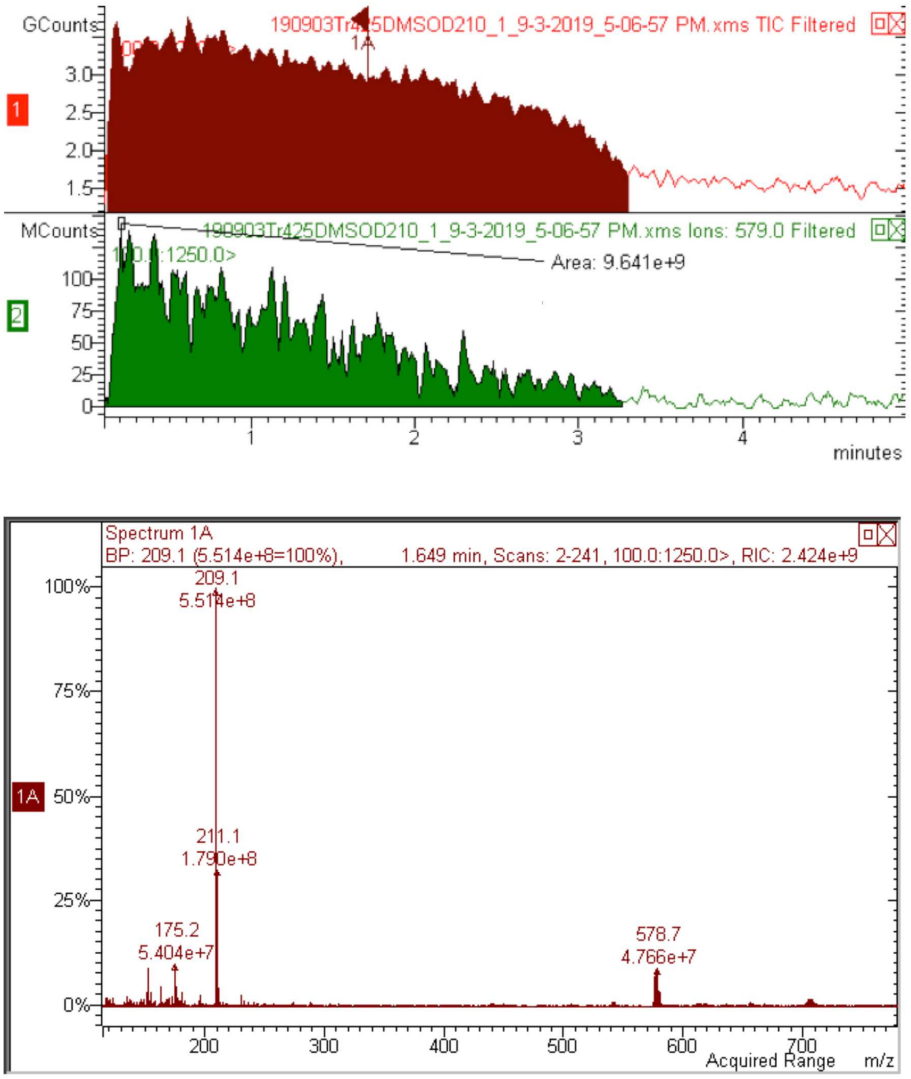

Fig. S 38: 1. Top in red: TIC = Total Ion Current from 0-3.2 min;
2. Middle in green: peak m/z = 579 integrated from 0-3.2 min to give an area of 9.641×10^9
3. Bottom: spectrum 1A, pertinent to TIC from 0-3.2 min.

Exemplary MS after 16 h:

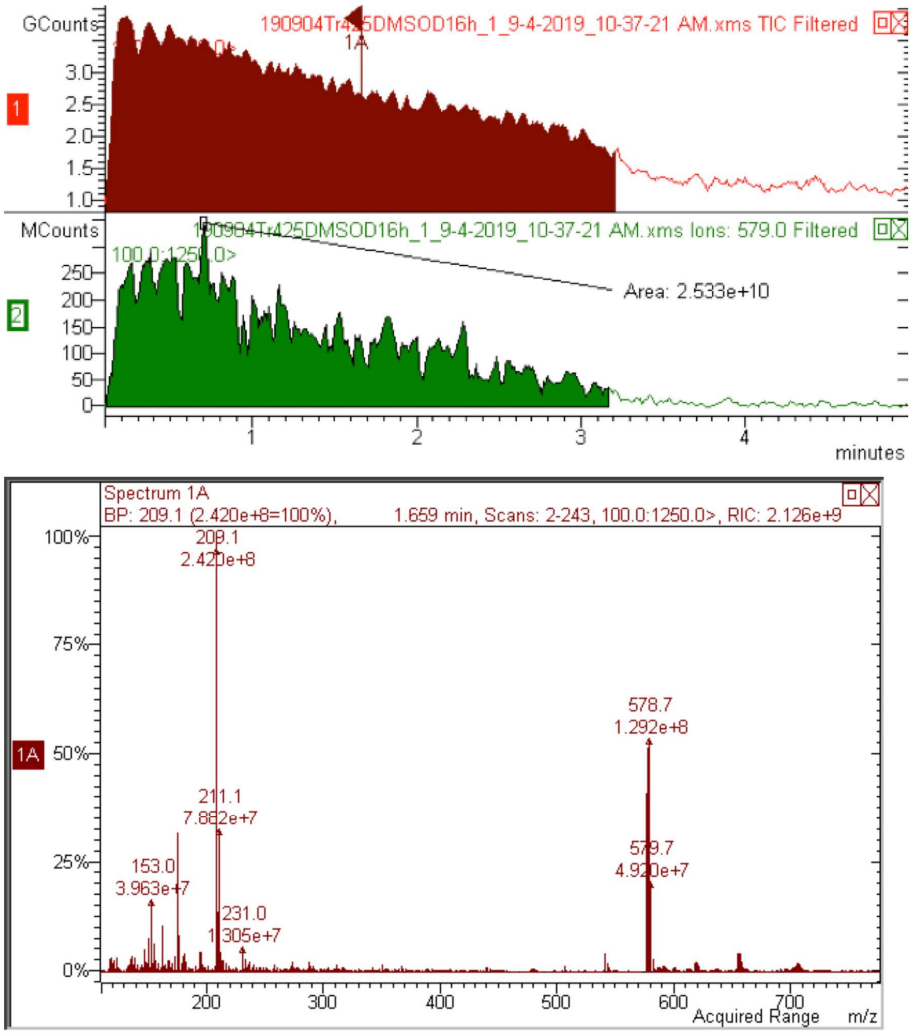

Fig. S 39: 1. Top in red: TIC = Total Ion Current from 0-3.2 min;
2. Middle in green: peak m/z = 579 integrated from 0-3.2 min to give an area of 2.533×10^{10}
3. Bottom: spectrum 1A, pertinent to TIC from 0-3.2 min.

Integration of peak m/z = 579 in spectra from 0-3.2 min recorded over time:

Time	***Area***
0 min	5.35×10^9
5 min	8.6×10^9
10 min	9.64×10^9
15 min	1.08×10^{10}
30 min	1.26×10^{10}
1 h	1.42×10^{10}
2 h	1.8×10^{10}
16 h	2.53×10^{10}

Confirmative MTT-assays with compounds 2c and 2d: were carried out with cells of the same lines yet of *distinctly different* passage numbers:

Table S 2: Means ± SD of IC_{50} (72 h) values [µM] of complexes **2c** and **2d** in MTT assays against human cancer cell lines[a] as calculated from four independent measurements

compounds	IC_{50} (72h) [µM]	
	2c[10b]	**2d**
[a]**518A2**	2.1 ± 0.3	> 50
[a]**HT29**	10.8 ± 1.0	> 50
[a]**DLD-1**	17.4 ± 1.0	> 50
[a]**HCT116**^{wt}	7.0 ± 0.8	> 50
[a]**HCT116**$^{-/-}$	5.3 ± 0.2	> 50

[a]518A2 – melanoma, HT-29 – colon adenocarcinoma, DLD-1 – Dukes type C colorectal adenocarcinoma, HCT116^{wt} – colon carcinoma (wildtype); HCT116$^{-/-}$ – colon carcinoma (p53 knock-out mutant).

5 AUFLISTUNG ALLER PUBLIKATIONEN UND TAGUNGSBEITRÄGE

5.1 PUBLIKATIONEN

- J.K. Münzner, T. Rehm, B. Biersack, A. Casini, I.A.M. de Graaf, P. Worawutputtapong, A. Noor, R. Kempe, V. Brabec, J. Kasparkova, R. Schobert, **Adjusting the DNA Interaction and Anticancer Activity of Pt(II) *N*-Heterocyclic Carbene Complexes by Steric Shielding of the *Trans* Leaving Group**, *J. Med. Chem.* **2015**, *58*, 6283−6292, DOI: 10.1021/acs.jmedchem.5b00896.

- T. Rehm, M. Rothemund, A. Bär, T. Dietel, R. Kempe, H. Kostrhunova, V. Brabec, J. Kasparkova, R. Schobert, ***N,N*-Dialkylbenzimidazol-2-ylidene platinum complexes – effects of alkyl residues and ancillary *cis*-ligands on anticancer activity**, *Dalton transactions* **2018**, *47*, 17367–17381, DOI: 10.1039/c8dt03360a.

- T. Rehm, M. Rothemund, J. K. Muenzner, A. Noor, R. Kempe, R. Schobert, **Novel *cis*-[(NHC)^1(NHC)^2(L)Cl]platinum(II) complexes – synthesis, structures, and anticancer activities**, *Dalton transactions* **2016**, *45*, 15390–15398, DOI: 10.1039/c6dt02350a.

- T. Rehm, M. Rothemund, T. Dietel, R. Kempe, R. Schobert, ***Synthesis, structures and cytotoxic effects in vitro of cis- and trans-[Pt^{IV}Cl$_4$(NHC)$_2$] complexes and their Pt^{II} precursors***, *Dalton transactions* **2019**, 48, 16358-16365, 10.1039/c9dt02438g.

- F. Schmitt, Kate D., J.K. Muenzner, T. Rehm, V. Novohradsky, V. Brabec, J. Kasparkova, M. Albrecht, R. Schobert, T. Mueller, **Effects of histidin-2-ylidene vs. imidazol-2-ylidene ligands on the anticancer and antivascular activity of complexes of ruthenium, iridium, platinum, and gold**, *J. Inorg. Biochem*. **2016**, *163*, 221-228, DOI: 10.1016/j.jinorgbio.2016.07.021.

- J.K. Muenzner, B. Biersack, A. Albrecht, T. Rehm, U. Lacher, W. Milius, A. Casini, J.-J. Zhang, I. Ott, V. Brabec, O. Stuchlikova, I.C. Andronache, L. Kaps, D. Schuppan, R. Schobert, **Ferrocenyl-Coupled *N*-Heterocyclic Carbene Complexes of Gold(I): A Successful Approach to Multinuclear Anticancer Drugs**, *Chem. Eur. J.* **2016**, *22*, 18953-18962, DOI: 10.1002/chem.201604246.

- H. Draut, T. Rehm, G. Begemann, R. Schobert, **Antiangiogenic and Toxic Effects of Genistein, Usnic Acid, and Their Copper Complexes in Zebrafish Embryos at Different Developmental Stages**, *Chem. Biodiversity* **2017**, *14*, e1600302, DOI: 10.1002/cbdv.201600302.

5.2 TAGUNGSBEITRÄGE

2017: 12th International Symposium on Platinum Coordination Compounds in Cancer Chemotherapy (ISPCC 2017), Sydney, Australien

Posterbeitrag: **Progressive Development of NHC Platinum Anti-Cancer Agents**
T.Rehm, M. Rothemund, and R. Schobert

2016: Gordon Research Conference on Metals in Medicine, Andover, NH, USA

Posterbeitrag: **Platinum(II) NHC Complexes: Novel Structural Motifs with distinct anti-cancer activities.**
T. Rehm, M. Rothemund, J. Münzner and R. Schobert

2015: Cost action CM1105 (Functional metal complexes that bind to biomolecules) working group 4 (Interactions of metallo-drugs on the cellular level) meeting, Bari, Italy

Vortrag: **Platinum(II) NHC Complexes: New Structural Motifs and Their Bearing on DNA Function.**

DANKSAGUNG

Nach der langen Zeit bis zur Fertigstellung dieser Arbeit möchte ich bei allen direkt oder indirekt daran beteiligten bedanken.

Zunächst gilt mein Dank Familie und Freunden, besonders Anna, für ihre Geduld und stete Unterstützung während all der Jahre des Studiums und der Promotion.

Vielen Dank auch an alle Kollegen am Lehrstuhl OC I für die gute Zusammenarbeit und die vielen unterhaltsamen Stunden vor und nach Feierabend, an Matthias Rothemund und Dr. Julienne Münzner ohne die all die Publikationen in dieser Form nicht möglich gewesen wären, an Dr. Ulrike Lacher für die Unterstützung bei analytischen Fragestellungen, an Silvia Kastner für die Organisation von allem Möglichen, an Dr. Bernhard Biersack für die regelmäßigen Ratschläge, die wissenschaftlichen Diskussionen und besonders die Unterstützung in meiner Anfangszeit, an Dr. Thomas Schmalz der uns allen immer mit Rat und Tat zur Seite stand und natürlich an alle anderen die nicht explizit erwähnt wurden. Danke!

Ein besonderer Dank geht natürlich an Prof. Dr. Rainer Schobert der es mir ermöglicht hat diese Arbeit an seinem Lehrstuhl zu erarbeiten, dabei für sämtliche wissenschaftliche Fragestellungen und neue Ideen immer ein offenes Ohr hatte und mir zudem die nötigen Freiheiten gelassen hat, um dieses interessante Thema nach meinen Vorstellungen anzupacken. Vielen Dank für die Möglichkeit meine Arbeiten auf mehreren Konferenzen vor internationalem Publikum vorstellen zu dürfen, aber nicht zuletzt auch für all die Gespräche und Diskussionen irgendwo zwischen Aquarium und Küche.

EIDESSTATTLICHE VERSICHERUNGEN UND ERKLÄRUNGEN

(§ 8 Satz 2 Nr. 3 PromO Fakultät)

Hiermit versichere ich eidesstattlich, dass ich die Arbeit selbstständig verfasst und keine anderen als die von mir angegebenen Quellen und Hilfsmittel benutzt habe (vgl. Art. 64 Abs. 1 Satz 6 BayHSchG).

(§ 8 Satz 2 Nr. 3 PromO Fakultät)

Hiermit erkläre ich, dass ich die Dissertation nicht bereits zur Erlangung eines akademischen Grades eingereicht habe und dass ich nicht bereits diese oder eine gleichartige Doktorprüfung endgültig nicht bestanden habe.

(§ 8 Satz 2 Nr. 4 PromO Fakultät)

Hiermit erkläre ich, dass ich Hilfe von gewerblichen Promotionsberatern bzw. -vermittlern oder ähnlichen Dienstleistern weder bisher in Anspruch genommen habe noch künftig in Anspruch nehmen werde.

(§ 8 Satz 2 Nr. 7 PromO Fakultät)

Hiermit erkläre ich mein Einverständnis, dass die elektronische Fassung der Dissertation unter Wahrung meiner Urheberrechte und des Datenschutzes einer gesonderten Überprüfung unterzogen werden kann.

(§ 8 Satz 2 Nr. 8 PromO Fakultät)

Hiermit erkläre ich mein Einverständnis, dass bei Verdacht wissenschaftlichen Fehlverhaltens Ermittlungen durch universitätsinterne Organe der wissenschaftlichen Selbstkontrolle stattfinden können.

……..

Ort, Datum, Unterschrift